TURBINE ENGINE COMPRESSOR BLADE CHECKOUT

FINAL REPORT

J. E. Bridges
H. R. Hegner, et al.

Air Force Aero Propulsion Laboratory
Research and Technology Division
Air Force Systems Command
Wright-Patterson Air Force Base, Ohio, 45433

FOREWORD

This report was prepared by IIT Research Institute of the Illinois Institute of Technology, Chicago, Illinois, under Air Force Project 8119, Task 811925, Contract AF33(615)-3640, "Turbine Engine Compressor Blade Checkout". This work was sponsored and administered under the direction of the Support Technology Division of the Air Force Aero Propulsion Laboratory, Air Force Systems Command. Mr. K. Hamilton, APFG, was the Project Engineer for the Air Force.

The studies presented began in April 1966 and were concluded in April 1967. This represents an effort by the Instrumentation and Recording Section, Electronics Research Division of IIT Research Institute on Project E6067. The overall program was under Mr. J.E. Bridges, Principal Investigator and H.R. Hegner, Project Engineer. Other contributors were R.M. Knox, R.B. Schwab and A.H. Hehn.

This report was submitted by the authors on 14 April 1967.

This technical report has been reviewed and is approved.

Robert D. Sherrill

ROBERT D. SHERRILL, Chief
Ground Support Branch
Support Technology Division

ABSTRACT

The ingestion of foreign objects into jet engines causes damage in the compressor assembly which is a major safety-of-flight and maintenance problem. While the engine is installed, the checkout of jet engine compressor rotor blades is a difficult and time consuming operation. Foreign object damage is normally not found until it severely affects engine performance. Therefore, new checkout techniques need to be developed to detect foreign object damage during flight line checkout while the engine is operating.

This program was initiated with an objective to demonstrate the feasibility of one or more techniques for a portable flight line checkout system that will determine foreign object damage to the compressor rotor blades of the installed jet engine. The compressor blades are to be inspected without requiring personnel to gain access to the engine front end and while the engine is motoring, idling, and running at 100 percent power or any setting in between.

The program was initiated by examining a wide variety of physical phenomena. The most promising techniques were then considered on an analytical basis, followed by preliminary laboratory evaluations on simple simulated compressor assemblies. After these investigations, the most promising techniques were evaluated on an actual compressor section from a J-47 class engine. Results pointed to the need for primary emphasis to be placed on electromagnetic techniques including millimeter wave, magnetic field, and eddy-current techniques. Electrometer and optical techniques did not prove to have promising applications on a practical basis. The feasibility of the promising techniques were verified by demonstrating them with experimental breadboards on the J-47 compressor assembly.

TABLE OF CONTENTS

ILLUSTRATIONS

ILLUSTRATIONS (Continued)

ILLUSTRATIONS (Continued)

ILLUSTRATIONS (Continued)

ILLUSTRATIONS (Continued)

ILLUSTRATIONS (Continued)

TABLES

1.0 INTRODUCTION

1.1 Objectives -- The ingestion of foreign objects into jet engines is a definite threat to flight safety and requires maintenance on many engines which otherwise could have remained in service. U.S. Air Force service records show that foreign object damage in jet engines is a major safety-of-flight and maintenance problem. Few objects that damage engines are identified, but most damage is caused by air base surface debris, parts of failed inlet components, and objects left in inlets by personnel. The inspection and checkout of compressor rotor blades while the jet engine is installed in the aircraft is generally a difficult and time consuming operation. Normally foreign object damage is not found until it severely affects engine performance in flight. Checkout techniques need to be developed to detect foreign object damage during on-ground inspections.

The specific objective of this program was to demonstrate the feasibility of one or more techniques for a portable flight line checkout system that will determine foreign object damage to the compressor rotor blades of a jet engine which is installed and running. The compressor blades are to be inspected without gaining access to the engine front end while the engine is motoring, idling, and running at 100 percent power or any rpm setting in between. The feasibility of the promising techniques are to be verified by demonstrating with experimental breadboards these techniques on an actual compressor assembly.

This section is presented, not only to introduce and define foreign object damage, but also to provide a survey of checkout techniques. This section also shows how the promising techniques can be ultimately incorporated into a complete flight line checkout system.

1.2 Summary -- Since the following sections present the detailed results of a wide variety of efforts, it is worthwhile to make a few comments relative to the program direction, final conclusions, and report organization.

The program was initiated with an examination of over 40 possible phenomena. Only seven were selected for analysis. Table I lists the techniques initially selected. The more promising techniques were then experimentally evaluated on a simple simulated compressor section which resembled a table-top fan. After these initial laboratory breadboard tests, only two techniques -- the millimeter wave interferometer and eddy-current detector -- appeared worthwhile for additional consideration.

These two techniques, as leading-edge defect detectors, were then evaluated on a laboratory mounted J-47 compressor section. Both the analysis and tests disclosed that either the normal axial variation in the position of the blade or the reworking of the blade caused spurious outputs for the eddy-current leading-edge defect detector. These problems eliminated the leading-edge eddy-current technique.

Test results with the millimeter-wave system were successful. The millimeter wave system is a quasi-optical system. It is used in the form of an interferometer so that adjacent areas on the same blade are compared. By this technique, most of the problems associated with the normal tolerance variations between blades and possible rework are greatly minimized. The millimeter wavelength was chosen to be comparable to the defect size in order to obtain the greatest sensitivity for defects in conjunction with the greatest immunity to various spurious responses. The millimeter-wave inspection system can be visualized as a probe containing two small flashlight like sources. Two beams of energy are focused on adjacent areas of the same blade. The returned energy from each source is compared in a bridge circuit, so that a defect illuminated by one source

causes a significant output. The amplitude of this output can be used to determine the approximate size of the defect.

The presently designed millimeter-wave system as tested on the actual compressor section of the J-47 engine appeared capable of resolving 0.03 inch radius leading edge defects on the first stage of the rotor. Further design improvements should increase the sensitivity and also permit detection of defects on the air foil contour area of the first stage as well as edge defects on the second stage of the compressor rotor section. Since a probe must be inserted, this technique appears to be the most useful for flight-line checkout techniques.

A second successful technique was developed during tests on the breadboard J-47 compressor section. It was discovered that the blades were magnetic and that if any one of these blades were struck by an object to cause a 0.015 inch radius defect, it would be permanently demagnetized. Brief tests at Wright-Patterson Air Force Base indicated that this magnetization is retained for normal flight conditions. To take advantage of this secondary evidence of foreign object damage, a very simple magnetic field sensor using a Hall-effect device was designed. It was mounted in a small hole located in the shroud above the row of compressor blades being monitored. At any speed of the compressor, this sensor easily detected blades which had been struck so as to cause significant damage, in the order of 0.015 inch radius or larger. This technique appears especially suitable for in-flight monitoring, especially during takeoff. Its output can be used with various flag-type indicators or on-board recorders.

An analysis of the specified tolerances, relative to blade positioning and rework, indicated the smallest ranges occurred at the blade tips. Tests and analysis also demonstrated that significant damage or crack development resulted in one or more of the tip parameters exceeding the specified tolerance ranges by a large value. By suitable tip parameter sensor design,

important evidence of foreign object damage or crack development can be monitored. To demonstrate this, an eddy-current sensor was placed in a small hole in the shroud above the row of rotor blades to be monitored. This sensor system was designed to detect overall twist or bending at the blade tip. While subject to a number of qualifications, breadboard tests on the J-47 compressor indicated that damage resulting in a 0.06 inch radius defect was easily detectable on the J-47 compressor section.

Analysis has also demonstrated that crack-development near the root of the blade results in significant changes at the blade tips, especially during conditions of high aerodynamic loading. Studies using the results of the J-47 breadboard tests indicated that a typical crack development can be detected at least 100 minutes prior to catastrophic failure. Thus, the tip parameter sensors are especially suitable for on-board, in-flight monitoring and may be used in conjunction with on-board recorders for foreign object damage (FOD) or with flag-type indicators for both FOD and crack development warning.

While the program has emphasized sensors, it is easily seen that the associated signal-processing is quite simple and well within the state-of-the-art. For example, a typical compressor section could have about 40 blades and be rotated as high as 12,000 rpm (200 rps). The blades passing by the sensors, under normal conditions, introduce a fundamental frequency of 8000 Hertz. To resolve differences between blades, a frequency response of about 12 times this fundamental frequency or about 100,000 Hertz is required. This upper frequency requirement is well within the state-of-the-art for very simple signal processing circuits. It should also be noted that none of the systems require extensive signal-processing, complex signature recognition, or any type of pattern recognition.

This program has demonstrated the feasibility of three techniques to detect foreign object damage; they are summarized

in Table I. No major problem areas or critical experiments have been identified. Thus, all aspects appropriate to a feasibility investigation were found favorable for these three systems.

It is recommended that a feasibility breadboard of a combined remnant magnetization and tip parameter sensor be developed. This intermediate step is necessary, not only to optimize the system, but to consider a variety of specific practical aspects. These aspects would include, for example, mechanical considerations of mounting on all jet engines, as well as investigating the effect of non-normal flight conditions on the remnant magnetization. Further development of the millimeter wave interferometer system is suggested as a flight-line checkout technique to determine the extent of FOD by resolving the position and size of the defect.

The remainder of the introduction considers background details of foreign object damage, as well as the various phenomena initially considered. This is followed by detailed presentations which include the unsuccessful systems as well. For those interested in only the more promising system, Table II indicates the portion of the report where these are discussed. Table III, summarizes the phenomena initially considered.

Table I

TECHNIQUES INVESTIGATED IN DEPTH

Selection	System	Type of Defect Detected	Current Analytical or Experimental Results	Future	Field Usage	Recommendation
Initially Selected Techniques or Phenomena	Millimeter-Wave Interferometer	Leading edge defects on 1st and 2nd stage. Defects on air foil contour area of 1st stage.	Detected 0.03" radius defects	Higher frequency system should resolve 0.005" leading edge defects. Also larger defects on air foil contour area of 1st stage and edge defects on 2nd stage.	Small Probe inserted into cowling for flight-line checkout.	Suitable for flight-line tests after development of higher frequency system.
	Electrometer	Leading Edge Defects, 1st stage	Insufficient resolution	- -	- -	Drop
	Eddy-current Techniques	Leading Edge Defects, 1st stage	Subject to normal axial position variation of blades	- -	- -	Drop
	Magnetic Field Techniques	Blade or leading edge defects, 1st stage	Subject to normal axial position, and variation of blade. Less sensitive than eddy-current techniques.	- -	- -	Drop
	Optical Technique	Leading edge or air foil contour area defects.	Subject to field usage problems, such as false alarms due to oil spots.	- -	- -	Drop
Evolved Techniques	Remnant Magnetic Field	Detects a hit blade on any row by noting disappearance of remnant magnetization.	Detected blade which was hit to cause a 0.015" radius defect.	Ready to be extended to feasibility breadboard.	Small unit mounted in shroud above stages for all engines employing magnetic compressor blades.	Consider for In-flight monitoring, especially during takeoff or near bird flyways. Can use for flight-line tests as well.
	Eddy-Current Blade Tip Parameter Monitor	Detect significant hits or crack development by noting blade twist or bending.	Detected blades which were twisted or bent by a hit capable of causing a 0.05" radius defect.	Ready to be extended to feasibility breadboard.	Small unit mounted in shroud above row of blades to be monitored.	Consider for use in-flight especially during takeoff or near bird flyways. Consider for in-flight monitoring to give about 1 hour warning of excessive crack development. Can use on flight-line as well.

Table II

RECOMMENDED SYSTEM

	Technical Discussion	Detailed Conclusions	General Conclusions	General Recommendations
Millimeter-Wave	p 38-89	p 88	p 212	p 216-217
Remnant Magnetic Field	p 89-94, 103-106, & 113-123	p 123	p 213-214	p 216-217
Eddy Current Tip Parameter Monitors	p 124-135, 158-171	p 171	p 213-214	p 216-217

1.3 Feasibility Test Criteria -- The contractual design goals called for detecting a variety of compressor rotor blade damage as given in Table III. These specifications were drawn largely from the Air Force Technical Orders for the J-79 turbine engine relative to reworking damaged blades. In the case of the J-47 turbine engine which was used as the demonstration breadboard system, the damage specifications obtained from the appropriate technical orders are also given in Table III.

At the outset of the work, the design goal was to resolve defects due to foreign object damage down to a minimum size. After tests were performed on the J-47 compressor, a secondary usage of certain techniques was established. This was to sense whether foreign object ingestion had taken place which would have caused damage in the order of the minimum size or greater as previously delineated. Such a detection system does not resolve specific geometrical mechanical damage features. Preferably the system should be able to (1) determine whether foreign objects have been ingested, and (2) whether the damage is significant.

In addition to the foregoing, the checkout system should meet other design objectives. These involve the minimization of operator judgement or subjective tests. In addition, special treatment of the blades was prohibited. Use of signature techniques which would require pattern recognition methods or making signature measurements on more than 10 engines was also prohibited. The use of techniques requiring engine sounds or long set-up times was also forbidden. It was desired that both flight-line and in-flight monitoring be achieved for more than one stage of compressor rotor blades while the engine was running.

Table III

TURBINE ENGINE COMPRESSOR ROTOR BLADE DAMAGE

Types of Blade Damage	Contract Goals				J-47 Turbine Engine			
	Air Foil Contour Area	Leading or Trailing Edge	Tip	Platform Edges	Air Foil Contour Area	Leading or Trailing Edge	Tip	Platform Edges
Nicks	0.005 in. deep	0.005 in. deep	-	0.005 in. deep	0.010 in. deep	0.010 in. deep	-	-
Dents	0.005 in. deep	0.005 in. deep	-	0.10 in. deep	0.010 in. deep	0.010 in. deep	-	-
Pits	1/64 in. deep	0.010 in. deep	-	-	1/16 in. diameter & 1/64 in. deep	1/64 in. diameter	-	1/16 in. diameter & 1/64 in deep
Scratches	Felt with scriber of 0.030 in. radius	-	-	0.005 in. deep	0.010 in. deep	-	-	-
Cracks	any	any	any	any	any	any	any	any
Curl	-	-	any	-	-	-	any	-

1.4 Typical Classes of Foreign Object Damage

1.4.1 General -- The ingestion of foreign objects into gas turbine engines has been the cause of many minor repairs, premature engine overhauls, and major aircraft accidents. Air Force Technical Orders specify nick and dent tolerances for gas turbine engines. When damage caused by the impact of an object exceeds that allowed in the technical orders, the engine must then be sent to an overhaul base for complete disassembly and repair.

The inspection of a gas turbine engine during overhaul may reveal indications of several malfunctions. Each malfunction or unsatisfactory condition found is described in the inspection report. A primary reason for the removal of the engine from service, based on information obtained during the inspection, is indicated in the report. Malfunctions, therefore, are reported either as the primary reasons for removal from service or as simultaneous failures also found during inspection. The data on the damage by foreign objects are compiled as: (1) total damage composed of both primary and simultaneous damage, and (2) primary damage only.

Foreign object damage is defined as including damage caused by objects originating outside the aircraft, objects left in the inlet duct by personnel, objects generated by failure within the inlet duct including screen components, and objects of unknown origin. Damages caused by objects generated by failure behind the inlet screen or engine face are considered internal failures. Foreign object damage is reported only when a nick or dent is observed that was clearly caused by the passage of an object through the engine. If an unexplainable major internal breakup of the engine has occurred, nicks or dents on the rotating parts are not reported as due to foreign objects.

The hazard to flying safety created by the ingestion of foreign objects into gas turbine engines cannot be evaluated directly from engine-overhaul statistics. Foreign objects may have caused major jet engine aircraft accidents, but confusion of the debris usually will have concealed the evidence required to prove the fact. Studies by the Air Force Directorate of Flight Safety Research have led to the statement that "axial flow compressor failure is the largest single factor contributing to the jet engine accident rate. Foreign object damage and metal fatigue in compressor rotor parts are principle factors in these failures." (Ref. 1). Therefore, it is important that foreign object damage be reduced in order that jet engine maintenance problems be minimized and flight safety improved.

1.4.2 Source of foreign object damage -- A study conducted by NASA Lewis Research Center (Ref. 2) involved a review of Air Force Disassembly Inspection reports prepared by gas turbine engine overhaul bases. This study includes a compilation of data which identifies particular objects that damaged the engines. These are listed in Table IV. The identifications were based on the following:

- The object was found in the damaged engine or otherwise positively identified
- The nature of the damage indicated the kind of object responsible
- A missing part from the inlet components could have caused the damage

Large objects may cause major break-ups of engine interiors (or accidents) and then become lost in the debris. Small objects may pass through the engine and become lost. Pebbles and other frangible objects may be broken into very small pieces and make identification improbable or of dubious value. Much of the damage is therefore attributed in the official reports to objects of unknown origin or identity. Rivets, screws, special fastenings, and screen segments that fail and/or become loose in the engine inlet are a known source of

Table IV

IDENTIFIED OBJECTS CAUSING PREMATURE OVERHAUL OF ENGINES

Objects	Number	Percent of engines over-hauled
Engine A		
Screen segments	23	19.3
Rocks and pebbles	5	4.2
Battle debris	1	0.8
Unknown	90	75.7
Total	119	100.0
Engine B		
Metal pieces	22	8.8
Rocks and pebbles	17	6.8
Screws and bolts	12	4.8
Failed parts	10	4.0
Safety wire	6	2.4
Tools	5	2.0
Cloth	2	.8
Battle debris	1	.4
Bird	1	.4
Animal	1	.4
Unknown	174	69.2
Total	251	100.0
Engine C		
Tool	1	0.9
Unknown	109	99.1
Total	110	100.0

damage. Spare parts and metallic debris left in the inlet by manufacturing, maintenance, and operating personnel are also known to have contributed to the problem.

The Disassembly Inspection Reports indicate that most of the damage in engines sent to overhaul bases is of moderate severity in the form of nicks and dents, the depths of which exceed limits specified by Air Force Technical Orders. The sizes of the nicks indicate that most of the damage is done by small objects. Small objects generated by the failure of inlet-duct components are sometimes identified.

Large objects seldom pass through the engines and are therefore found unless a major accident results and the evidence is lost. Large objects such as tools, failed parts, and spare parts left in the engine inlet have been identified, although comparatively infrequently. Objects left in engine inlets, including tools, parts, and scrap, during final assembly and preparation for initial flight tests by aircraft manufacturers and overhaul agencies may constitute the major cause of damage when engines are intially operated. Debris from the air-base surface, including pebbles, concrete, and metallic objects, is believed to cause most of the damage after the engines have been placed in service by the operating agencies.

1.4.3 Mode of entry for foreign object -- The mode of entry of objects generated or left in the engine inlet is self-evident. Airport debris may be blown into engine inlets by the blast of other jets or may be thrown in by landing-gear wheels. Other investigations of the modes of entry (Refs. 3, 4, and 5) conclude that the engine air-inlet stream, unaided by outside influences, will not cause the ingestion of objects from the ground surface if the airflow is uniform and undisturbed by vortex formations.

The ingestion of foreign objects from the ground by vortices formed between the engine inlet and the ground was investigated

at NASA Lewis Research Center (Ref. 6). The presence of vortices is evidenced by dust and water whirls and occasionally by visible cores. The visible core of a vortex formed at an engine inlet is composed of condensed water droplets. The condensation of these droplets results from a static temperature equal to or less than the dewpoint temperature at the vortex-core pressure. The reduced temperature in the vortex core is indicative of a low-pressure region.

The study of ingestion by vortices showed that pebbles, typical of objects that damage jet engines, were projected into the air by the vortices and were drawn into the engine by the high-velocity inlet-air stream. Vortex formation depended on engine speed, engine height, and surface wind. The possibility of ingesting airport surface debris is enhanced by:

- Increased engine speed
- Increased engine size
- Reduced engine-inlet height above the ground surface
- Reduced wind or taxi speed

Pebbles on smooth surfaces are less likely to be projected upward into the inlet by a vortex than when they are lodged in a crack. When exposed on a smooth surface, the pebbles were swept aside by the circular motion outside the vortex core but were not projected upward. Pebbles lodged in cracks and thus constrained from lateral motion were projected into the air when a vortex core passed over the crack.

Thus, from available information, the nature and modes of entry of foreign objects of major importance are as follows:

- Inlet components released by failure and drawn into the engine
- Objects left in the inlet by personnel and drawn into the engine
- Air-base debris thrown into the engine inlet by the blast of other jets or aircraft landing gear wheels
- Air-base debris ingested by engine-inlet vortices

1.4.4 Failure modes

1.4.4.1 Failure statistics -- The ingestion of foreign objects may cause a direct impact failure but more frequently will produce nicks, gouges, and dents in both rotor and stator blades. The immediate effect in some cases is impaired efficiency, but the more serious effects are points of stress concentration, which may with time result in fatigue failure.

Statistics on compressor failures other than foreign objects damage are relatively ineffective in determining the true severity of the compressor reliability problem. For example, available statistics show that 6.5 percent of one engine type were removed prematurely from the aircraft primarily because of compressor difficulties. In another engine type, 8.8 percent of the engine removals were attributed to the compressor. However, neither the Engine Removal Reports nor the Disassembly Inspection Reports used for statistical failure data include any of the fatigue failures where blades actually separated from their attachments. Since a broken compressor blade is generally carried through succeeding compressor stages and starts a chain reaction of blade failures, a single blade failure may virtually destroy the entire engine and frequently the aircraft. Consequently, these results are not listed in the Disassembly Inspection Reports, since the engine is not repairable and must be scrapped. A compressor failure in which a single blade failed in the first stage is shown in Figure 1. The damage accumulated until it burst through the casing at the seventh stage.

A limited amount of compressor statistics can be obtained from accident reports. In many cases, however, the damage is so extensive that the original cause cannot be traced and thus is listed as unknown. Accident reports from 1953, which include 205 accidents caused by jet-engine failure or malfunction, show the compressor to be responsible for 26.8 percent of the accidents. In almost half of these cases the airplane was also destroyed.

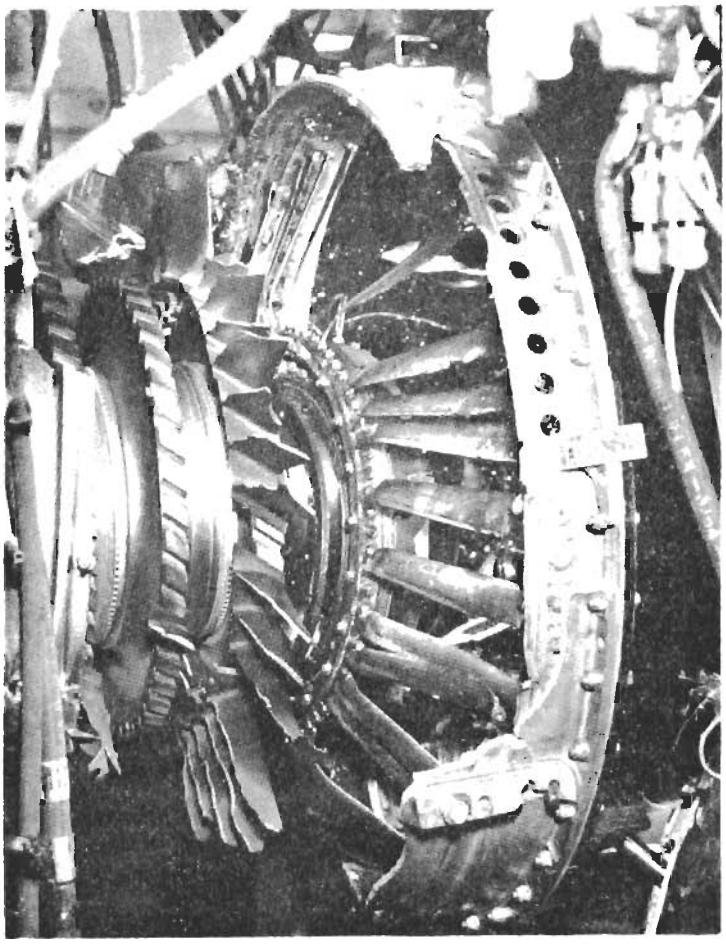

FIGURE 1 DAMAGE RESULTING FROM FATIGUE OF BLADE ROOT IN SECOND ROTOR STAGE

1.4.4.2 Failure mechanisms -- Very few compressor failures have occurred as a result of direct stress imposed by centrifugal or steady aerodynamic loading. The centrifugal stress varies with the stage (Figure 2). Even the highest centrifugal stress of 36,000 pounds per square inch (psi) in the first stage at the rated speed of the engine is only a fraction of the strength available from the compressor blade material. The bending stresses due to the steady state gas forces at rated speed are only 15 to 25 percent of the centrifugal stresses. Obviously, other factors are primarily responsible for the failures.

1.4.4.3 Principal types of failures -- The principal causes of compressor failures, in order of frequency of occurrence, are: (1) foreign object damage, (2) vibration fatigue, (3) stress-corrosion cracking, and (4) blade-surface erosion.

Foreign object damage -- The axial flow compressor rotor blades are the first moving objects encountered by foreign matter entering a jet engine. Because every other row of blades in a compressor is stationary and immediately obstructs any motion imparted to foreign particles by the intervening rotor blades, damage is caused to a large percentage of the total number of blades in each row of a multistage compressor. Also, the cantilever-type attachment and the thin leading and trailing edges of the airfoils make the axial flow units extremely susceptible to foreign object damage as can be seen from Figure 3.

With the conventional blade materials used, the direct impact of a foreign object seldom causes the blade to break unless the object is unusually large. The damage consists mostly of small gouges and nicks in the airfoil (Figure 4). These nicks in themselves are not disastrous, but they concentrate the stresses normally present, and thus, induce or greatly accelerate fatigue failures. Therefore, the nicks near the base of the airfoil or at the sharp leading or trailing edge

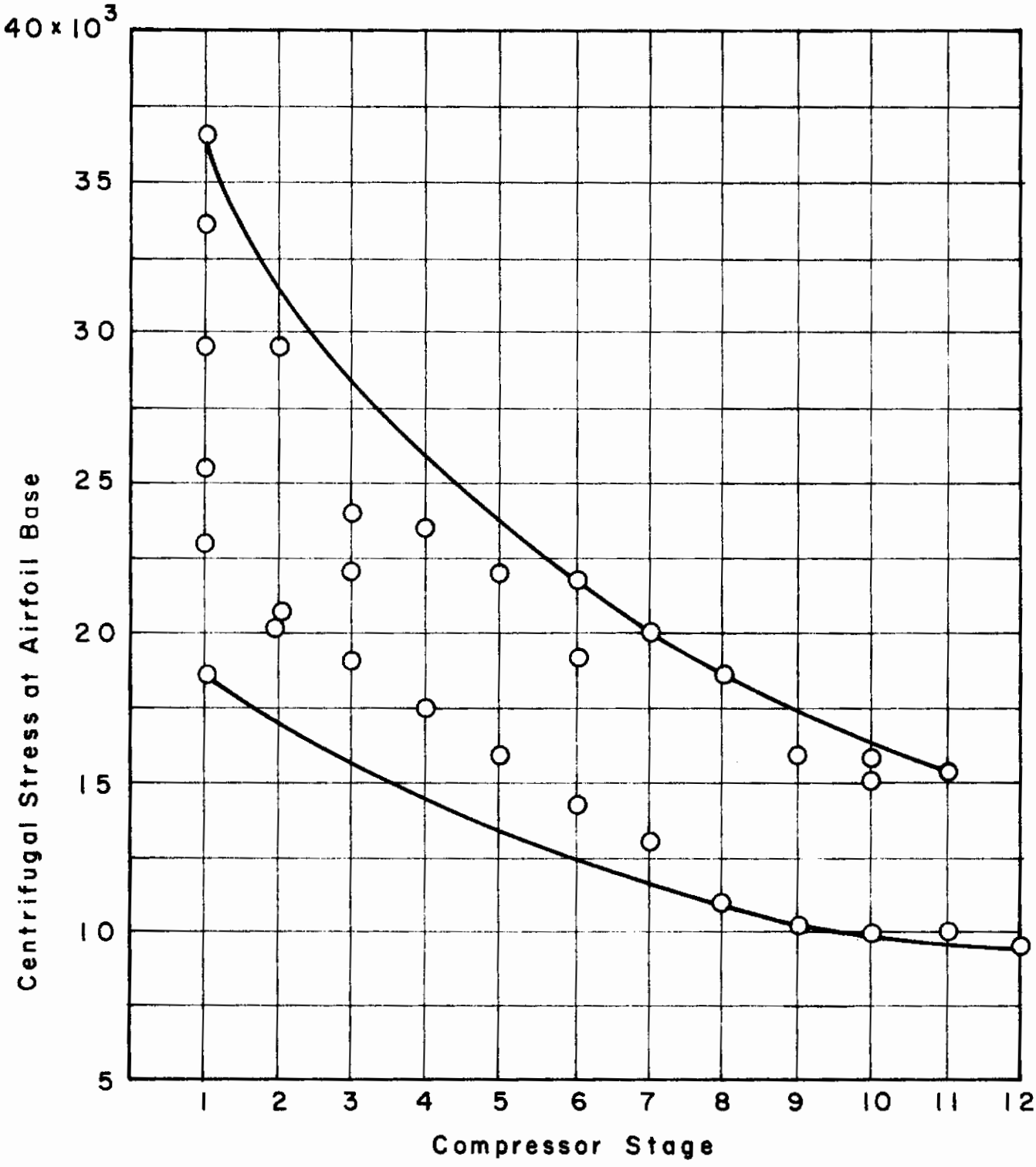

FIGURE 2 RANGE OF CENTRIFUGAL STRESSES IN ROTOR BLADES OF VARIOUS STAGES

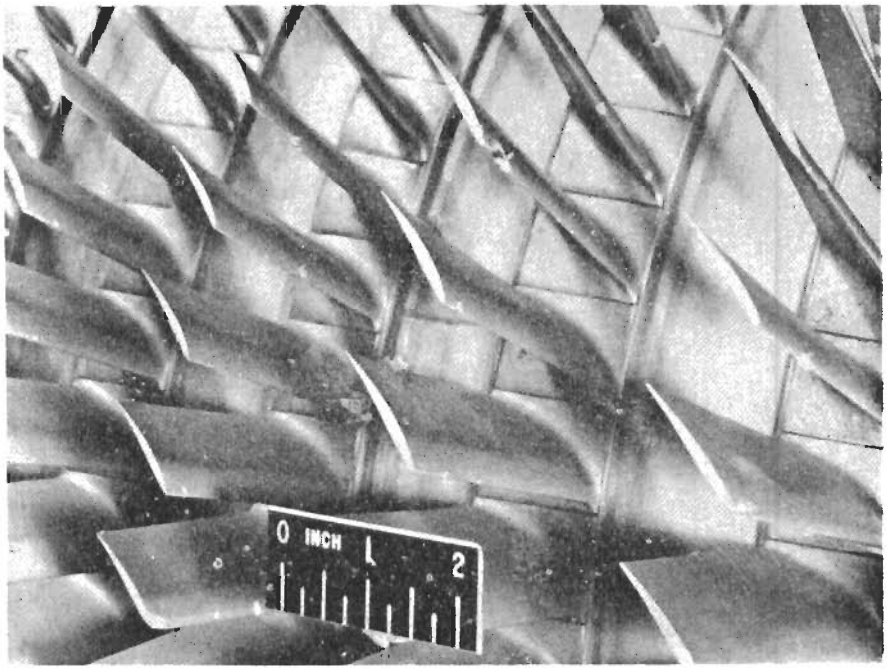

FIGURE 3 DAMAGE RESULTING FROM FOREIGN OBJECT ENTERING INLET

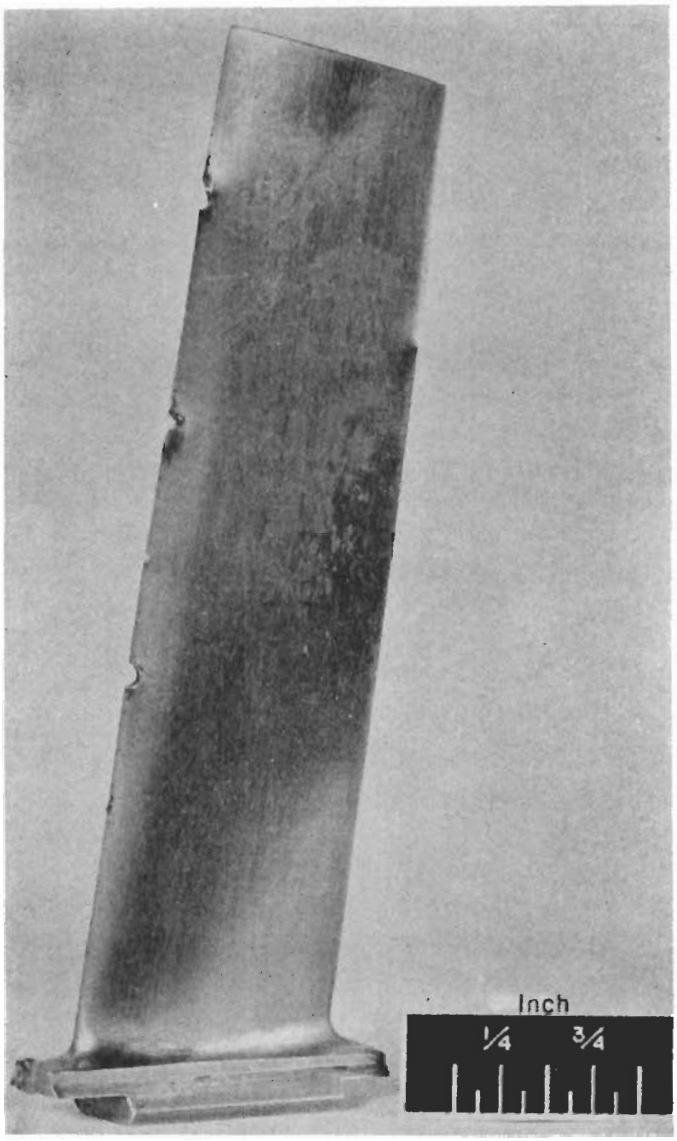

FIGURE 4 GOUGES IN COMPRESSOR BLADE CAUSED BY FOREIGN OBJECT

are of greater concern than damage to the airfoil body. Engine manufacturers have set up arbitrary limits on the number, size, and location of such nicks which essentially agree with the program design goals (Ref. 2).

Foreign object damage is a serious problem because of the large numbers of blades involved and the expense of disassembly, blade replacement, and compressor rebalancing. The number of rotor blades per stage varies from 17 to over 130 (Figure 5), the total per compressor averaging about 800 rotor blades. Occasionally, as many as 75 percent require replacement. Figure 6 shows the typical result of a foreign object passing through a compressor. The number of blades hit in the first eight stages was relatively constant.

Because the number of blades per stage increases toward the rear of the compressor, the first stage had the highest percentage of damage. The peaks in the curves indicate that the foreign object lingered slightly in the tenth stage. The values do not include stator blades, which are not nearly as critical because of the absence of centrifugal loads.

Vibration fatigue -- Fatigue usually occurs in the rotor blades but is occasionally experienced in the stator blades or rotor disks at the blade recesses because of vibratory loads from the blades. The blade vibrations are generally induced by pulsations in the airflow. In most cases of blade failure, the fractures occur in the airfoil section near the base and show progressive damage typical of pure fatigue. The origin of the failure is usually on the convex surface at the maximum camber point where the bending stress is maximum during vibration. Fatigue failures may also originate in the trailing edge of the airfoil. In other cases, the failure is in the fastening. Frequently fatigue failures originate at random locations on the airfoil where stresses are not ordinarily high but are magnified by stress concentrations arising from toolmarks or nicks made by foreign objects. The bending stresses due to

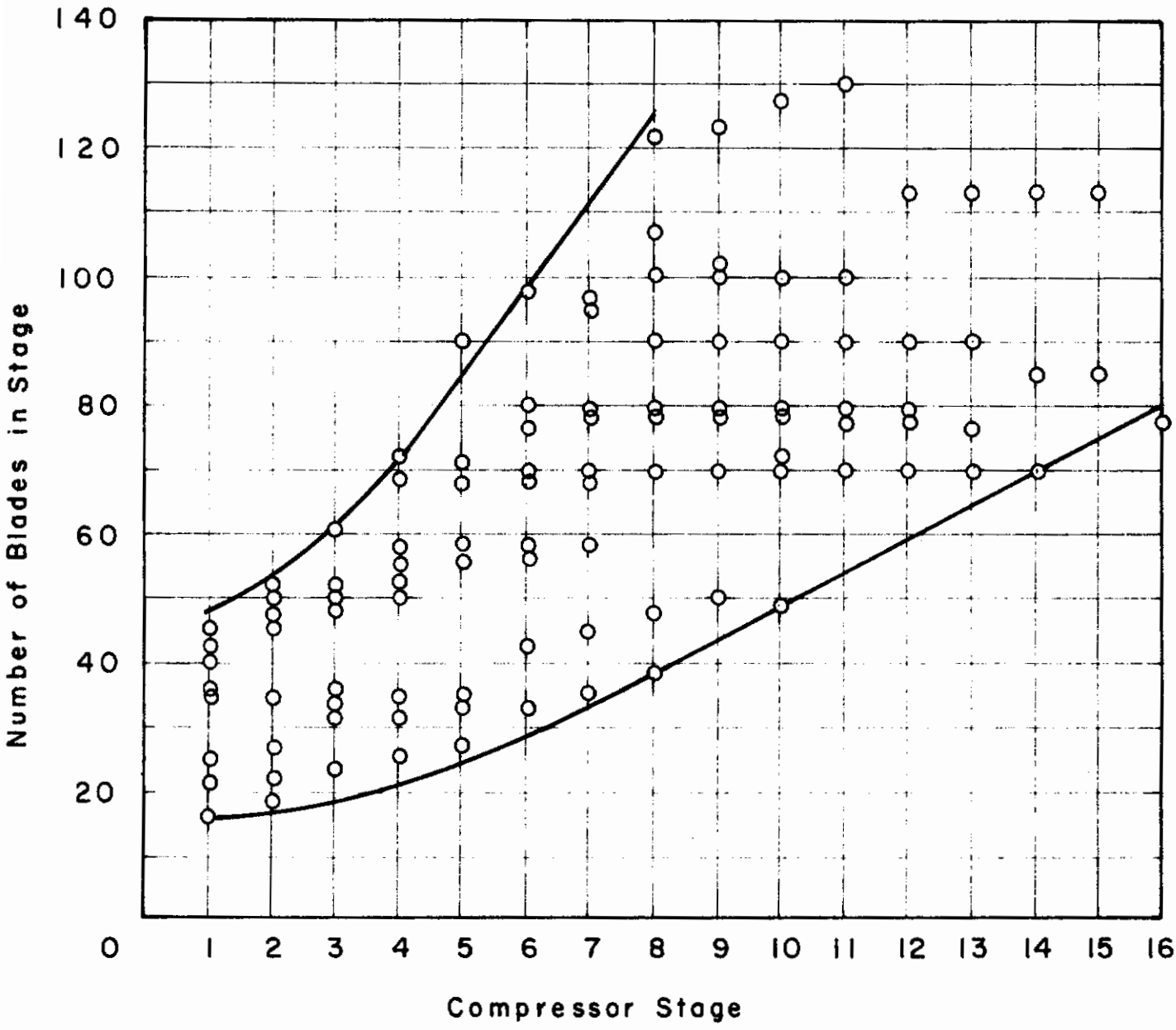

FIGURE 5 RANGE OF NUMBER OF ROTOR BLADES IN EACH STAGE OF CONVENTIONAL JET-ENGINE COMPRESSOR

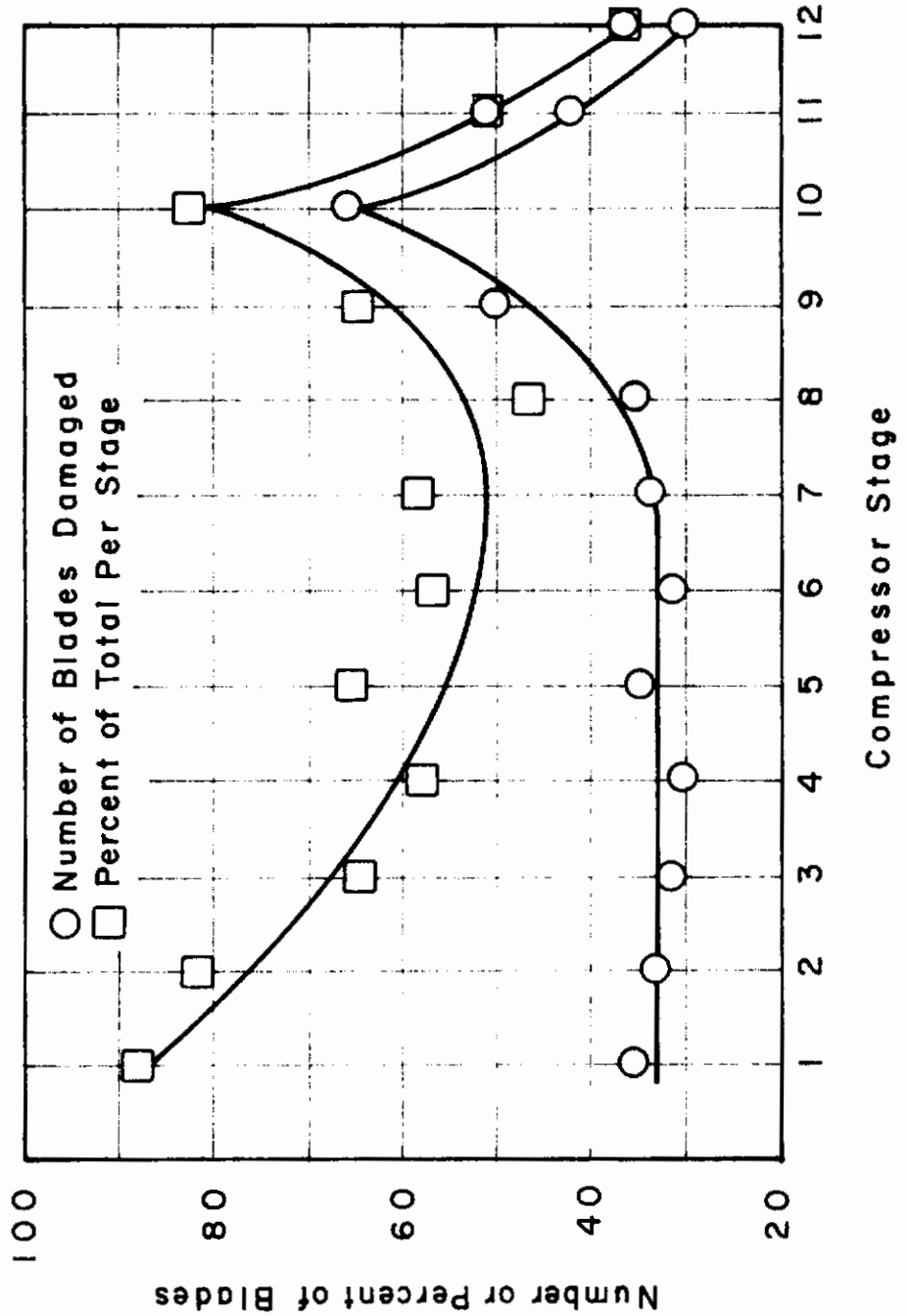

FIGURE 6 NUMBER OF BLADES DAMAGED BY FOREIGN OBJECT IN TYPICAL AXIAL-FLOW COMPRESSOR

vibration are superimposed on the steady centrifugal and gas-bending stresses. All stresses are magnified by the stress concentration caused by the abrupt changes in cross section.

Vibratory stresses of ±30,000 to ±40,000 psi have commonly been measured in conventional jet engines (Refs. 3 and 4), while vibratory stresses as high as ±80,000 psi have been observed in experimental units. Figure 7 is a modified fatigue diagram, a plot of vibratory stress against number of cycles to produce failure for a typical blade material. The horizontal portion of the curve establishes the endurance limit, the vibratory stress that can be endured indefinitely without causing failure. This endurance limit is lower than that normally presented for this material, but the curve has been modified to include the effect of the steady stresses imposed on a rotor blade at the speed at which blade vibrations are most prevalent. The high vibratory stresses are generally pronounced at 50 to 70 percent of rated speed. The time required to produce failure can be readily determined from the blade natural frequency and its vibratory stress.

Stress-corrosion cracking -- A difficulty called stress-corrosion cracking has recently been encountered with the 12 percent chromium iron alloy currently being used for nearly all compressor blades. Although the actual mechanism for this process has not been completely established, the cracks (Figure 8) are known to appear under the following circumstances.

As a result of the strengthening heat treatment and quenching at 1750°F, residual stresses due to fabrication techniques are frozen into the material according to the theory outlined in Refs. 5 and 6. The residual stresses tend to assist moisture in the air, and particularly in salty atmospheres, in penetrating and reacting with the grain boundary material. Another theory suggests that the problem is simply one of hydrogen embrittlement and is independent of residual or operating stresses (Ref. 7). In either case, because of extreme thinness, the trailing edges of the blades are most vulnerable to cracking.

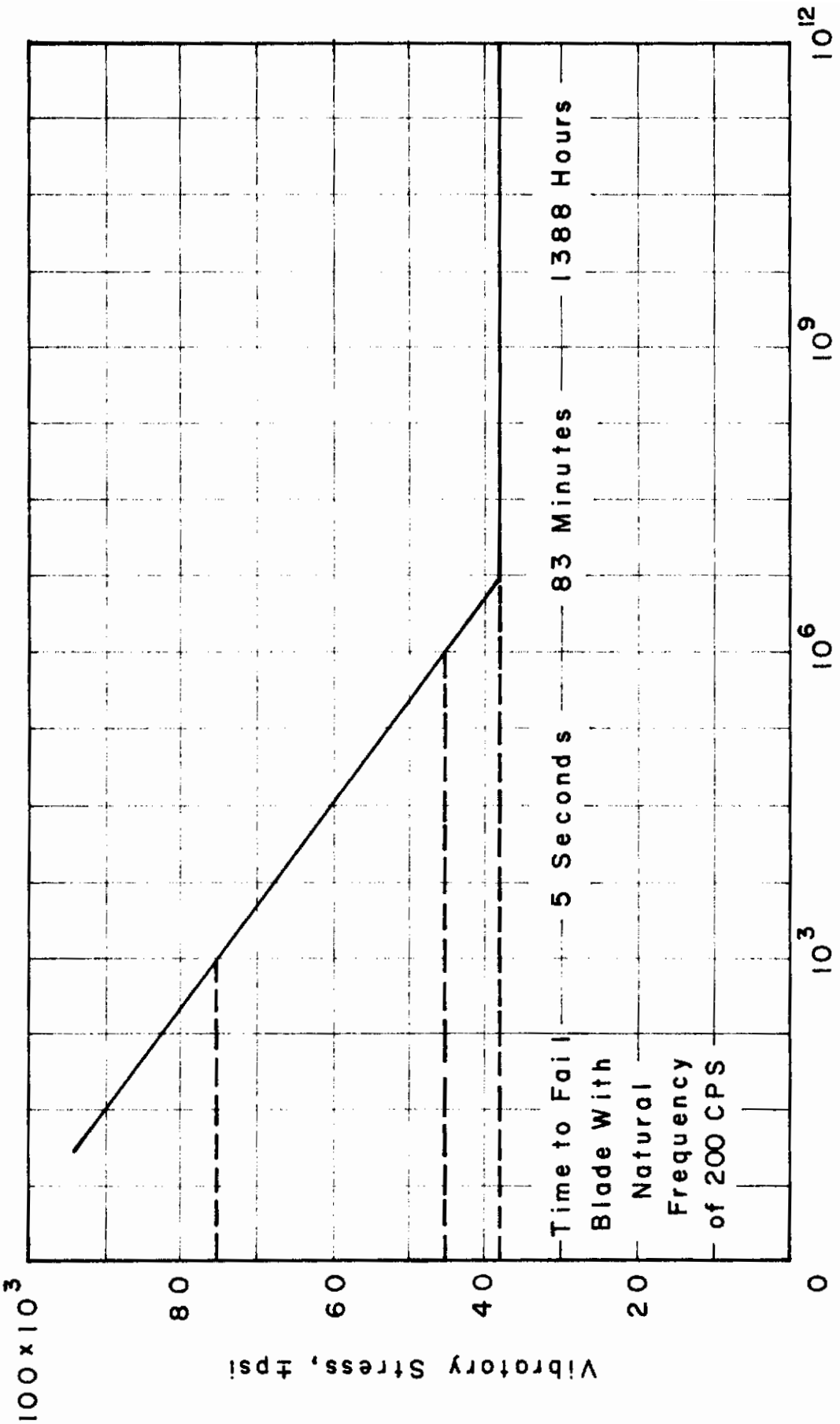

FIGURE 7 MODIFIED FATIGUE DIAGRAM FOR TYPICAL COMPRESSOR-BLADE MATERIAL

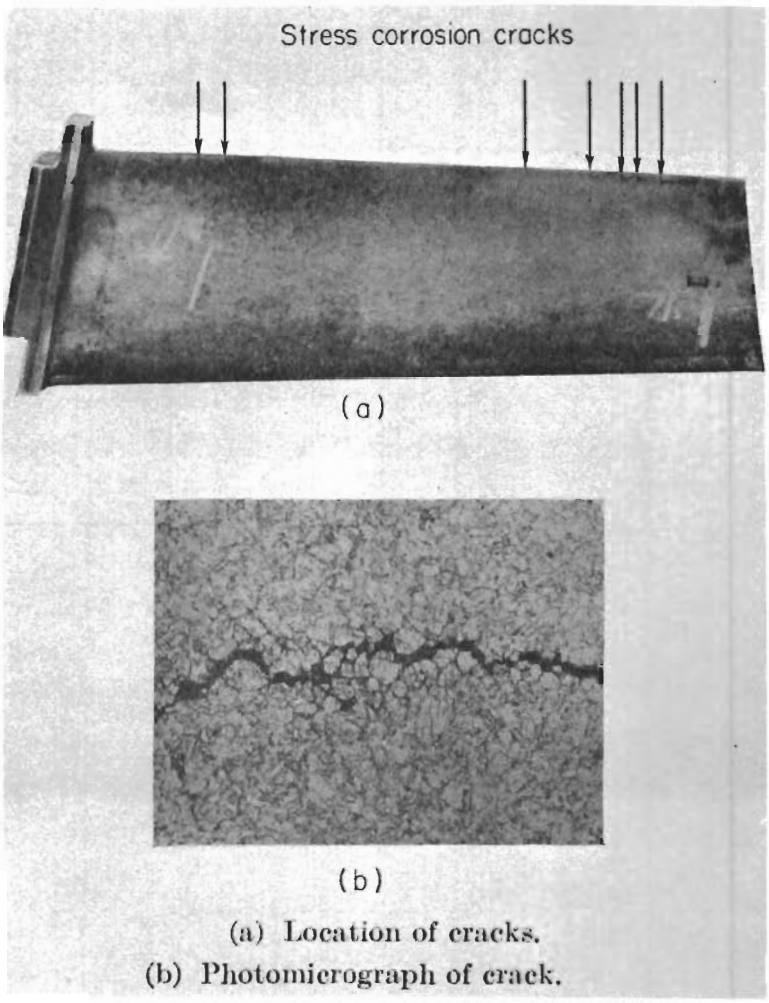

(a) Location of cracks.
(b) Photomicrograph of crack.

FIGURE 8 TYPICAL BLADE CRACKED BY STRESS CORROSION

During fabrication, these blades are given several heat treatments. The first, which occurs after the blade has been formed, is intended to produce an optimum microstructure and relieve residual stresses due to forging. The blade is then finished and the edges polished. A second heat treatment is applied to relieve residual stresses introduced during the finishing operation. The properties of the blade, and in particular its resistance to stress corrosion, depend on the temperatures used in these heat treatments. The practice of one manufacturer in applying the first heat treatment is to solution-treat the blade at 1750°F and blast-air cool it. The tempering treatment following the quenching is at 1000°F for approximately 2 hours. This results in high Rockwell hardness values of C-32 to -38 which give high tensile and endurance strength; but such blades have had stress-corrosion problems. Another manufacturer also uses a solution treatment at a temperature of 1750°F, but tempers at a higher temperature of 1140°F for 2 hours during the first heat treatment with a resultant softening to a Rockwell hardness level of C-20 to -26. The final heat treatment in both cases is a stress-relief anneal at 950°F during which the hardness is not changed. Although the lower hardness of blades made by the second method results in lower tensile strength and endurance limit, improved resistance to stress-corrosion cracking, as well as other improved properties such as higher internal damping capacity and higher impact resistance (Ref. 6), accompany the lower hardness. In the study by this manufacturer of 109 compressor failures due to stress corrosion, only one compressor contained soft blades, while 101 contained only hard blades. The other seven compressors had both hard and soft blades.

The stress-corrosion cracks themselves are not very serious, but in the presence of vibration, the crack is propagated until ultimately the blade fails from fatigue.

Blade-surface erosion -- Erosion may be due to dust, sand, water, or similar particles. The British conversion from aluminum to steel blading was due to the common occurrence of erosion of aluminum blades. Erosion effects are gradual and readily detectable during inspection so that any blades in an aircraft suffering from erosion would probably be withdrawn from service before disintegration occurred.

1.5 Survey of Techniques -- The design goals listed in the statement of work generally require some type of indirect or remote sensing technique which can detect foreign object blade damage. The physical phenomena may be best categorized by remembering that checkout is the technology of determining the status of components. Four major checkout techniques which can be used are (1) electromagnetic, (2) nuclear, (3) chemical, and (4) acoustical. These areas can be further divided into how the systems are employed such as "passive", as exemplified by an infrared mapping system, and "active" such as a radar system. Tables V and VI summarize the various physical phenomena initially considered and associated with electromagnetic, nuclear, chemical, or acoustical type communication employed as passive or active systems. The electromagnetic areas include everything from the shortest wavelengths (X-rays) to the longest wavelengths (ELF waves). The application or use of nuclear particles such as alpha or beta rays must be carefully considered, since a personnel hazard exists. The application of chemical techniques to the foreign object blade damage problem is not now apparent. Acoustical techniques were excluded by the statement of work.

Table V

SUMMARY OF PASSIVE TECHNIQUES INITIALLY CONSIDERED

Physical Phenomena	Passive Source	Likely Propagation	Typical Sensor	Possible Detection Methods	Tentative Comments
Electromagnetic	X-Ray (Non-Existant)	Direct or Through Walls	Imaging Phosphor	--------	Passive X-Ray not applicable
	Visible Light	Line-of-Sight or fiber optic	Photodiode or TV Camera	Area-to-Area Blade-to-Blade Image Comparison	Partially excluded by work statement, especially if operator judgment is required.
	Black-Body Radiation I-R Millimeter Microwave WHF, VHF, HF	Line-of-Sight only for IR Reflection from walls for other wavelength	Bolometer Scanning Radiometer	Possible Emissivity Change Caused by Damage	Useable emissivity change, if any, caused by damage only conjectural
	Low Frequency	Through Walls	Magnetometer	Blade-to-Blade Comparison of Magnetic Field	Convenience of technique attractive but sensitivity to small damage areas questionable
Nuclear	Seeded Coating of α or β Particles	Through Walls	Gieger Counter	Damage causes reduced emission blade-to-blade comparison	Required special treatment of blades and therefore exluded by work statement
Chemical	---------	----------	----------	--------	Immediate application not apparent
Acoustical	Ultrasonic whistles or turbulence caused by defect	Line-of-Sight or reflection	Ultrasonic microphone	Blade-to-Blade Comparison	Should be able to resolve small defects over entire blade. Existance of useable ultrasonic "hot spots" questionable. Possibly excluded by work statement
	Sonic Noise	Mechanically conducted or air propagated	Microphone	Correlation Techniques	Definitely excluded by work statement

Table VI

SUMMARY OF ACTIVE TECHNIQUES INITIALLY CONSIDERED

Physical Phenomena	Active Source	Likely Propagation	Typical Sensor	Possible Detection Methods	Tentative Comments
Electromagnetic	X-Ray Tube	Through Walls	Imaging Phosphor	Blade-to-blade Comparison	Possible long-term hazard to personnel. Practical field device hard to visualize
	Visible or I-R Laser	Line-of-sight reflection	Phototube or TV Camera	Blade-to-blade Comparison	Sensitivity to recognize damage over normal variations may be impaired by blade's surface reflectivity. Implementation difficult, however, should be considered. Use of technique for visual inspection excluded by work statement.
	Submillimeter or millimeter vacuum tubes and antenna	Line-of-sight or reflection off walls or blades	Hetrodyne radar-type receiver	Area-to-area blade-to-blade of doppler. Polarization, phase angle or amplitude comparisons	Theoretically should resolve defects over normal variances over entire blade surfaces. Serious consideration should be given to techniques using these wavelengths; implementation difficult.
	Microwave WHF, VHF, HF, MF				Application not now apparent
	Near electric or magnetic field	Line-of-sight to small area on edge of blade	Array of electro-static or eddy current transducers/ sensors on strut	Small area comparison of capacity or eddy current near edge of blades	Should readily resolve nicks on edges and possibly could resolve some defects on surface. Minor modification required, but serious consideration should be given.
Nuclear					Same as X-Ray
Chemical					Application not apparent
Acoustical	Ultrasonic transducer and reflector	Line-of-sight or reflection	Ultrasonic microphone and reflection	Similar to millimeter	Similar to millimeter wave except that ultrasonic energy is radically affected by air turbulence and is strongly attenuated.

1.6 Electromagnetic Technique Considerations -- Of the four major checkout techniques initially comsidered, the electromagnetic techniques indicated the most promise. The important physical effects related to indirect or remote sensing active systems using electromagnetic techniques generally have to do with energy backscatter.

If energy impinges upon a surface or a round object, energy is backscattered or sidescattered and some energy is absorbed on the surface of the object. If the object size or "hole" is small compared to the wavelength, then the energy is said to be scattering in the Rayleigh region. Here, the scattered energy is not sensitive to minor surface variations. Where the wavelength becomes the same order of magnitude as the imperfection diameter, the Rayleigh-MIE region, then special effects begin to occur. First, surface or internal resonance effects appear. When this happens, backscattering or sidescattering is either greatly enhanced or reduced. Certain modes of oscillation are set upon the object or in a hole so that polarization is radically affected as well.

If the wavelength is further decreased on the same object, a region known as the MIE scattering region is entered. Here, the surface or internal resonances exist in great profusion and changes in polarization and backscattered energy are sensitive to variation in wavelength or mechanical positioning. In such a case, normal mechanical variations might obscure the true nature of the backscattered energy. Thus, an optimum wavelength might exist which is comparable to the damaged area dimensions but not so small as to be sensitive to existing normal variations.

This is illustrated in Figure 9, where a pit in a compressor rotor blade is indicated. In Figure 9a, the wavelength is large compared with the area of the pit, and as a result, the total energy that is returned or reflected is a function not only of the imperfection introduced by the pit but of the larger area of the blade as well. In Figure 9b the wavelength is chosen to

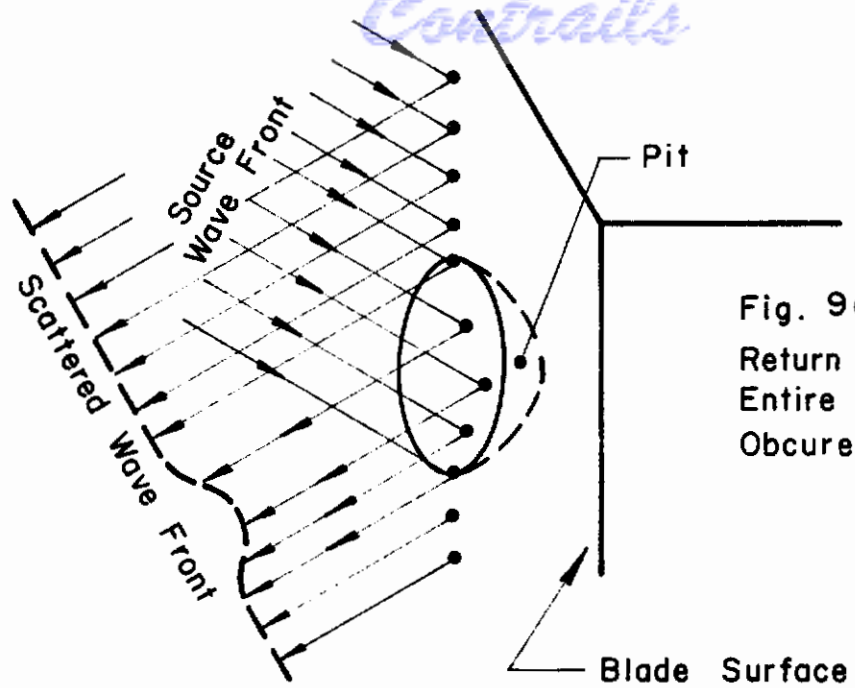

Fig. 9a Rayleigh

Return Signal Arises From Entire Surface and Obcures Defect

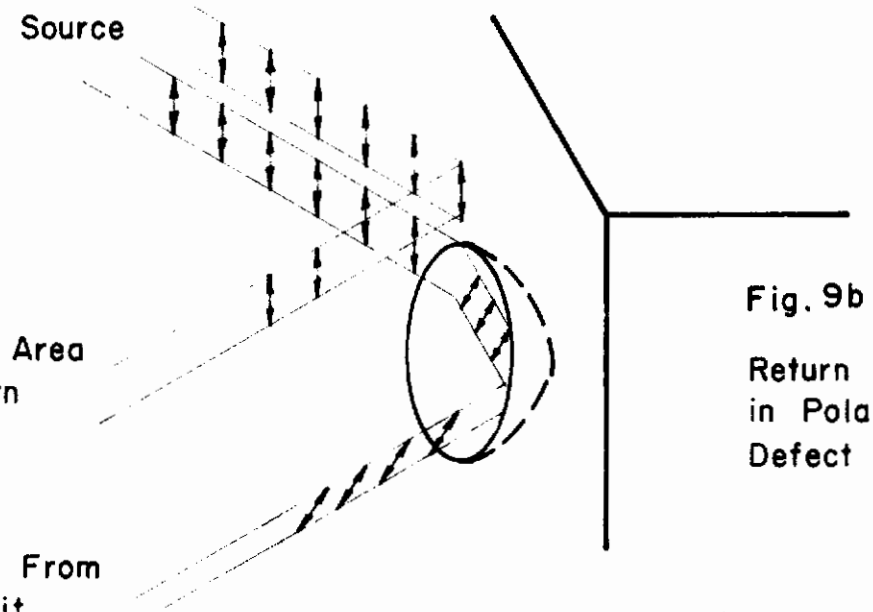

Fig. 9b Rayleigh Mie

Return From Defect Changed in Polarization From Non-Defect Area

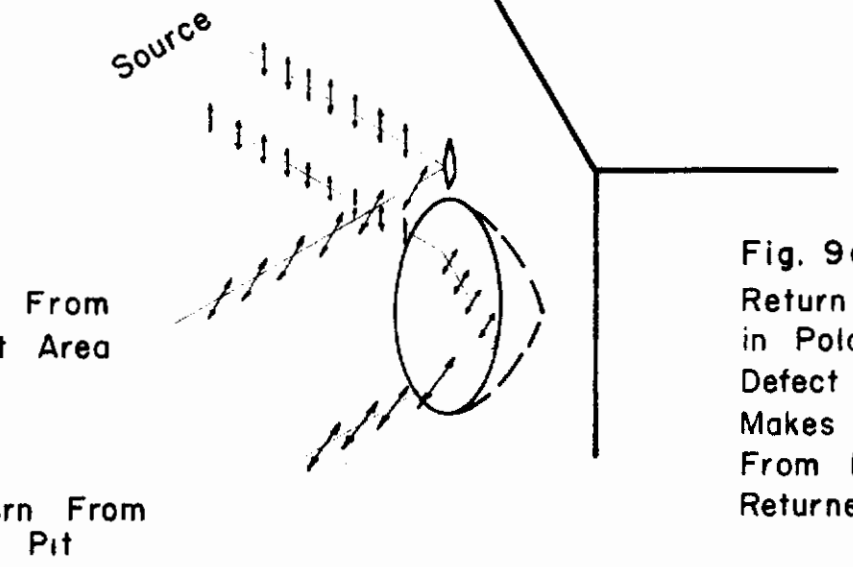

Fig. 9c Mie

Return From Defect Changed in Polarization but Smaller Defect on Machined Surface Makes This Indistinguishable From Polarization of Signals Returned From Adjacent Areas

FIGURE 9 EFFECT OF WAVELENGTH ON SCATTERING

be of about the same order as the diameter of the pit. In this case the energy can be focused in a more localized area, and the energy which does enter into the pit can undergo one or more internal reflections of such a nature as to change the plane of polarization. Where the wavelength is extremely small with respect to the dimensions of the pit, better focus can be achieved, but owing to normal mechanical variations, polarization or phase techniques could not be used reliably.

Since direct access to the aircraft turbine engine front end is not always possible, it may be necessary in some instances to "bounce" the energy off the walls of the air intake one or more times. Thus, the nature of the surfaces is of interest in regard to how the energy is reflected off the surfaces. If visible or infrared energy is used, then the surface finish must be highly polished in order to avoid a nonspecular reflection. If millimeter wavelengths are employed, the usual surface finish is less critical since the wavelength is large in comparison to the surface imperfections, and specular reflection with little absorption can be obtained. This is illustrated in Figure 10a and 10b. In the case of a nonmetallic surface, the millimeter and submillimeter waves are also reflected but perhaps not as effectively as in the case of metal. For infrared and invisible light, these could be absorbed in the plastic or paint-like material.

The desirability of utilizing passive or active systems having wavelengths comparable to the defect dimensions has been mentioned. This could also be considered on an area or volume basis. In the case of area, a compressor blade area of from 4 to 10 $inch^2$ is not unusual. The pit and damaged areas under consideration are approximately five orders of magnitude less than the total area of the blade. Thus, systems which depend, for example, on the total reflected energy from a blade or total capacitance with respect to some remotely located probe must have a sensitivity of at least one part in 10^6. This type

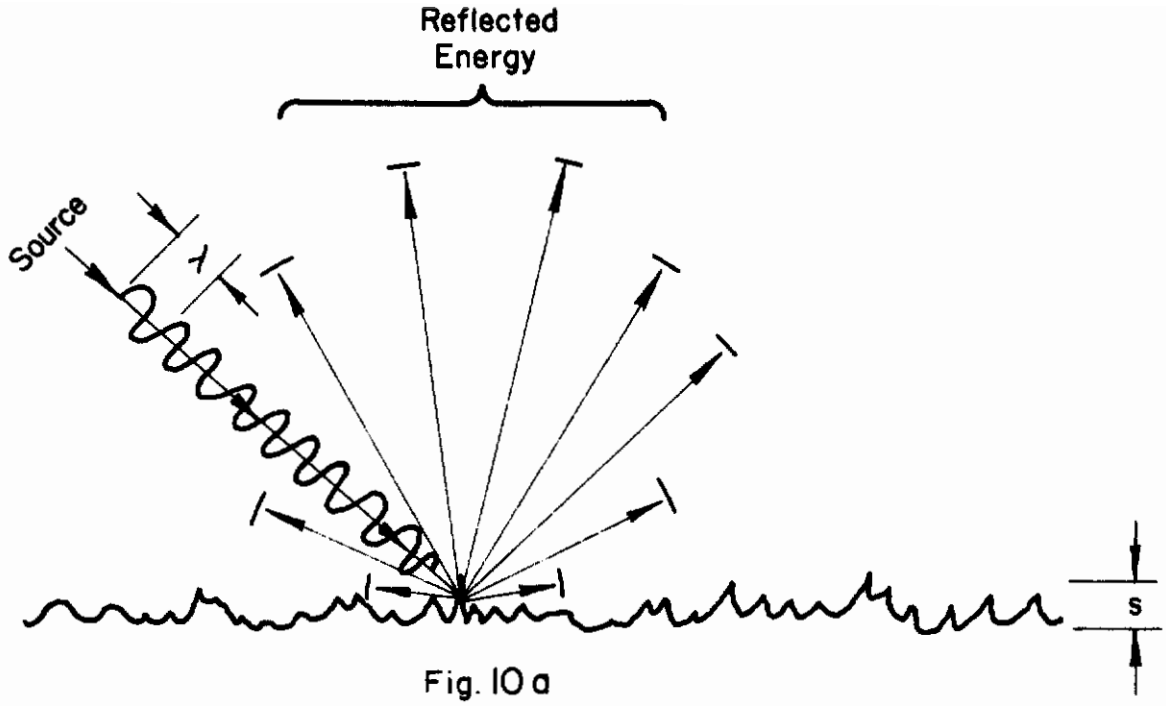

Fig. 10a

Diffuse Reflection $\lambda \lesssim$ "S", Surface Roughness
Reflected Beam is Non-Existant

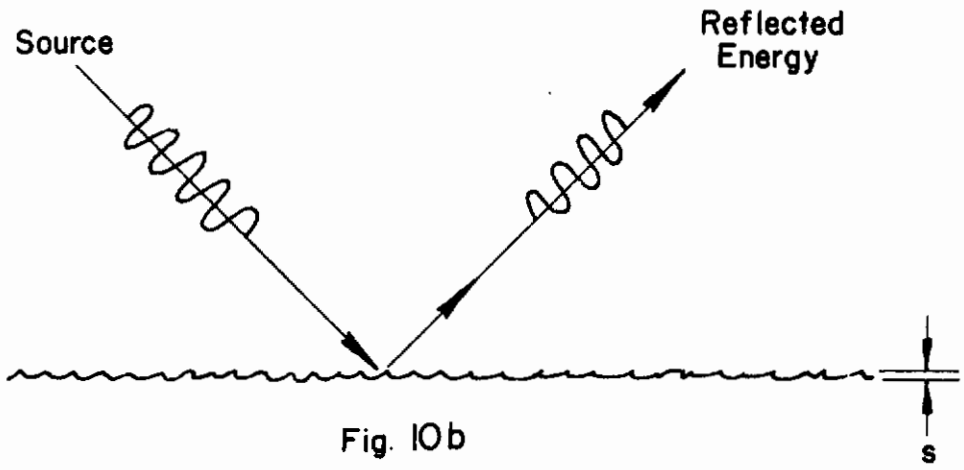

Fig. 10b

Specular Reflection $\lambda >> S$, Reflected Beam
Remains Intact

FIGURE 10 WAVELENGTH AND SURFACE ROUGHNESS EFFECTS

of sensitivity is not readily achieved, although bridge type comparison techniques can give a factor of from 10^3 to 10^5 improvement. To utilize a bridge-type comparison, either a reference blade or signature could be made available. This is probably not desirable, however, since each individual turbine engine may have its own idiosyncracies and thus exclude this type of correlation or profile recognition.

To overcome this difficulty, a blade-to-blade or adjacent-area-to-adjacent-area type of comparison technique can be used. Blade-to-blade sensing is complicated by the variations and mechanical positioning between adjacent blades.

The advantages of utilizing the smaller wavelengths, which can be focused and used in some type of scanning action over the blades, are obvious. Here, adjacent-area-to-adjacent-area comparison techniques can be utilized to increase the energy density of a spot and thereby the effective sensitivity by several orders of magnitude or more. In addition, a great improvement in sensitivity is achieved if some focusing is employed.

Also, there are other constraints worthy of consideration in view of the fact that the turbine engine is rotating. For example, in order to detect a small area rotating at approximately 10,000 rpm, a system must have a bandwidth in excess of 500,000 Hz and preferably 10 or 20 MHz in order to detect a perturbation introduced by a defect.

Other problem areas and considerations include normal mechanical tolerance, variations in the ambient or background noise, and the mechanical layout for accessability. In addition, there are a variety of other constraints mentioned in the statement of work which preclude the use of monitoring the total engine sounds or employing pattern recognition techniques.

1.7 General System Considerations -- Early in the program, some thought was given as to how each technique might be incorporated into the overall checkout system. It appeared feasible to consider the following possibilities. The first involves sensing systems which could be inserted into the cowling primarily for tests on the flight-line. This would require modification of the cowling to the extent that certain key-holes or lugs would have to be permanently installed so that the test apparatus could be positioned in a reasonably repeatable manner. Techniques which are ammenable to this type of installation would probably have some type of scanning feature so that the first few stages of compressor rotor blades could be scanned. The millimeter wave technique to be described in Section 2.1 appears to be most suitable for this type of procedure. If the higher millimeter wave frequencies are employed, as recommended, the size of the unit can be made quite small so that a minimum perturbation of the air flow during the flight-line test would occur.

Other techniques based on the detection of edge defects requires a line of sensors positioned parallel to the leading edge of the first stage rotor blades. It was envisioned that a series of sensors on some type of scanning mechanism could be placed on a strut (either permanently installed or installed by means of a key-hole positioning technique). These would scan and evaluate the first stage compressor rotor blades for edge defects (nicks, dents, and pits). A third technique is envisioned as a sensor positioned external to the shroud but still very close to the blade tips. This would permit either flight line or in-flight monitoring to determine whether foreign object damage had taken place. The sensor requirements, however, require this class of sensors placed very close to the blade tips. This is accomplished by drilling a small hole in the shroud and placing the sensor in this hole. Currently, many of the commercial airlines drill small holes in the shroud

to permit inspection of the rotor blades. These are described in subsequent sections.

Since a variety of signature recognition techniques were generally either precluded or discouraged in the contractual effort, the major emphasis was placed on the sensor system. This emphasis resulted in rejecting a number of techniques which might have been successful had some form of memory system been incorporated. Sufficient resolution did exist in at least one of these sensor systems with appropriate immunity to the normal tolerance variations.

2.0 SPECIFIC APPROACHES

2.1 Millimeter Wave Techniques

2.1.1 Introduction -- A technique is presented for the detection of foreign object damage in compressor rotor blades by scattering microwave energy from the blades. The basic system is a bridge circuit known as an "interferometer". The blade with a defect presents a different impedance than a blade without a defect when illuminated by microwave radiation. The primary difference is in the phase shift introduced by the defect. Other techniques are also possible, such as those based on doppler shift or other scattering mechanisms.

During this program, two interferometer systems have been constructed and tested, one at 15 GHz and one at 88 GHz. These systems have been tested at various stages of development in order to establish the potential capability of the technique for defect detection. The early tests were somewhat rudimentary but served as a guide in the development of the more sophisticated interferometer at 88 GHz. Even the 88 GHz interferometer system is limited by inadequate source power and a very insensitive detection system. As such, it has not as yet demonstrated the limit of its capability.

Detection of defects 0.030 inch deep and 0.050 inch across has been achieved, and it is estimated that the 88 GHz interferometer should be capable of detection of defects less than half that size. An interferometer operating at 220 GHz should have the capability of measuring leading edge defects in the 0.005 inch to 0.010 inch range (see Section 2.1.3.3.6). In the sections to follow, an analysis of the interferometer is given. The results of experimental investigations conducted during the program are then presented. A consideration of the relationship of defect dimensions to systems response is given. A discussion of a possible system for examination of defects while scanning blades with curved edges or surfaces is presented. Conclusions are stated in the final section.

2.1.2 Analysis of an interferometer system -- Figure 11 shows a block diagram of the basic interferometer system considered. Shown is a system employing two focusing horn lens antennas where the blades pass through the focal point of the lenses. As an alternative to the blade-to-blade comparison technique, the lenses can be focused on adjacent areas of the same blade. Because of variations in the location of blades, the latter method offers more promise. In the interferometer, the two reflected signals are compared in amplitude and phase in the difference arm of a Magic Tee (signal processor) which is basically a microwave bridge circuit.

Surface perturbation unbalances an otherwise balanced bridge which is indicated by the presence of a pulsed signal in the output caused by a defect in one of the blades.

Since the Magic Tee was chosen as the signal processor, a brief mathematical description of this device in terms of scattering coefficients is in order. Such a description will be shown to be essential in the analysis of the system. The Magic Tee is a four-port waveguide structure consisting of two colinear arms, one E-plane branch arm and one H-plane branch arm. This type of arrangement is ullustrated in Figure 12. The behavior of a Magic Tee can be described by a scattering matrix $[S]$ which relates the input signals to the output signals.

$$[S] = \tfrac{1}{2} \begin{bmatrix} 0 & 0 & 1 & 1 \\ 0 & 0 & 1 & -1 \\ 1 & 1 & 0 & 0 \\ 1 & -1 & 0 & 0 \end{bmatrix} \qquad (1)$$

From microwave circuit theory, $[S][a] = [b]$ where $[a]$ is a matrix composed of all signals entering the ports of the Magic Tee and $[b]$ is a matrix composed of all signals leaving the ports of the Magic Tee.

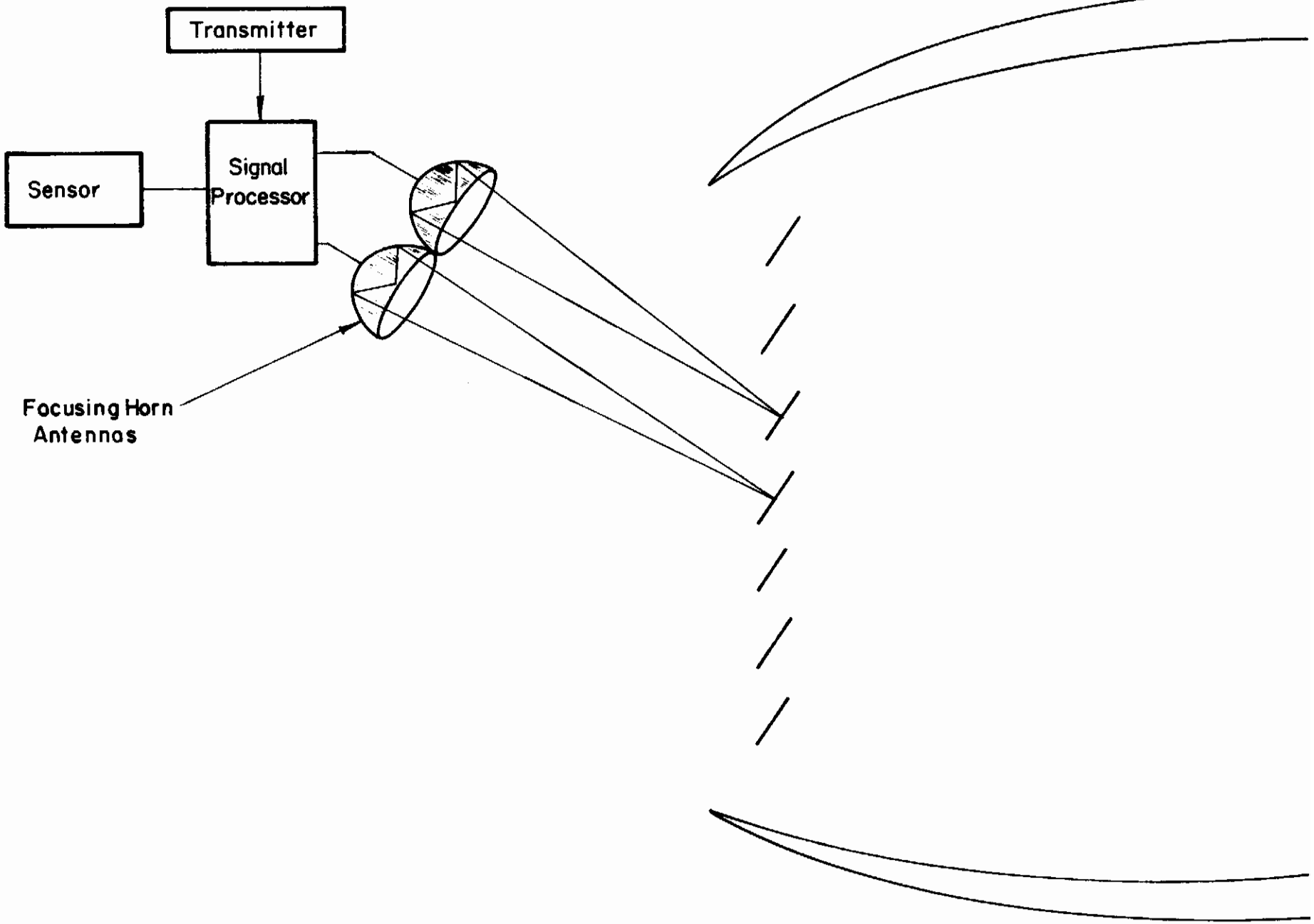

FIGURE 11 BASIC INTERFEROMETER SYSTEM
(BLADE - TO - BLADE COMPARISON)

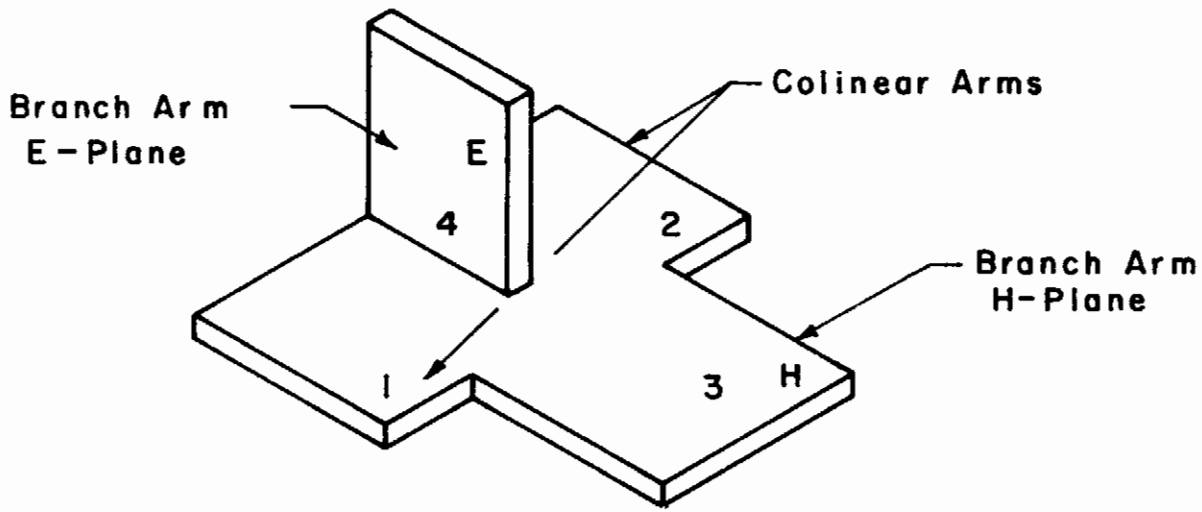

FIGURE 12 MAGIC TEE

a = normalized incident wave into the port which is proportional to the incident transverse electric field.

b = normalized reflected wave out of the port which is proportional to the reflected transverse electric field.

The incident power, or power into any port, is:

$$P_{in} = \tfrac{1}{2}\, a\, a^* = \tfrac{1}{2}\, |a|^2 \qquad (2)$$

The reflected power, or power leaving any port, is given by

$$P_{out} = \tfrac{1}{2}\, b\, b^* = \tfrac{1}{2}\, |b|^2 \qquad (3)$$

Initially, the basic interferometer system to be analyzed is shown in Figure 13. (A second case will be considered subsequently in which a general time-varying impedance also appears at port 1.) Port 1 is short circuited and is to provide the phase shift required to have a null at port 4 when the reflected signal a_2 in port 2 is the result of backscatter from a non-defective blade. The movable short circuit is used to simulate the return signal from another blade with no defects. A variable phase shifter in arm 2 of the Magic Tee is used to properly balance the bridge circuit under no defect conditions. Impedance z(t) is the time varying input impedance of the elliptical reflector which focuses the electromagnetic energy onto a moving metallic surface. In fact, z(t) would be a periodic function of time since a blade or moving metallic surface crosses the antenna beam periodically (see Figure 11). Detection is accomplished by a crystal video detector whose output waveform is displayed on a scope. Surface roughness results in a bridge unbalance which is observed visually on the scope as a change in the shape of the waveform. Note that the system of Fig.13 can detect both amplitude and phase variations in the reflection coefficient $\Gamma(t)$ due to backscatter from a moving defect.

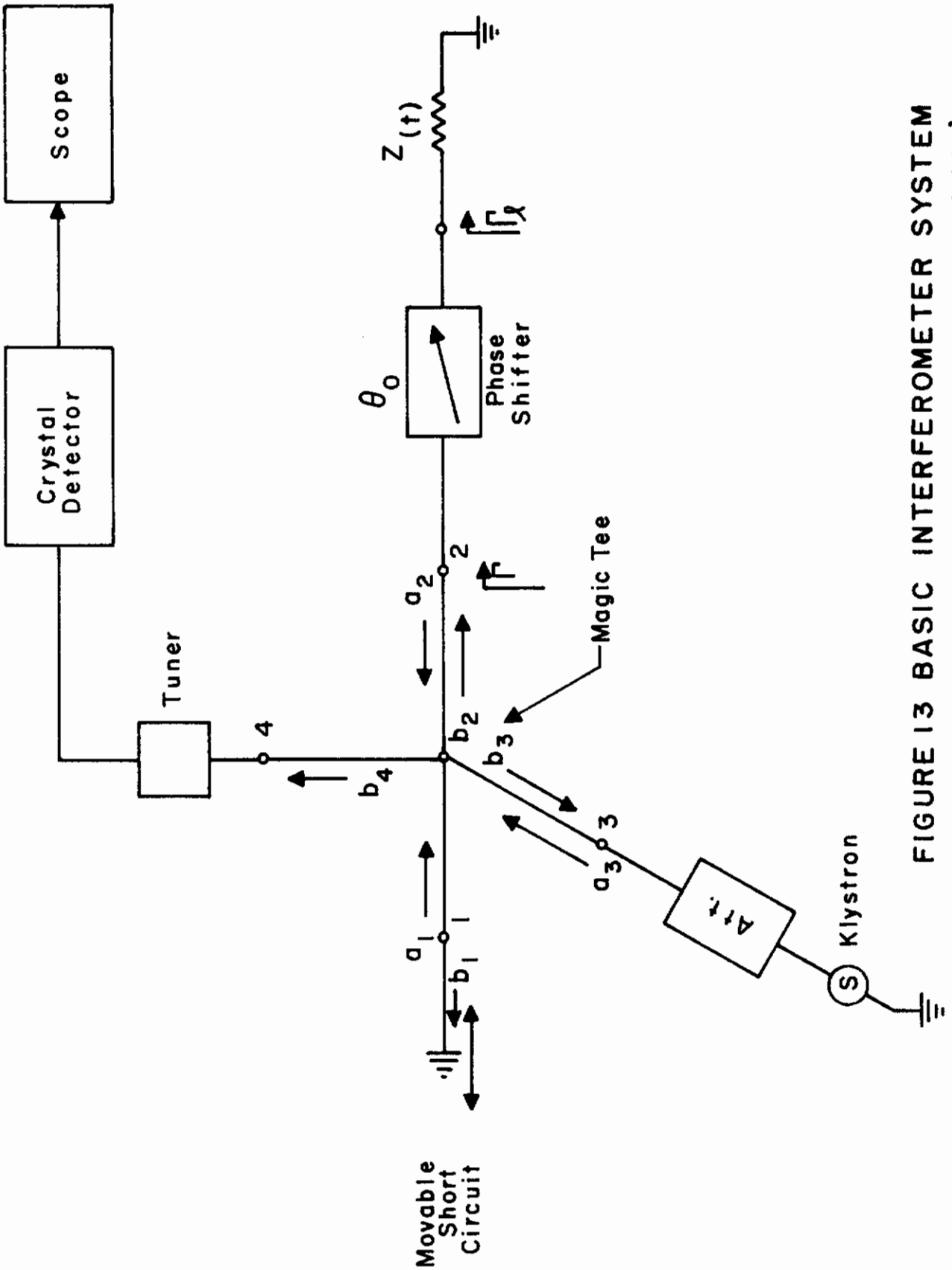

FIGURE 13 BASIC INTERFEROMETER SYSTEM
(BLADE TO BLADE COMPARISON)

An analysis of the system in Figure 13 is necessary if one is to determine critical system parameters which might be optimized to improve the sensitivity of the system. From Figure 13, it is seen that:

$$\Gamma_\ell = \frac{z(t)-1}{z(t)+1} = |\Gamma_\ell(t)| \quad e^{j\theta(t)} \tag{4}$$

$$\Gamma(t) = \frac{a_2}{b_2} = |\Gamma_\ell| \quad e^{j\left[\theta(t) + \theta_o\right]} \tag{5}$$

where

$z(t)$ = input impedance of elliptic reflector antenna normalized with respect to the characteristic impedance of the waveguide,

$\Gamma_\ell(t)$ = reflection coefficient at the load $z(t)$,

$\Gamma(t)$ = reflection coefficient at the input of the phase shifter.

The input matrix of the Magic Tee is:

$$\left[a\right] = \begin{bmatrix} a_1 \\ a_2 \\ a_3 \\ 0 \end{bmatrix} \tag{6}$$

The output matrix is

$$\left[b\right] = \begin{bmatrix} b_1 \\ b_2 \\ b_3 \\ b_4 \end{bmatrix} \tag{7}$$

where $b_1 = -a_1$ since port 1 is short circuited. Combining Equations (1), (6), and (7) results in

$$\begin{bmatrix} b_1 \\ b_2 \\ b_3 \\ b_4 \end{bmatrix} = \tfrac{1}{2} \begin{bmatrix} 0 & 0 & 1 & 1 \\ 0 & 0 & 1 & -1 \\ 1 & 1 & 0 & 0 \\ 1 & -1 & 0 & 0 \end{bmatrix} \begin{bmatrix} a_1 \\ a_2 \\ a_3 \\ 0 \end{bmatrix} \qquad (8)$$

Using Equations (3) and (8), it is readily shown that:

$$P_{out\ 4} = \frac{|b_4|^2}{2} = \tfrac{1}{4} \left| a_1 - a_2 \right|^2 \qquad (9)$$

and since

$$a_1 = -\frac{1}{\sqrt{2}}\ a_3,$$

$$a_2 = |\Gamma|\ e^{j(\theta+\theta_o)},\ \&\ b_2 = |\Gamma|\ e^{j(\theta+\theta_o)}\ \frac{a_3}{\sqrt{2}}$$

Equation (9) becomes

$$\frac{P_{out\ 4}}{P_{in\ 3}} = \tfrac{1}{4} \left\{ 1 + |\Gamma(t)|^2 - 2|\Gamma(t)| \cos \left[\theta(t) + \theta_o \right] \right\} \qquad (10)$$

Now the output crystal detector current as a function of time is given by

$$i(t) = k\ P_{out\ 4} \qquad (11)$$

where k is a proportionality constant determined by the conversion efficiency of the crystal video detector. It is to be noted that the detected output waveform depends on both the magnitude and phase of the load reflection coefficient. Equations (10) and (11) can be used as a guideline for explaining experimental observations on various simplified models of the actual geometrical configuration. Specifically, the measurements reported in subsequent sections on the 15 GHz interferometer can be interpreted with the aid of Equation (10). The 15 GHz interferometer is of the type shown in Figure 13. Some preliminary measurements on the 88 GHz interferometer were also made with one of the antennas replaced by a sliding short.

The 88 GHz interferometer was designed for operation as a two-antenna system with the output nulled when the two antennas are focused on a defectless blade. The above analysis must, therefore, be modified to allow for a time-varying impedance on port 1. The ratio of output power to input power is then given by

$$\frac{P_{out\ 4}}{P_{in\ 3}} = \tfrac{1}{4}\left\{|\Gamma_1|^2 + |\Gamma_2|^2 - 2|\Gamma_1|\ |\Gamma_2| \cos\left[\theta_2 - \theta_1 + \theta_0\right]\right\} \quad (12)$$

where $|\Gamma_1|$ and θ_1 are the magnitude and phase angle of the reflection coefficient caused by the blade at the focus of antenna 1. Similar definitions hold for $|\Gamma_2|$ and θ_2. The phase angle θ_0 is the phase shift introduced by the variable phase shifter. Ideally, if the antennas are illuminating adjacent areas on the same blade and there is no defect present, then

$$|\Gamma_1| = |\Gamma_2| \equiv |\Gamma|$$

and

$$\theta_1 - \theta_2 = 0$$

and

$$\theta_0 = 0$$

so that Equation (12) becomes

$$\frac{P_{out\ 4}}{P_{in\ 3}} = \tfrac{1}{4}\left\{2|\Gamma| - 2|\Gamma|\right\} = 0 \quad . \quad (13)$$

In actual practice, the phase shifter makes it possible to compensate for minor phase differences in Γ_1 and Γ_2 so that the argument for the cosine term in Equation (12) can be made zero and the system can be nulled. In practice, too, it may also be necessary to introduce variable attenuators into arms 1 and 2 to provide a means to compensate for small differences in $|\Gamma_1|$ and $|\Gamma_2|$. For simplicity, these have been omitted from the analysis but can be easily introduced, if necessary.

It is now apparent that Equation (10) is merely a special case of Equation (12) where Γ_1 has unity magnitude (for a short circuit) and zero phase. The operation of the two interferometers is different, however, as will be illustrated in the discussions to follow.

2.1.3 Experimental results

2.1.3.1 Introduction -- Two interferometer systems have been implemented during the course of the program. The first was built at 15 GHz and is of the single antenna type shown in Figure 13. This system was checked out with and without an antenna using simulated compressor blades. It was again tested with the antenna on the J-47 compressor section.

The second interferometer operates at 88 GHz and uses two antennas, one on arm 1 and one on arm 2 of the hybrid. This interferometer was checked out initially as a single antenna system, and then as a two-antenna system on simulated compressor blades. It was then tested statically by scanning an actual compressor blade. Finally, it was tested on the J-47 compressor section.

The results of all of these tests are reported in the following sections.

2.1.3.2 Measurements using 15 GHz single antenna interferometer

2.1.3.2.1 Measurement of simulated blades with no antenna -- The interferometer system of Figure 13 has been implemented in the laboratory as shown in Figure 14. There were preliminary tests conducted during the fabrication of the antenna. The klystron output (operating at 15 GHz) passes through a wave meter and variable attenuator and then enters port 3 of the hybrid or Magic Tee. On port 1 is a tunable short and on port 2 is a variable phase shifter. A diode detector on port 4 is connected to a low noise preamplifier which, in turn, is connected to an oscilloscope.

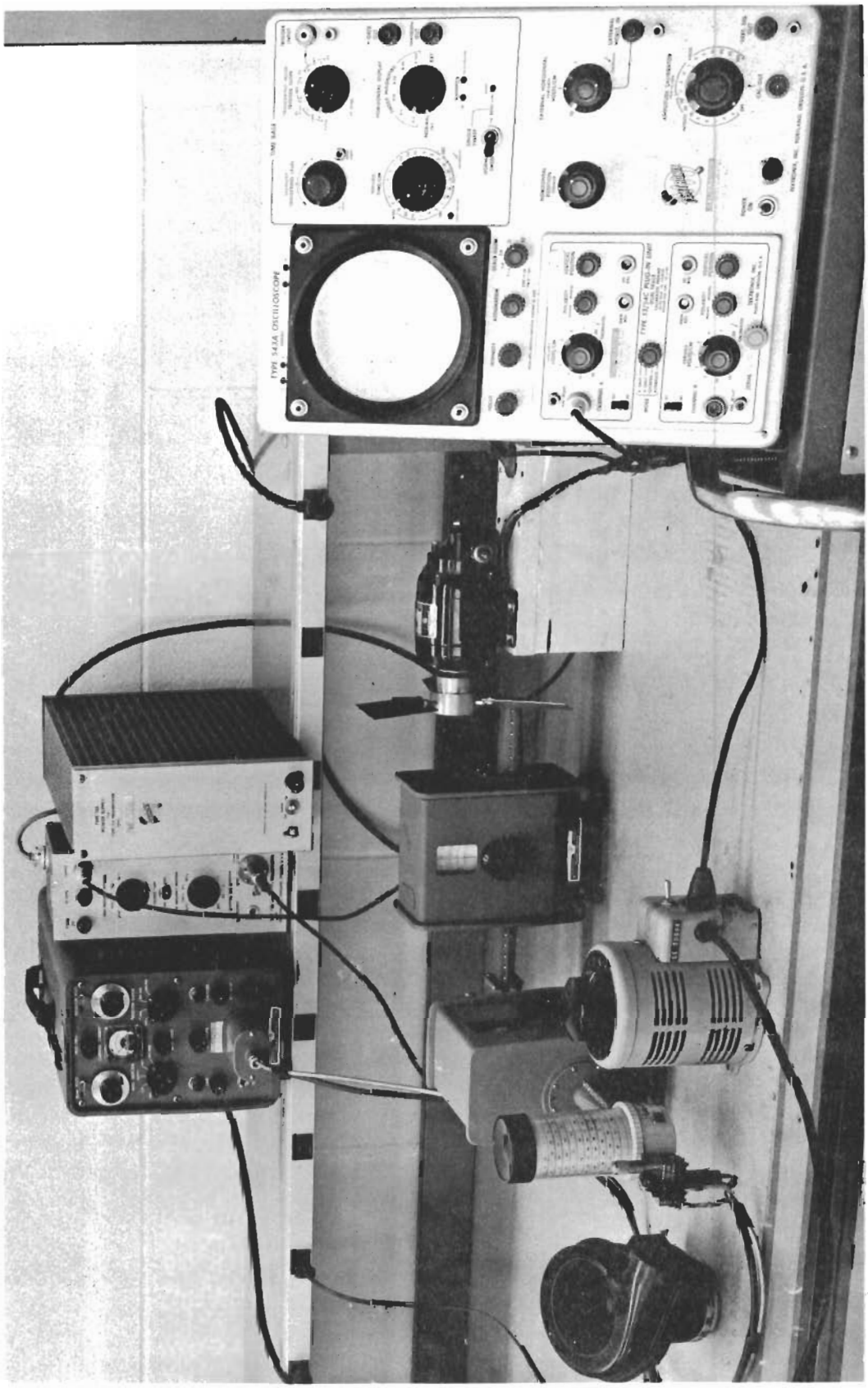

FIGURE 14 LABORATORY IMPLEMENTATION OF A WAVEGUIDE INTERFEROMETER

Figure 15 is a closer view of the simulated compressor blades. The blades turn clockwise. A large and small defect can be seen in the leading edge of blade #1 (the lower blade). A piece of copper tape on the trailing edge of blade #2 (the near blade) serves as a marker for identification on the oscilloscope display.

Two series of measurements will be discussed here and correlated with the theory of Section 2.1.2. The oscilloscope records in Figure 16 show the successive changes which resulted from making a defect in the leading edge of blade #1 and increasing the size of the defect. Figure 16 is a display of the power out of port 4 of the hybrid as a function of time. The blades were adjusted so that the response of the leading edge of the three blades was nearly identical. Blade #1 on the left was slightly lower at the start of the experiment. For the reflections shown in Figure 16 the phase angle of the phase shifter was adjusted so that the three pulses were maximized. Referring to Equation (10), this means that the term $\cos\left[\theta(t) + \theta_o\right]$ was equal to -1, or that the total instantaneous phase as the leading edge passes the waveguide is 180 degrees (the actual reading on the phase shifter was 292 degrees).

A small defect was made in the leading edge of blade #1 with no measurable effect. The defect size was increased to an approximately semicircular shape 0.140 inch wide by 0.070 inch deep. The response of the three blades is shown in Figure 16b with blade #1. A small but measurable drop in the response is observable. The size of the defect was progressively increased to the dimensions 0.250 inch wide by 0.135 inch deep. This response is shown in Figure 16c. The response of blade #1 is down to 55 percent of that of the other blades.

At this point, it was recognized from Equation (10) that with the cosine function maximized, the rate of change of amplitude with changes in phase was minimized. The maximum slope of the cosine function would be where the cosine function is zero; but then, the amplitude variations would be zero. Thus, a compromise

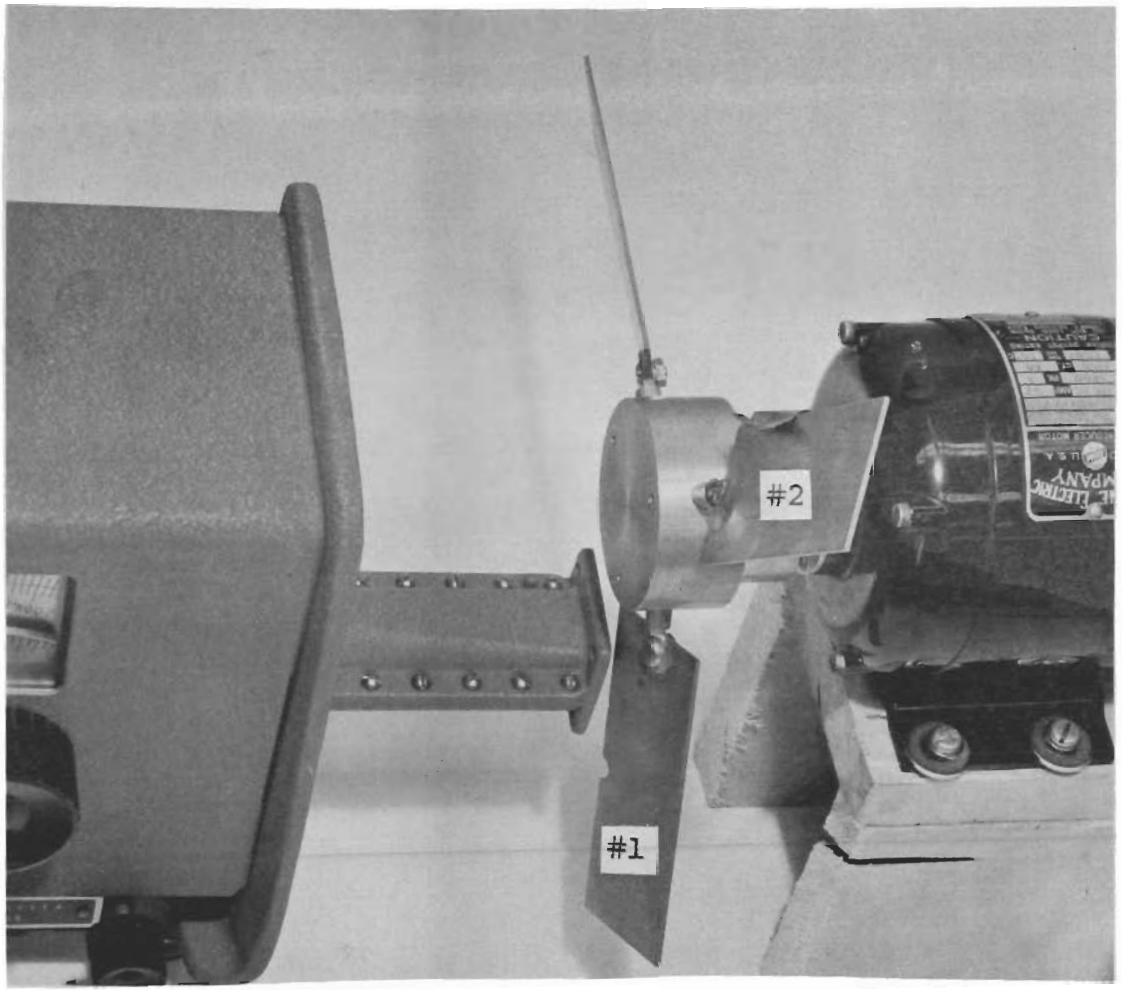

FIGURE 15 SIMULATED COMPRESSOR BLADE SHOWING LARGE AND SMALL DEFECTS IN THE LEADING EDGE

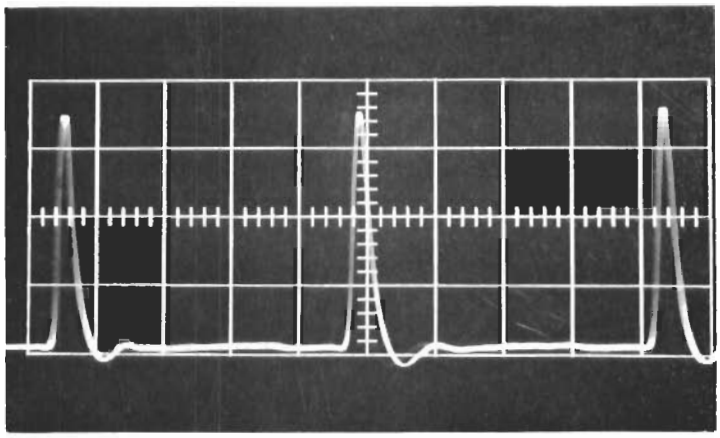

(a) No Defect in Blade 1

Horiz: 10 μs/cm
Vert: 2.5V/cm
Phase Shift: 292°

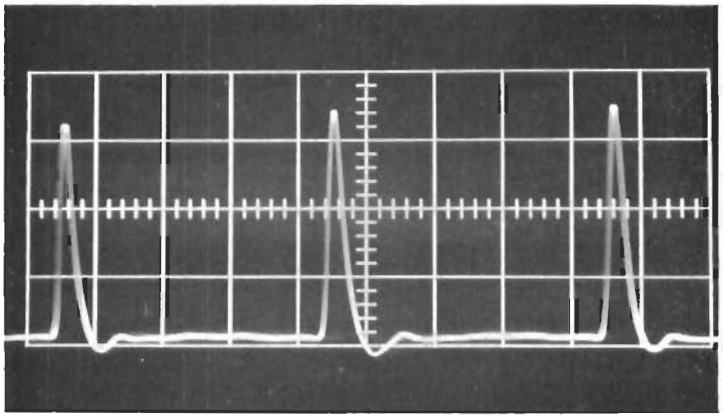

(b) Defect 0.140 in. Wide x 0.070 in. Deep

Horiz: 10 μs/cm
Vert: 2.5V/cm
Phase Shift: 292°

FIGURE 16 SIGNAL OUTPUT AT PORT 4 OF THE HYBRID

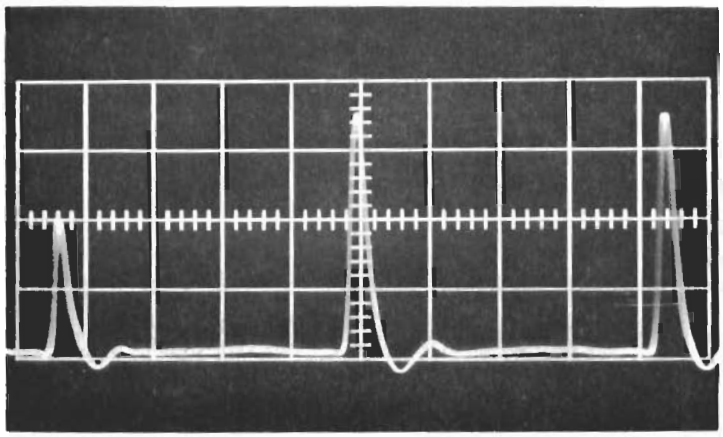

(c) Defect 0.250 in. Wide x 0.135 in. Deep

Horiz: 10 μs/cm
Vert: 2.5 V/cm
Phase Shift: 292°

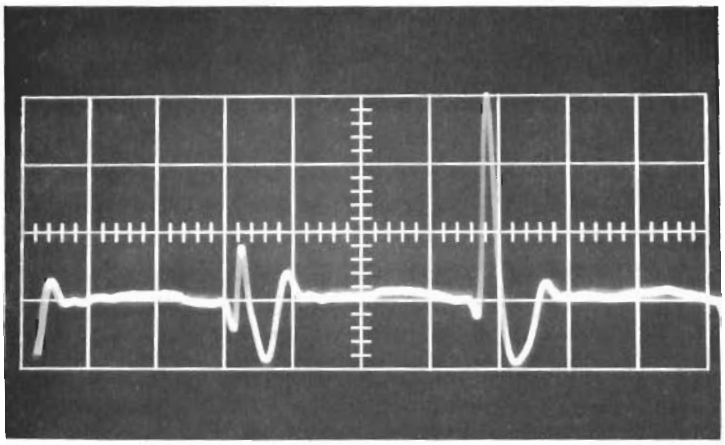

(d) Defect 0.250 in. Wide x 0.135 in. Deep

Horiz: 10 μs/cm
Vert: 1.5 V/cm
Phase Shift: 318°

FIGURE 16 SIGNAL OUTPUT AT PORT 4 OF THE HYBRID

is necessary to an angle which is greater or less than 90 degrees from the position of peak response. Figure 16d shows a shift in phase from the maximum point of 52 degrees (phase shifter reads 318 degrees). The response of all three blades dropped, as expected from Equation (10), but the response of blade #1 dropped in greater proportion because the output was more dependent on phase shift changes. The pulse of blade #1 dropped to 25 percent of the other blades, which would be a more easily distinguishable change than the former change of 55 percent.

For a second experiment, the positions of the simulated compressor blades were adjusted so that the first defect no longer passed across the waveguide opening. The response of the three blades, with the amplitude of each pulse maximized, is shown in Figure 17. The response of the three blades is nearly the same. A small defect 0.050 inch wide by 0.025 inch deep was made in blade #1 and, as before, under conditions of maximized response (phase shifter set at 275 degrees), the response of blade #1 dropped a noticeable amount as shown in Figure 17b. With the phase shift increased to 74 degrees (phase shifter set to 312 degrees), the relative drop in response for blade #1 became even more pronounced (blade #1 is in the center). The relative response of blade #1 is 87 percent, which could be a recognizable change in a properly instrumented system.

2.1.3.2.2 Measurement of simulated blades with antenna -- This section begins with a discussion of the horn-lens antenna followed by the experimental results achieved using this antenna with the 15 GHz interferometer.

2.1.3.2.2.1 Microwave focusing-horn antenna -- The purpose of the horn-lens antenna is to provide a small spot of electromagnetic energy propagating with a plane phase front at the compressor blade. The operation of the horn-lens antenna is shown schematically in Figure 18. A photograph of the antenna is shown in Figure 19. The first section of the antenna is a

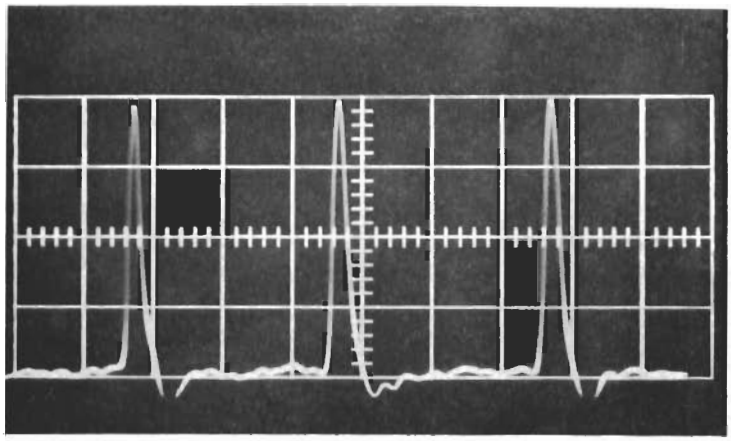

(a) No Defect in Blade 1

Horiz: 5 μs/cm
Vert: 1 V/cm
Phase Shift: 275°

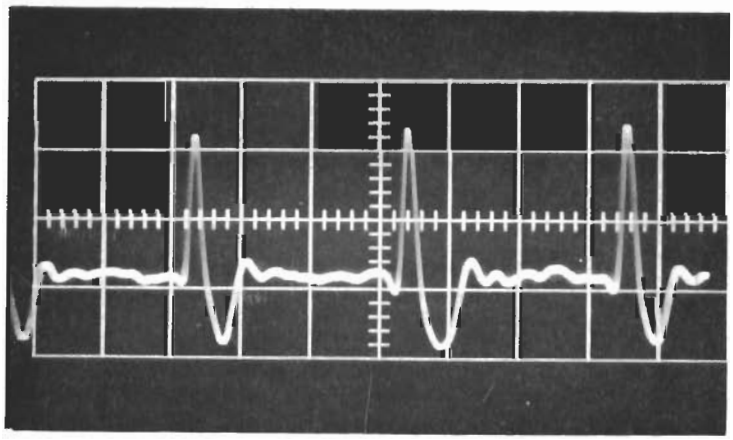

(b) Defect 0.050 in. Wide x 0.025 in. Deep

Horiz: 5 μs/cm
Vert: 1 V/cm
Phase Shift: 305°

FIGURE 17 SIGNAL OUTPUT AT PORT 4 WITH BLADES SHIFTED

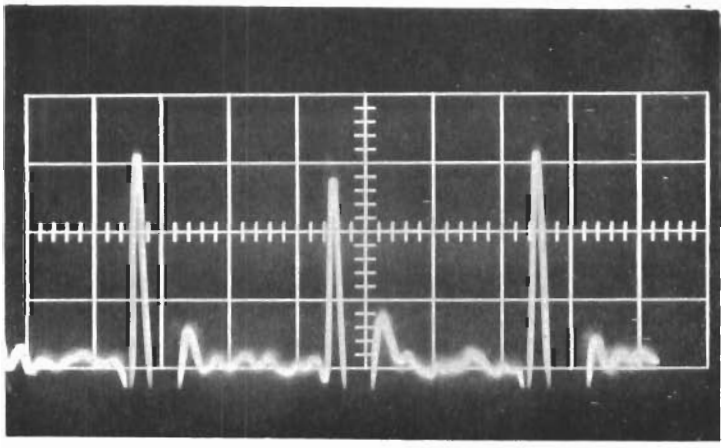

(c) Defect 0.050 in. Wide x 0.025 in. Deep

Horiz: 5 μs/cm
Vert: 0.5V/cm
Phase Shift: 312°

FIGURE 17 SIGNAL OUTPUT AT PORT 4 WITH BLADES SHIFTED

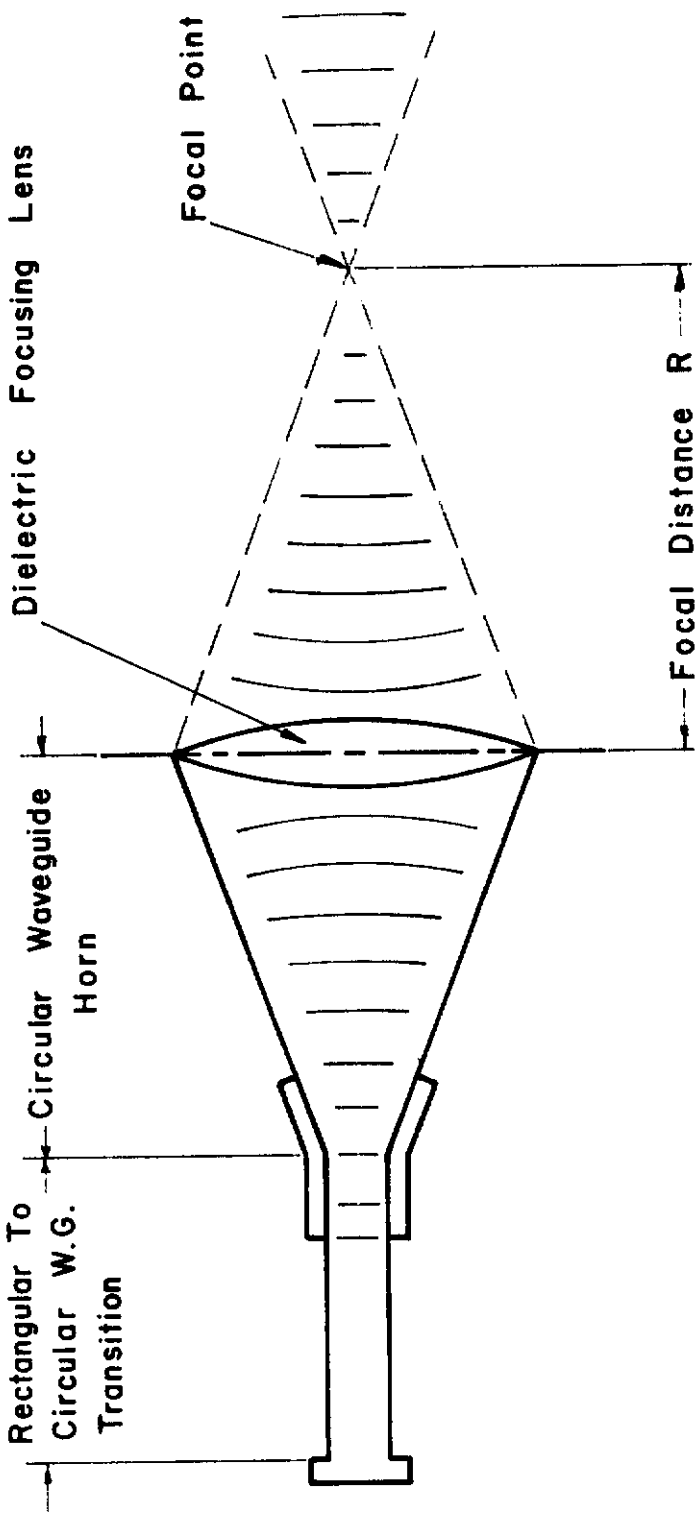

FIGURE 18 CIRCULAR WAVEGUIDE HORN ANTENNA WITH FOCUSING DIELECTRIC LENS

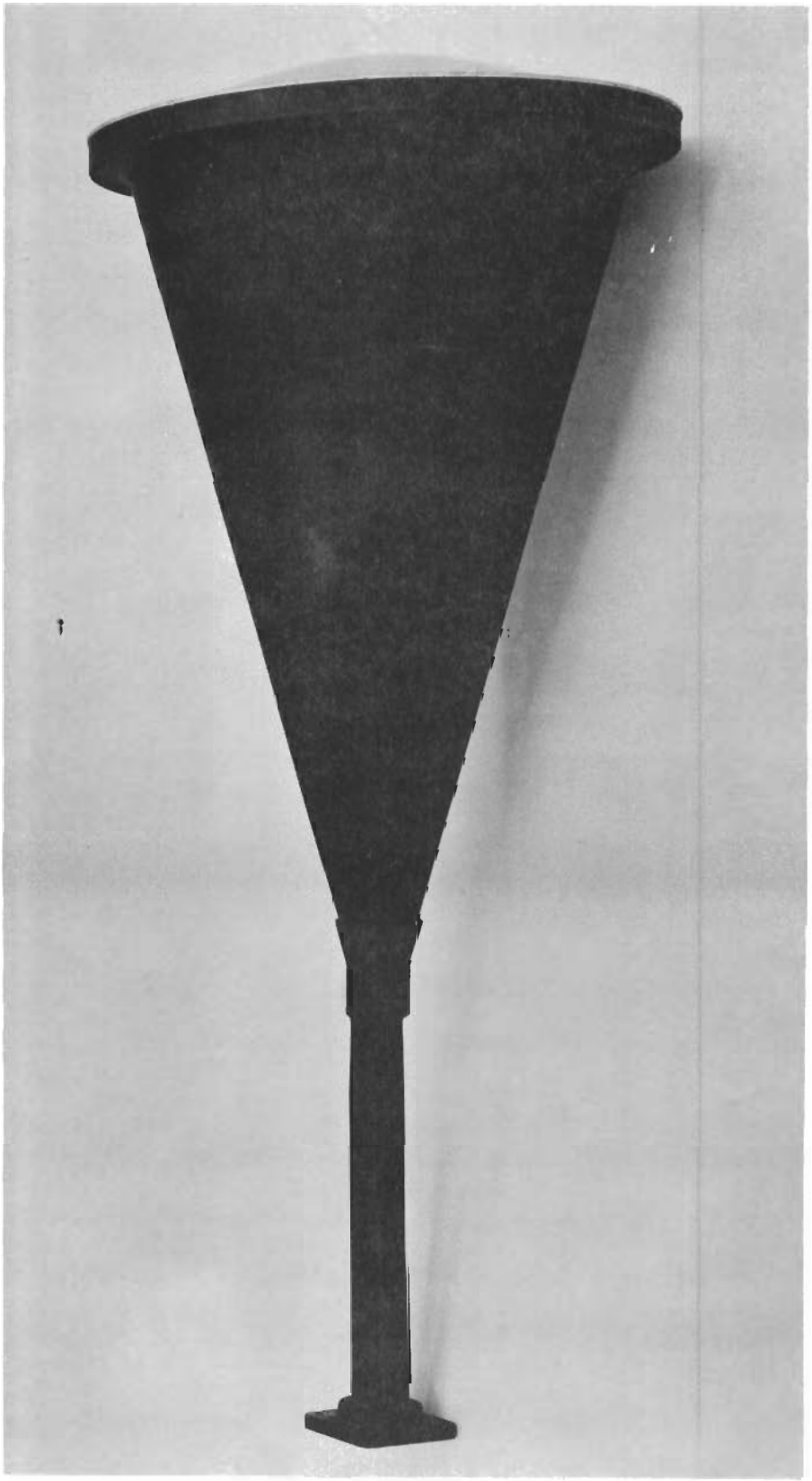

FIGURE 19 KU-BAND HORN-LENS ANTENNA FOR SPOT FOCUSING OF THE ELECTROMAGNETIC ENERGY

transition from rectangular Ku-band waveguide to circular wave-guide. The next section is a 10-inch conical horn which opens to a 6-inch aperature. The phase front of the electromagnetic energy gradually transforms from planar to spherical along the length of the horn. At the aperture of the horn is a dielectric lens. The inner section (to the left of the center line) of the lens causes the spherical phase front to become planar again. The outer section of the lens refocuses the plane wave beam to a spot at a distance called the focal distance. On the far side (right side of the figure) of the lens the phase front is spherical near the lens but becomes planar at the focal point.

The theoretical diameter of the spot of electromagnetic energy is given by (Ref. 9)

$$d = \frac{2R\lambda}{D}$$

where

d = diameter of the circle where the field intensity is -10 db from the intensity at the center of the spot

R = focal distance of the outside surface of the lens

λ = wavelength of the electromagnetic energy

D = lens diameter

The focal distance used for the outer lens surface was 9 inches. Therefore, the spot diameter should theoretically be 3λ, which at 15 GHz is 2.32 inches. Field intensity patterns indicated a spot diameter of 2.64 inches measured 9 inches from the lens. The horn-lens antenna is, therefore, performing very nearly as expected.

2.1.3.2.2.2 Laboratory investigations -- The focusing horn-lens antenna was used to illuminate the set of simulated compressor blades. The experimental apparatus is shown in Figure 20 and a closer view of the blades in Figure 21.

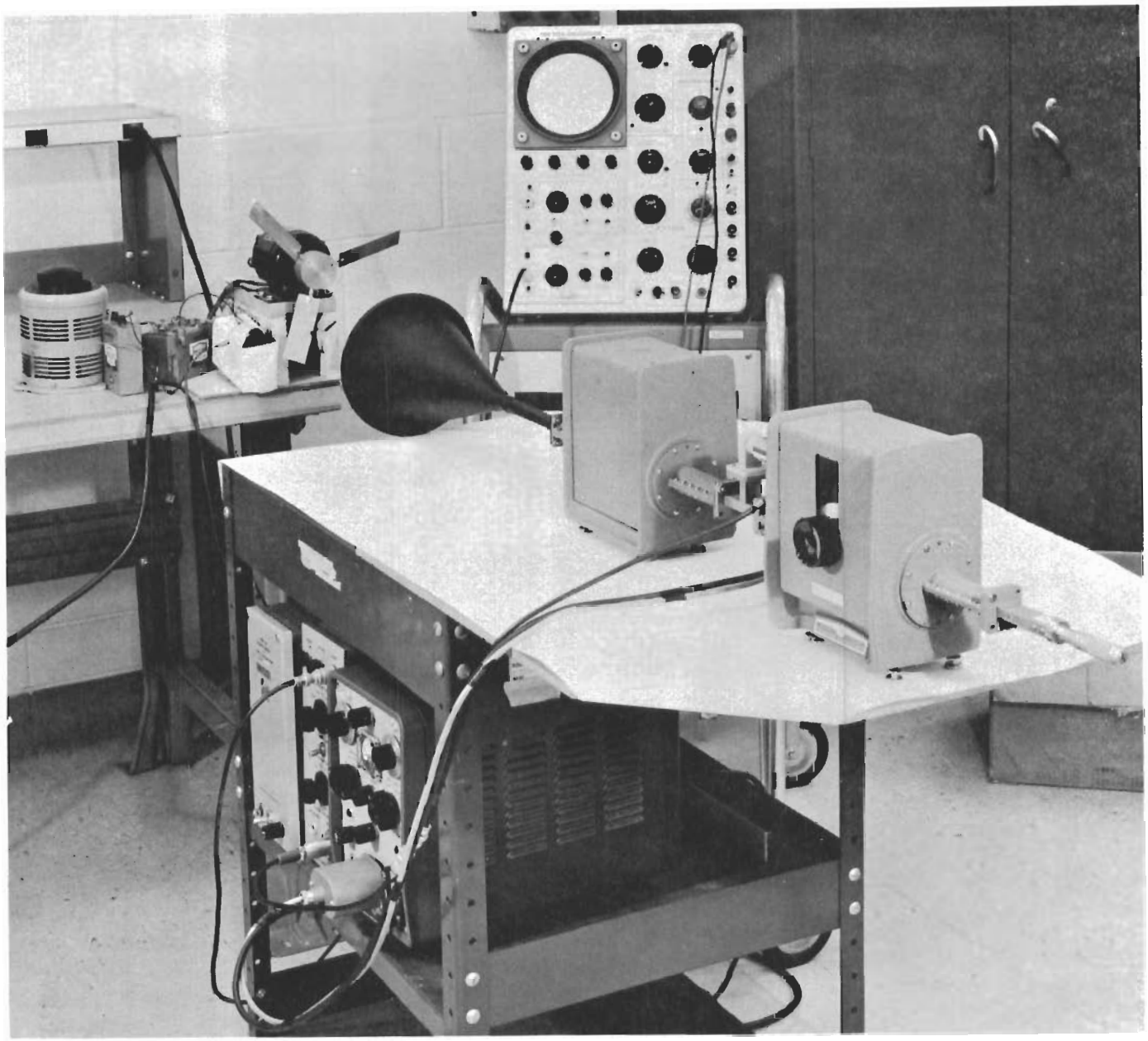

FIGURE 20 INTERFEROMETER WITH HORN-LENS FOR DEFECT DETECTION AT A DISTANCE OF 9 INCHES

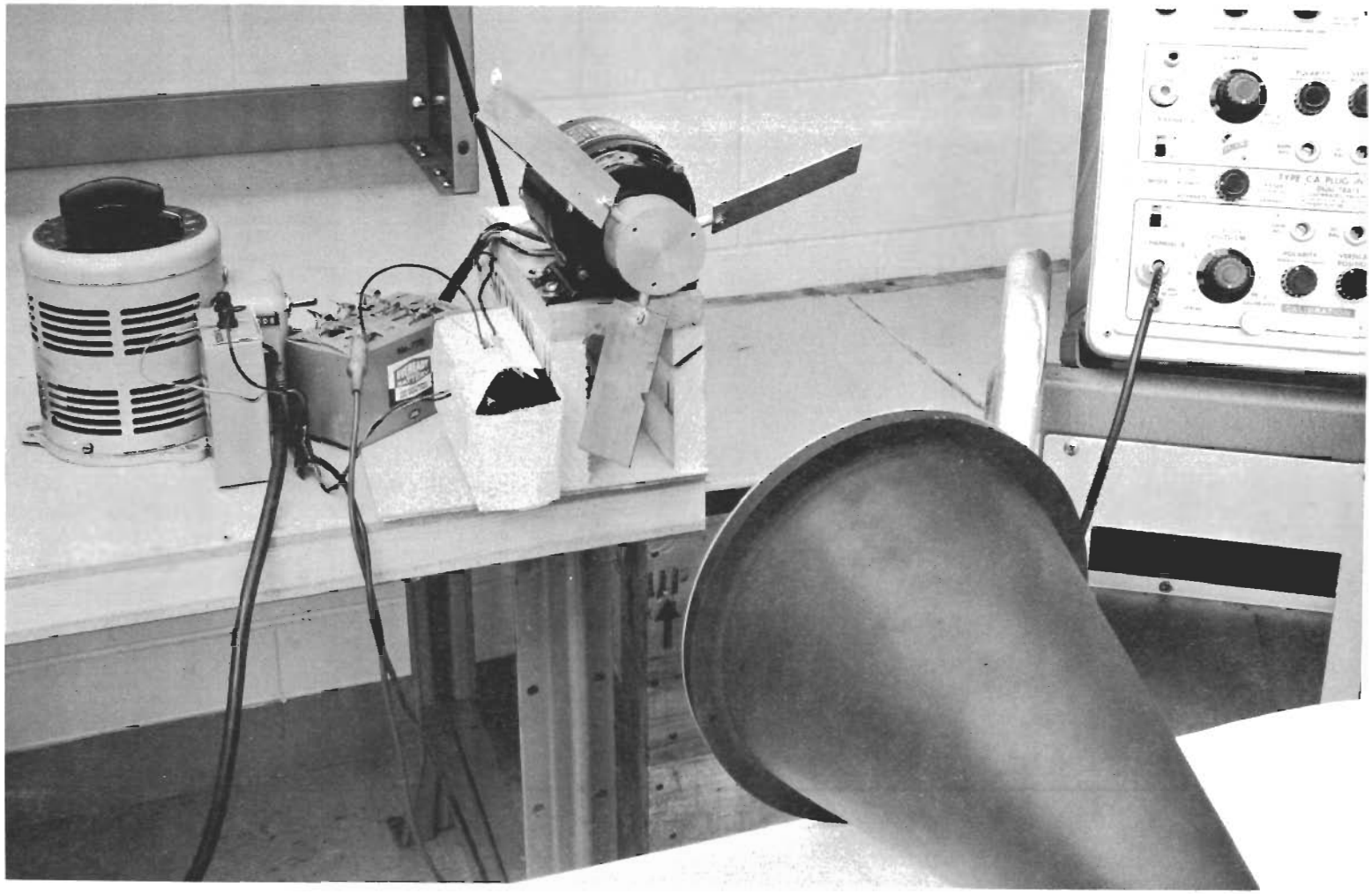

FIGURE 21 VIEW OF SIMULATED COMPRESSOR BLADES AND HORN-LENS ANTENNA (SHOWN ARE THE VARIAC FOR SPEED CONTROL AND OPTICAL TRIGGERING CIRCUITRY)

The initial set of measurements with the antenna system was performed with the compressor blades oriented perpendicular to the axis of the antenna so that only the edge of the blade was illuminated. Initially, the response of the three blades with no defects was identical. Figure 22a shows the response when blade #1, on the left, had a semicircular flaw of 0.125 inch radius. The relative response is 52 percent. The phase shifter was adjusted for peak response in Figure 22a. The effect of changing the phase by 32 degrees is demonstrated in Figure 22b where the blade with a defect shows a drop to 34 percent, compared with a blade having no defect. These results are, therefore, consistent with those given previously when no antenna was used. One reason for beginning these experiments by illuminating only the edge of the blade was to determine whether the return signal would be observable above the noise of the microwave detector. Figure 23 shows that the signal-to-noise ratio with the present instrumentation system is sufficient so that it is not necessary to use a mixer (superheterodyne) type of receiver.

The second set of measurements was made with the simulated compressor blades oriented at 30 degrees with respect to the direction of the incident electromagnetic energy. The response of the three blades was nearly identical and was maximized for a phase angle of θ_o = 17 degrees. The response of the three blades when blade #1 had a 0.125 inch radius defect is shown in Figure 23a. The response of blade #1 was 63 percent of the other blades. Introducing a phase shift of 40 degrees (θ_o = 357) causes an additional drop in the response of blade #1. The response was 22 percent of the other blades in this case. Again the effect of the defect was more pronounced when the phase shift was changed from the angle of peak amplitude response.

The next set of measurements were performed with the blades at an angle of 45 degrees with respect to the direction of incidence of the electromagnetic energy. The response of the three blades with no defect in blade #1 is shown in Figure 24a.

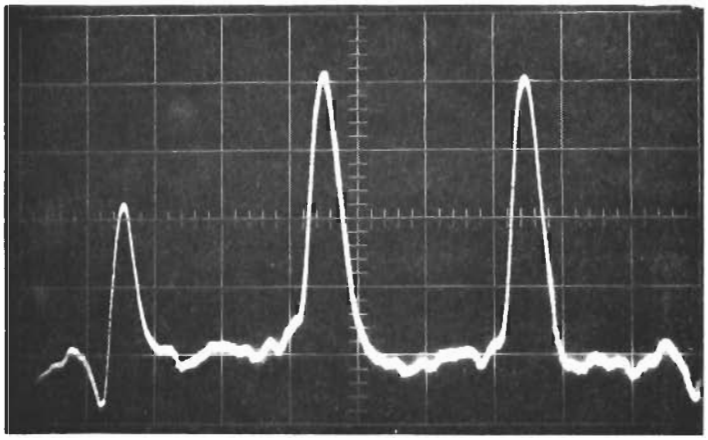

(a) Blade 1 Has a 0.125 in. Radius Defect

Horiz: 10 ms/cm
Vert: 0.5 v/cm
Phase Shift: 230°

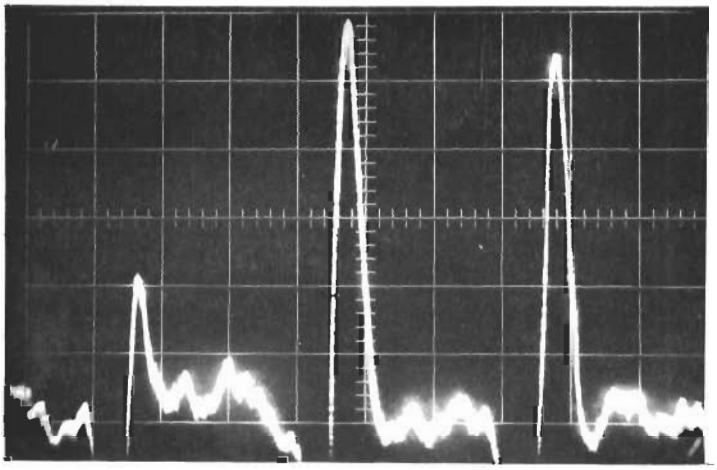

(b) Blade 1 Has a 0.125 in. Radius Defect

Horiz: 10 ms/cm
Vert: 0.2 v/cm
Phase Shift: 214°

FIGURE 22 RESPONSE OF SIMULATED COMPRESSOR BLADES WHICH ARE ORIENTED PARALLEL TO THE DIRECTION OF INCIDENCE

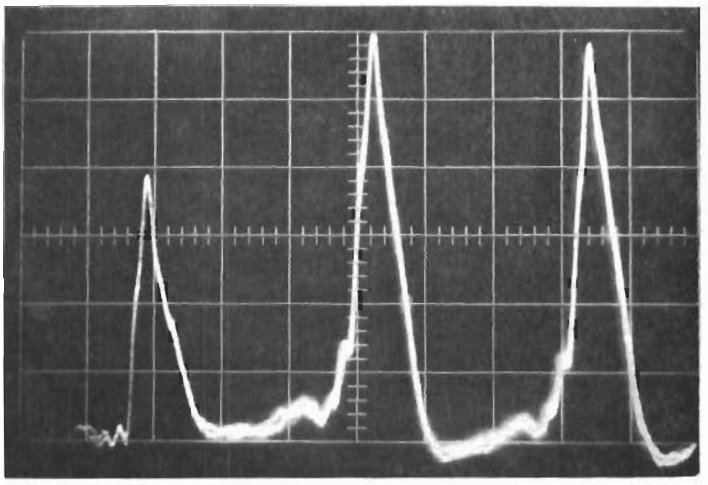

(a) Blade 1 Has a 0.125 in. Radius Defect

Horiz: 10 ms/cm
Vert: 0.16 v/cm
Phase Shift: 17°

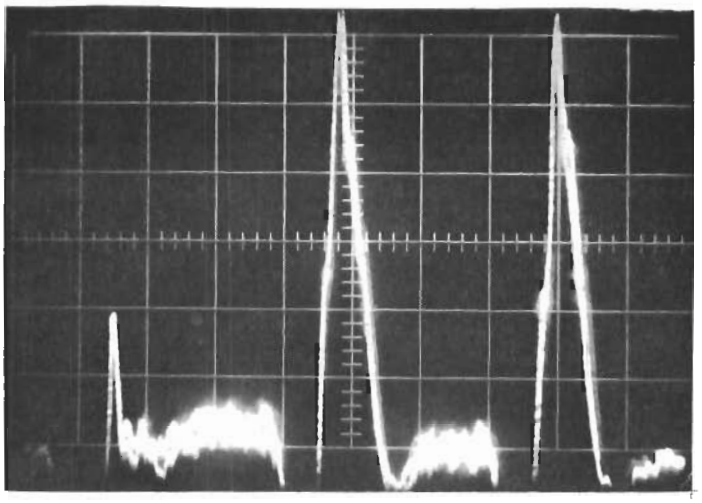

(b) Blade 1 Has a 0.125 in. Radius Defect

Horiz: 10 ms/cm
Vert: 0.08 v/cm
Phase Shift: 357°

FIGURE 23 RESPONSE OF SIMULATED COMPRESSOR BLADES WHICH ARE ORIENTED AT AN ANGLE OF 30° TO THE DIRECTION OF IMPEDANCE

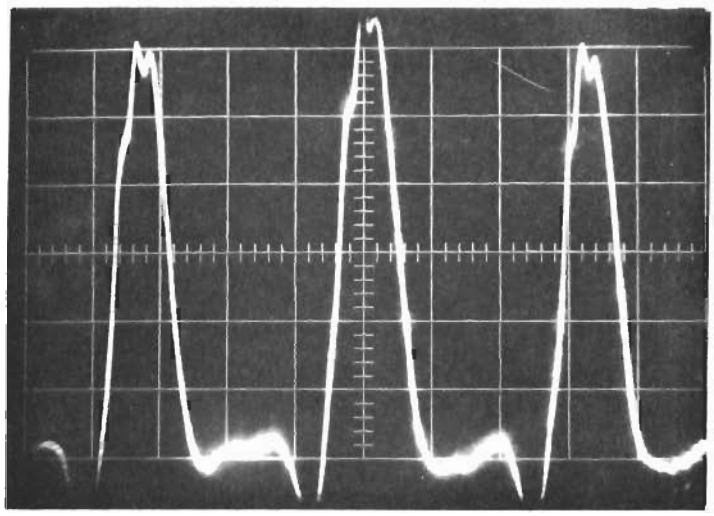

(a) No Defect in Blade 1

Horiz: 10 ms/cm
Vert: 0.18 v/cm
Phase Shift: 32°

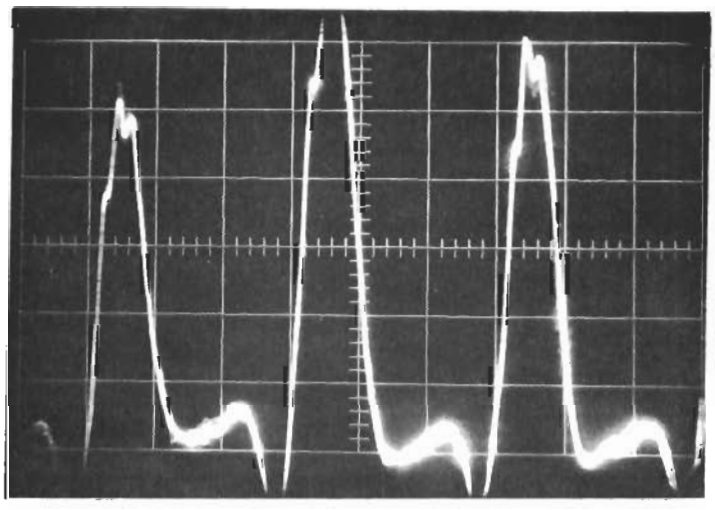

(b) Blade 1 Has a 0.125 in. Radius Defect

Horiz: 10 ms/cm
Vert: 0.18 v/cm
Phase Shift: 32°

FIGURE 24 RESPONSE OF SIMULATED COMPRESSOR BLADES WHICH ARE ORIENTED AT AN ANGLE OF 45° TO THE DIRECTION OF INCIDENCE

The phase angle was adjusted for maximum response. With a 0.125 inch radius defect the response was as shown in Figure 24b (same vertical scale factor and phase shift).* The response due to the blade with the defect was 83 percent of the other blades, somewhat less than in previous instances with the same size defect. Another observation was that changing the phase angle did not increase the percent drop in response as in the previous cases when the blades were oriented at a smaller angle with respect to the illumination. This decrease in sensitivity is attributed to the fact that with the present operating frequency (15 GHz) the spot of illumination is rather large. The spot diameter is large compared to the width of the blade, and as the position angle is increased, the backscatter from the entire blade begins to predominate (note the broadening of the response in Figure 24). Therefore, the contribution of the defect to the overall reflection coefficient (in both magnitude and phase) becomes of less consequence.

2.1.3.2.3 Measurement on the J-47 compressor section using the horn-lens antenna -- The focusing horn-lens antenna was used to illuminate the first stage of rotor blades in the J-47 compressor section. A photograph of the 15 GHz interferometer system is shown in Figure 25. The compressor cover was removed for clarity in the photograph but was in position at the time of the measurements. There were no changes in the measurement technique from that used with the simulated blades.

The previously used method of comparison of the amplitude response with and without a defect was not useable for these measurements. Previously, the shape and position of the simulated

---

* Only blade #3 can be used as a reference in these measurements because blade #2 did not vary with phase shift in the same manner as did blades 1 and 2.

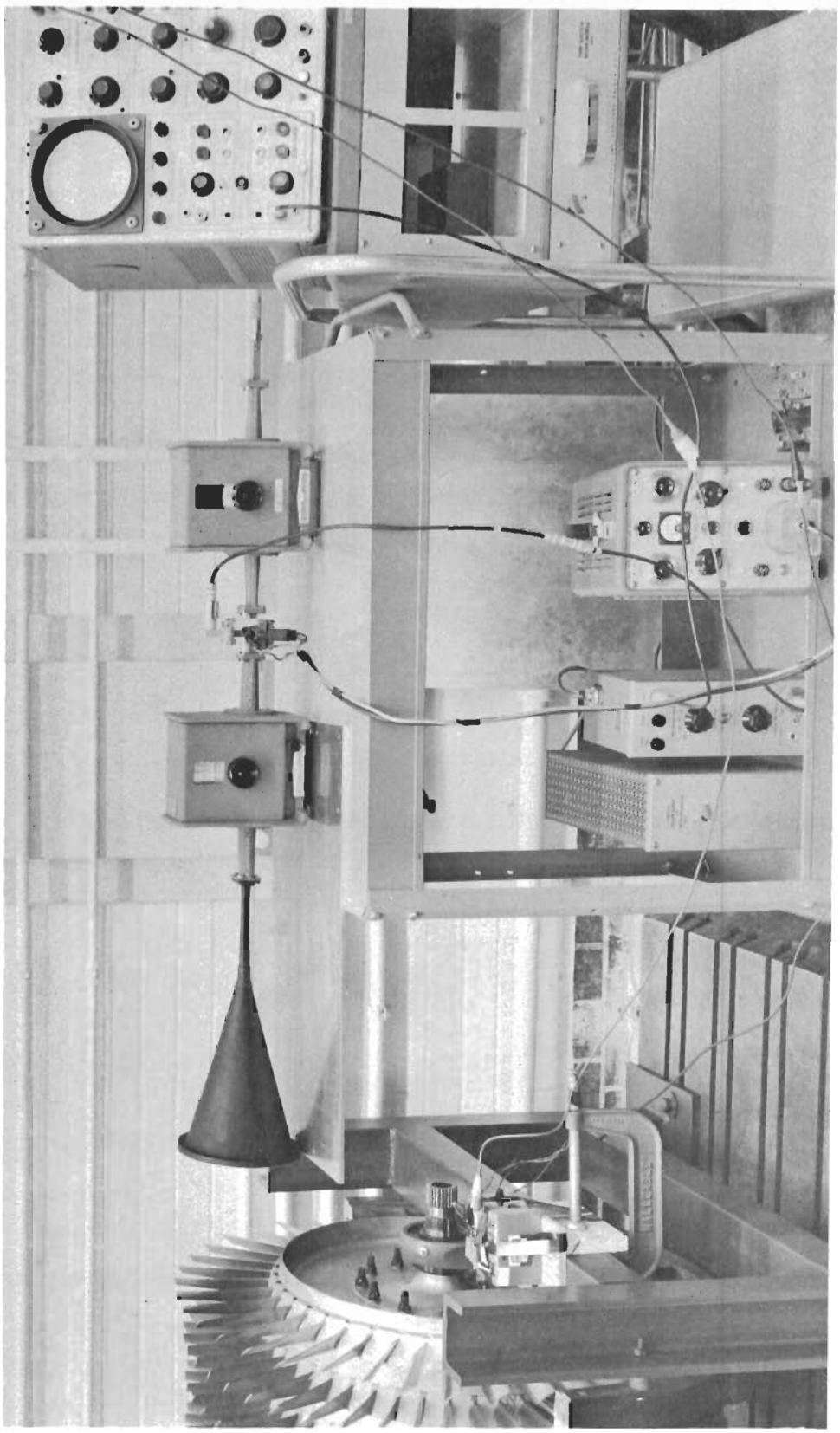

FIGURE 25 15 GHz INTERFEROMETER FOR LABORATORY MEASUREMENT OF DEFECTS IN THE COMPRESSOR SECTION BLADES

blades was controllable and it was possible to use a blade-to-blade comparison of two blades, one with a defect and one without. This was not possible with the compressor section blades because no two adjacent blades showed the same change in response as the phase shift was varied. Therefore, it was necessary to run a series of measurements on a blade as a function of phase angle and then repeat the measurements with a defect in the blade. Photographs were taken to assure that there was no change in the response of the interferometer during the time that the compressor was stopped and the defect introduced into the blade. Typical response photographs are shown in Figure 26. In Figure 26a is shown the response of four of the compressor blades. The response, after a semi-circular defect of 0.125 inch radius was introduced into the blade nearest the center of the display, is shown in Figure 26b. The phase shift setting was 20 degrees less than that for peak amplitude response. The effect of the defect was to reduce the amplitude to 87 percent of its former value. The response of the other blades shown was virtually identical for the two sets of measurements.

The above measurement is included in the set of data shown in Figure 27. It has been shown theoretically and experimentally in previous results that adjusting the phase angle away from the setting for maximum amplitude response causes the interferometer to be more sensitive to phase shift and, therefore, to show a greater amplitude decline for a given defect size. The curve of Figure 27 shows how the sensitivity of the interferometer was affected by variation of the phase shift around the point of maximum amplitude response. The effect follows the pattern of previous results with a slight discrepancy of the phase angle for minimum sensitivity. This could be a measurement error or it might also result if the defect was not illuminated exactly at the region of maximum field intensity.

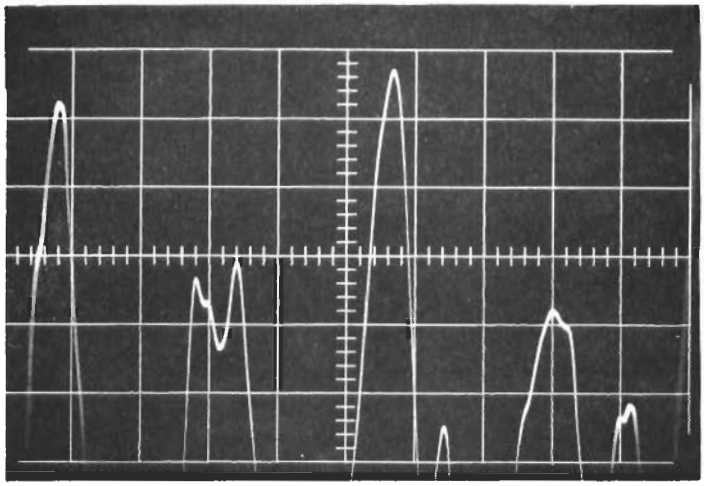

a. No Defect Present

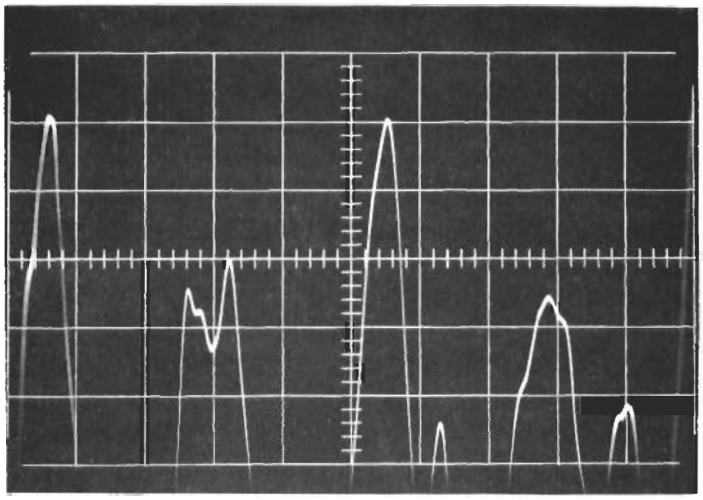

b. 0.125 in. Defect Present in Blade Nearest the Center of the Display. Phase Shift = 20 Degrees

FIGURE 26 RESPONSE OF INTERFEROMETER SYSTEM TO PASSAGE OF FOUR COMPRESSOR BLADES

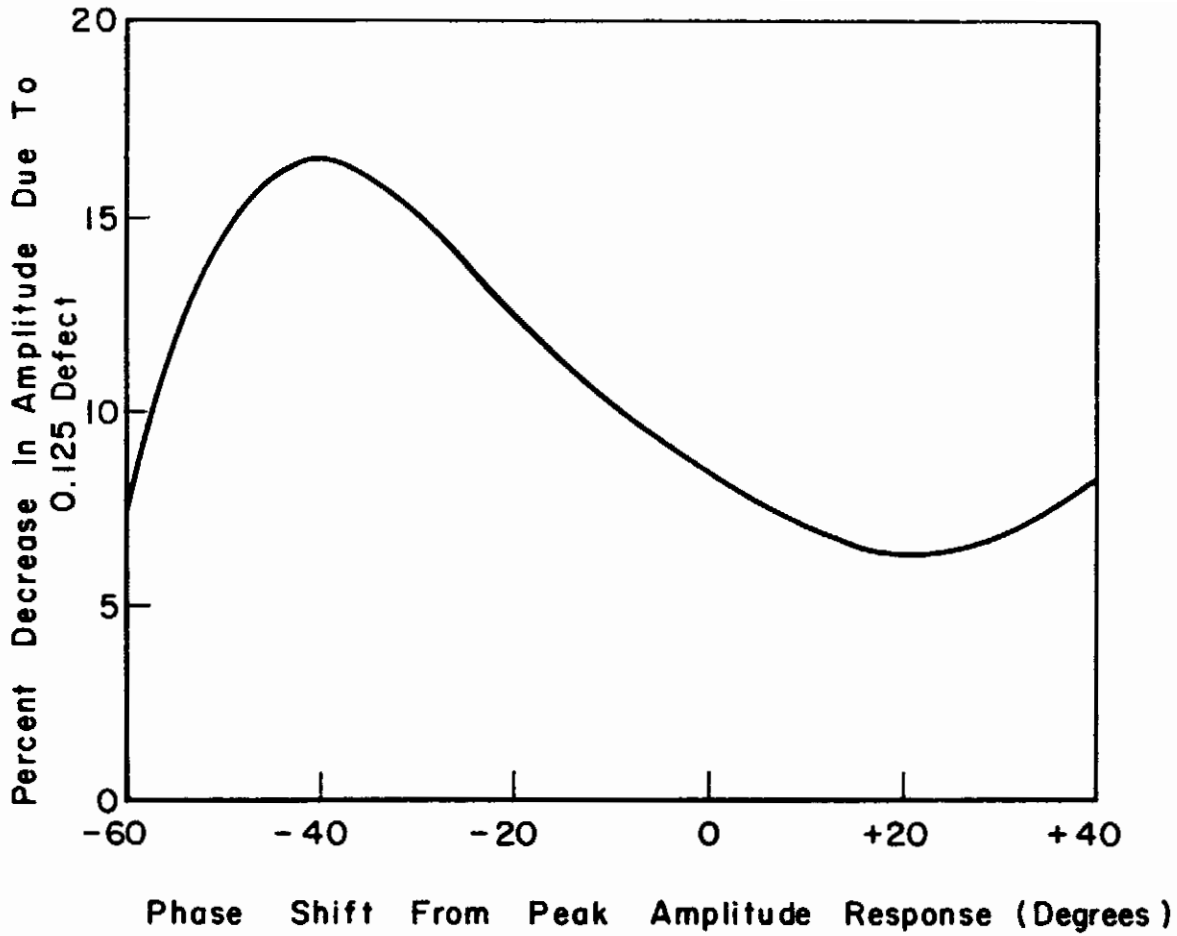

FIGURE 27 PERCENT AMPLITUDE DECREASE DUE TO DEFECT AS A FUNCTION OF PHASE SHIFT .

Comparison with results of measurements taken on the simulated compressor blades shows that the sensitivity with the actual compressor blades is comparable to that when the simulated blades were set at an angle of 45 degrees to the direction of illumination. This is not surprising because the tangent of the leading surface of the compressor blade (which is slightly curved) is approximately 45 degrees with respect to the axis of the compressor.

Some measurements were made with the illumination turned at an angle to the compressor axis so that it was more parallel to the blade axis. This should improve the sensitivity of the interferometer to the phase shift of the defect. However, when the illumination is not normal to the plane of rotation of the blades, then the blade has a time varying phase shift due to the blade rotations. Since the single antenna interferometer has a fixed phase reference, the phase setting introduced by the phase shifter becomes meaningless due to the time-varying phase shift of the blade (it moves toward the source as it passes through the spot of illumination). Therefore, it is impossible to adjust the phase shifter for optimum sensitivity. Experimentally, it was found that no improvement in sensitivity was achieved when the direction of illumination was other than parallel to the compressor axis.

Such a technique may, however, achieve improvement in the sensitivity of the millimeter wave system where the reference short is a compressor blade so that the phase shift in both arms of the interferometer is the same irrespective of motion of the blade in the direction of illumination.

2.1.3.3 Measurements using the 88 GHz dual antenna interferometer

2.1.3.3.1 Introduction -- A millimeter wave interferometer capable of operation in the 60 to 90 GHz range has been constructed. The klystron and isolator have a center frequency of 88 GHz. Two horn-lens antennas have been designed, fabricated, and tested.

The previously given theory predicts a 10 db spot diameter of 0.200 inch for a lens diameter of 1.0 inch and a focal distance of 0.75 inch. Measurements indicated that the spot diameter was approximately 0.200 inch.

One configuration of the dual antenna interferometer is shown in Figure 28. The arrangement of the components was varied slightly in a later configuration in order to insert an attenuator in one arm of the circuit. The final configuration, which was used for all tests, can be seen in Figure 29, which is a view of the system in position for measurement of a defect on the J-47 compressor section. The hybrid was modified to include tuning for establishing initial balance of the bridge when the antennas were radiating into free space.

The tests conducted, following initial evaluation of the system,were as follows:

1) Static tests on a simulated compressor blade.
2) Dynamic tests on a simulated compressor blade.
3) Static tests on an actual compressor blade.
4) Dynamic tests on the J-47 compressor section.

2.1.3.3.2 Static test on a simulated compressor blade -- These tests were conducted by illuminating the edge of one of the simulated blades shown previously in Figure 15 with both antennas. The interferometer is first balanced by adjusting the phase shifter, hybrid tuner, and attenuator as necessary. Use of the attenuator was generally not required. Then the defect was introduced in front of one of the antennas, thereby causing an unbalance in the interferometer and a signal at the output. The results of these later tests are shown in Figure 30 . In Figure 30a is the system output in the balanced condition. The klystron was modulated at a 1000 Hz rate and some unbalance is noted. These measurements were made prior to introducing a tuner into the hybrid, and the unbalance here is due to mismatch in the hybrid. It was possible to pass the blade in front of the

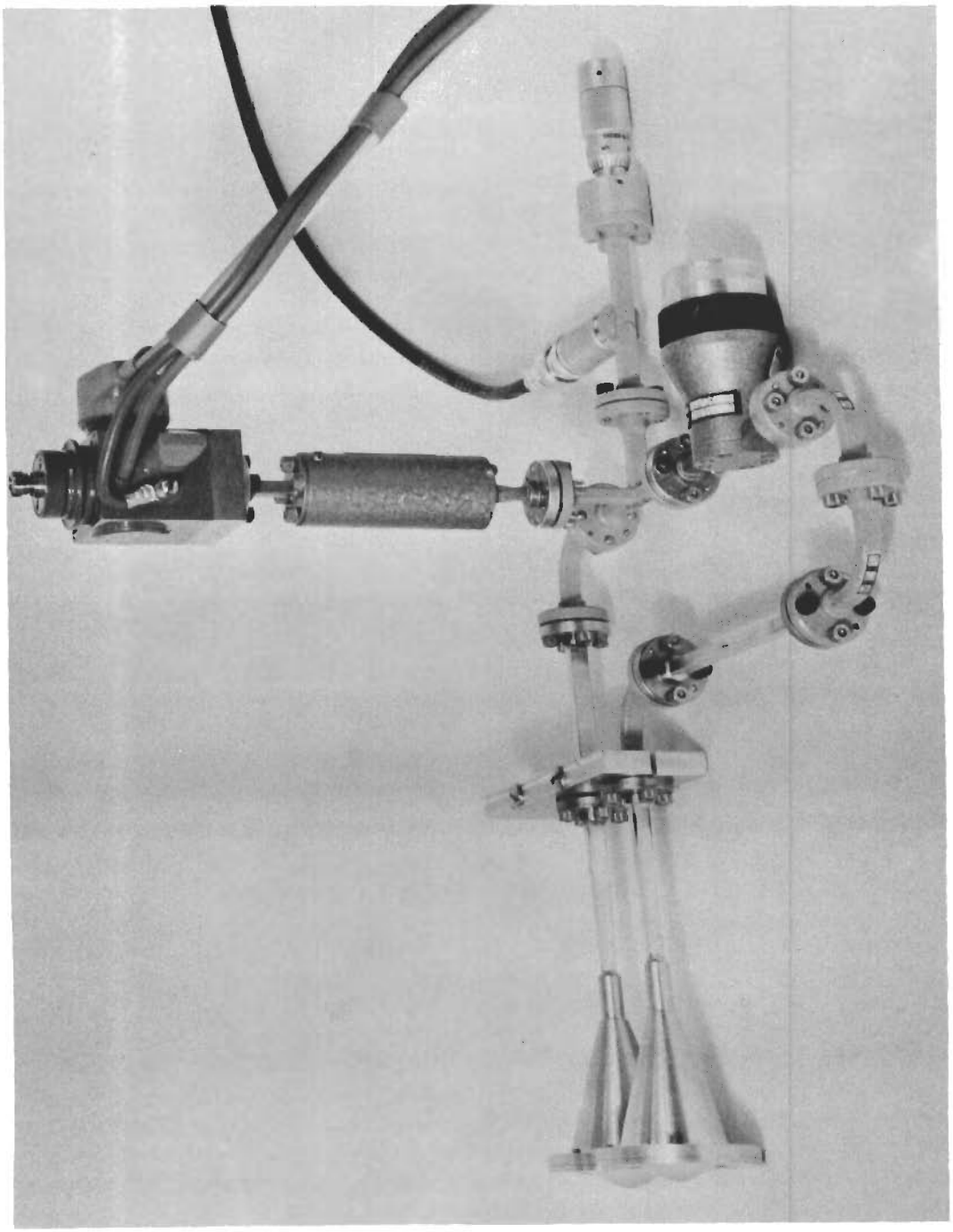

FIGURE 28 DUAL ANTENNA INTERFEROMETER FOR OPERATION AT 88 GHz

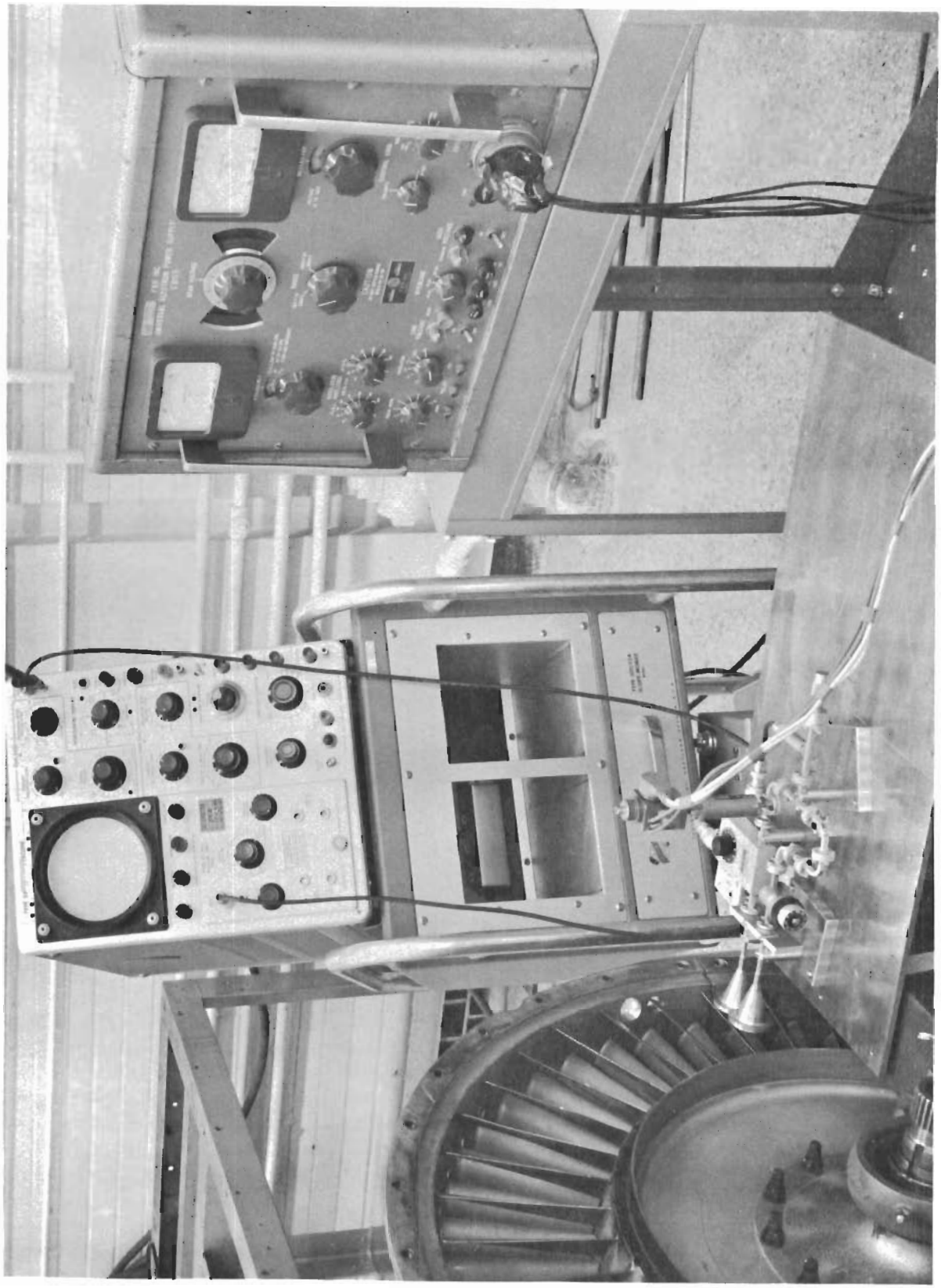

FIGURE 29 DUAL ANTENNA INTERFEROMETER TEST SET-UP

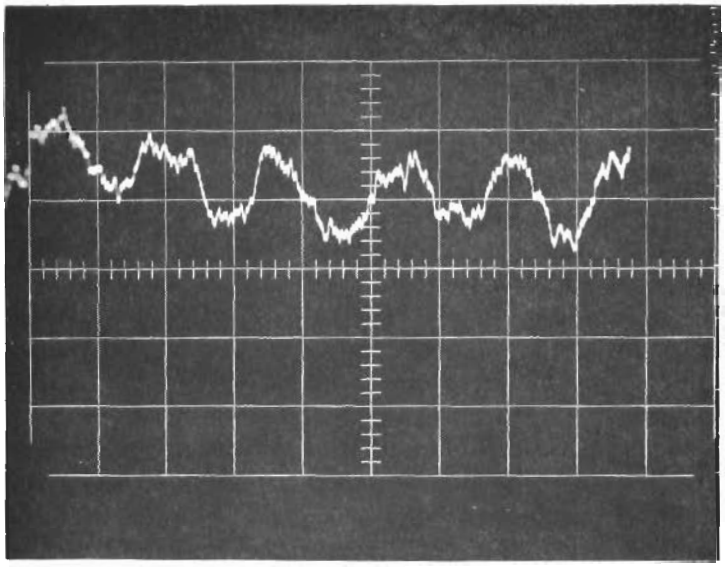

a. No Defect in Blade
0.01 v/cm

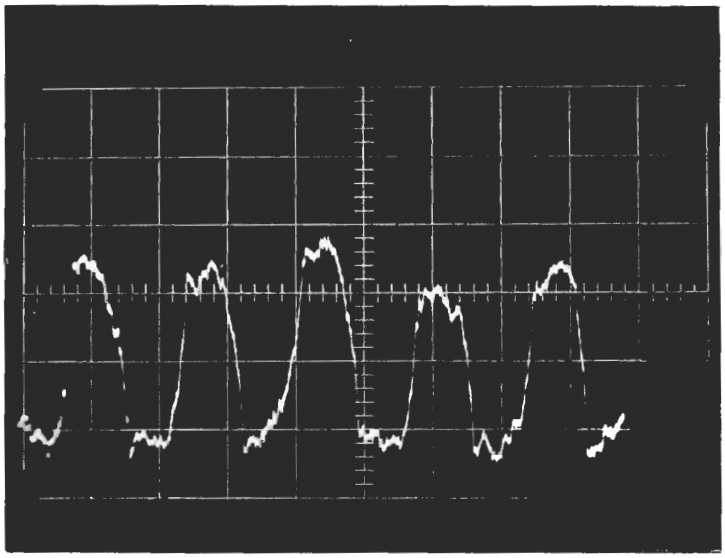

b. Defect of 0.015 in. Radius
0.01 v/cm

FIGURE 30 STATIC DEFECT DETECTION OF A SIMULATED COMPRESSION BLADE

horns with no effect on the output. In Figure 30b is shown the interferometer output when a 0.015 inch radius defect was introduced. The method of introducing the defect for these tests was to remove copper tape covering the defect. The tape was 0.005 inch thick and must be considered part of the defect. Therefore, the defect was actually about 0.025 inch deep. A noticable increase in the output results.

At this point, it is well to note that the balanced type of interferometer requires increased source power as well as a much lower detector noise level than the single antenna type in which variations in the peak deflection were observed. The low-power source and the poor signal-to-noise ratio of the direct detector had hindered all of the measurements made with the 88 GHz system. Improved low noise amplifiers for use with the direct microwave detector have been used; and most of the measurements were made in a screen room to reduce interference. The basic sensitivity limitation, however, is that of the direct microwave diode detector. This problem can be best circumvented through the use of a superheterodyne receiver which will improve the sensitivity by 40 db or more, as well as increasing the source power. However, such equipment was not available for these tests so that the results reported here represent less than the ultimate capability of the interferometer because of the high noise level. Such equipment, while too expensive for an initial feasibility study, is commercially available.

2.1.3.3.3 Dynamic tests on a simulated compressor blade -- Next, the simulated compressor blades were rotated. The system was again balanced for minimum output as shown in Figure 31a. No modulation was used in this case, and the signal is merely noise and interference. However, one of the blades was turned broadside, and it gave the response shown at the fourth vertical division. This should be ignored as it is of no interest in this test. In Figure 31b is shown the response of the interferometer with the same 0.015 inch defect as above (which should be considered

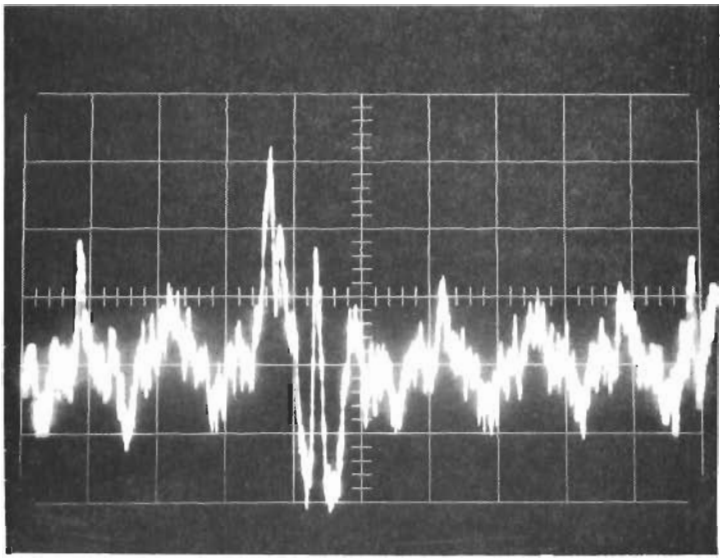

a. No Defect in Blade
0.01 v/cm

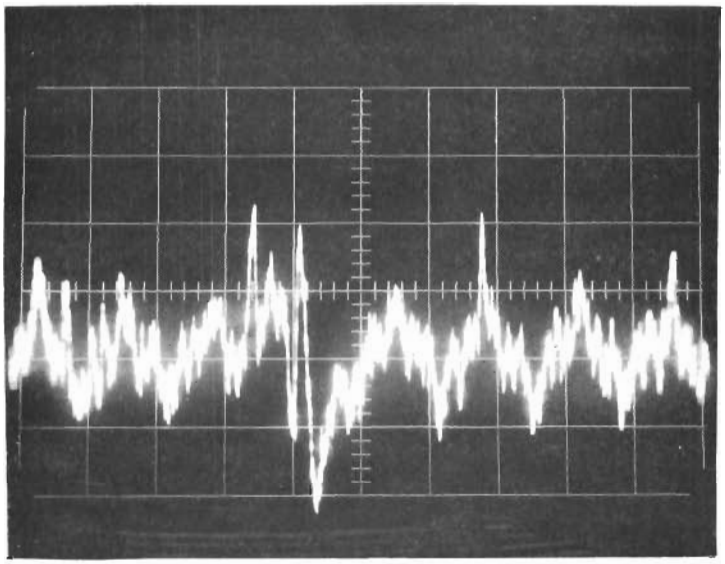

b. Defect of 0.015 in. Radius
0.01 v/cm

FIGURE 31 DYNAMIC DEFECT DETECTION OF A SIMULATED COMPRESSOR BLADE

a 0.025 inch radius defect). The output occurs near the seventh vertical division. Once again, the poor signal-to-noise ratio is evident.

2.1.3.3.4 Static tests on actual compressor blade -- In these tests, a J-47 compressor rotor blade was mounted so that it could be moved vertically in front of the pair of antennas. This test simulates the scanning of the leading edge of the blade by the antennas. Since the test was static, the klystron was again modulated at 1000 Hz. The base of the blade was set at an angle of 30 degrees with the direction of illumination, which closely duplicates orientation of the blade in the J-47 compressor section.

Initially, measurements were made with the interferometer intentionally unbalanced as in the 15 GHz interferometer. Figure 32a shows the maximum output of the interferometer in the unbalanced condition with no defect in front of either antenna. Figure 32b shows the change in the output when the blade was "scanned" so that a defect was in front of one of the antennas. The signal level dropped to 65 percent of its former value due to the presence of the defect which was 0.030 inch deep and 0.030 inch across.

The above test was repeated with the interferometer initially balanced. Figure 33a shows the output with no defect. When the blade was scanned so that a defect was in front of one of the antennas, the output was as shown in Figure 33b.

2.1.3.3.5 Dynamic tests on the J-47 compressor section -- The 88 GHz interferometer system was mounted so that it could "scan" radially any rotor blade on the J-47 compressor section. Movement axially was also provided so that the "spot" could be focused on the leading edge of the blade. A blade with no defects was selected and a defect 0.030 inch deep and 0.050 inch across was introduced. Static tests were conducted with results essentially the same as reported above. The compressor section was rotated and by means of appropriate triggering the blade to be examined was located on the oscilloscope display. It was

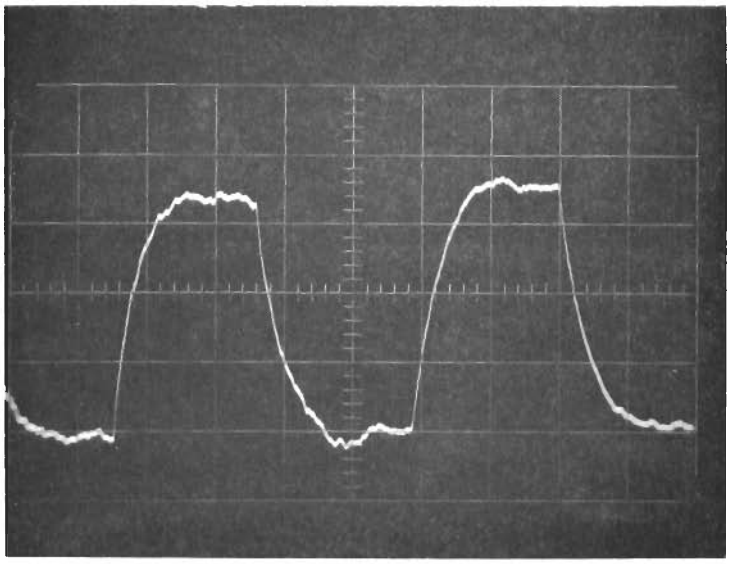

a. No Defect
0.01 v/cm

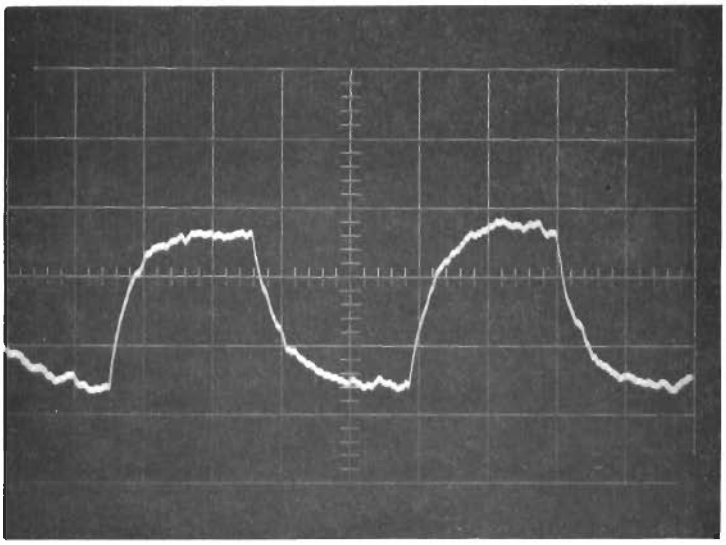

b. Defect 0.030 in. x 0.030 in.
0.01 v/cm

FIGURE 32 STATIC DEFECT DETECTION OF AN ACTUAL COMPRESSOR BLADE (UNBALANCED INTERFEROMETER)

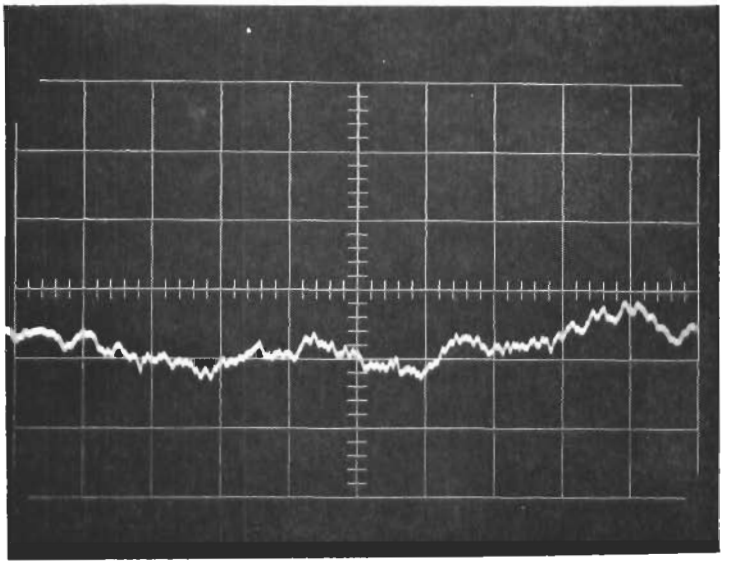

a. No Defect
0.01 v/cm

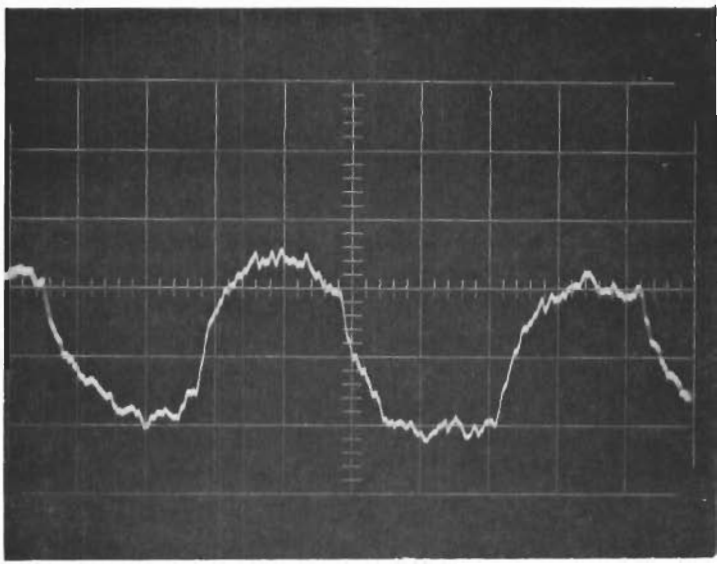

b. Defect 0.030 in. x 0.030 in.
0.01 v/cm

FIGURE 33 STATIC DEFECT DETECTION OF AN ACTUAL COMPRESSOR BLADE (BALANCED INTERFEROMETER)

centered on the display and then the interferometer was balanced by adjusting the phase shifter with both antennas illuminating portions of the blade with no defect. The oscilloscope display is shown in Figure 34a. The interferometer was made to scan the blades radially until one of the antennas was centered on the defect. The output due to the defect is shown in Figure 34b. The 0.030 inch defect is easily discernible. Two defects approximately 3 inches apart were detected in this manner.

2.1.3.3.6 Extrapolations of results -- The full potential of the 88 GHz bridge-type interferometer system is not being realized because of the relatively high noise level of the diode detector. As indicated previously, this noise level would be reduced 40 db or more by using a superheterodyne receiver. It is expected that the system resolution would be thereby improved 2 to 6 times. Thus, a resolution to 0.015 inch is a virtual certainty. Increasing the source power also adds to the system's dynamic range and improves the signal-to-noise ratio.

Additional resolution improvement is, of course, achieved in direct proportion to an increase in frequency. A frequency increase to 220 GHz is made easily (operation at higher frequencies is possible but the selection of commercially available components is more limited). Thus, a resolution improvement of

$$\frac{220}{88} = 2.5$$

is not difficult to achieve. This means that defects of 0.006 inch deep can be detected.

In the 88 GHz system, the "spots" are 1.0 inch apart. The success of the present antenna design indicates that the lens diameters could have been reduced. If we assume that the lens diameter could have been reduced by 25 percent with no frequency increase, then at 220 GHz the separation of the spots would be

$$1.0 \times \frac{3}{4} \times \frac{1}{2.5} = 0.30 \text{ inch}$$

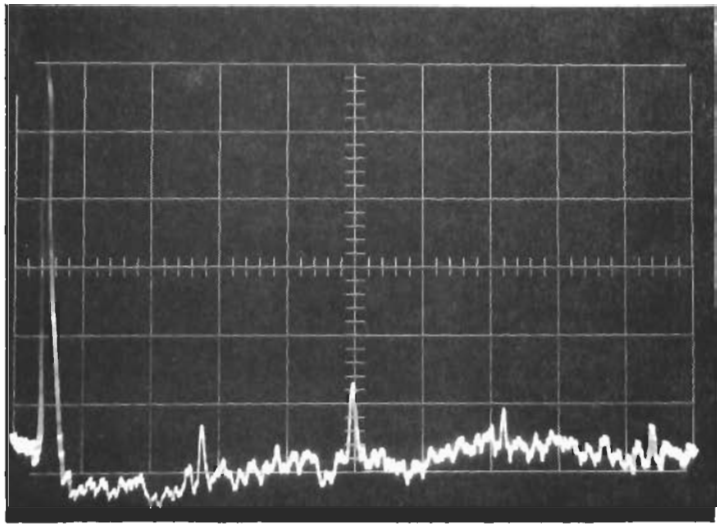

a) No Defect
0.01 v/cm

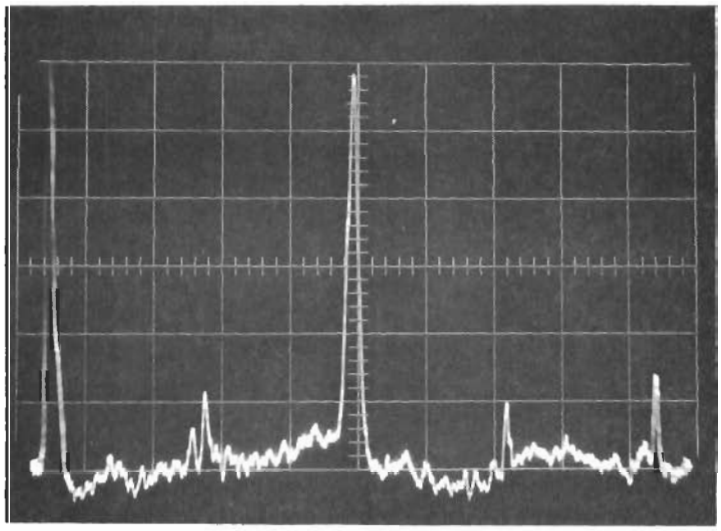

b) Defect 0.030 in.
deep x 0.050 in.
across - 0.01 v/cm

FIGURE 34 DYNAMIC DEFECT DETECTION OF THE J-47 COMPRESSOR SECTION

The corresponding spot diameter would be 0.080 inch and the focal distance would be

$$R = \frac{dD}{2\lambda} = \frac{0.080 \times 0.030}{2 \times 0.0537} = 0.224 \text{ inch}$$

If this separation between lens and blade is too small then the lens diameter can be increased or the frequency increased. Alternatively, a poorer resolution will result if the spot diameter is increased along with the focal distance.

2.1.3.3.7 Determination of defect size -- It is expected that establishing the relationship between defect size and shape to the magnitude of the interferometer output will be largely an empirical process. However, some assistance in establishing this relationship may be provided through analytical modeling of the defect. The defect, in simplified model, can be treated as a waveguide discontinuity. As such, it is possible to relate the effect on the interferometer output signal to the variation of the dimensions of the discontinuity.

The following considerations are given with regard to measuring the size and depth of the defect independently. If we consider that the defect can be described by a mean area A_m and a mean depth d_m, it may be possible to conduct the measurement in such a way as to determine A_m and d_m essentially independent of each other. The assumption is first made that in Eq. (12) the magnitude of the reflection coefficient, $|\Gamma_1|$, is influenced primarily by A_m and that the phase shift, θ_1, is influenced primarily by d_m. It has been demonstrated (see Figure 27) that the amplitude variations of the interferometer can be made either insensitive or strongly sensitive to the phase shift variations caused by d_m. Therefore, two measurements could be performed; one in which θ_o is adjusted so that the variation of the cos θ term with phase shift θ_1 (in Eq. 12) is negligible, and the second in which θ_o is adjusted so that the phase shift θ_1 has a strong influence on the interferometer. It should then be possible to correlate the difference of these measurements with d_m and the

first measurement with A_m. One possible limitation of this dual measurement is that the first measurement, where the effect of phase shift is suppressed, is less sensitive. The usefulness of this dual measurement technique can be evaluated empirically.

2.1.3.3.8 Implementation of the millimeter defect detection system -- Since the "no defect" condition is one of a balanced interferometer, it is necessary to maintain this balance as the pair of antennas is scanned over the edge or surface of a blade which is curved and/or misaligned in the radial direction.

Balance can be maintained through the use of negative feedback from the output of the interferometer to an electronically controlled phase shifter in one of the arms of the bridge. This feedback arrangement is illustrated in Figure 35 .

As the antennas are scanned in the y direction along the blade at a rate of y' inch per second, a difference

$$\Delta d_t = d_1 - d_2 \tag{14}$$

may develop in the distances of the two antennas from the blade surface. This difference represents a phase shift which unbalances the bridge and causes a voltage V to develop at the amplifier output. Assume that another output voltage V_f from the amplifier, which has appropriate polarity to act as negative feedback, is used to control an electronic phase shifter and thereby maintain the balance of the bridge.

Assume the feedback voltage is related to the tracking error by a system constant K_1

$$V_f = K_1 \Delta d_t \tag{15}$$

Also, let the tracking error be related to the tracking displacement y by a constant K_2.

$$\Delta d_t = K_2 y \tag{16}$$

Thus, from (15) and (16)

$$V_f = K_1 K_2 y \tag{17}$$

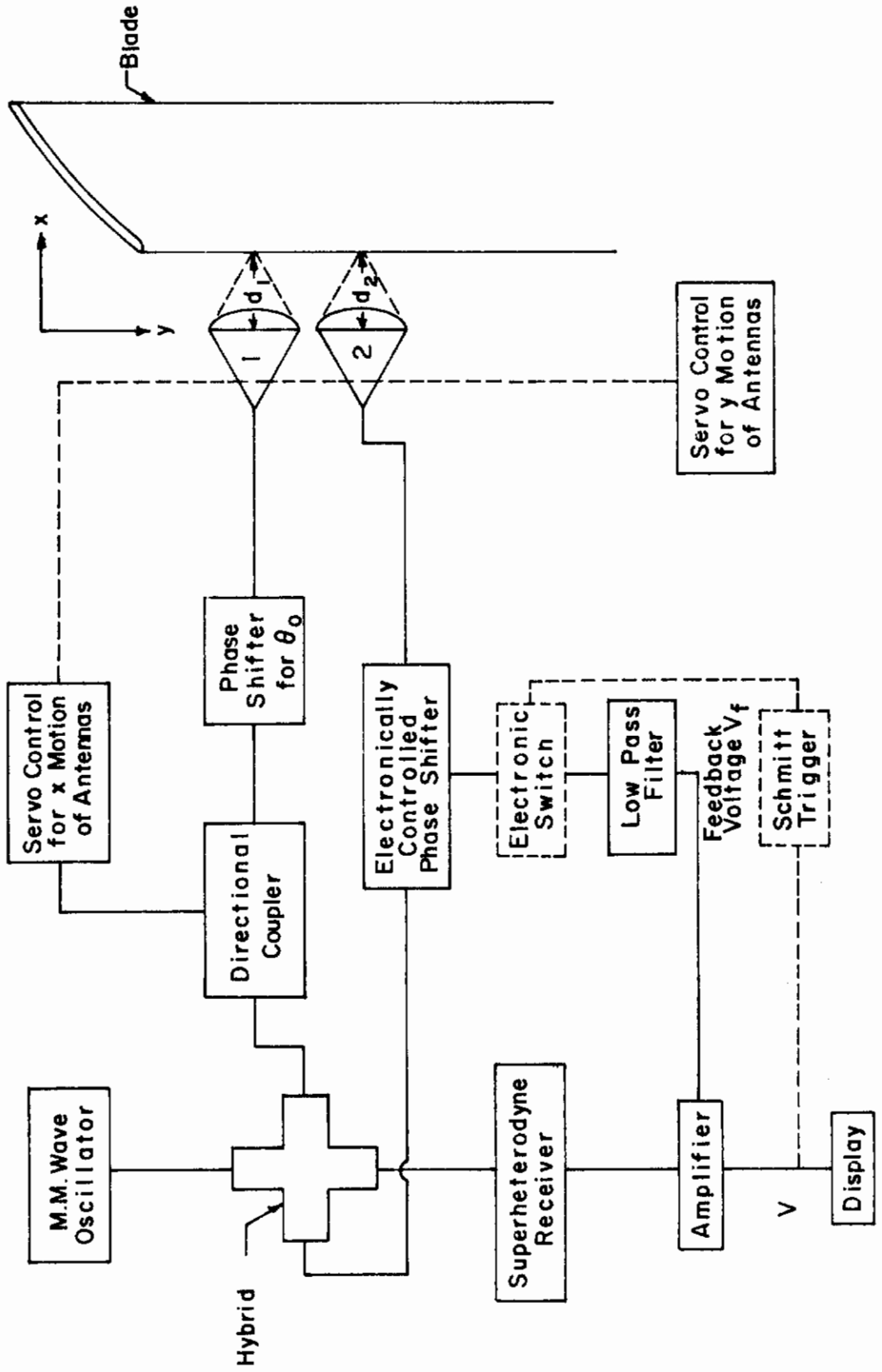

FIGURE 35 BLOCK DIAGRAM OF IMPLEMENTATION OF THE MILLIMETER WAVE INTERFEROMETER FOR DEFECT DETECTION

Therefore, the rate of change of feedback voltage is proportional to the tracking velocity y' multiplied by the very small constant K_2.

$$f_t = \frac{dV_f}{dt} = K_1 K_2 \frac{dy}{dt}$$

$$f_t = K_1 K_2 y' \tag{18}$$

A very low frequency f_t can be associated with the rate of change of feedback voltage due to tracking error.

Next, assume that one of the antennas is incident upon a defect and the edge of this defect makes a 45-degree angle with both the X and Y axes. In this case, a displacement Δd_d occurs due to the defect which is exactly equal to the change of y along the edge of the defect. The resulting feedback voltage is then related to y by

$$V_f = K_1 y \tag{19}$$

and the rate of change of the feedback voltage is

$$f_d = \frac{dV_f}{dt} = K_1 y' \tag{20}$$

A frequency f_d may be associated with the rate of change of feedback voltage due to a defect. The ratio of the frequencies

$$\frac{f_d}{f_t} = \frac{K_1 y'}{K_1 K_2 y'} = \frac{1}{K_2} \tag{21}$$

is very large since K_2 is an extremely small constant.

Returning, now, to the discussion of the operation of the system of Figure 35 , we observe that some means must be provided to prevent the feedback loop from nulling the bridge when a defect is in front of one antenna. This is done by inserting a low pass filter with a cutoff frequency, fc, such that

$$f_t < f_c \ll f_d \tag{22}$$

This is easily done because, as was shown above,

$$f_d >> f_t \tag{23}$$

An alternative viewpoint of the functions of the filter circuit is obtained by examining the response of a typical low-pass filter to a transient step input of V_f volts. The response of a series L, shunt C filter is

$$V_{fo} = V_f \ (1-\cos w_o t) \tag{24}$$

where

$$w_o^2 = \frac{1}{LC}$$

Initially, the filter output is zero and it will remain at a negligable value during the time that the defect is causing an unbalance in the bridge provided w_o is small enough. If, however, w_o is too small, the filter will not permit the balancing of tracking error voltage. A suitable compromise value for w_o should be possible.

If, however, a suitable value for w_o is not possible, then the electronic switch and Schmitt trigger (shown dashed in Figure 35) can be employed. In this case, w_o is made large enough so that only the initial transient caused by the defect is rejected by the filter. Then, an unbalance voltage will develop during the period that the defect is scanned by the antenna. The Schmitt trigger threshold voltage would be set so that the electronic switch (which is normally closed) will disable the feedback circuit when the large unbalance of a defect is present but not when the small unbalance due to tracking error is present.

The above system is intended to illustrate the functional operation of a millimeter-wave defect detection system and is not intended to represent the only possible configuration for such a system. Such a configuration, however, makes possible the detection

of defects on compressor blade edges and surfaces which are curved or misaligned in the radial tracking direction of the antennas.

Another form of mechanical control over the antenna motion that is required is the movement in the x direction; that is, toward or away from the blade. The intensity of the electric field in the vicinity of the focal distance varies nearly sinusoidally in the x direction. For maximum sensitivity it is necessary that the maximum of electric field occur at the blade surface. When this is the case, the return signal is also maximized. If the return signal is sampled by a directional coupler (see Figure 35) in one arm of the bridge, then by using this signal, to control the servo mechanism for x direction motion, it is possible to continually adjust the position of both antennas so that maximum electric field appears at the surface of the blade. Since both antennas move together, no unbalance in the bridge occurs due to small displacements in the x direction.

2.1.3.3.9 Conclusions -- It has been demonstrated that an interferometer system operating at 88 GHz with marginal sensitivity can detect defects of the order of 0.030 inch. The ultimate detection capability of the present system with a sensitive receiver was estimated to be 0.015 inch or less. These results were extrapolated to a 220 GHz system which was concluded to offer a defect detection capability in the 0.005 inch to 0.010 inch range. A block diagram representing a possible system for defect detection while scanning the edge or surface of a blade was discussed. While many practical problems must be considered, it is believed that the basic conceptual feasibility of such a system has been established.

2.2 Magnetic Field Techniques

2.2.1 Introduction -- One phenomenon discovered on a previous program for the Air Force, "Investigation of Secondary Effects for the Checkout of Nonelectronic Systems" (Technical Report AFAPL-TR-65-57), was that the distortion of the earth's magnetic field by moving parts can be detected some distance away by means of a Hall-effect magnetometer or a loop sensor. Therefore, the magnetometer or loop sensor can be used to measure the distortion created by the movement of compressor blades through the earth's magnetic field.

Sensing signals in this frequency range offers advantages inasmuch as these signals tend to readily penetrate enclosure walls made of nonmagnetic material, thereby permitting a simple field set-up. If the mechanical movement is slow enough, the change of the magnetic field easily propagates through nonmagnetic panels. In the case of a turbine engine, the rotational speed is too fast to employ reliable signals penetrating the thick aluminum shroud. Minor modifications, therefore, are required to allow the magnetometer probe to be placed nearer the blades.

During the program, the Hall-effect magnetometer and loop sensor systems were experimentally evaluated on simulated and actual compressor rotor blades to determine the feasibility of using magnetic field techniques to detect foreign object damage. Initially, it was demonstrated on simulated compressor blades that a Hall-effect magnetometer could detect blade movement even if the blade material was nonmagnetic. It was then demonstrated that a single probe magnetometer system could detect leading edge defects of the order of 0.10 inch diameter or larger in rotating blades. The magnetic field techniques were finally evaluated on the J-47 compressor section with two magnetic field sensors in order to perform an adjacent-area-to-adjacent-area leading edge comparison. Due to the wide variations of blade-to-blade positions and tilt in an actual compressor, the two sensor system can

only marginally detect leading edge defects down to 0.060 inch diameter.

Experimental investigations were performed that demonstrated the feasibility of using the remnant magnetization of a compressor rotor blade to determine if foreign object damage has occurred. The magnetization of a hit blade radically changes when foreign object ingestion occurs, and this change is easily detected with a Hall-effect magnetometer sensor which could be permanently mounted in the compressor enclosure. Simulated foreign object hits of sufficient energy to produce 0.015 inch leading edge defects were easily resolvable.

2.2.2 Sensors

2.2.2.1 Hall-effect magnetometer -- In order to sense magnetic fields, a Hall-effect magnetometer can be used. This device responds to the magnetic field rather than to the time rate-of-change of the field as in a loop, thereby providing the following advantages:

- Ability to measure magnetic fields at a point.
- Direct one-point calibration independent of frequency.
- True spectral responses to magnetic fields (frequency-independent).
- No distortion of magnetic field (Hall-effect probe without flux collectors).

The IITRI Hall-effect magnetometer consists of a Hall-effect magnetic field probe and portable auxiliary equipment housed in an instrument case (Figure 36). The auxiliary equipment consists of an amplifier, Hall-element bias supply, calibrator, and battery charger. The major environment factor that affects the successful operation of the Hall-effect magnetometer during subaudio magnetic field measurements is the amplitude of waveforms arising from power lines. These are generally 60 Hz or 400 Hz signals and their harmonics. These signals tend to mask out the desired signals, or they may overload various measurement circuits.

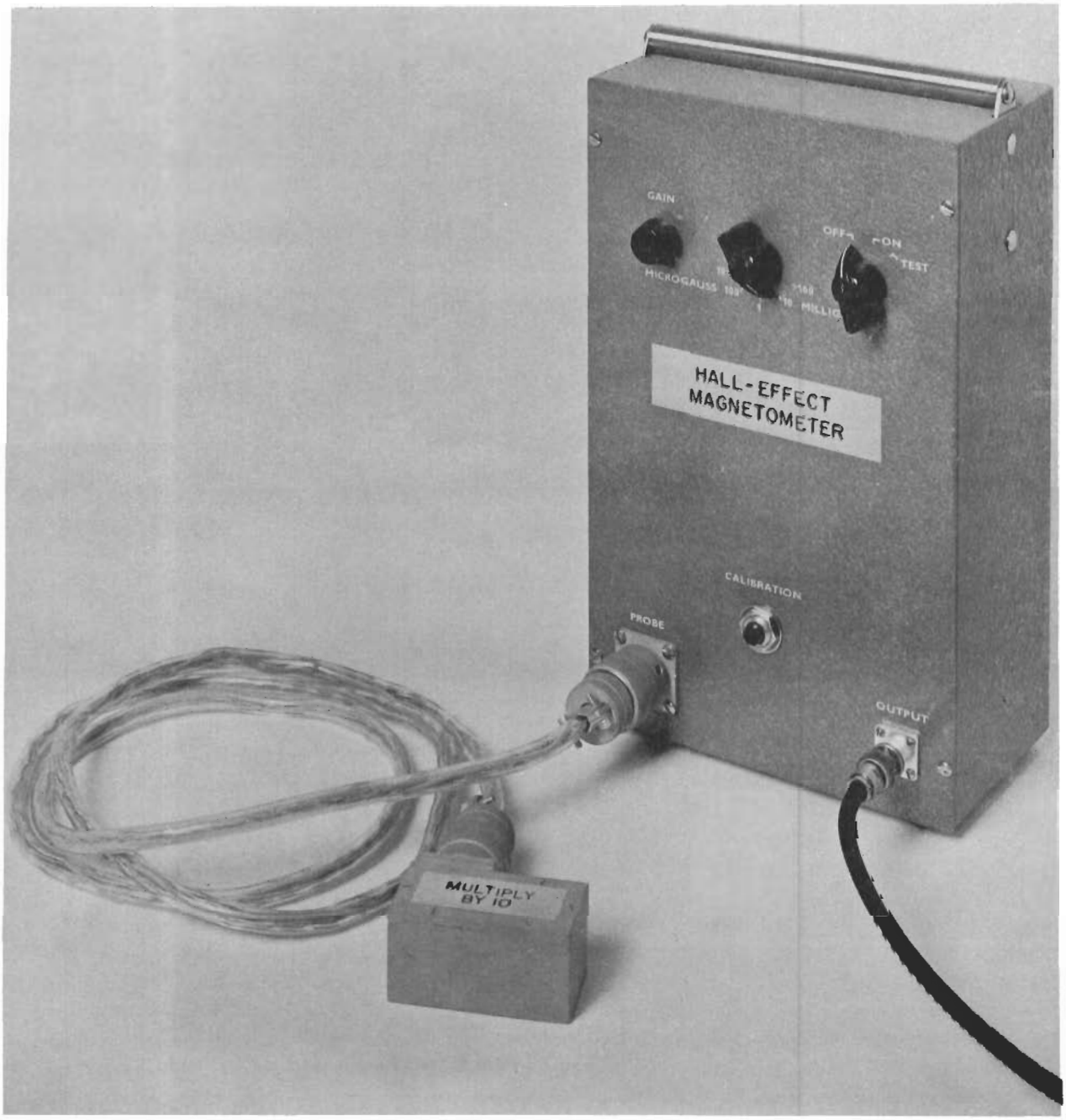

FIGURE 36 HALL-EFFECT MAGNETOMETER

The general specifications for the Hall-effect magnetometer are as follows:

1) Sensitivity (per cycle per second for unit signal-to-noise ratio)

   (a) Magnetic fields to 10^{-7} gauss

   (b) Currents to 10^{-5} ampere (at frequencies below 100 Hz the sensitivity decreases by an order of magnitude)

2) Frequency Range (within 3 db)

   0.7 Hz to 1,000 Hz

3) Output Signal (for maximum setting of GAIN control)

   At least 1 volt rms

4) Range of Measurable Signals

   (a) Magnetic fields from 10^{-7} gauss to 1 gauss

   (b) Currents from 10^{-5} amp to 0.5 amp

5) Dynamic Range

   (a) Maximum setting of GAIN control (40 db)

   (b) Minimum setting of GAIN control (80 db)

6) Loading Impedance

   600 ohms or higher

The Hall-effect probe consists of a Hall-element with flux collectors. Three probes with flux collectors are available which differ in the lengths of the flux collectors. The most sensitive probe is capable of detecting magnetic fields of the order of 10^{-7} gauss per cycle per second (signal-to-noise ratio of unity) or better in the range of frequencies above 100 Hz. At lower frequencies, the presence of 1/f noise reduces the sensitivity of the probe.

The response of the probe to extraneous signals due to inductive pickup is very low. For a single-frequency signal the inductive pickup is at least 60 db lower than the measured value. The length of the most sensitive probe is about 17 inches. A second probe has a sensitivity about 10 times lower, and its length is 2.5 inches (see Figure 36). The third probe is constructed differently from the other two. Its total length, Hall-element and flux collectors, is only 0.5 inch. It is mounted at the end of a flat rod and is, therefore, more versatile, i.e., it can be used to measure fields in confined spaces as well as next to current-carrying conduits. The sensitivity of this probe to magnetic fields is in the order of 10^{-6} gauss per cycle per second.

The Hall-effect probe, which utilizes high permeability materials as flux collectors, will exhibit nonlinear behavior due to the saturation of the ferrites. Hence, the degree of nonlinear performance will depend on the size of the magnetic flux density present in the probe. To avoid generation of nonlinear terms in the probes, the most sensitive probe is used for the measurement of fields below 10 milligauss, the medium one for fields below 100 milligauss, and the least sensitive one for fields below one gauss. It should be noted that the calibration levels of all three probes were set at these limiting values of measured magnetic fields. Thus, each probe should be used only for the measurement of magnetic fields which are below the level of the calibration field. This should assure a linear operation which may contain nonlinear terms not exceeding 60 db below the measured fields. However, when two large fields are present, the highest magnitudes of fields which render linear performance are even smaller, i.e., if two fields of 10 milligauss each are applied to the most sensitive probe, the nonlinear terms may be as high as 50 microgauss, which is about 46 db below the magnitude of the measured fields. A satisfactory performance of the probes will be obtained when the measured magnetic fields are maintained an

order of magnitude below the respective calibration levels.

Another aspect of the nonlinear behavior of the probes is due to the presence of the earth's magnetic field. In the case of the most sensitive probe, the orientation of the probe affects its response within ±5 percent. Hence, to obtain precise measurements this probe should be recalibrated every time it has to be moved.

The amplifier consists of two parts: (1) the preamplifier and (2) amplifier. The preamplifier consists of an input transformer and three transistor stages. The input transformer is made of very high permeability laminations. The transformer is followed by the step attenuator and an amplification stage. Suitable Hall-element bias and calibration circuits are also provided.

2.2.2.2 Ferrite loop sensor -- Another type of magnetic field sensor is a ferrite loop sensor. This sensor responds to the time rate-of-change of magnetic fieldsinstead of the magnitude of the field as in the case of the magnetometer. Two typical ferrite loop sensors are shown in Figure 37. With this type of sensor, only the change in the fringing magnetic field appears at the output of the sensor and any dc field present does not effect the output.

2.2.3 Magnetic field measurements

2.2.3.1 Preliminary measurements, seeded fields for defect detection -- An experimental investigation was performed in the laboratory with a Hall-effect magnetometer system to measure the distortion of the earth's magnetic field by moving simulated compressor blades. This investigation was performed on a breadboard system consisting of a high-speed air turbine (80,000 rpm maximum) driving a 3-inch diameter brass disc on which was mounted simulated compressor blades. The sensor system consisted of a Hall-effect magnetometer and an oscilloscope for displaying the output of the magnetometer. A strobatac was used to monitor the rpm of the air turbine.

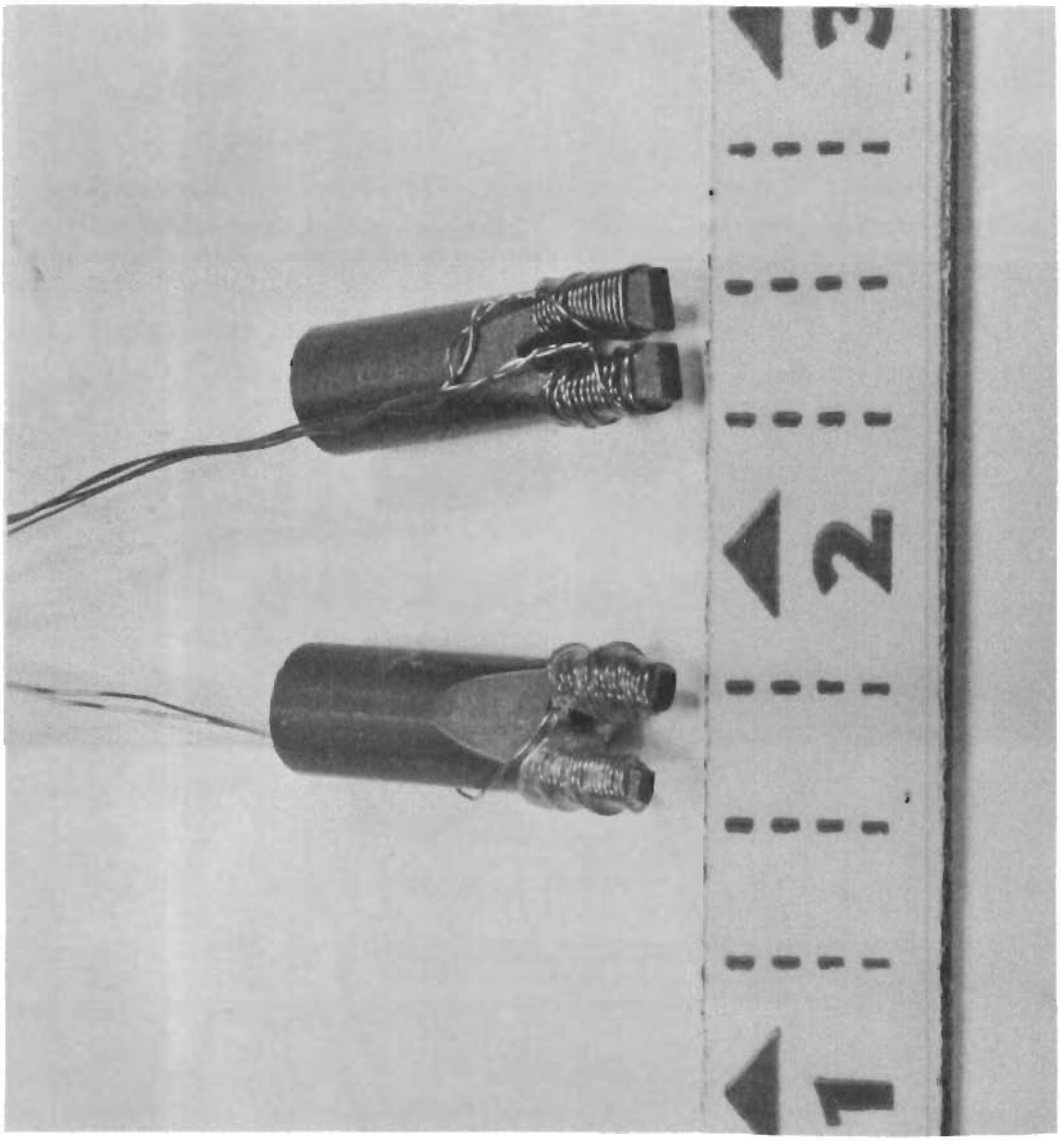

FIGURE 37 FERRITE LOOP SENSORS

Initially, an investigation was performed to determine if the Hall-effect magnetometer could be used to detect the movement of simulated compressor blades made of both nonmagnetic and magnetic materials. This investigation was performed with the previously described breadboard and sensor systems with the addition of a small horseshoe magnet placed adjacent to the Hall-effect probe as shown in Figure 38. The magnet was used to "seed" the breadboard system by setting up a constant value (dc) magnetic field near the blades to be inspected. The magnetometer system detected the movement of the simulated compressor blades fabricated with nonmagnetic materials (copper, aluminum, brass, and stainless steel) and magnetic materials (steel and iron). In the case of the magnetic material blades, the external magnetic field set up by the horseshoe magnet greatly enhanced the sensing of the movement of the simulated blades. For the nonmagnetic material blades, the external magnetic field is required to sense the movement of the simulated blades. The blade movement appears as pulses obtained from the output of the magnetometer each time the simulated blades rotate past the Hall-effect probe.

Next, an experimental investigation was performed to determine if the magnetometer system could detect defects in rotating blades. During this experiment four identical aluminum blades with various defect sizes were mounted on the brass disc. The four blades inspected are shown in Figure 39 and contain the following defects:

(1) Blade No. 1 - None

(2) Blade No. 2 - 0.1 in. x 0.1 in.

(3) Blade No. 3 - 0.2 in. x 0.2 in.

(4) Blade No. 4 - 0.2 in. x 1.2 in.

The magnetometer output pulses obtained for the four blades are shown in Figure 40. These results were obtained with the same test set-up as shown in Figure 38. As can be seen from Figure 40, blade defects appear as variations in the amplitude of the

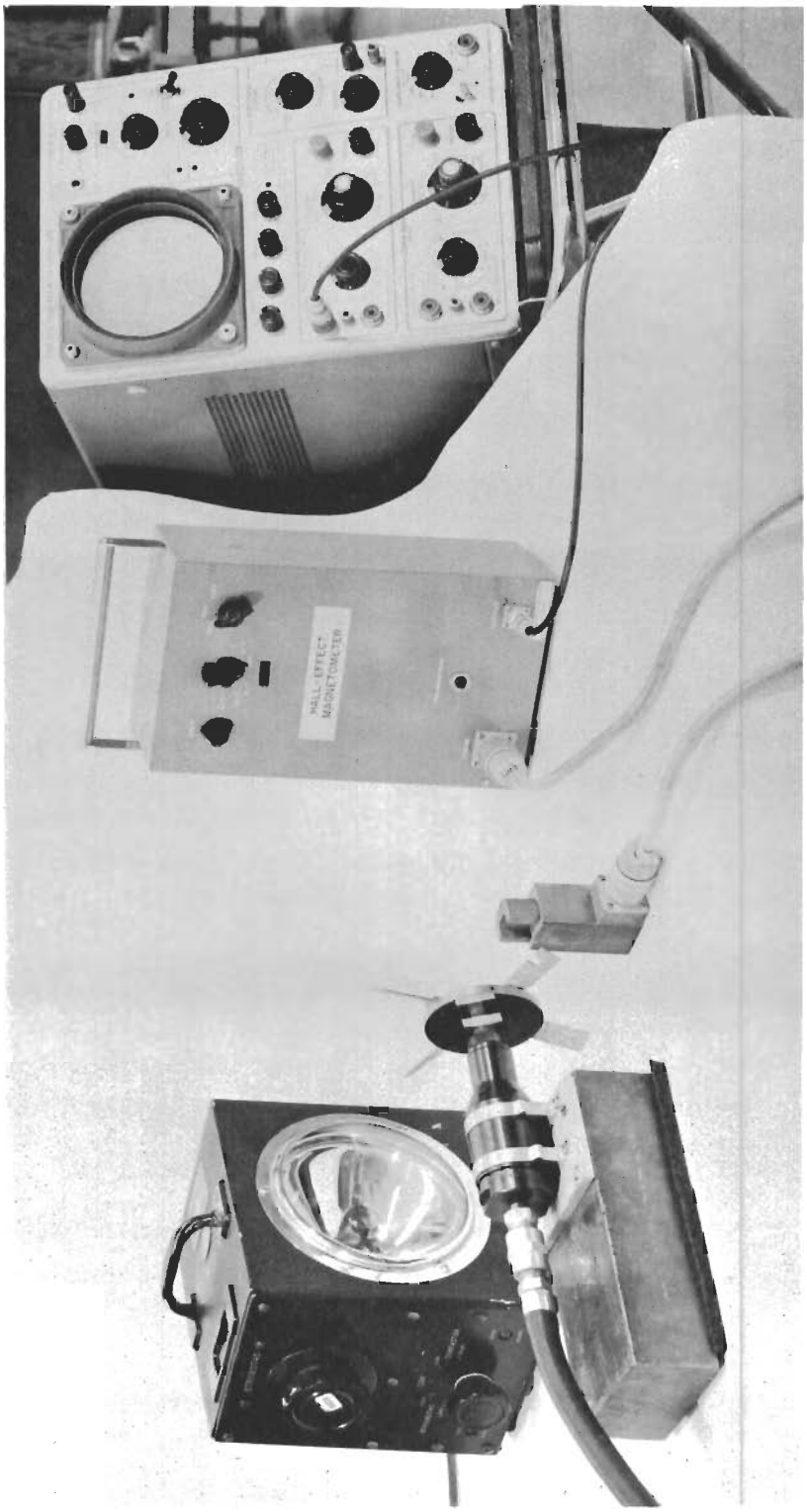

FIGURE 38 HALL-EFFECT MAGNETOMETER INSTRUMENTATION SET-UP

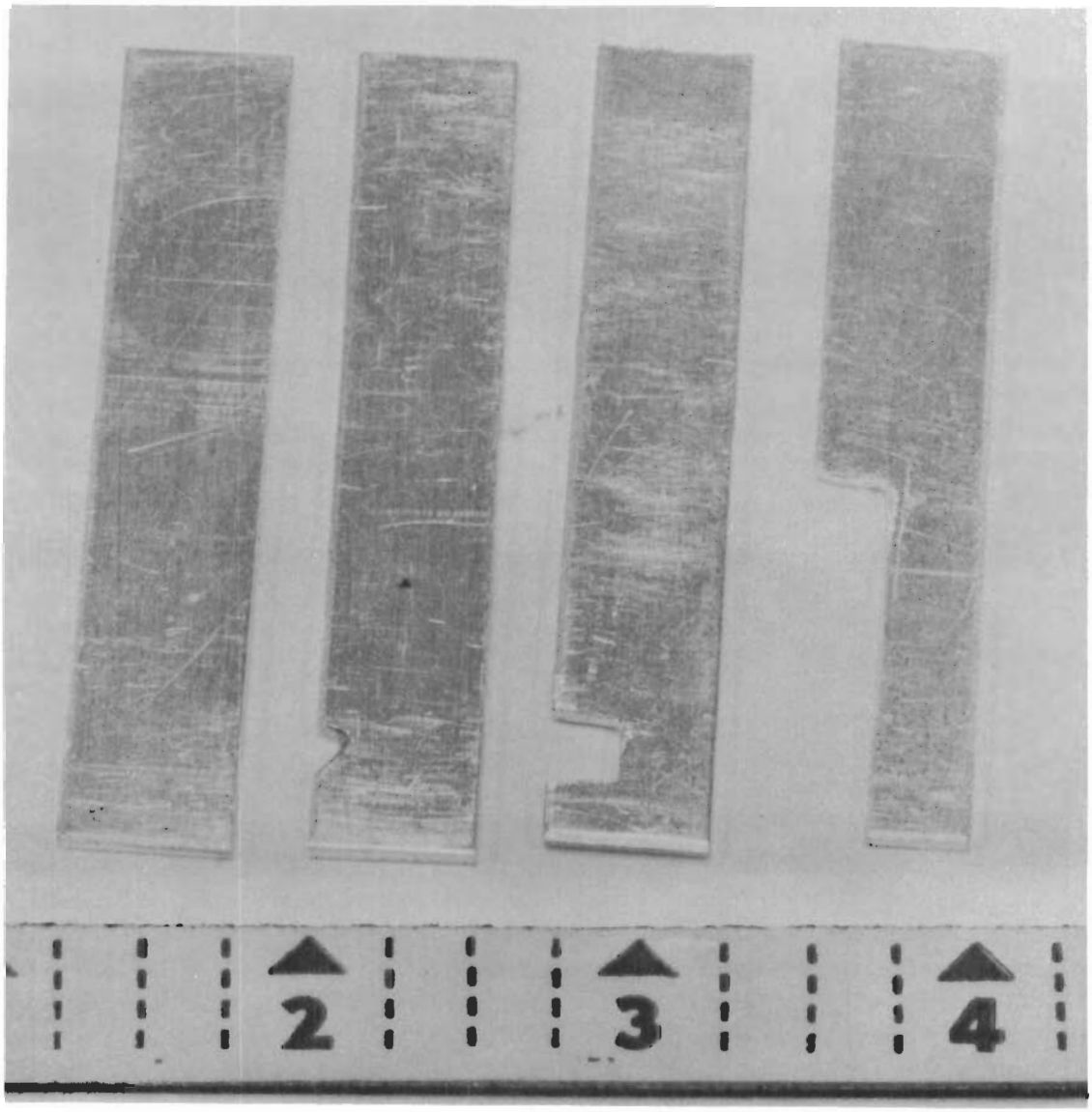

FIGURE 39 SIMULATED ALUMINUM COMPRESSOR BLADES

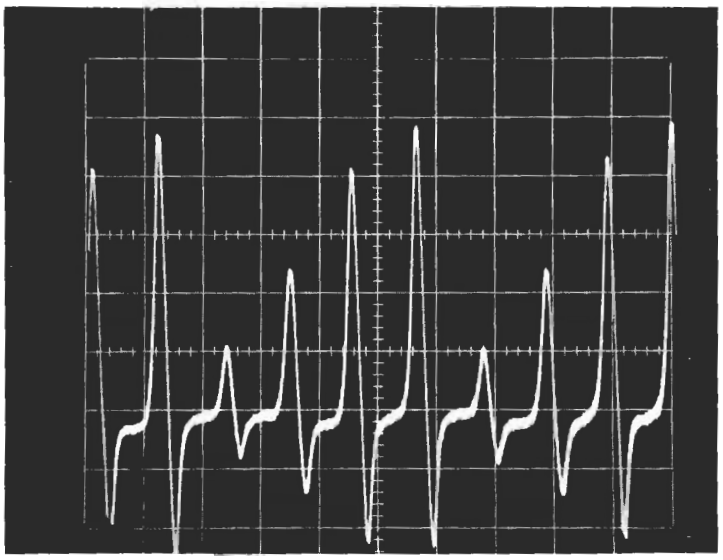

Horiz: 5 msec/cm
Vert: 1 volt/cm

FIGURE 40 MAGNETOMETER OUTPUT PULSES FOR FOUR ALUMINUM BLADES (AIR TURBINE SPEED 1400 RPM)

magnetometer output pulses. The amplitude of the output pulses increases as the size of the defect decreases. The pulse amplitude variation obtained for each of the four blades inspected is given below.

Blade No.	Defect Size	Pulse Amplitude
1	None	5.2 volts
2	0.1 in x 0.1 in	4.5 volts
3	0.2 in x 0.2 in	2.6 volts
4	0.2 in x 1.2 in	1.4 volts

Laboratory tests were performed to determine if the magnetometer system could detect defects in rotating blades constructed of both nonmagnetic and magnetic materials. During this experiment, identical aluminum (nonmagnetic) and steel (magnetic) blades with various defect sizes were mounted on the brass disc. The four blades inspected were twisted to simulate an actual compressor blade (see Figure 41) and contained the following defects:

(1) Blade No. 1 - None

(2) Blade No. 2 - 0.1 in. x 0.1 in.

(3) Blade No. 3 - 0.2 in. x 0.2 in.

(4) Blade No. 4 - 0.2 in. x 1.2 in.

The magnetometer output pulses obtained for the four blades mounted on the brass disc are shown in Figure 42. These results were obtained with the test set-up shown in Figure 38. As can be seen from Figure 42, blade defects appear as variations in the amplitude of the magnetometer output pulses. The amplitude of the output pulses increases as the size of the defect decreases. The pulse amplitude variation obtained for each of the four blades inspected is given below.

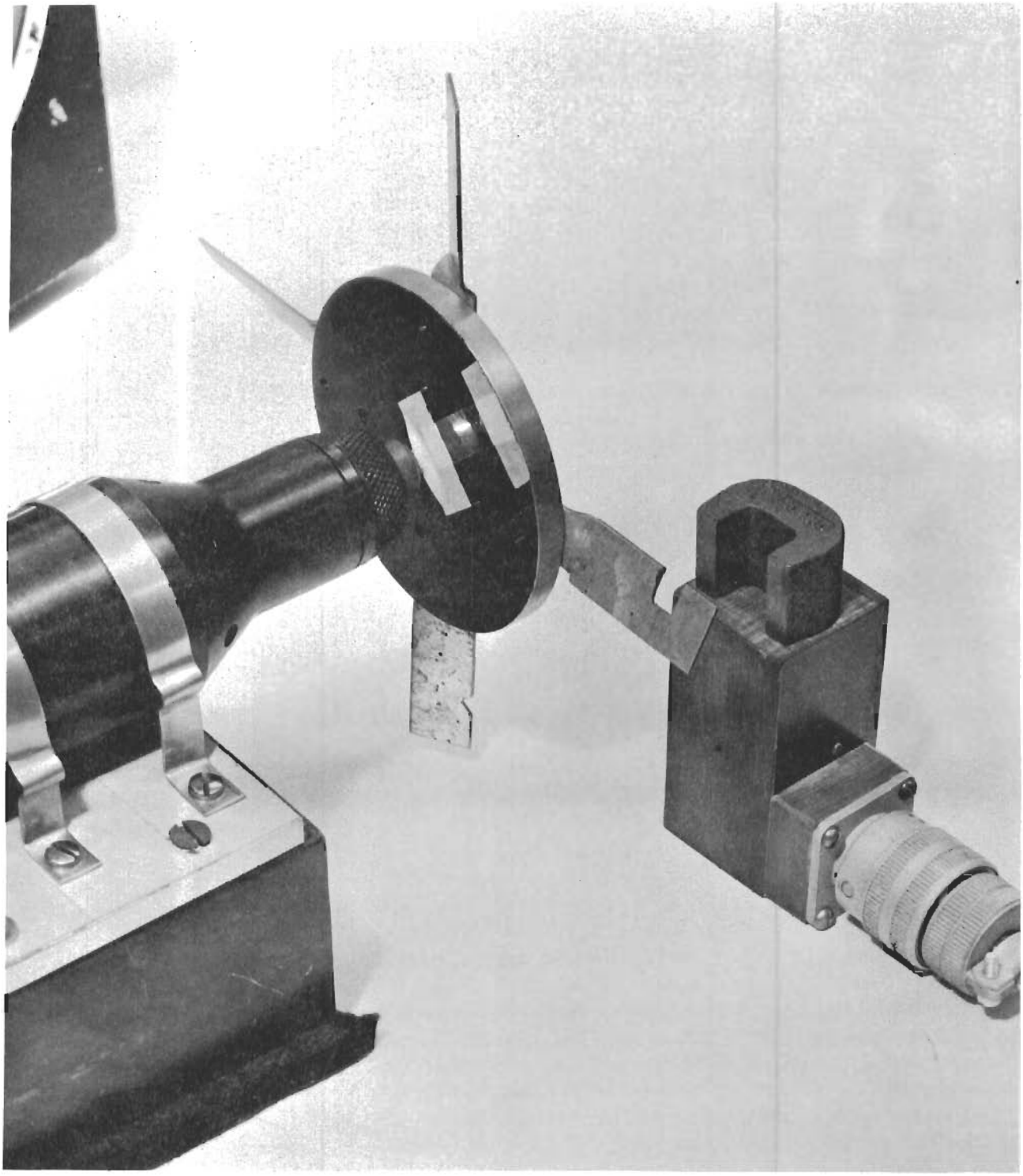

FIGURE 41 HORSESHOE MAGNET PLACED ADJACENT TO HALL-EFFECT PROBE

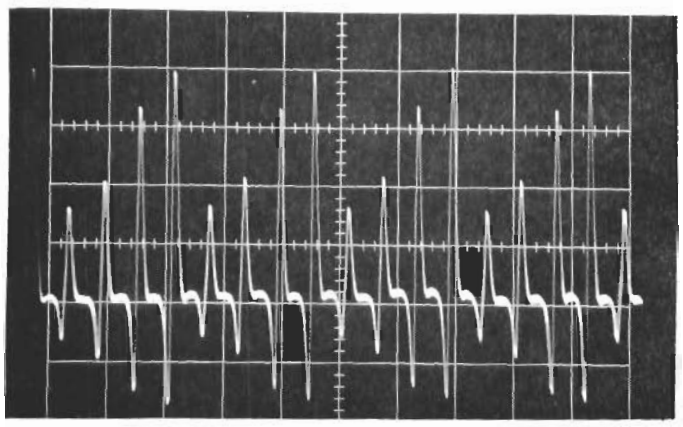

4 3 2 1
Blade Sequence

Horiz: 5 msec/cm
Vert: 1 v/cm

(a) Four Aluminum Blades

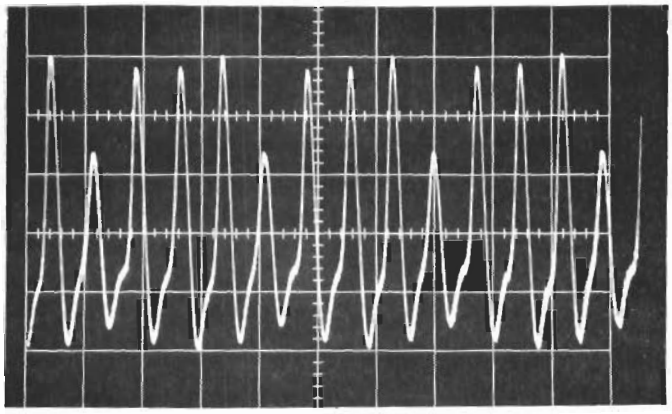

4 2 3 1
Blade Sequence

Horiz: 5 msec/cm
Vert: 1 v/cm

(b) Four Steel Blades

Figure 42 MAGNETOMETER OUTPUT PULSES FOR ROTATING COMPRESSOR BLADES (AIR TURBINE SPEED, 4000 RPM)

Blade No.	Defect Size	Pulse Amplitude Aluminum	Pulse Amplitude Steel
1	None	4.0 volts	3.8 volts
2	0.1 in x 0.1 in	3.4 volts	3.5 volts
3	0.2 in x 0.2 in	2.2 volts	3.6 volts
4	0.2 in x 1.2 in	1.6 volts	2.1 volts

Therefore, it has been demonstrated that with a single Hall-effect magnetometer probe, defects in aluminum and steel blades of the order of 0.1 inch or larger can be detected. It should be possible to obtain similar results with most other nonmagnetic and magnetic metal blades. The size of the defect detectable could be improved by using two magnetometer probes connected in a bridge arrangement and by making an adjacent area to adjacent area comparison.

2.2.3.2 Preliminary measurements, change in remnant fields for foreign object damage -- An investigation was also performed to determine if foreign object ingestion would change the magnetization of a blade in a way which is easily detectable.

A stage 1, J-47 compressor rotor blade was magnetized by placing the blade in an 11,000 gauss magnetic field for approximately five minutes. The magnitude of the magnetic field density, B, at the blade surface was measured at various locations with a gaussmeter. Figure 43 indicates the regions of the blade where the B field was measured, and Table VII lists the magnetic field variations. The results are given before and after the blade was hit with a "foreign object" (hammer) on its leading edge.

Next, two stage 1, J-47 compressor rotor blades were magnetized in a 7,000 gauss magnetic field for approximately two minutes. The magnitude of the magnetic field density at the blade surface was measured at various locations and recorded as with the previous test. The blades were then hit on their leading

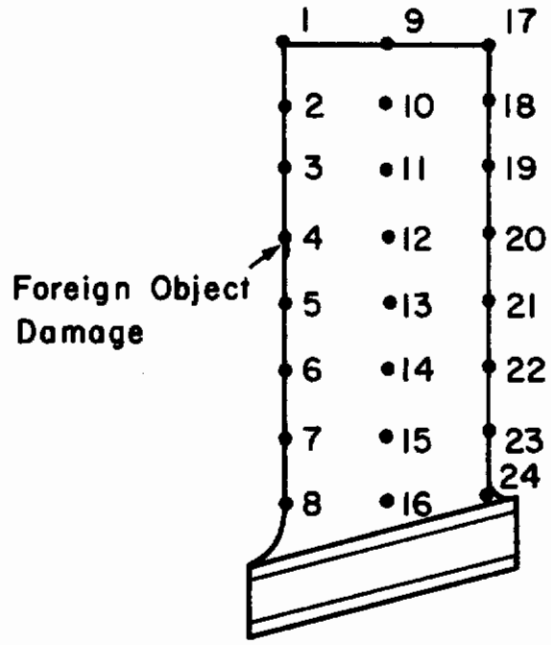

FIGURE 43 B FIELD MAPPING OF FIRST STAGE J-47 COMPRESSOR ROTOR BLADE.

Table VII

COMPRESSOR BLADE MAGNETIC FIELD MEASUREMENTS

Blade Location	Magnetic Field Density, B, (Gauss) Before Damage	After Damage
1	160	42
2	29	16
3	23	16
4	16	16
5	13	14
6	11	14
7	19	15
8	19	16
9	15	15
10	15	15
11	10	10
12	10	10
13	13	14
14	11	14
15	14	14
16	15	15
17	25	15
18	23	15
19	21	15
20	21	15
21	13	15
22	13	15
23	13	15
24	13	15

edge with a NATO 30 caliber round by firing at the blade with a projectile velocity of approximately 2,700 ft/second. After the blade was hit, the blade magnetization decreased to a very low level over the entire blade surface (less than 1 gauss).

These preliminary tests indicate that the magnetization of a blade changes when a foreign object hits the blade. For the case of leading edge damage, the largest changes occur at the leading and trailing edges in the upper third of the blade. These magnetization changes could easily be detected with a Hall-effect magnetometer sensor.

2.2.4 Compressor section measurements

2.2.4.1 Use of remnant field for edge detection of defects -- The magnetic field monitoring techniques that was explored on the J-47 compressor section utilizes the time rate-of-change of a magnetic field (loop sensor) instead of the magnitude of the field as in the case of a magnetometer because of its ease of installation on the compressor. This system is in many respects quite similar to that of the eddy current technique described in Section 2.3. In both cases, the fringing magnetic field is distorted by the blade edge, and this is reflected in the differential output signal of two detectors. The detectors are placed on a strut parallel to the leading edge. In the eddy current system, the change in the fringing field varies the inductance of a parallel resonant circuit to provide an output signal which is magnified by the "Q" of the circuit. In this magnetic field system, only the change in the fringing field due to a possible edge defect appears in the output, and thus any dc bias field does not effect the output. This technique also requires the blades to be uniformly magnetized, such as by a coil around the shroud.

The initial efforts using this technique employed the 0.040 inch gap ferrite detectors used in the eddy current investigations. The differential output of the two detectors was monitored directly using the experimental set-up in Figure 44. The tests were conducted

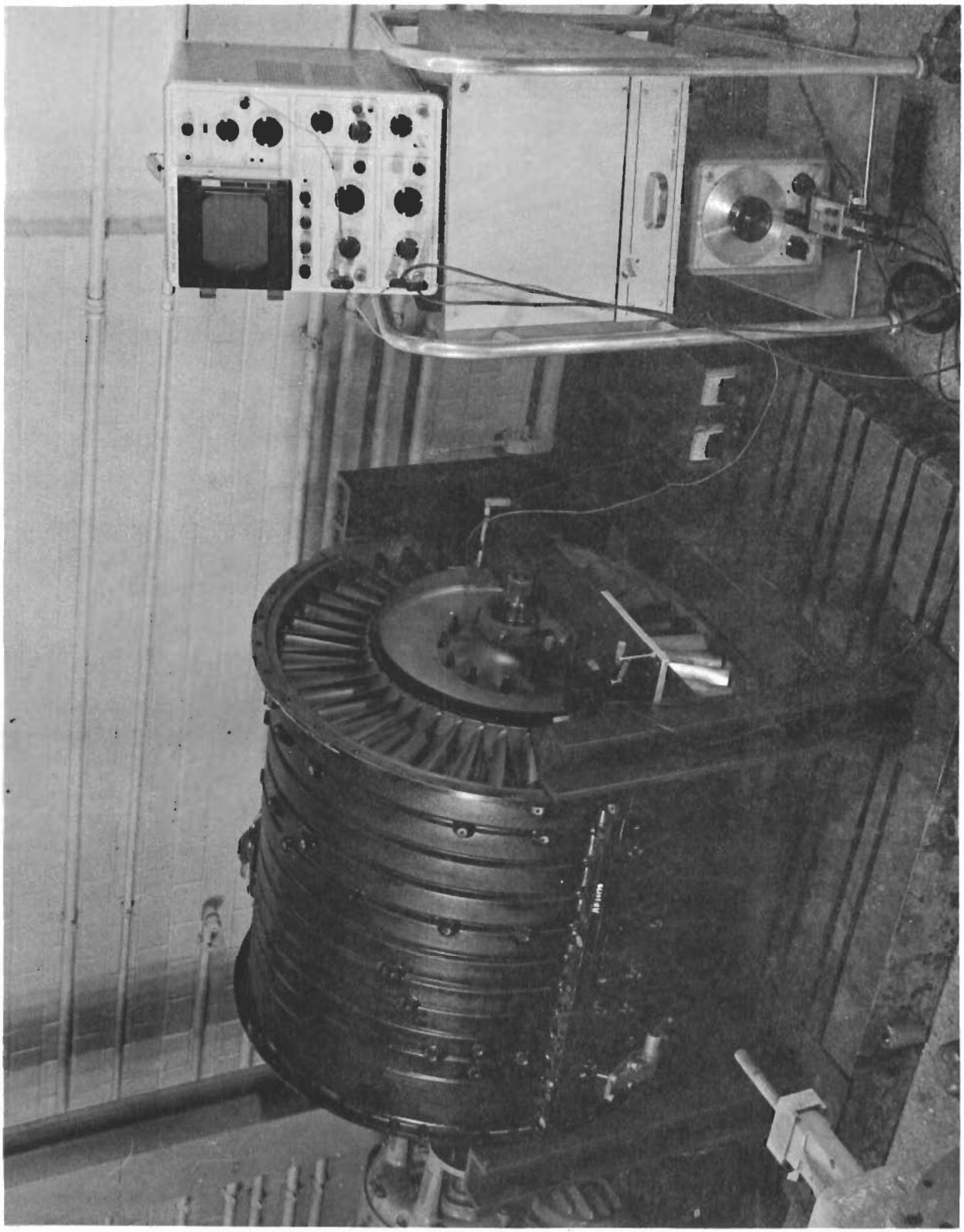

FIGURE 44 MAGNETIC FIELD SYSTEM EXPERIMENTAL TEST SET-UP

on the compressor section as described in Section 3.1. The results of these tests when viewing 1/8 inch and 1/16 inch diameter defects are given in Figures 45 and 46 and are tabulated in Table VIII. The variation in the output for good blades appears to be less than that obtained for eddy current techniques. The abnormally large output seen from blade 11 may be due to its "harder" magnetic characteristics allowing it to retain a larger magnetic moment as the blades were magnetized with a bar magnet.

The use of two detectors in a differential circuit as employed above ideally compensates for blade-to-detector spacing, but at the same time, it amplifies the blade slope variations. In an attempt to compensate for the blade tilt variations, a third detector was employed. In this application, two detectors were connected differentially. The output of this pair would then be proportional to the difference in spacing between each of them and the blade edge. A third detector placed between the above two detectors should then read the average spacing of the two outer most detectors because its blade to detector spacing is the average value of that of the other two detectors. Thus, the differential output of the center detector with respect to the two outside detectors would ideally be independent of blade slope variations. Dynamic tests run on the J-47 compressor, however, did not provide a significant improvement over the two detector system. This discrepency was attributed to slight differences in the detector structures and the blade-to-detector spacing variations.

Another passive monitoring sensor employed is shown in Figure 47. The Comb detector is mounted at an angle of 45 degrees with respect to the blade being scanned such that points along the blade are sequentially scanned as the blade passes over the detector. This concept is attractive in that a linear scan along the blade is automatically converted into a time varying signal. The detector length and angle were chosen such that as one blade leaves the lower end of the detector, the succeeding blade enters the upper end of the detector. Thus, the voltage waveform out of

Defect Diameter = 0.0"

Defect position

Detector Output

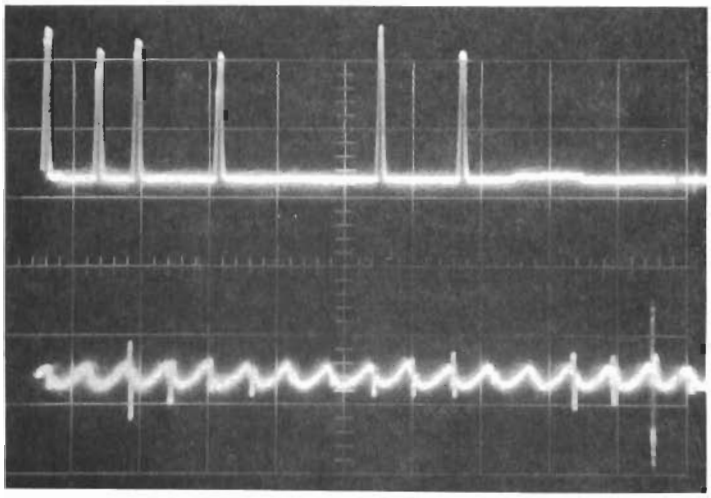

5msec/cm

2m v/cm

Defect Diameter = 0.125"

Defect position

Detector Output

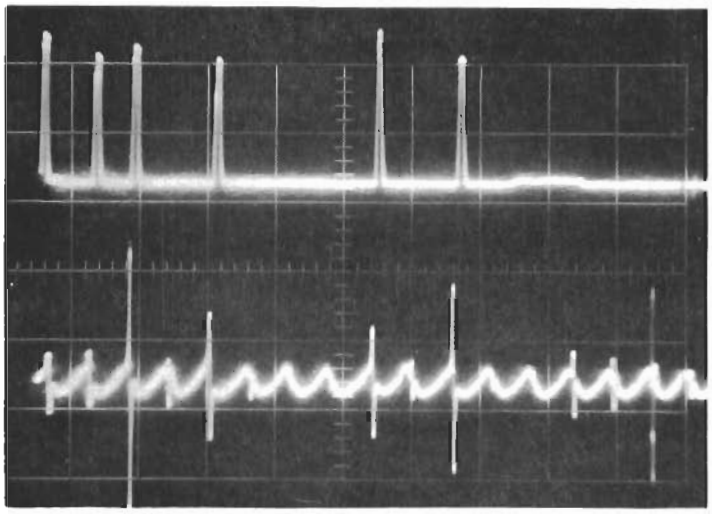

5msec/cm

2m v/cm

Test Condition

Detector Gap = 0.040"
Blade #10 to Detector Spacing = 0.010"
Detector center-to-center spacing = 0.375"

FIGURE 45 MAGNETIC FIELD DETECTOR OUTPUT

Defect Diameter = 0.0"

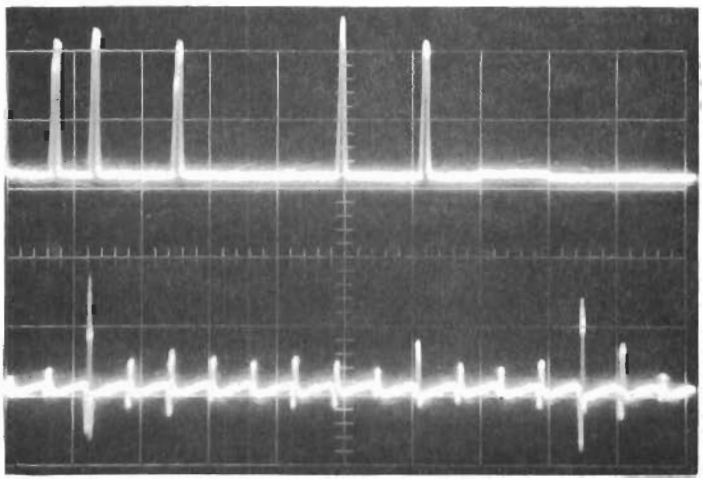

Defect Diameter = 0.062"

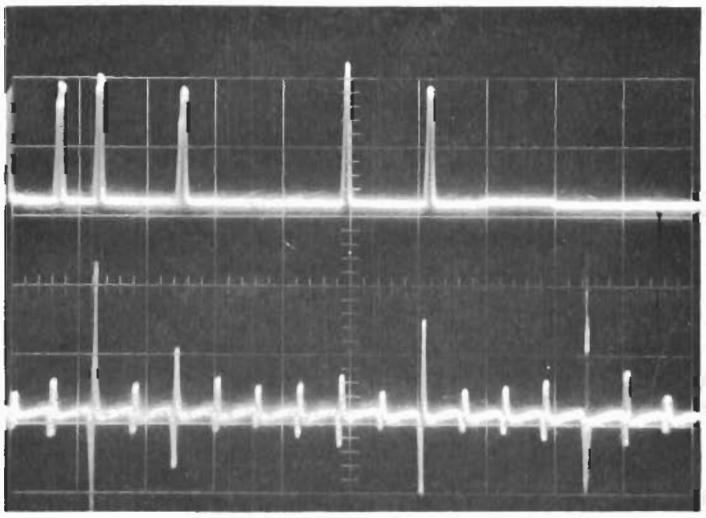

Test Condition

Detector Gap = 0.040"
Blade #10 to Detector Spacing = 0.010"
Detector center-to-center spacing = 0.375"

FIGURE 46 MAGNETIC FIELD DETECTOR OUTPUT

Table VIII

MAGNETIC FIELD TEST RESULTS

Blade Number	Dimension A (mils)	Slope S_{AB} (mils/inch)	Vout (Defect) / Vout (No Defect) 0.125" Defect	0.062" Defect
* 25	10	26.3	2.33	1.5
* 24	4	39.3	2.22	2.0
* 23	36	30.8	3.34	1.7
22	36	28	1.21	1.06
* 21	20	35	3.5	1.74
20	23	30.2	1.0	1.13
19	23	36.6	1.2	1.15
18	9	36.6	1.2	1.10
* 17	21	34.8	3.16	1.15
16	18	34.8	1.08	1.3
* 15	33	37.7	3.86	2.64
14	2	33.8	1.0	1.0
13	17	33	1.11	1.7
12	23	33	1.15	1.25
11	36	33	1.06	1.57
10	48	28	1.15	1.0
9	17	33	1.0	1.45

* Blades Containing Defects

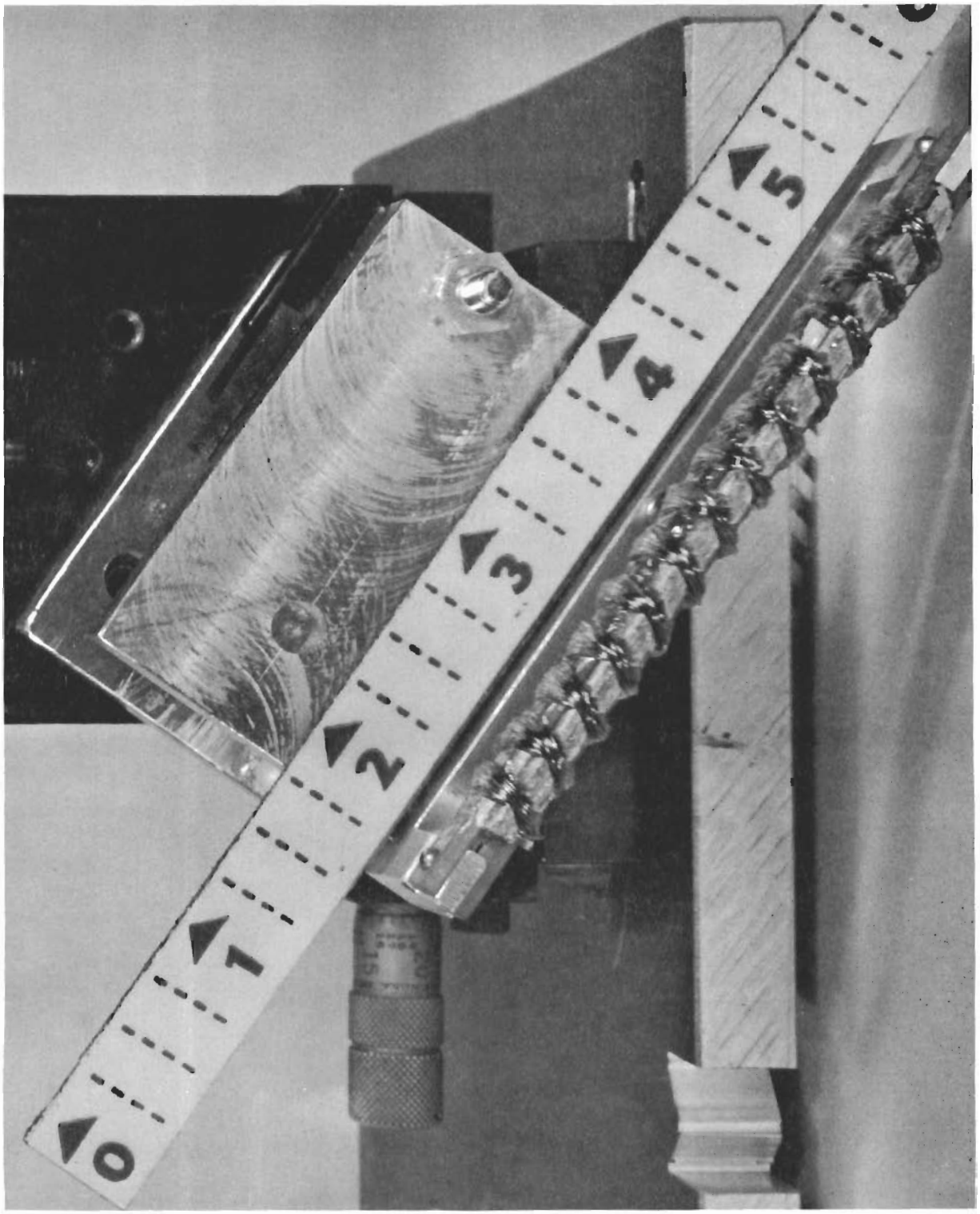

FIGURE 47 MAGNETIC FIELD COMB DETECTOR

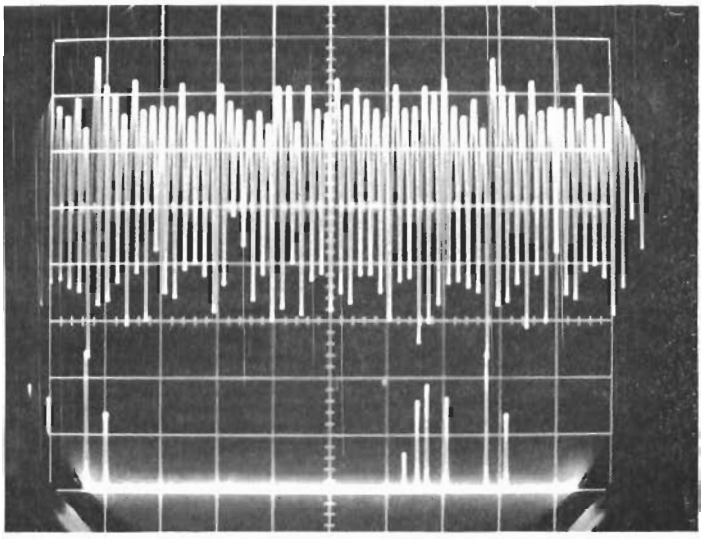

a. 0.125" Defect
20 msec/Div.

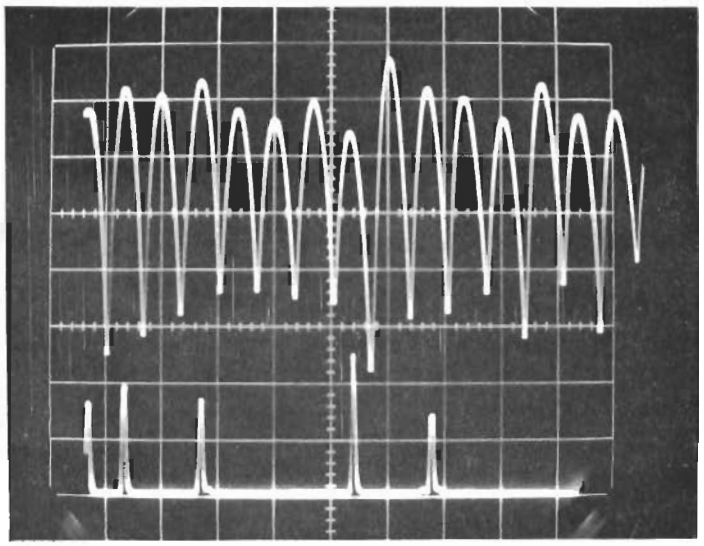

b. 0.125" Defect
5 msec/Div.

FIGURE 48 COMB DETECTOR OUTPUT FOR 0.125" DEFECT

the detector corresponds to a series of 2.5-inch segments of the blade leading edge. The results of this technique are seen in Figure 48. The defective blades in the upper photograph are seen to be indistinguishable from the other blades. An examination of the lower photograph reveals that the detector output is a function of the gross magnetic field surrounding the blade. Thus, the perturbation of the blade's magnetic field due to a defect is merely added to that obtained from the remainder of the detector and is thus masked by the gross field of the blade.

2.2.4.2 Tip detection of remnant magnetic field using actual compressor blades -- The effect of foreign object ingestion on blade magnetization was explored on the J-47 compressor section by utilizing the Hall-effect magnetometer. The sensor system consisted of the Hall-effect magnetometer and an oscilloscope for displaying the output signal. The sensor consisted of a Hall-element without flux collectors mounted in a plexiglass holder which was screwed into a hole in the compressor enclosure (see Figures 49 and 50). This hole was drilled above the tips of the first stage compressor rotor blades. Each of the stage 1 rotor blades were magnetized with a bar magnet. The magnetized blades appear as a pulse at the output of the magnetometer each time a blade rotates past the Hall-effect probe as shown in Figure 51. The results are also given after one of the blades was hit with a light ball-peen hammer on its leading edge to cause a visible (about 0.015 inch) defect.

As was demonstrated during the preliminary laboratory tests described in section 2.2.3.2, the magnetization changes when a foreign object hits the blade. Here, the hit blade is indicated by the absence of a pulse. These tests indicate that the reduction in pulse amplitude is a function of the size of the object and also the velocity with which the object hits the blade. It was also demonstrated that a "FOD hit" (as simulated by a light ball-peen hammer) of sufficient force to cause a noticeable (0.015 inch) defect radically demagnetized the blade. This demagnetization

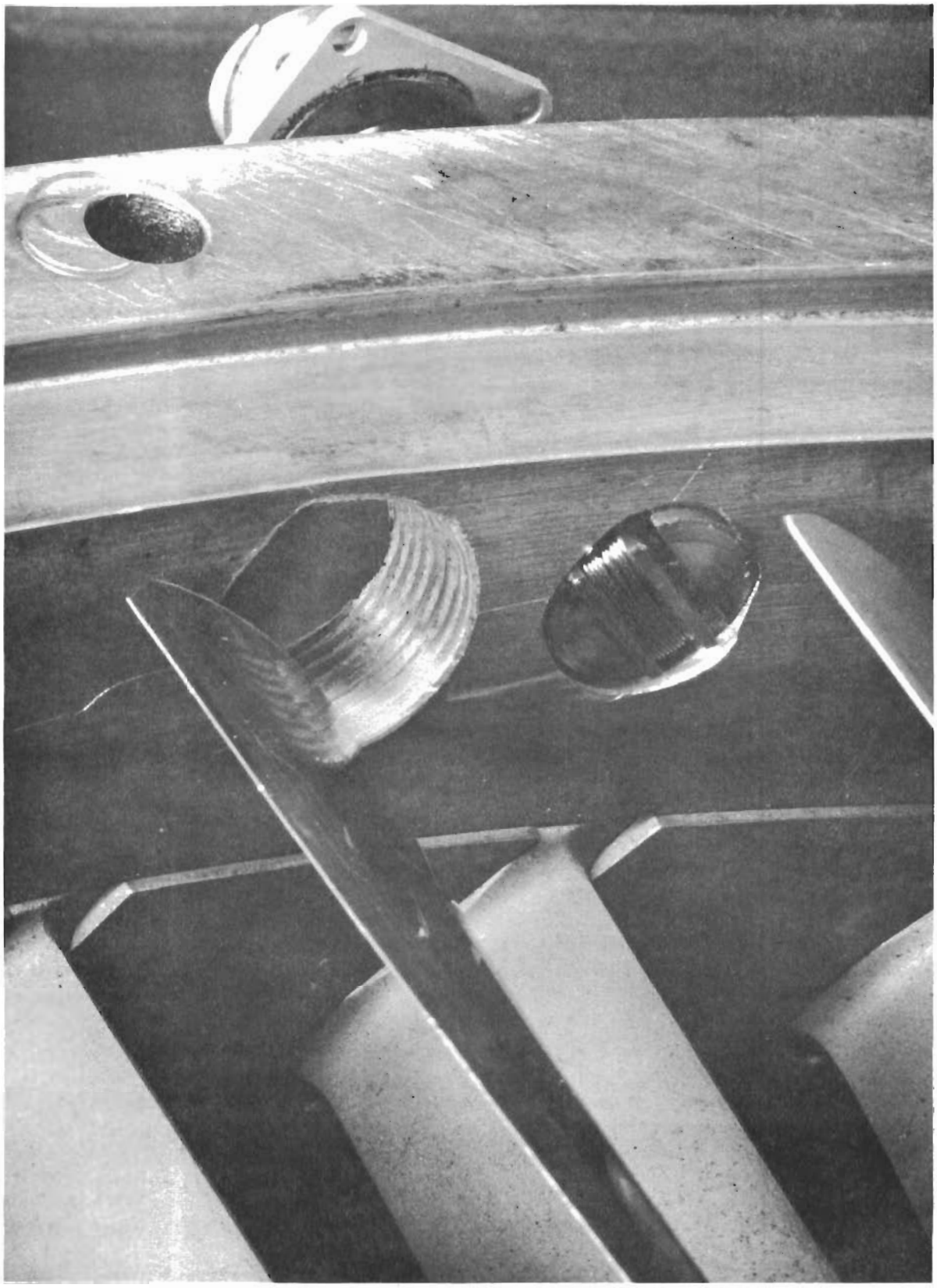

FIGURE 49 HALL ELEMENT SENSOR

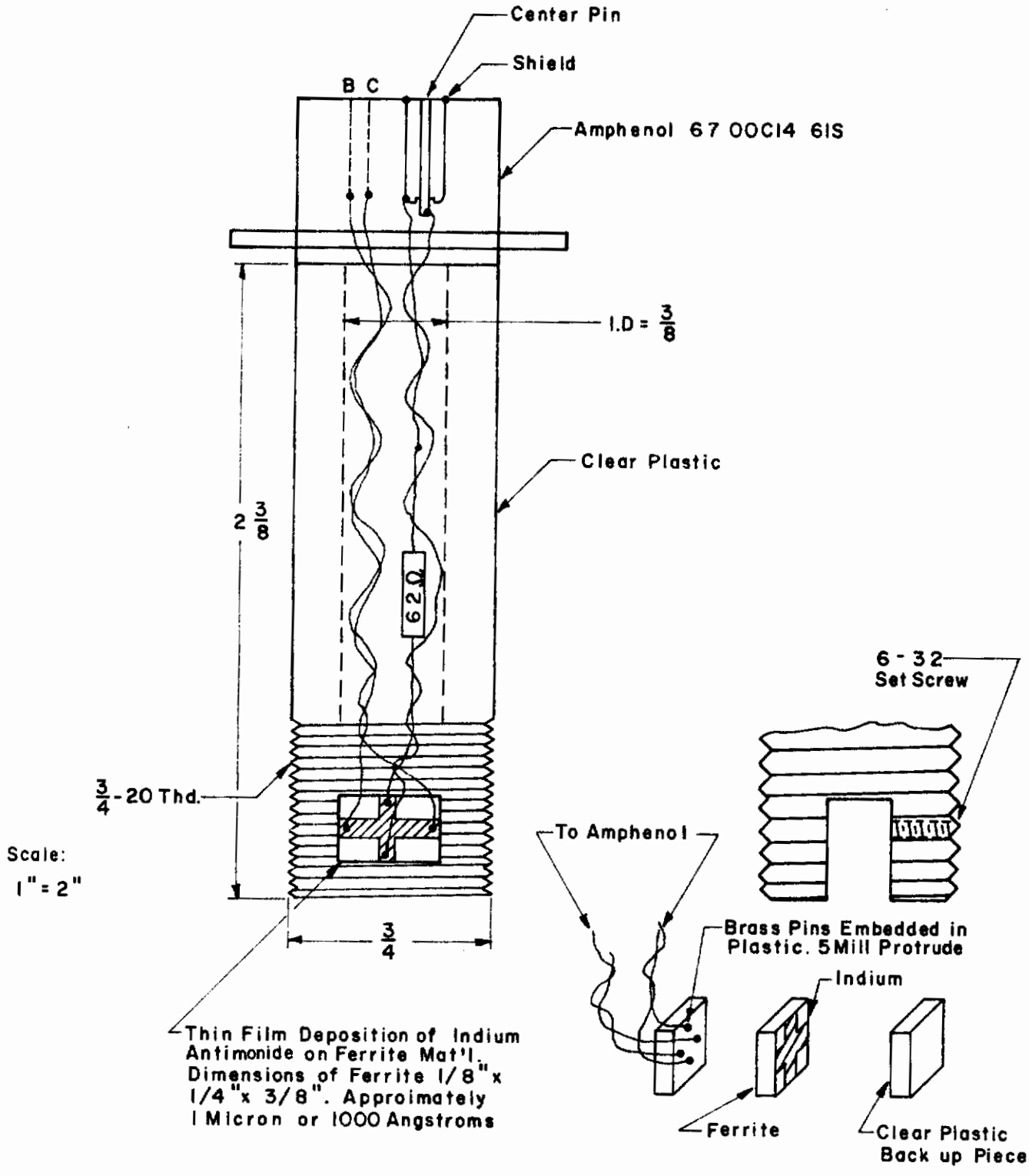

FIGURE 50 HALL ELEMENT SENSOR CONSTRUCTION

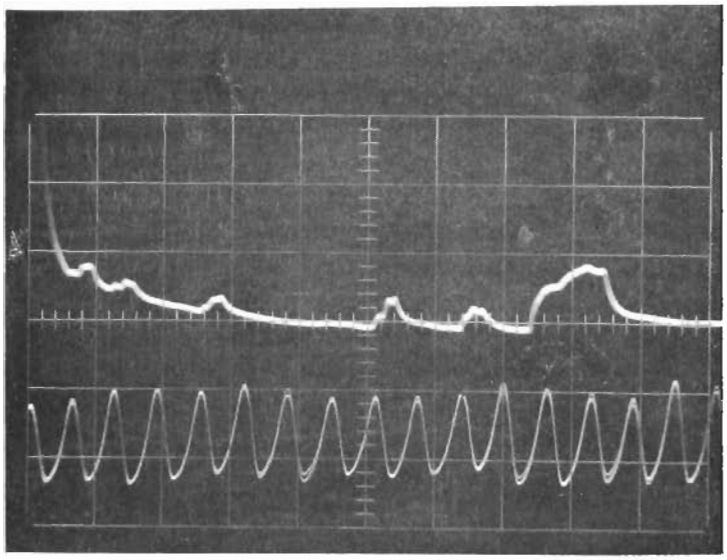

a. All Compressor Rotor Blades Magnetized

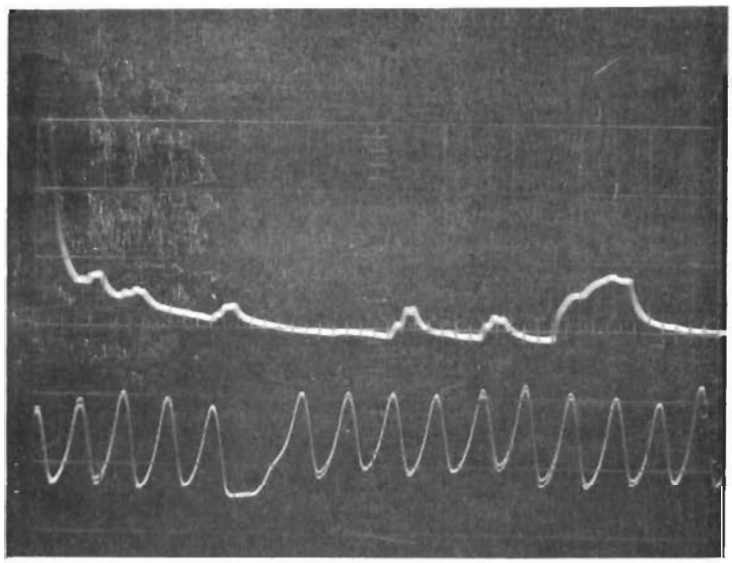

b. Fifth Blade Past Trigger Signal Hit with Hammer

FIGURE 51 BLADE MAGNETIZATION TEST ON J-47 COMPRESSOR SECTION

was easily detectable on the actual compressor section.

Before the feasibility of this technique can be shown, it also had to be demonstrated that magnetized compressor blades remain magnetized after running the aircraft turbine engine under normal operating conditions. Preliminary tests were performed on the J-47 compressor section in order to demonstrate this assumption. A number of stage 1, compressor rotor blades were magnetized and monitored with the Hall-effect probe while running the compressor at various speeds up to 1800 rpm. No noticeable change in pulse amplitude was obtained for speeds up to 1800 rpm. The next step was to demonstrate this on a complete aircraft turbine engine running at maximum power in a test cell.

2.2.4.3 Field tests -- Field tests were performed at Wright-Patterson Air Force Base, Ohio, in order to demonstrate that magnetized compressor rotor blades retain their magnetization even if the turbine engine is operated at maximum power. This investigation was performed on a complete J-85 turbine engine installed in a test cell. The sensor system consisted of a Hall-effect magnetometer and an oscilloscope for displaying the output signals. The sensor consisted of a Hall-element mounted in a plexiglass rod which was mounted above a 0.5-inch hole drilled in the compressor enclosure above the tips of the stage 1 compressor rotor blades (see Figure 52). After each of the stage 1 compressor rotor blades were magnetized with a bar magnet, the engine was motored at approximately 200 rpm and the sensed magnetic field time-history was obtained. The magnetic field time-history consisted of output pulses of approximately the same amplitude for each of the 31 stage 1 rotor blades. The magnetic field waveform was also obtained after the engine was operated during two operational cycles.

During the initial test, the engine was first idled at 12,230 rpm for eight minutes, next cruised at 14,900 rpm for eight minutes, and then run at maximum power (16,550 rpm) for five minutes. During the next test, the engine was first idled for

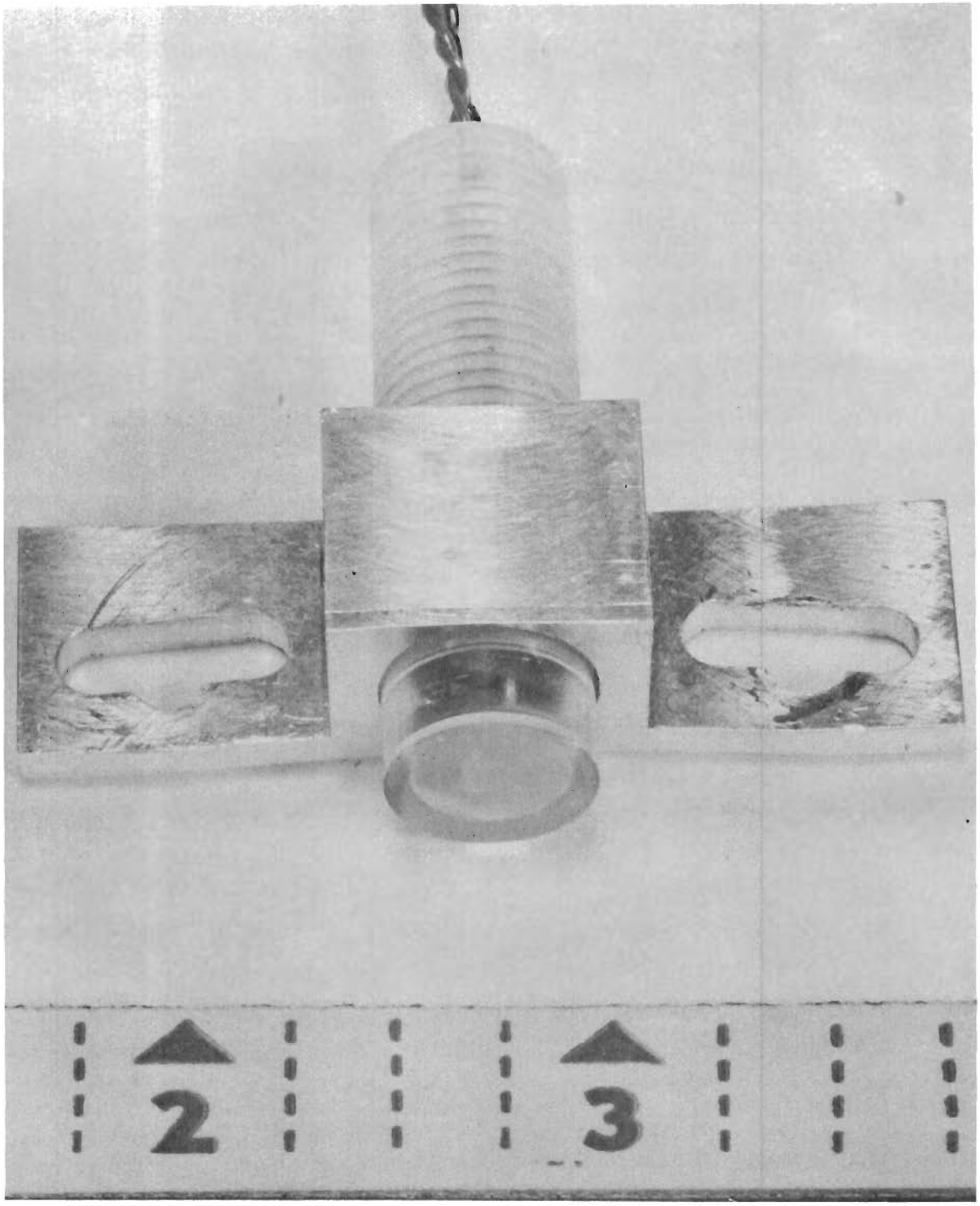

FIGURE 52 HALL ELEMENT SENSOR

three minutes and then accelerated as rapidly as possible to maximum power where it was operated for three more minutes. No noticeable change in the magnetic signatures was obtained after each of these test runs.

2.2.5 Implementation of remnant magnetic field detection system -- A possible signal processing system which could be used with the Hall-effect sensor to monitor the effect of foreign object ingestion on blade magnetization is given in Figure 53 . Waveforms at various points of the system are presented in Figure 54 . The sensor consists of a Hall-element in a holder mounted in a hole above the blade tips in the compressor enclosure similar to the sensor shown in Figure 49. The sensor is initially positioned mechanically to provide a maximum output signal for a normally magnetized blade. The sensor output V_A is amplified, detected, and shaped resulting in signal V_B (see Figure 54). Signal V_B is applied to the inputs of two integrator circuits with time constants T_1 and T_2 where $T_1 >> T_2$ resulting in output waveforms V_C and V_D respectively. Signals V_C and V_D are applied to the two inputs of a high gain differential amplifier which provides a negative pulse V_E whenever a pulse is missing at point B (blade demagnetized). This negative pulse triggers a flip-flop from a 0 state to a 1 state and provides a positive output signal V_F (output 2) which indicates that a foreign object of sufficient force to cause a noticeable defect has been ingested. The flip-flop output (point F) and monostable multivibrator output (point B) are applied to the inputs of an AND gate which provides pulse signals V_G that are gated on and off each time a Hall sensor output pulse is below the predetermined threshold level (blade hit). The gated pulses drive a counter which provides output pulses inversely related to the number of hit blades. With additional signal processing, this system could provide digital outputs proportional to the number of hit blades as well as the location of the hit blades.

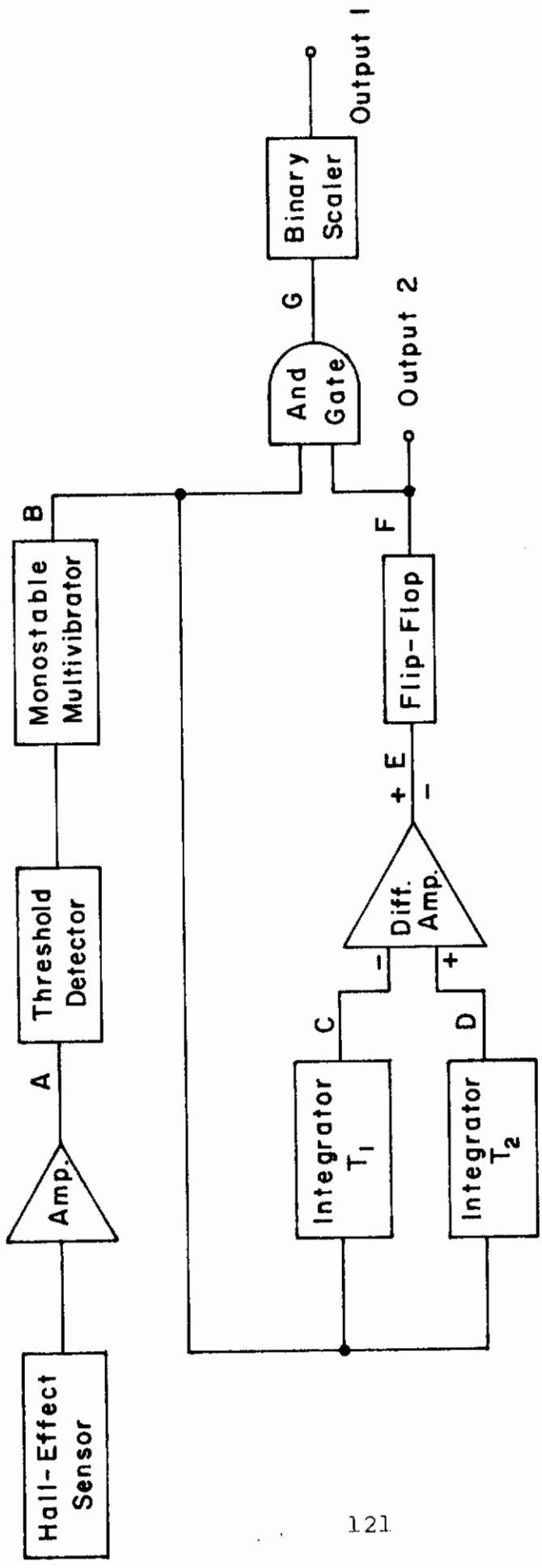

FIGURE 53 PROPOSED REMNANT MAGNETIC FIELD PROCESSING ELECTRONICS

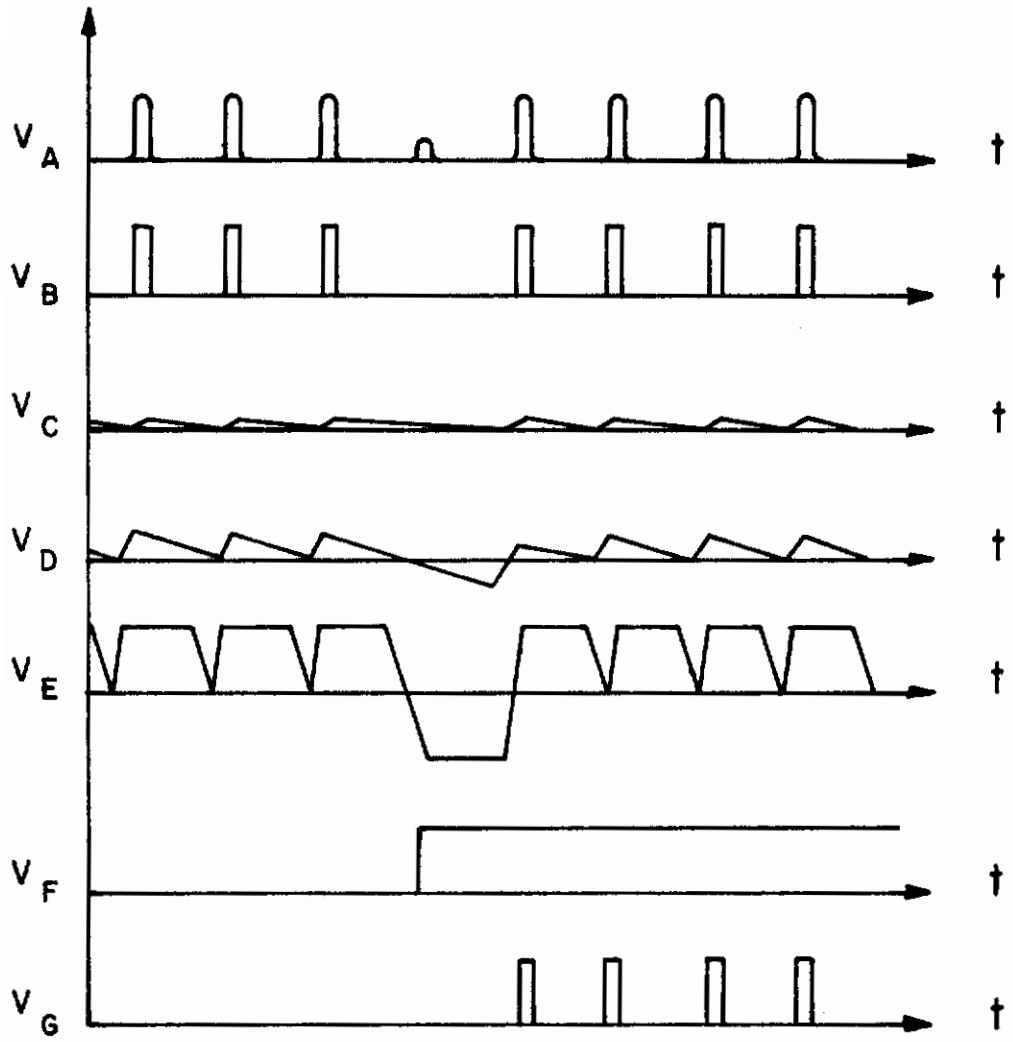

FIGURE 54 REMNANT MAGNETIC FIELD PARAMETER WAVEFORMS

The proposed signal processing system uses in general commercially available circuits. In fact many of the circuits proposed are available in integrated circuit form occypying the volume of a single transistor. The system given in Figure 53 is not necessarily the optimum system but only one suggested system.

2.2.6 Conclusions of magnetic field techniques -- It has been demonstrated that when the compressor rotor blades in an aircraft turbine engine containing magnetic material blades have been magnetized, they retain their magnetization under normal operating conditions, unless a foreign object has been ingested by the engine. If an object is ingested into the compressor section, the hit blades will have a reduction in pulse amplitude which is a function of the size and velocity of the object. Simulated foreign object damage hits of sufficient energy to cause 0.015-inch defects appeared to be clearly resolvable.

Detection of leading edge defects by noting changes in the remnant magnetization by some type of detectors placed on a strut parallel to the leading edge appeared to be marginal. Minor variation in magnetic hardness along the leading edge of a normal blade is always possible, since this is not controlled during manufacture. The normal axial displacements and tilts of the blades appear to contribute greatly to the unreliability of this technique. While not tested on the J-47 compressor because of the high level of remnant magnetization, similar conclusions appear possible for the "seeded" magnetic field techniques described in Section 2.2.3.1.

2.3 Eddy Current Techniques

2.3.1 Introduction -- The use of eddy current phenomena in the detection of foreign object damage in compressor rotor blades may be implemented in several ways. In general, a current is induced in the surface to be inspected and the reflected impedance of the drive coil or the voltage induced in the pickup coil is correlated with surface defects, surface geometry, material conductivity and permeability, and coil-to-surface spacing. Since only surface defects are to be monitored, the eddy current technique used must minimize the influence of the other parameters. In the case of blade edge inspection, the spacing and geometry variations as a function of distance from the blade root as well as from blade-to-blade impose severe restrictions on the eddy current detection of small blade edge defects.

Laboratory tests on simulated compressor blades containing calibrated defects were used to obtain an optimum detector geometry and circuit. This detection system was then employed on an actual J-47 compressor section to monitor edge defects under operating conditions. These tests indicated the detection of 1/8 inch diameter defects was not possible due to normal blade tilt and spacing variations. Subsequent static tests were performed on the compressor to define the detector parameters required as a function of minimum detectable defect size and maximum blade parameter variations. Due to the wide variation of blade edge parameters, other locations with more consistant geometries were sought. Normal variations of blade tip parameters are more closely controlled, so tests using the eddy current detection scheme were implemented on the blade tip. The results of these tests appear quite promising to detect evidence of significant FOD or fatigue cracks, but do not provide a unique indication of defect size and position.

2.3.2 Parameter optimization -- An important eddy current parameter is the choice of eddy current frequency to be employed. The choice of operating frequency is determined by two constraints.

One constraint is the skin depth, which is the depth of penetration of the eddy current in the blade edge. For maximum sensitivity, the skin depth should be, at most, equal to the minimum defect depth to be detected. The second factor influencing the frequency of operation is the required system bandwidth, which is proportional to the speed of operation of the aircraft turbine engine. An estimate of the system bandwidth can be obtained by considering the time required for a point on the tip of the compressor blade to transverse a 1/16-inch detector. In the case of the J-47 turbine engine this time is 0.040/rpm seconds. Thus, operation at a motoring speed of 1000 rpm yields 40 μ seconds observation time, while operation at an idle speed of 5000 rpm yields 8 μ seconds observation time. This requires the use of eddy currents whose frequency spectra are in the range of 1 to 10 MHz. Since the skin depth is inversely proportional to the square root of the frequency, conductivity, and permeability of the blades, this factor will be a function of the particular blades used. Calculations using representative materials indicate that the skin depth will be below 0.010 inch for these frequencies.

The second area of optimization in the development of an eddy current sensor is the coil geometry. As with optical inspection techniques, the minimum detectable defect is directly proportional to the viewing aperature of the detector. One means of attaining a small viewing aperature involves using a small coil of large diameter wire within a copper cylinder having a small hole at the viewing end as shown in Figure 55. This radiating coil is then pulsed with microsecond pulses of high currents resulting in a sharply defined magnetic field. This pulsed technique was rejected over continuous current techniques due to the added synchronization problems. Although the use of a pulsed technique would work for sine wave excitation, the losses associated with the drive coil make it very inefficient. Therefore, in an attempt to define a relatively small viewing aperature, the ferrite structures of Figure 56 were employed.

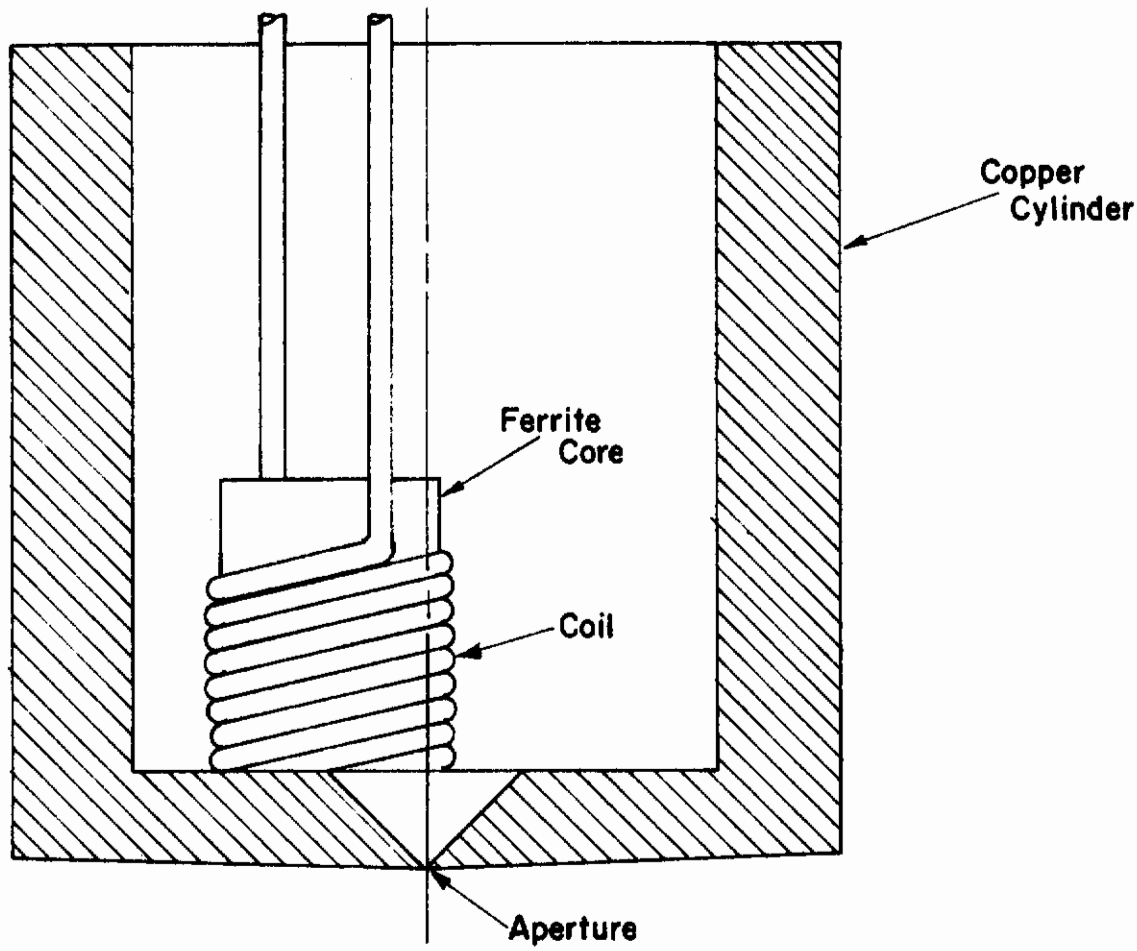

FIGURE 55 EDDY CURRENT MASKING TECHNIQUE

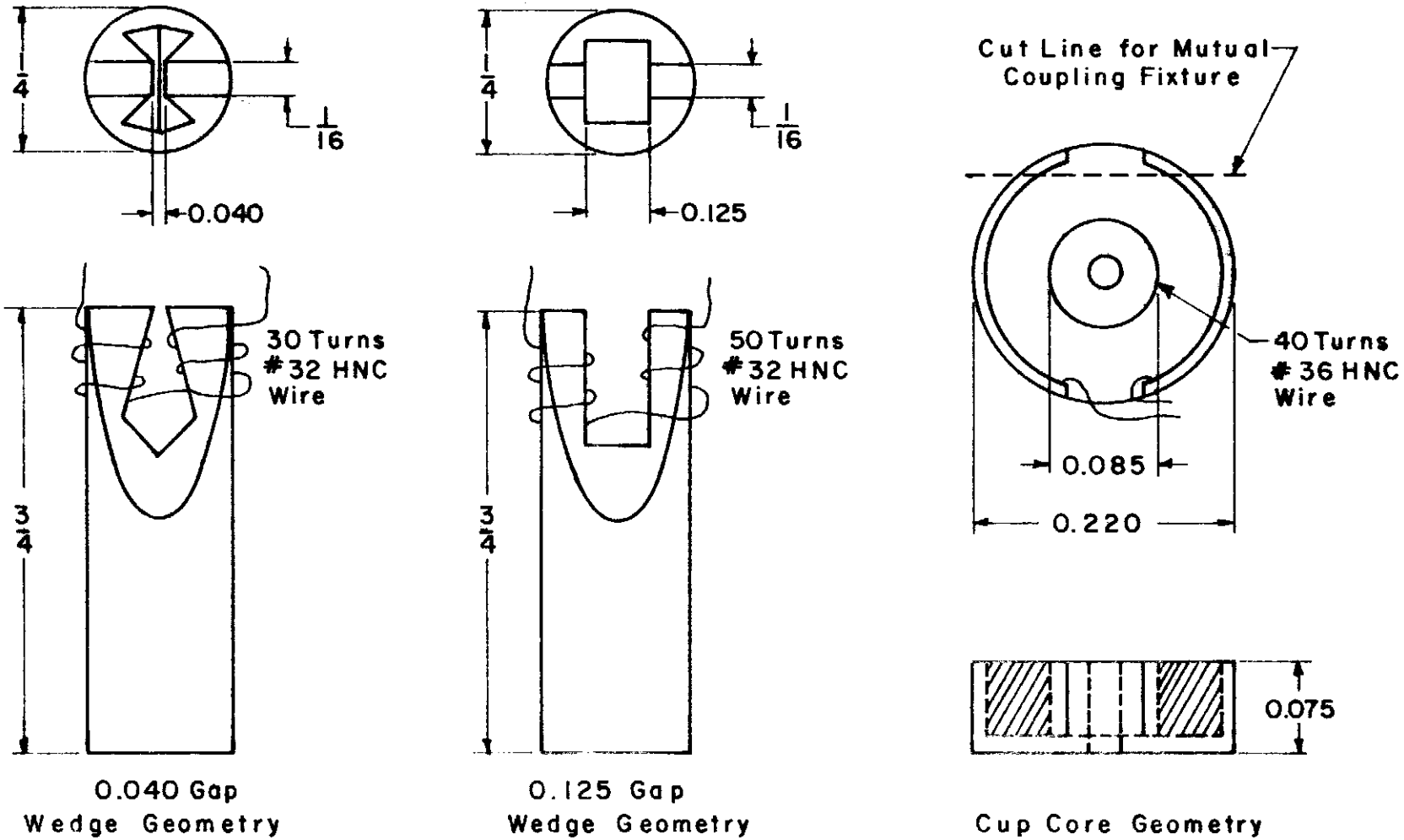

Mat'l: Indiana General CF-501

Mat'l: Seimens Type
B65501

FIGURE 56 FERRITE DETECTOR STRUCTURES

In order to obtain a quantitive evaluation of these detectors, tests were performed on simulated compressor blades fabricated from 1.5 by 5-inch sheets of 0.025 inch and 0.064 inch aluminum and 0.040 inch steel. Semicircular defects varying from 1/16 inch to 1/4 inch in diameter were drilled in the blade edges. Static evaluation of the ferrite detectors with respect to defect size, ferrite geometry, and blade-to-detector spacing was performed after mounting the detectors in the test fixture in Figure 57. A typical set of results using 0.064 inch aluminum is seen in Figure 58. Here, the coils were used in the parallel resonant bridge circuit of Figure 59. This bridge circuit was balanced by varying the relative current drive and resonant frequency of the arms with no blade present. The results of Figure 58 indicate a substantial gain in sensitivity via the use of a wedge geometry over that of a cup-core geometry. The increased sensitivity is due to two factors. First, the wedge geometry provides a magnetic field concentration in the area of the blade edge. Thus, a given defect affects a greater percentage of the total magnetic field. Second, the use of a smaller air gap allows a higher inductance, and thus, an increased Q in the resonant circuit. As might be expected, an optimum air gap exists for the wedge geometry. In this case, a trade-off exists between the minimum detectable defect, which places an upper bound on the gap size, and the maximum detector-to-blade spacing which determines a lower bound on the air gap.

The use of eddy currents to detect defects can be implemented through monitoring the mutual coupling between a drive and pickup coil, the impedance reflected into the drive coil, or a combination of both of these techniques. In an attempt to optimize the detection system, both the mutual coupling and the reflected impedance techniques were investigated. The test fixture used to evaluate the mutual coupling technique is shown in Figure 60. In order to minimize the stray coupling between the drive and pickup coils, pairs of cup cores as shown in Figure 56 were machined

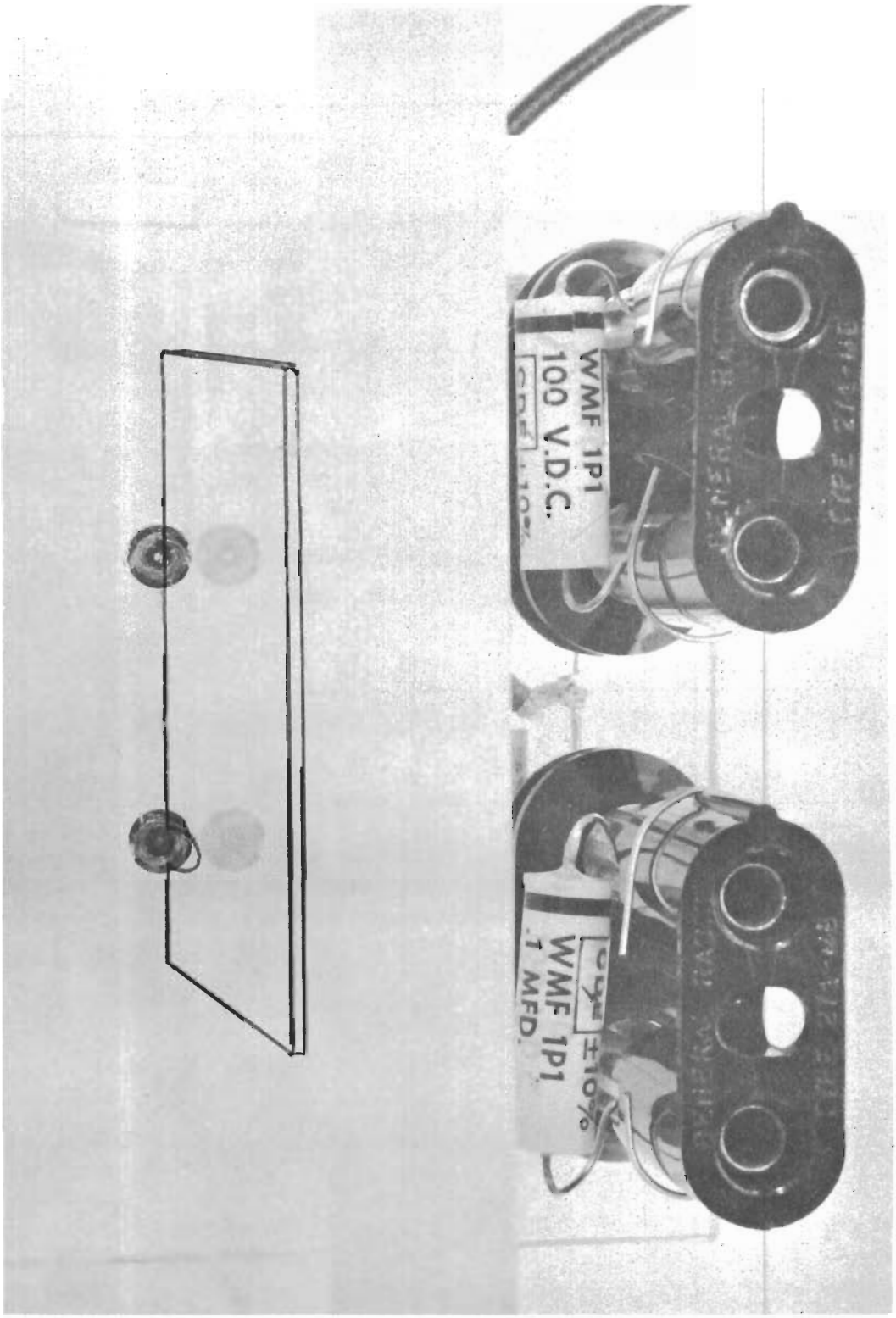

FIGURE 57 RESONANT BRIDGE TEST FIXTURE

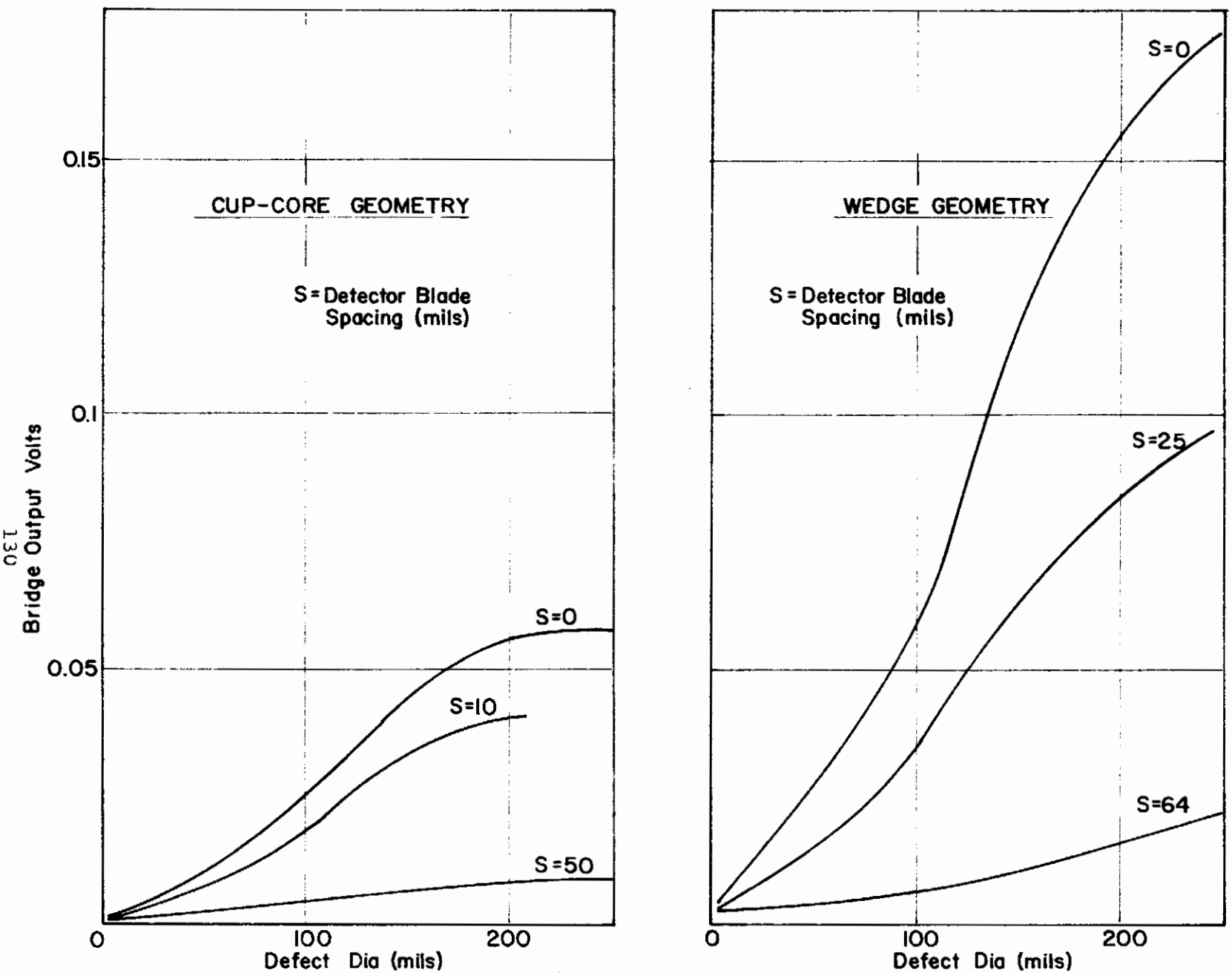

FIGURE.58 RESONANT BRIDGE OUTPUT AS A FUNCTION OF DEFECT DIAMETER FOR 0.064" ALUMINUM & 70 KHZ DRIVE

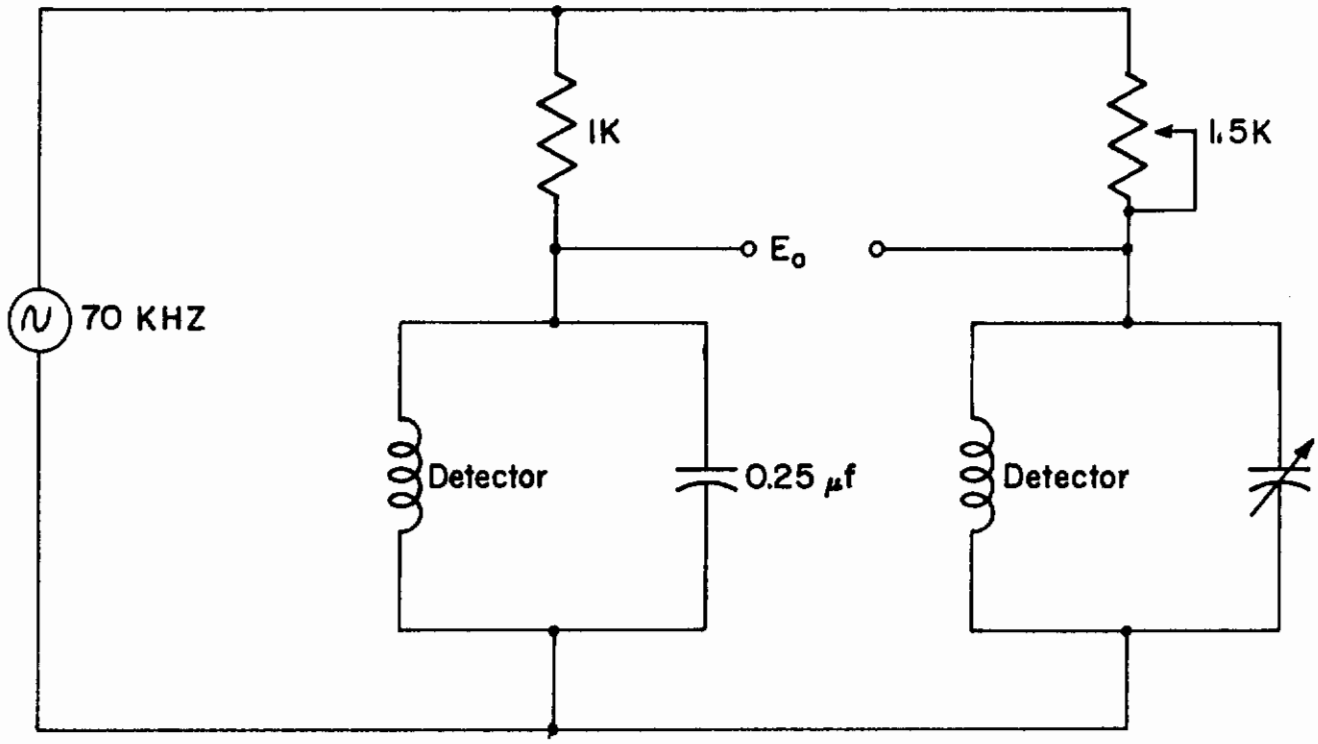

FIGURE.59 RESONANT BRIDGE CIRCUIT

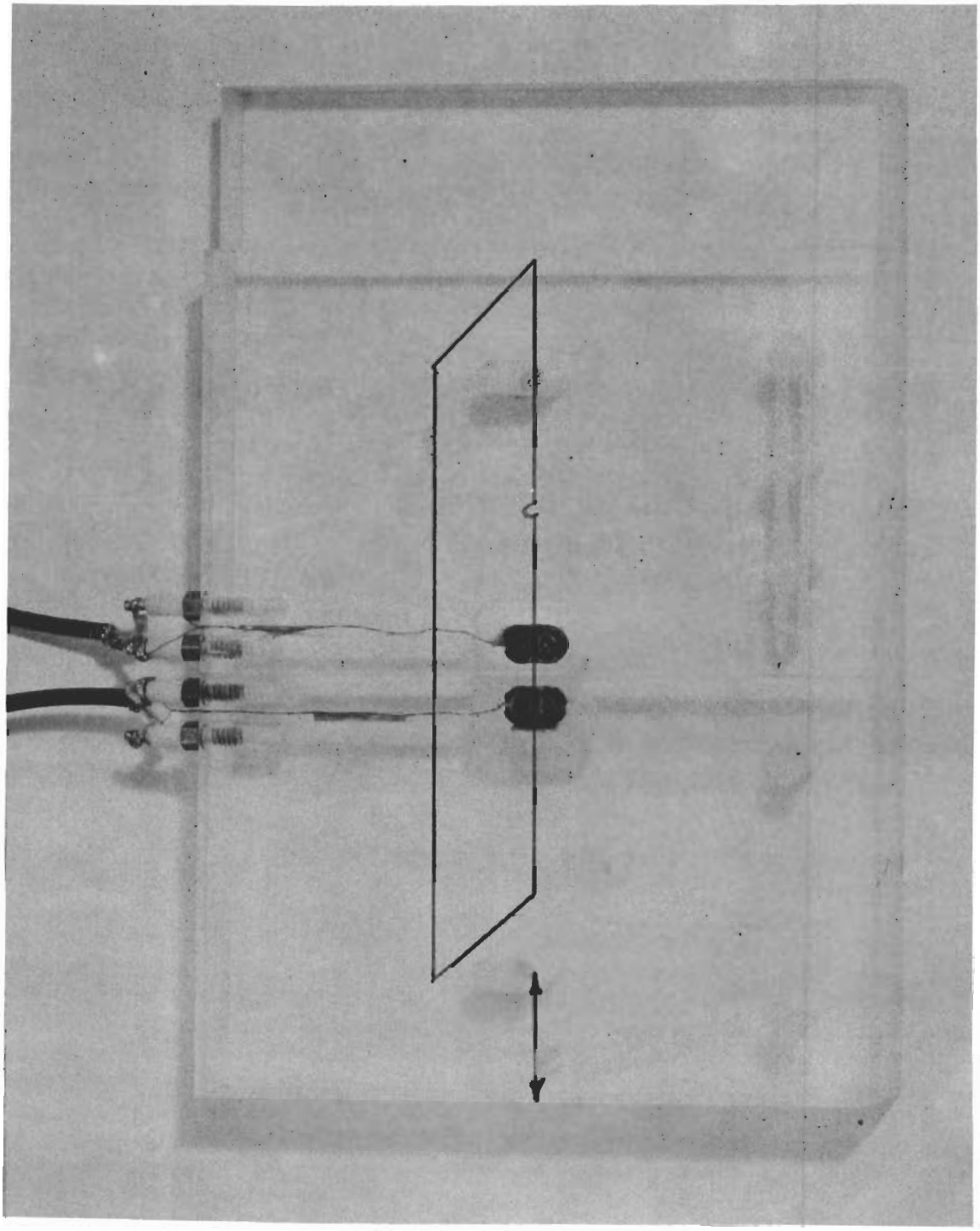

FIGURE 60 MUTUAL COUPLING TEST FIXTURE

flat on one side. These cores were then positioned as shown in Figure 60 and wound with figure-eight coils to provide a concentration of the magnetic field at the faces of the cup core. The simulated compressor blades were then positioned perpendicular to the faces of the cup cores and moved across their surface (Figure 60). The drive coil thus induces an eddy current in the blade edge which in turn induces a voltage in the pickup coil.

Results of these tests are given in Figure 61. Here the maximum signal output occurs for a good blade, and the output decreases with increasing defect size and coil-to-blade spacing. The considerable variance that appears in the data is partially due to the variation of the angle of the blade with respect to the plane of the coils. Since the system output is inversly proportional to defect size, more signal processing is required than if the output were directly proportional to defect size. This disadvantage can be overcome by employing a third coil to excite eddy currents in the blade and then measuring the output differentially across the two ferrite cup core pickup coils. This technique, however, requires careful layout as the pickup coils must be balanced with respect to direct pickup from the drive coil.

The detection of blade defects via the change in reflected impedance from the blade is most effectively utilized by employing the coils in a resonant circuit. The use of a resonant circuit provides noise rejection of frequencies off resonance and provides a system gain proportional to the Q of the tuned circuit. One application of the resonant circuit is in the resonant bridge network of Figure 59 and test fixture of Figure 57 described previously. As seen in Figure 58, this technique provides a very sensitive means of detection of blade defects whose output voltage is directly proportional to the defect size. This technique, however, suffers from the disadvantage that the relative blade-to-coil spacing must remain constant to obtain a minimum output for good blades.

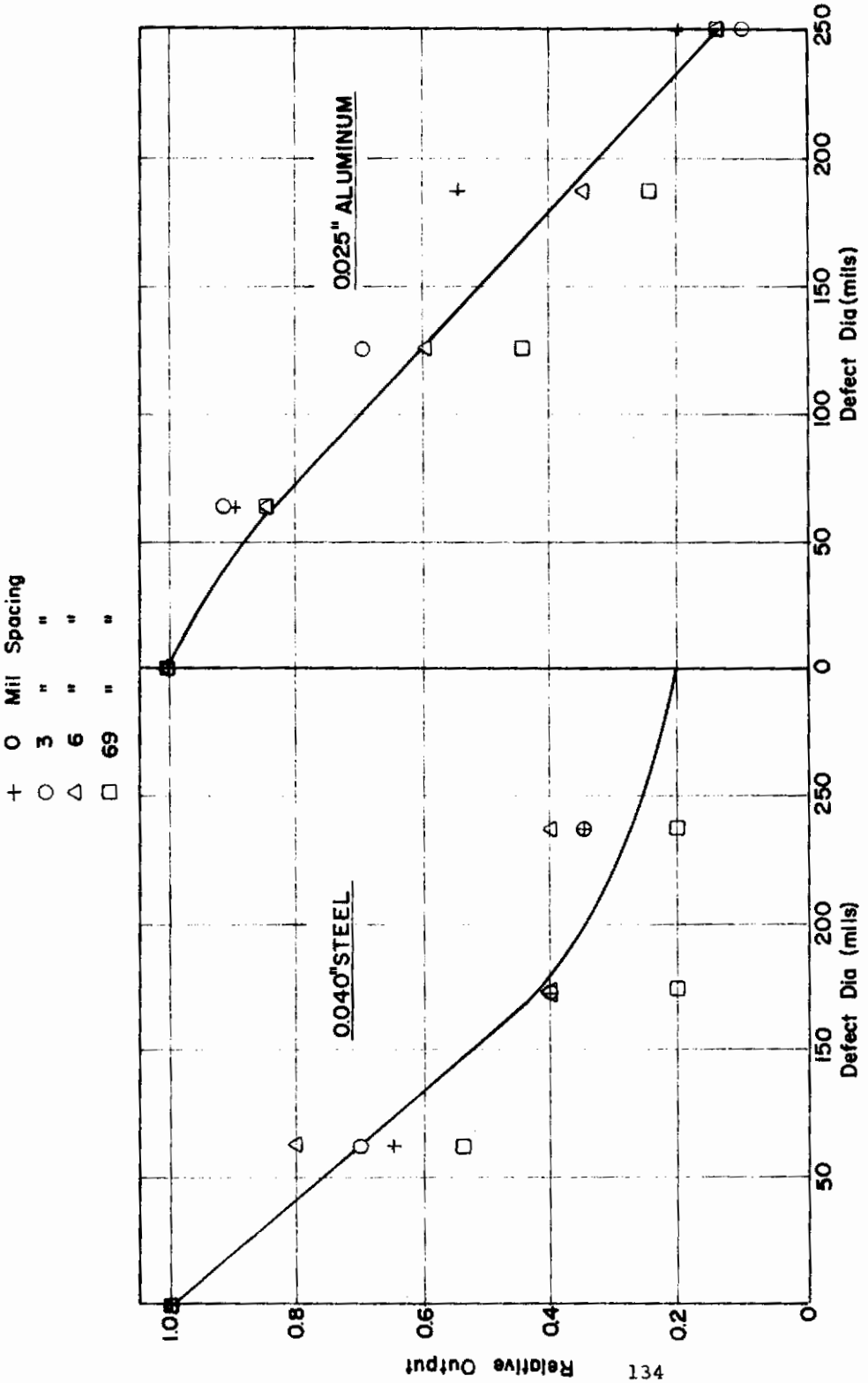

FIGURE 61 RELATIVE OUTPUT OF MUTUAL COUPLING TEST AS A FUNCTION OF DEFECT DIAMETER

A second disadvantage of the resonant bridge technique is the difficulty of maintaining a balanced bridge at the frequencies involved. This will be particularly true in the adverse environment encountered in the field.

Another technique employing a resonant circuit was also investigated. This technique employs an FM discriminator circuit with the detecting coil in a series resonant circuit as seen in Figure 62. In this case, however, the discriminator circuit is driven with a constant frequency oscillator, and the discriminator characteristics are shifted as a function of the detecting coil inductance and Q. The coil inductance and Q can in turn be correlated with the blade defect size. The results of tests using this circuit at a frequency of 2.5 MHz are given in Figure 63. The use of this circuit minimizes the geometrical balance problems encountered in the bridge technique, but as in the case of the mutual coupling technique, a maximum output occurs for a good blade. An added advantage of this technique is that it allows the use of feedback to maintain a stable operating point. Here, the DC output from the discriminator may be used in conjunction with a variable capacitance diode in the oscillator circuit to vary the drive frequency proportional to changes in the resonant frequency of the detector circuit. Thus, highly stable components are not required, since frequency drift is automatically compensated.

2.3.3 Blade edge measurements -- The use of eddy current checkout techniques on the J-47 compressor section involved the use of the resonant bridge circuit described in section 2.3.2. This circuit was employed over the other eddy current circuits investigated in the laboratory for two reasons. One, this technique provides the greatest sensitivity and allows a simple threshold system for signal processing because the circuit output is proportional to defect size. Two, the use of a technique whose output is proportional to the difference in two adjacent areas of the same blade tends to eliminate small

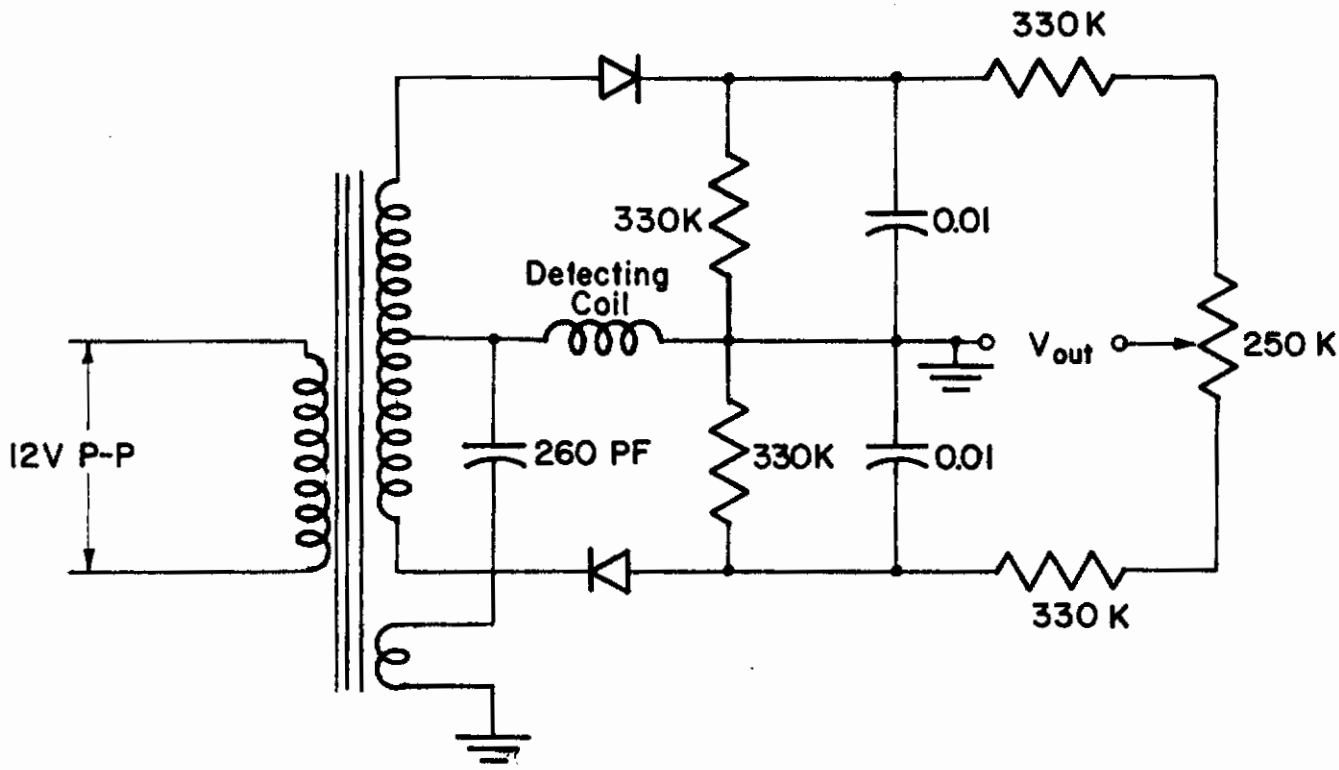

FIGURE 62 DISCRIMINATOR CIRCUIT

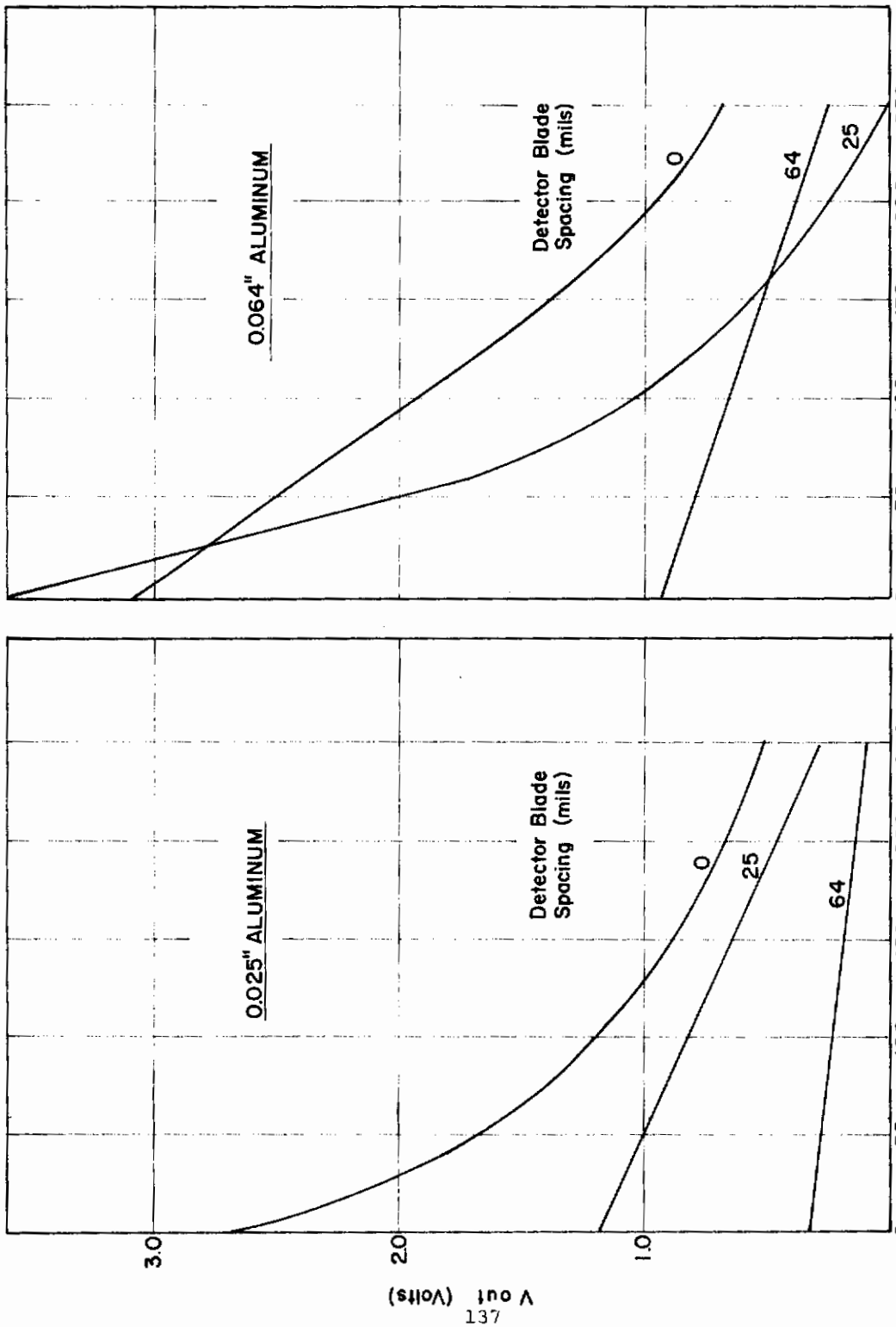

FIGURE 63 DISCRIMINATOR OUTPUT AS A FUNCTION OF DEFECT DIAMETER FOR OPERATION AT 2.5 MHZ

variations in blade parameters.

The resonant bridge circuit was evaluated on the J-47 compressor section by cutting calibrated defects into six of the compressor rotor blades. These defects, varying in diameter from 1/8 inch to 1/128 inch, were cut into the blades as shown in Figure 64. Care was taken in the placement of the defects so that all defects of a given size are at a constant distance from the axis of the compressor. Thus, a given detector position, as seen in Figure 65, allows scanning all blades with the same defect size. The defects were placed in blades whose blade-to-detector spacings ranged over a 0.032 inch span and whose slope variations ranged over a span of 0.014 inch/inch. Thus, the variation in the circuit output for blades having the same defect allows an estimate of the signal variation caused by the extraneous factors of blade spacing and blade tilt.

The tests conducted on the compressor involved careful adjustment of the x, y, and z axis of the micrometer stage, seen in Figure 65, as well as a rotation of the micrometer about the vertical axis to balance the circuit with the detectors in front of a particular blade. The oscilloscope photographs of Figures 66 thru 69 show the circuit output where the upper photograph in each case is taken with both detectors viewing good blade areas while the lower photograph is taken with one detector viewing a 0.125 inch defect. The upper trace on each photograph indicates the positions of defective blades. A summary of the test results is tabulated in Table IX. Here the blades beginning with blade number 25 and ending with blade number 8 correspond to consecutive blades from left to right in the photographs of Figures 66 thru 69. The ratio of the resonant bridge circuit output with a 0.125 inch defect to that without a defect is given. Also included in Table IX are the blade spacing and slope values as these factors inject extraneous signals into the system masking the circuit output due to defects.

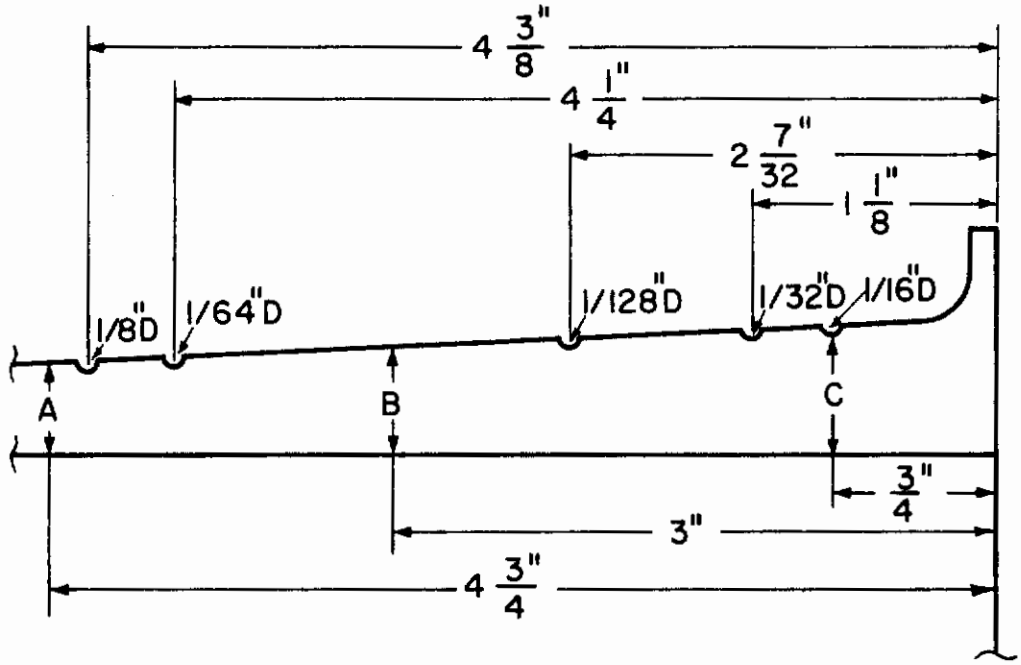

FIGURE 64 POINTS OF MEASUREMENT OF RELATIVE COMPRESSOR BLADE SPACING .

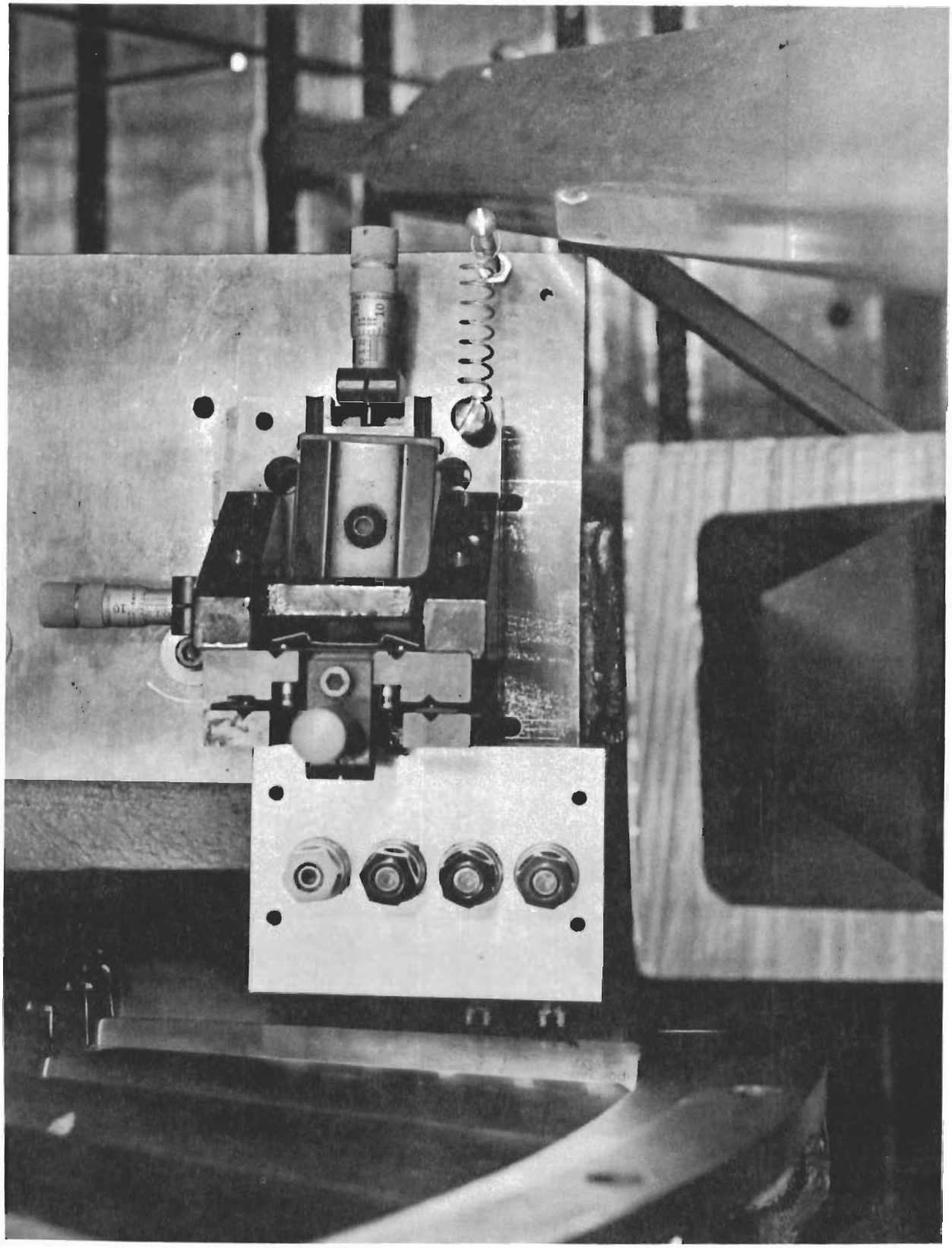

FIGURE 65 EDDY CURRENT DETECTION SYSTEM

Defect Diameter = 0.0"

Defect position

Circuit output

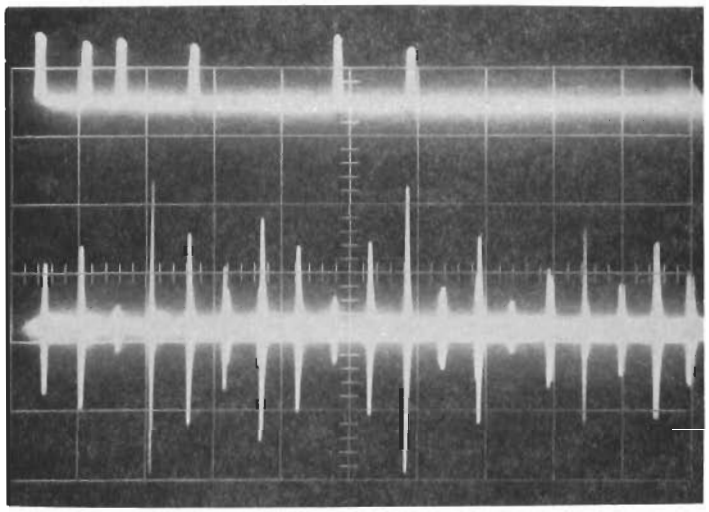

5msec/cm

10mv/cm

Defect Diameter = 0.125"

Defect position

Circuit output

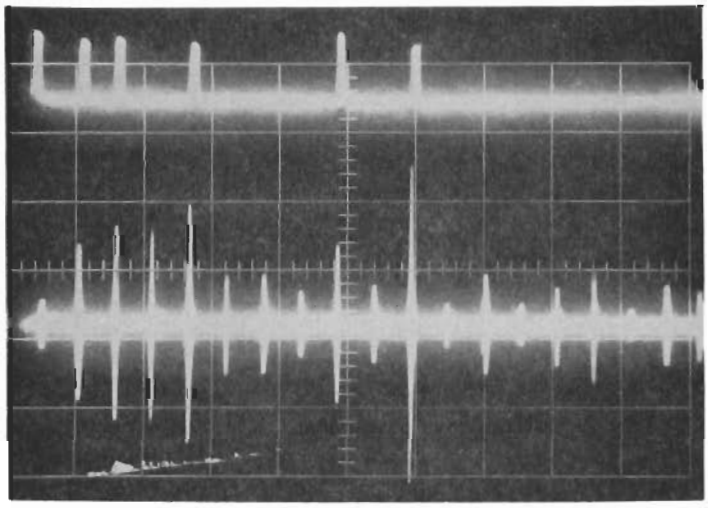

5msec/cm

10mv/cm

Test Condition

Balance on blade #25
Detector gap = 0.125"
Detector Center-to-Center Spacing = 0.375"
Blade #10 to detector Spacing = 0.010"

FIGURE 66 EDDY CURRENT TEST #1

Defect Diameter = 0.0"

Defect position

Circuit output

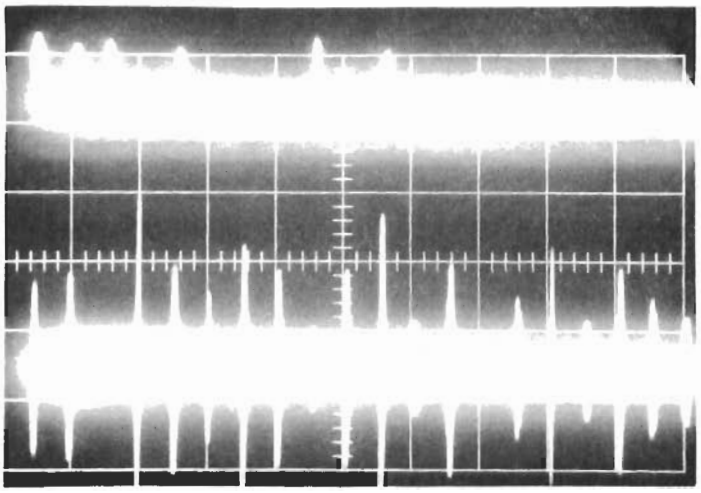

5msec/cm

10mv/cm

Defect Diameter = 0.125"

Defect position

Circuit output

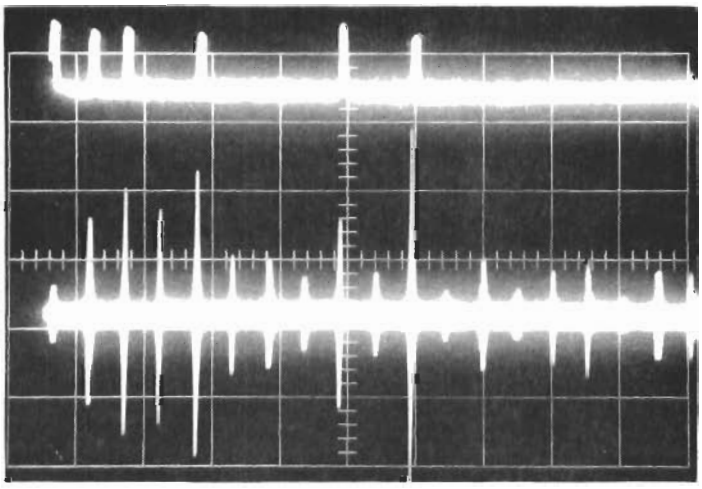

5msec/cm

20mv/cm

Test Condition

Balance on blade #23
Detector gap = 0.125"
Detector center-to-center spacing = 0.375"
Blade #10 to detector Spacing = 0.010"

FIGURE 67 EDDY CURRENT TEST #2

Defect Diameter = 0.0"

Defect position

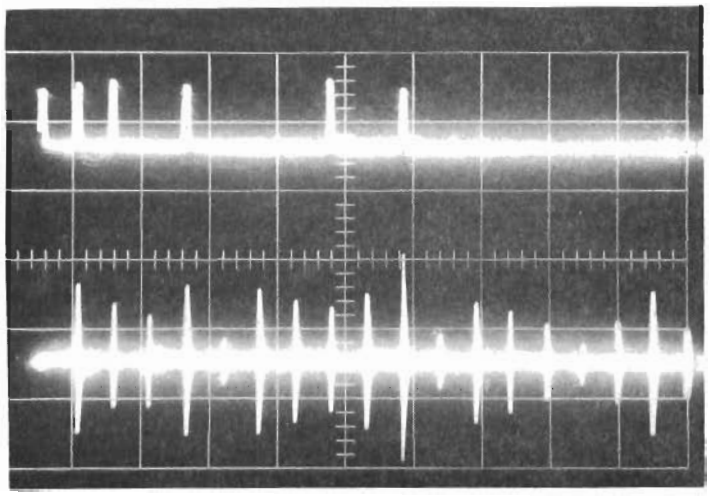

5msec/cm

Circuit output

10mv/cm

Defect Diameter = 0.125"

Defect position

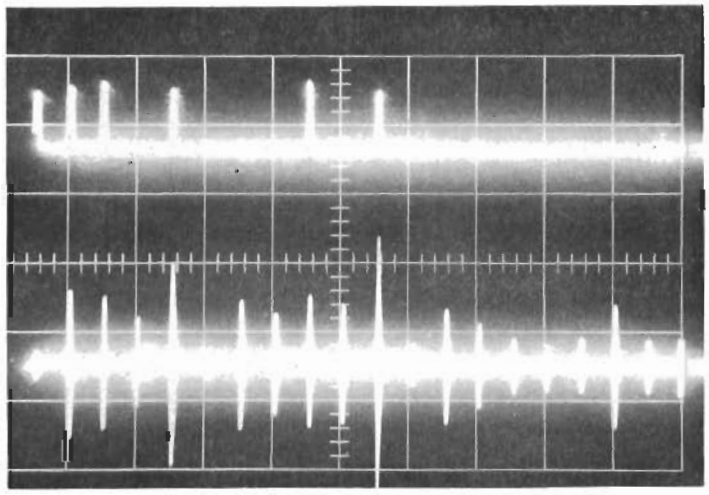

5msec/cm

Circuit output

10mv/cm

Test Condition

Balance on Blade #10
Detector gap = 0.125"
Detector center-to-center spacing = 0.750"
Blade #10 to detector Spacing = 0.010"

FIGURE 68 EDDY CURRENT TEST #3

Defect Diameter = 0.0"

Defect position

Circuit output

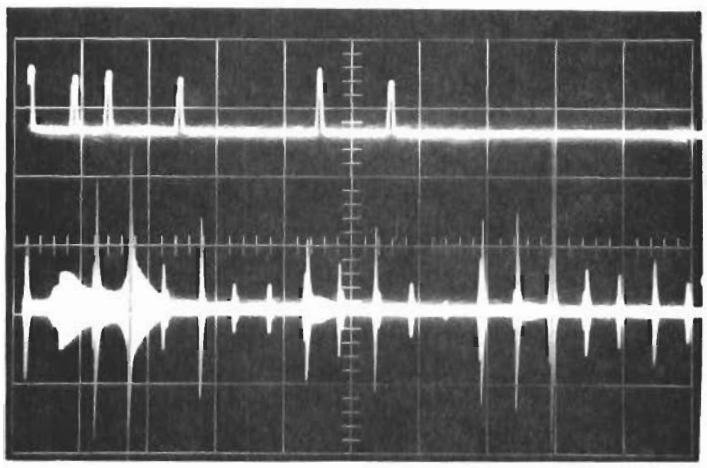

5msec/cm

10mv/cm

Defect Diameter = 0.125"

Defect position

Circuit output

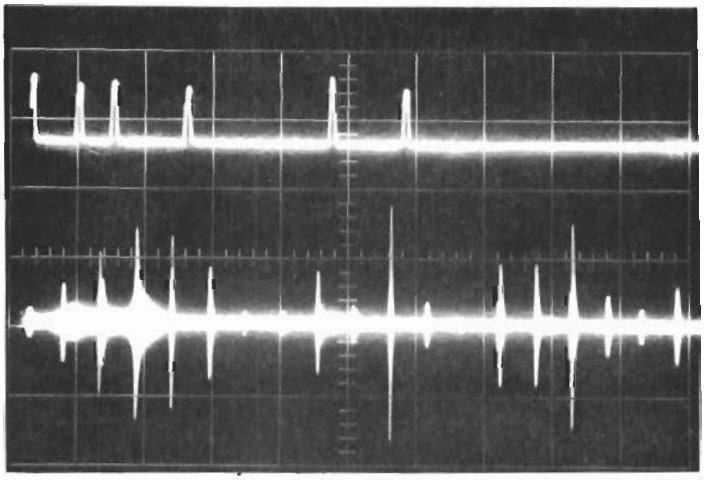

5msec/cm

20mv/cm

Test Condition

Balance on blade #23
Detector gap = 0.040"
Detector center-to-center spacing = 0.375"
Blade #10 to detector spacing = 0.010"

FIGURE 69 EDDY CURRENT TEST #4

Table IX

SUMMARY OF EDDY-CURRENT TEST RESULTS

Blade Number	Dimension A (Mils)	Slope S_{AB} (Mils/inch)	Vout (with 0.125" Defect) / Vout (with 0.00" Defect) Test #1	Test #2	Test #3	Test #4
* 25	10	26.3	0.82	0.69	1.56	0.28
* 24	4	39.3	1.92	2.00	1.00	2.00
* 23	36	30.8	8.00	8.20	1.29	1.10
22	36	28	1.31	1.31	0.97	1.08
* 21	20	35	2.44	2.82	1.38	4.07
20	23	30.2	1.56	1.56	0.69	1.12
19	23	36.6	0.89	0.88	0.92	1.00
18	9	36.6	0.80	0.78	0.85	1.00
* 17	21	34.8	4.53	4.43	1.30	1.45
16	18	34.8	0.91	0.88	0.89	0.78
* 15	33	37.7	2.20	2.43	1.24	3.40
14	2	33.8	1.07	1.13	0.74	1.66
13	17	33	1.06	1.09	0.98	1.72
12	23	33	1.66	1.80	0.83	1.33
11	36	33	1.30	1.33	0.73	1.25
10	48	28	1.19	1.03	1.14	1.20
9	17	33	0.77	0.66	0.71	1.38
8	12	37	0.93	0.92	0.86	1.00

* Blades containing defects.

The results of these tests as presented in Table IX indicate that at least three variables exist between blades. Two of these variables are the spacing and slope variation between blades. A third variation appears since the output ratio from blades which have no defects vary over a range from 0.66 to 1.8. Since the blade material should be relatively homogeneous, the variation must be attributed to combinations of two factors. Since the detectors are moved approximately 0.5 inch between the two measurements, the circuit output variation could be caused by the variation in blade geometry as a function of length. A second factor may be the slight misalignment of the detectors causing a change in blade-to-detector spacing as the detectors are moved across the blades.

Test #1 and #2 are included in Table IX to demonstrate the circuit output variation due to balancing the detectors on different blades. In this case, the detectors used were the wedge geometry with a 0.125 inch gap and a 0.375 inch center-to-center spacing. The results of the two tests are seen to agree quite well on most of the blades. Test #3 was included to demonstrate the effect of increasing the detector center-to-center spacing from 0.375 inch to 0.75 inch. The results of this change was to decrease the output ratios obtained with defective blades. This reduction may be expected, however, since the signal derived from the blade-to-blade slope variations are amplified. Test #4 was included to demonstrate the effect of reducing the detector gap width. These detectors employed 0.040 inch gaps and a 0.375 inch center-to-center spacing. In this case, as in the others, detection of 0.125 inch diameter defects requires comparison with a normal signature of the turbine. Even under these conditions, the defect of blade #25 could not be detected.

The results of the differential eddy current detectors are difficult to analyze due to the variation of differential detector spacings as a function of blade slope. The single ended

data of Figures 70 and 71 were thus taken to eliminate this parameter. The results of this test are tabulated in Table X. Here, the detector output is seen to correlate very well with the blade-to-detector spacing. As seen from the ratio $Vout_{Defect}/Vout_{Normal}$ the single ended system is not able to detect a 0.125 inch diameter defect. In this case, the variation in output due to a defect is masked by the larger signal due to blade spacing. An extraneous signal is alos injected into the measurement since the no-defect signal is obtained from a point on the blade 0.250 inches from the defect position.

The above single ended data has indicated an excellent correlation of detector output with blade spacing. Due to the apparent inability of the detector to see a 0.125 inch diameter defect, tests were run in an attempt to determine the detector field of view. In these tests, a single eddy current detector was used as in the dynamic tests above except the system static output voltage was balanced at a given blade-to-detector spacing to provide a zero output voltage from the differential amplifier as seen in Figure 72. The test data of Table XI was obtained by alternately cutting and measuring operations to eliminate the spacing and geometry variations imposed by moving the detector. The results of Table XI and the single ended dynamic tests of Figure 71 are plotted in Figure 73 .

Also from Table XI, the millivolt change in output for the removal of edge areas progressively displaced from the axis of the sensor detector was developed and is presented in Figures 74 and 75. While the data was developed for the progressive removal of two small areas (either 20 mils x 10 mils, 40 mils x 10 mils, or 60 mils x 10 mils) each symmetrically displaced from the axis, the results are normalized in terms of a single 20 x 10 mils area at the mean distance from the axis. The error range is chosen to be approximately one percent of the maximum voltage noted. This error is more suggestive than accurate, since the spread could be interpreted to indicate even larger errors.

5msec/Div

0.5V/Div

0.0" Defect

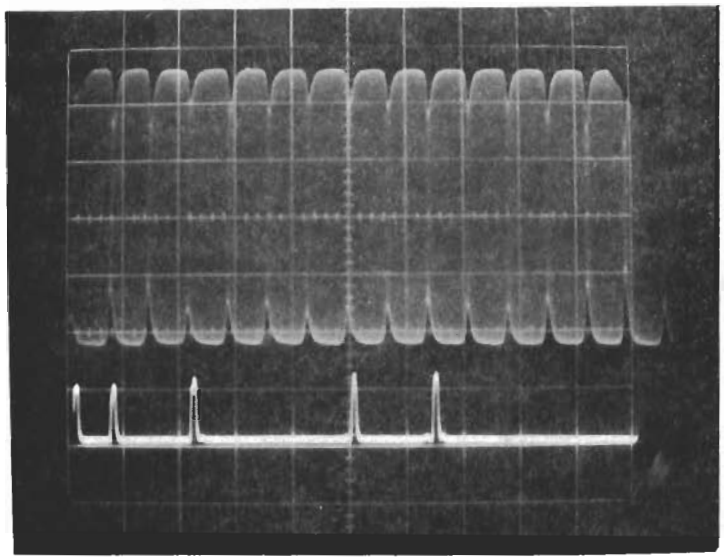

5msec/Div

0.5V/Div

0.125" Defect

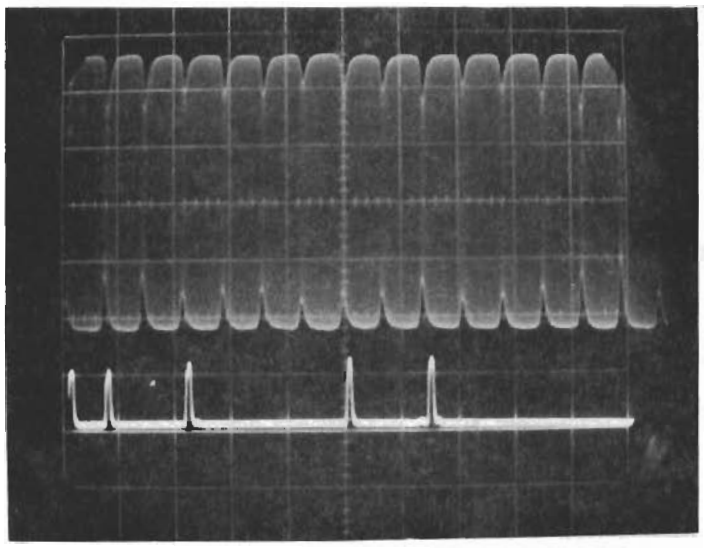

Test Conditions
Detector Gap = 0.125"
Blade #23 to Detector Spacing = 0.050"

FIGURE 70 SINGLE ENDED EDDY CURRENT OUTPUT

5msec/Div

50mv/Div

0.0" Defect

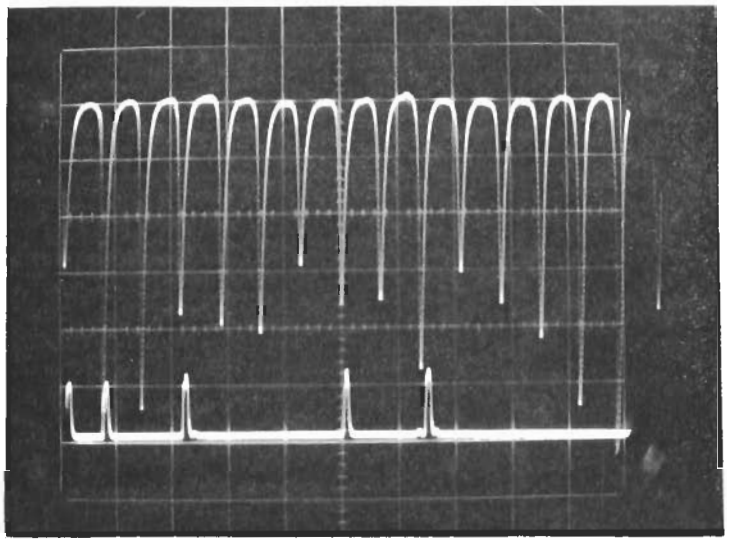

5msec/Div

50mv/Div

0.125" Defect

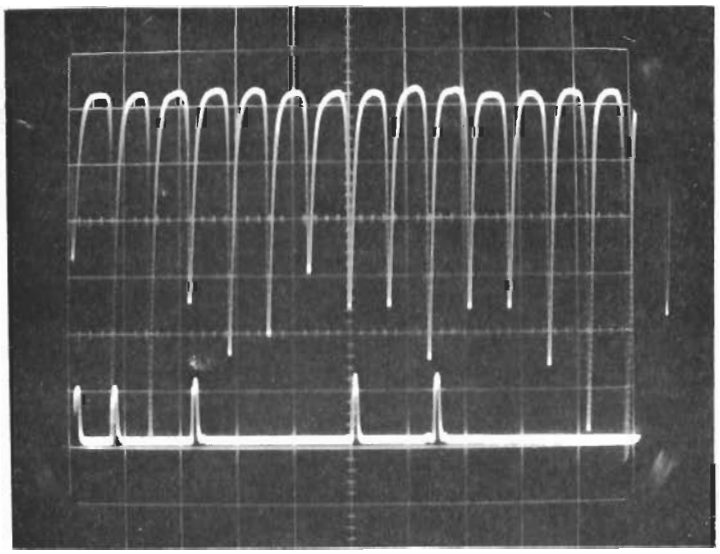

Test Conditions
Detector Gap = 0.125"
Blade #23 to detector Spacing = 0.050

FIGURE 71 DEMODULATED SINGLE ENDED EDDY CURRENT OUTPUT

Table X

SINGLE ENDED EDDY-CURRENT TEST RESULTS

Blade Number	Dimension A (Mils)	Slope S_{AB} (Mils/inch)	Vout 0 Defect (mv)	Vout 0.125" Defect (mv)	Vout Defect / Vout Normal
* 24	4	39.3	142	147	1.03
* 23	36	30.8	268	287	1.07
22	36	28	268	298	1.11
* 21	20	35	187	184	.985
20	23	30.2	195	230	1.18
19	23	36.6	203	216	1.07
18	9	36.6	145	161	1.11
* 17	21	34.8	179	193	1.08
16	18	34.8	174	190	1.09
* 15	33	37.7	234	242	1.03
14	2	33.8	153	192	1.26
13	17	33	179	192	1.07
12	23	33	208	242	1.17
11	36	33	266	297	1.12
10	48	28	316	327	1.03
9	17	33	184	200	1.09

* Blades containing defects.

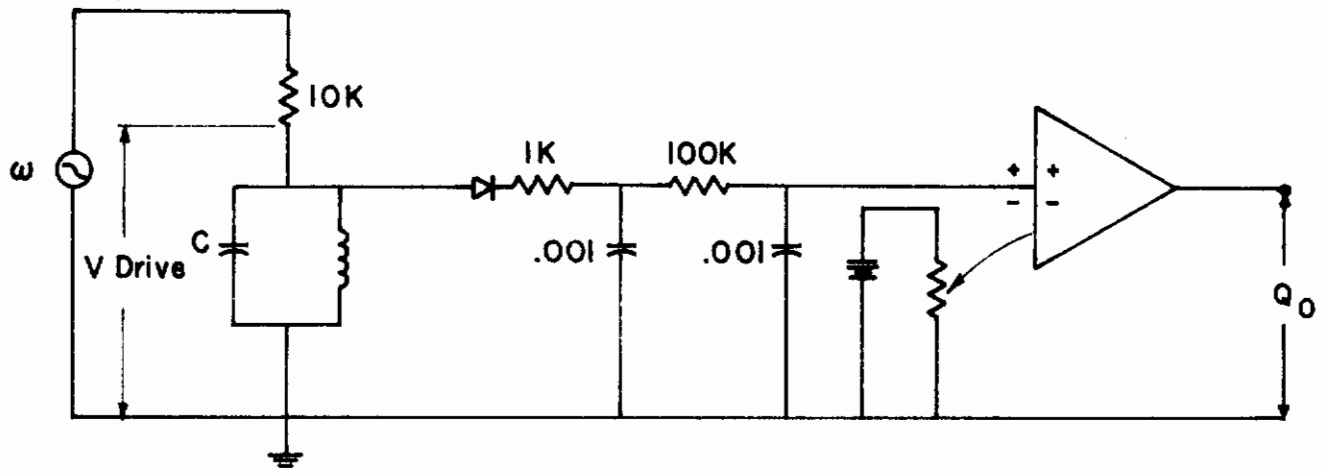

	0.125 Inch Gap Detector	0.040 Inch Gap Detector
ω	110 KC	130 KC
V Drive	2.8 V P-P	1.7 V P-P
Q	18.5	15
C	0.04	0.06

FIGURE 72 DIFFERENTIAL AMPLIFIER WITH ZERO OUTPUT VOLTAGE

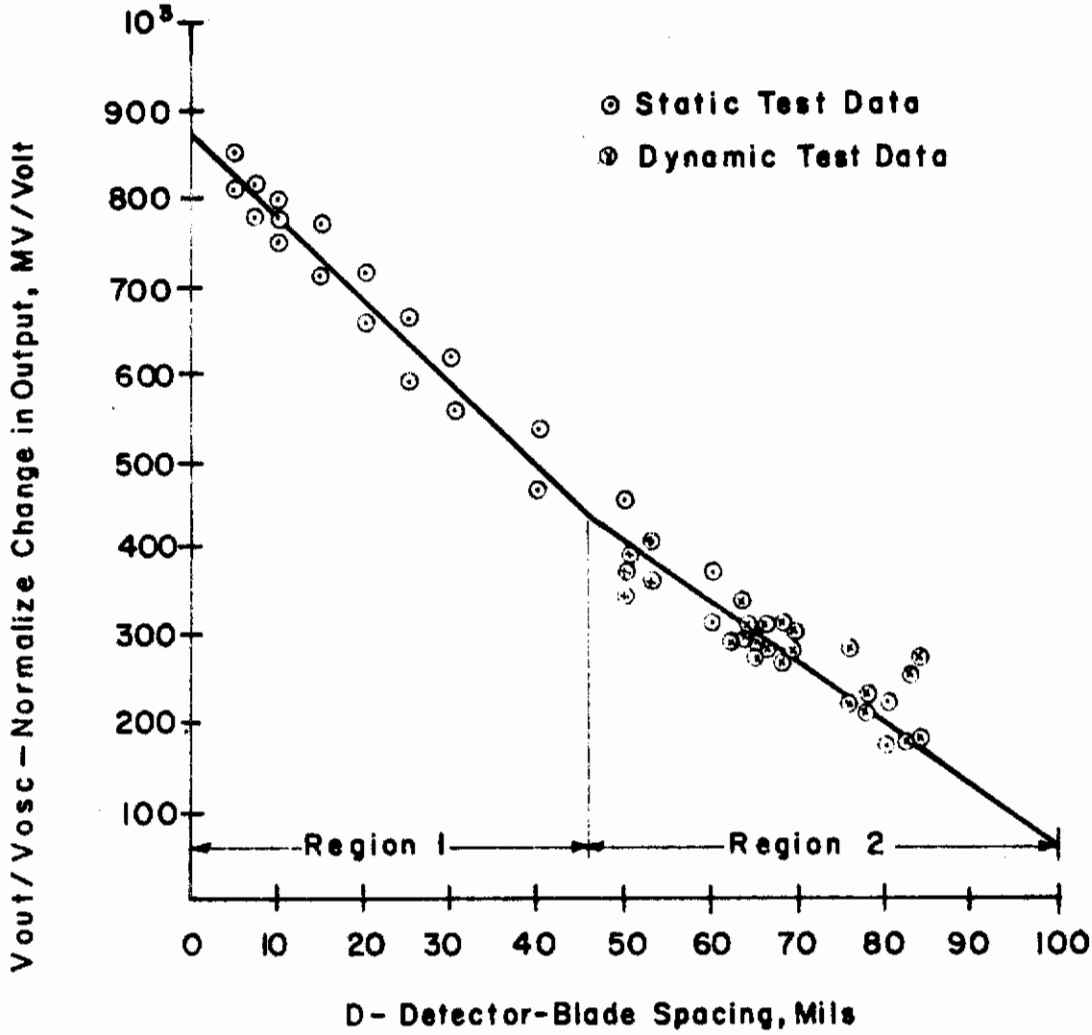

FIGURE 73 EDDY CURRENT OUTPUT CHANGE VS. DETECTOR TO BLADE SPACING(RESONANT CIRCUIT)

Slope@ Region 1 = - 9.45 mv v/mil
Slope@ Region 2 = - 7.10 mv v/mil

Table XI

MEASUREMENT OF DETECTION REGION

Detector Gap = 0.125 in.

Blade-Detector Spacing = 0.050 in.

Cut depth (mils)	Cut width (mils)	E_o (mv)	Blade-Detector Spacing (mils)	E_o (mv)
0	0	0	50	0
10	47	7	51	10
10	87	17	52	20
10	127	26	53	30
10	167	39	54	41
10	207	53	55	51
10	247	64	56	61
10	287	80	57	72
10	327	94	58	82
10	367	108	59	92
			60	102

Blade-Detector Spacing = 0.100 in.

Cut depth (mils)	Cut width (mils)	E_o (mv)	Blade-Detector Spacing (mils)	E_o (mv)
0	0	0		
10	47	0	100	0
10	87	2	102	7
10	167	6	104	13
10	247	13	106	17
10	327	19	108	24
10	407	25	110	30
10	487	27		
10	567	30		

Table XI (Cont'd.)

MEASUREMENT OF DETECTION REGION

Detector Gap = 0.040 in.

Blade-Detector Spacing = 0.050 in.

Cut depth (mils)	Cut width (mils)	E_o (mv)	Blade-Detector Spacing (mils)	E_o (mv)
0	0	0		
10	47	3	50	0
10	87	8	52	12
10	127	20	54	24
10	167	32	56	35
10	207	42	58	50
10	247	52	60	60
10	287	65		

Blade-Detector Spacing = 0.100 in.

Cut depth (mils)	Cut width (mils)	E_o (mv)	Blade-Detector Spacing (mils)	E_o (mv)
0	0	0		
10	47	0		
10	87	2	100	0
10	127	4.5	110	16
10	207	8		
10	287	11		
10	367	12		
10	487	14		
10	607	16		
10				

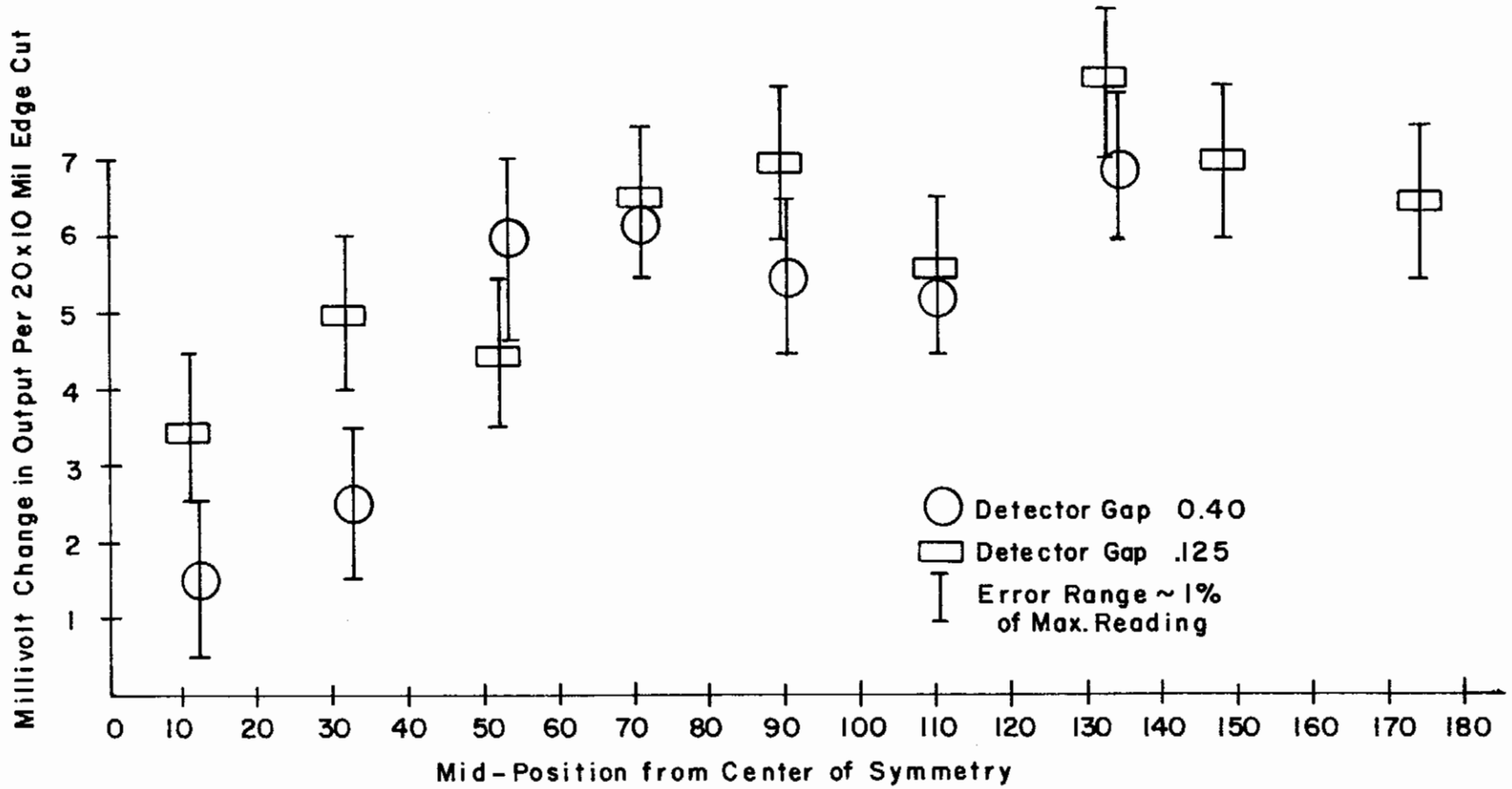

FIGURE 74 REMOVAL OF A 20 x 10 AREA PROGRESSIVELY DISPLACED FROM A CENTER OF SYMMETRY. BLADE TO DETECTOR SPACING OF .50 MILS

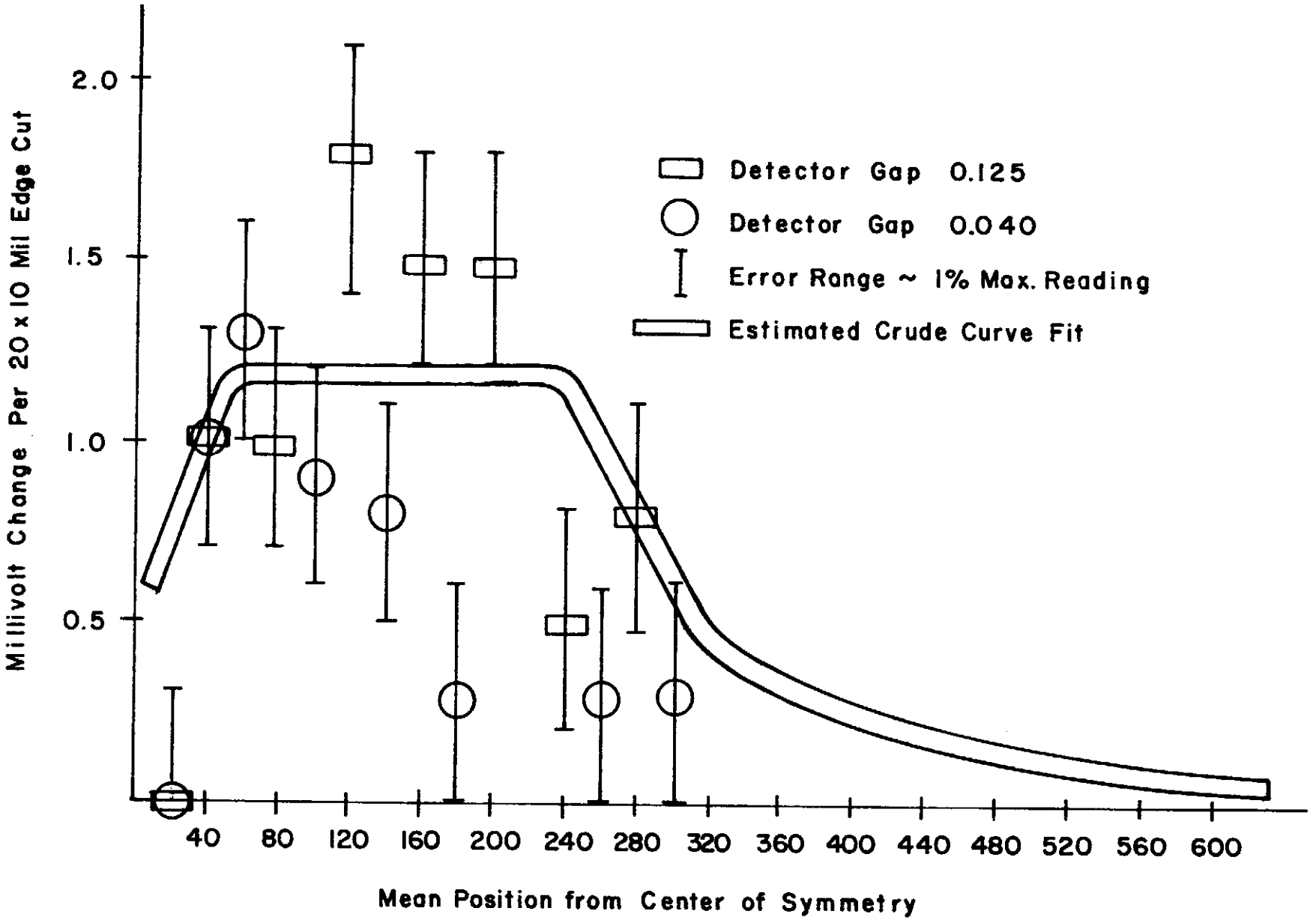

FIGURE 75 REMOVAL OF A 20 x 10 AREA PROGRESSIVELY DISPLACED FROM A CENTER OF SYMMETRY. BLADE TO DETECTOR SPACING OF .100 MILS

The displays of Figures 74 and 75 suggests that the performance is not significantly different for either a 40 mil or 125 mil detector gap. It also suggests a measureable response for 20 x 10 mil areas or edge defects as far out as ± 500 mils from the axis of the detector.

A brief analysis was undertaken which attempted to relate all parameters to optimize the detectability in terms of normal blade axial displacement, tilt, and detector parameters. A model was chosen which characterized the detector as having a well defined "beamwidth" and which assumed the normal blade displacement and tilts to have gaussian characteristics. This analysis, when carried forward logically, led to the questionable conclusion that an operable edge-defect eddy-current system could be devised by employing two sensor-detectors very close together. While such an arrangement is progressively less sensitive to tilt and other variants, it ultimately reduces the signal as well.

Just how close one can bring the two sensor-detectors is of great practical importance. Using the axis separation previously employed of 0.375 inches, it is seen from Figure 75 that this is about as close as the two detectors can be placed. For example, since the detectors operate differentially, a significant change must occur in one relative to the other. Consider a 20 x 10 mil defect spaced 40 mils from one sensor and spaced (in the opposite direction) 220 mils from the other detector. For these spacings, as shown in Figure 75, each detector experiences nearly identical changes in output voltage, thereby producing no indication of an edge defect. Thus, the axial spacing of 375 mils between detectors used for test results cited in Tables IX and X are close to optimum. Since the results of these tables demonstrated the inability to reliably detect damage by the eddy-current-edge detector technique, this technique in its present form should not be pursued further.

2.3.4 Blade tip measurement -- A second type of compressor blade defect detection utilizes an eddy current system to sense various manifestations of foreign object damage appearing at the blade tips as seen in Figure 76. Other sensors, such as millimeter wave or a magnetometer can also be employed. This system has several advantages over the edge-measurement techniques described previously. First, the detector mounting requires only a hole in the compressor shroud positioned radially out from the compressor section being monitored. This would allow the use of a permanently installed sensor. Second, all stages of compressor rotor blades can be monitored, if desired. Third, the manufacturing tolerances on the rotor blade tip to case distances are much tighter than corresponding tolerances on the blade edge. Thus, the detector output for normal blades is well defined and is less likely to mask the system output due to blade defects.

This system concept, (employing either eddy-current, millimeter wave, or magnetic sensors) can be used to monitor three classes of defects. First, the detectors can monitor the blade tip for tip damage such as tip curl. In this mode, the detectors could be used differentially as in the blade edge measurments. In the second class of defects, the position and/or twist of the blade tip is monitored as a precursor of blade edge or blade body damage. In this case, the lower limit of detectable damage must be sufficient to have caused yielding under the impact stress. Here, the correlation of system output with defect size is dependent upon the position of impact along the blade length, since forces near the blade tip have a larger bending moment than those near the root. Foreign object geometry also influences the system output. For example, a sharp object will cause local blade deformation with a minimum stress on the total blade.

As an example of possible system outputs using an eddy-current twist detector, the test results of Figures 77 and 78 are included. Here the damage was inflicted using a dull chisel and

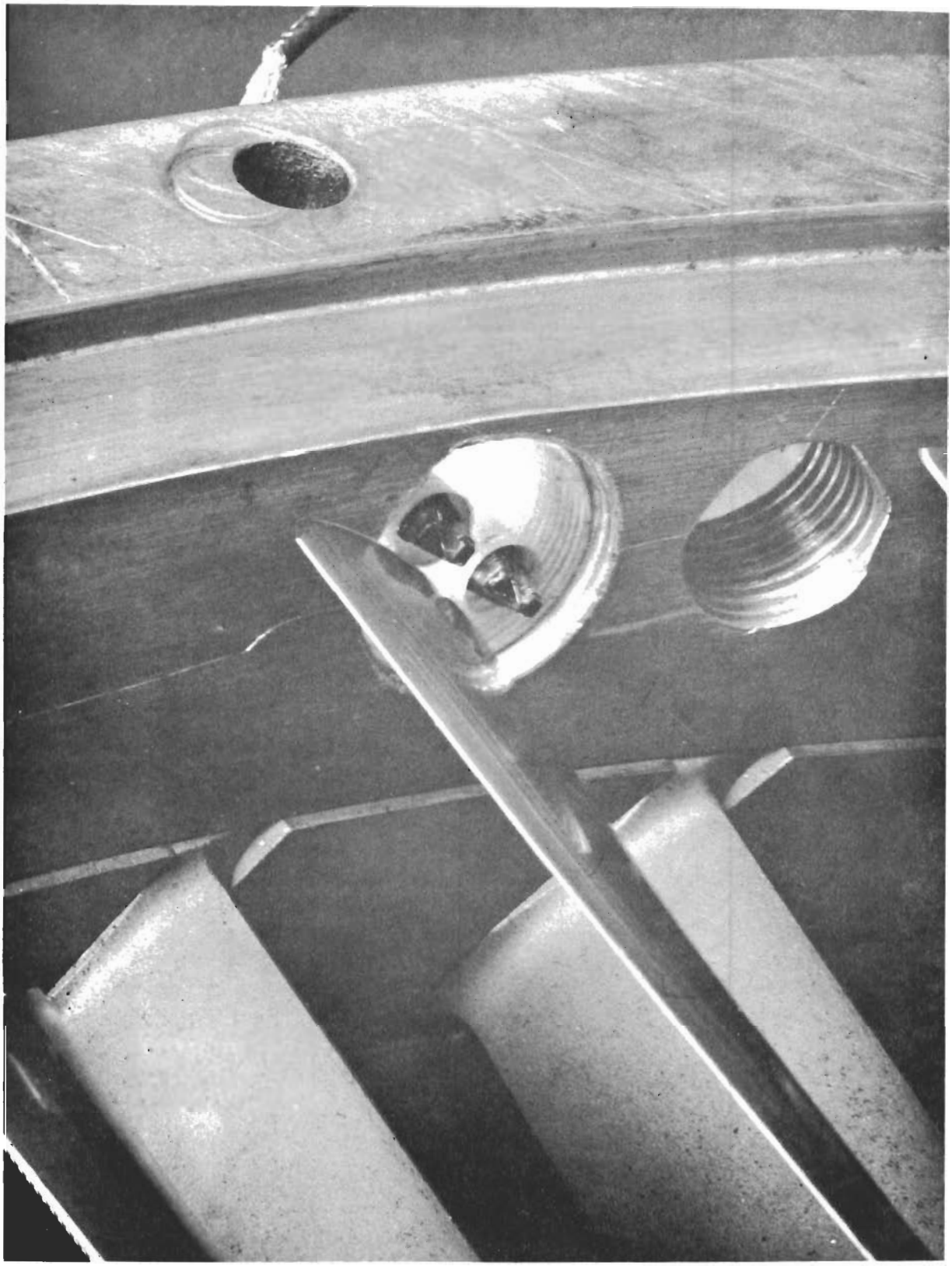

FIGURE 76 RELATIVE POSITION OF EDGE DETECTOR TO COMPRESSOR BLADES

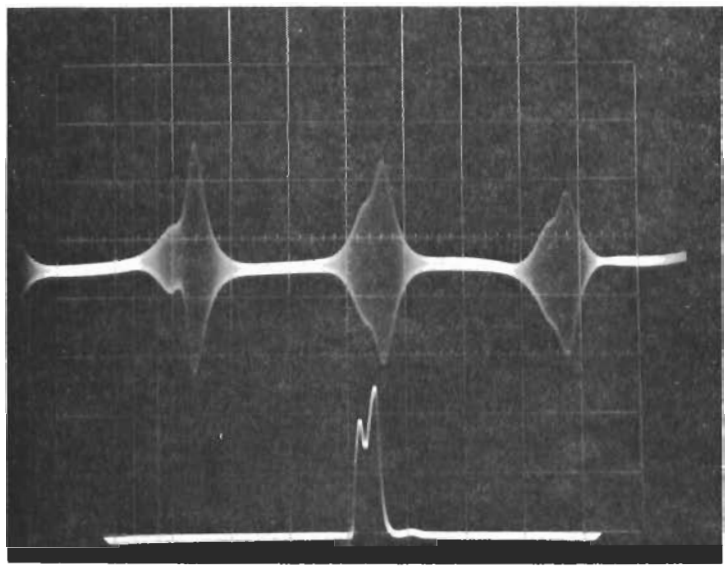

#1 3.26msec +1% 3.20msec -1%

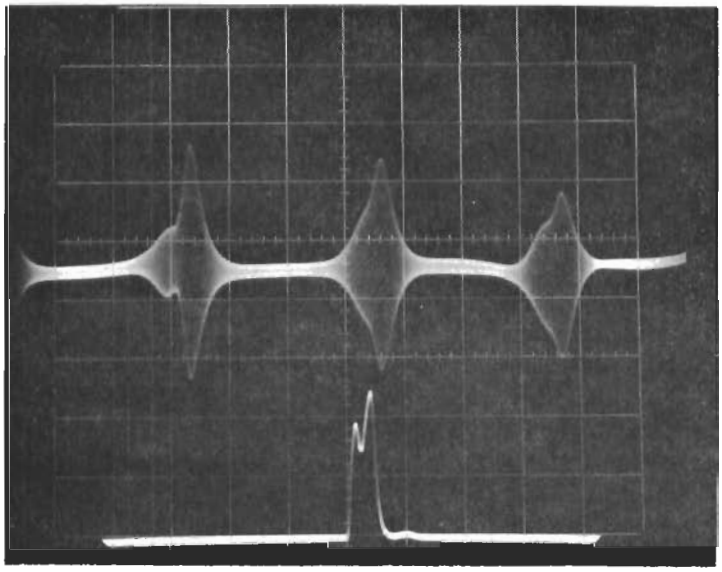

#2 3.31msec +2.5% 3.16msec -2.5%

FIGURE 77 DIFFERENTIAL TIP DETECTOR OUTPUT AS A FUNCTION OF TIP DISPLACEMENT

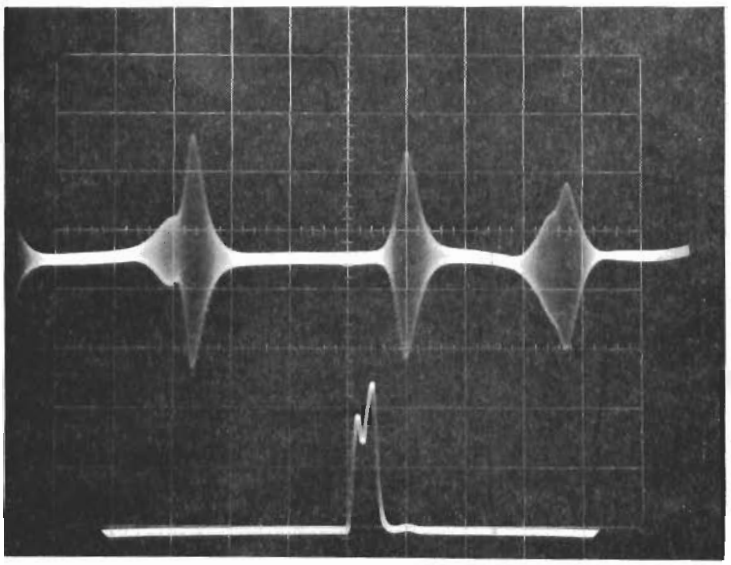

#3

3.68 msec +14%

2.74 msec -15%

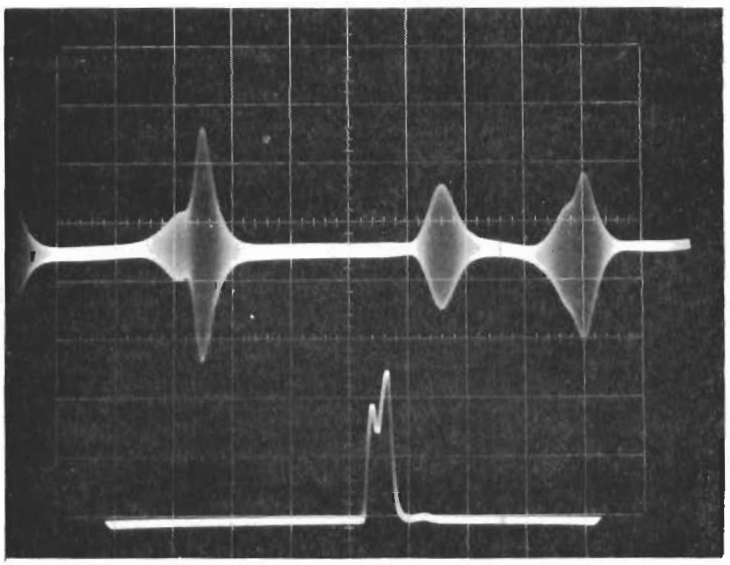

#4

4.10 msec +26.8%

2.42 msec -25%

FIGURE 78 DIFFERENTIAL TIP DETECTOR OUTPUT AS A FUNCTION OF TIP DISPLACEMENT

a hammer. The point of impact was three inches from the blade root and at the blade edge. The direction of impact was along a line normal to the blade length and at 120 degrees from the blade width. Impact #1 caused a triangular deformation approximately 1/16 inch deep and 1/16 inch wide. Successive impacts increased defect size to 3/32 inch by 3/32 inch as seen in photograph #4 in Figure 78. The timing variations as measured from the photographs of Figures 77 and 78 range from a $\pm$ 1 percent variation in photograph #1 to a + 26.8 percent and - 25 percent variation in photograph #4. When using a caliper as the measuring device, normal blade tip-to-blade tip spacing measurements on the J-47 compressor at IITRI ranged from 2.22 inches to 2.37 inches. Thus, the normal variation in blade spacing is approximately + 3.3 percent and - 3.7 percent from the average spacing. This then determines the lower limit of detectability of blade tip spacing measurements.

The third class of defects detectable using the blade tip measuring technique results from the aerodynamic loading of the blades. In this case, the tip twist and bending for a given aerodynamic load is a function of the defect depth and its distance from the blade root. The results of theoretical studies on blade deformation performed by Armstrong (Ref. 8) are seen in Figures 79, 80, and 81. In this case, as in the other detection systems, the minimum resolvable defect size is a function of the range of variation of the measured parameter in a normal compressor section. The minimum resolvable blade twist is seen in Figures 82 and 83. Here the normal blade angle is seen to be approximately 40 degrees. A variation of 8 degrees of blade twist is easily detectable requiring a crack length in the order of 0.180 inches. The system possesses a greater sensitivity to blade tip displacement since the bending movement along the blade length is larger. Since the normal blade tip spacing variation ranges from - 3.7 percent to + 3.3 percent of the average spacing, this limits the resolution in this mode. This results in a $\pm$ 0.8 degree

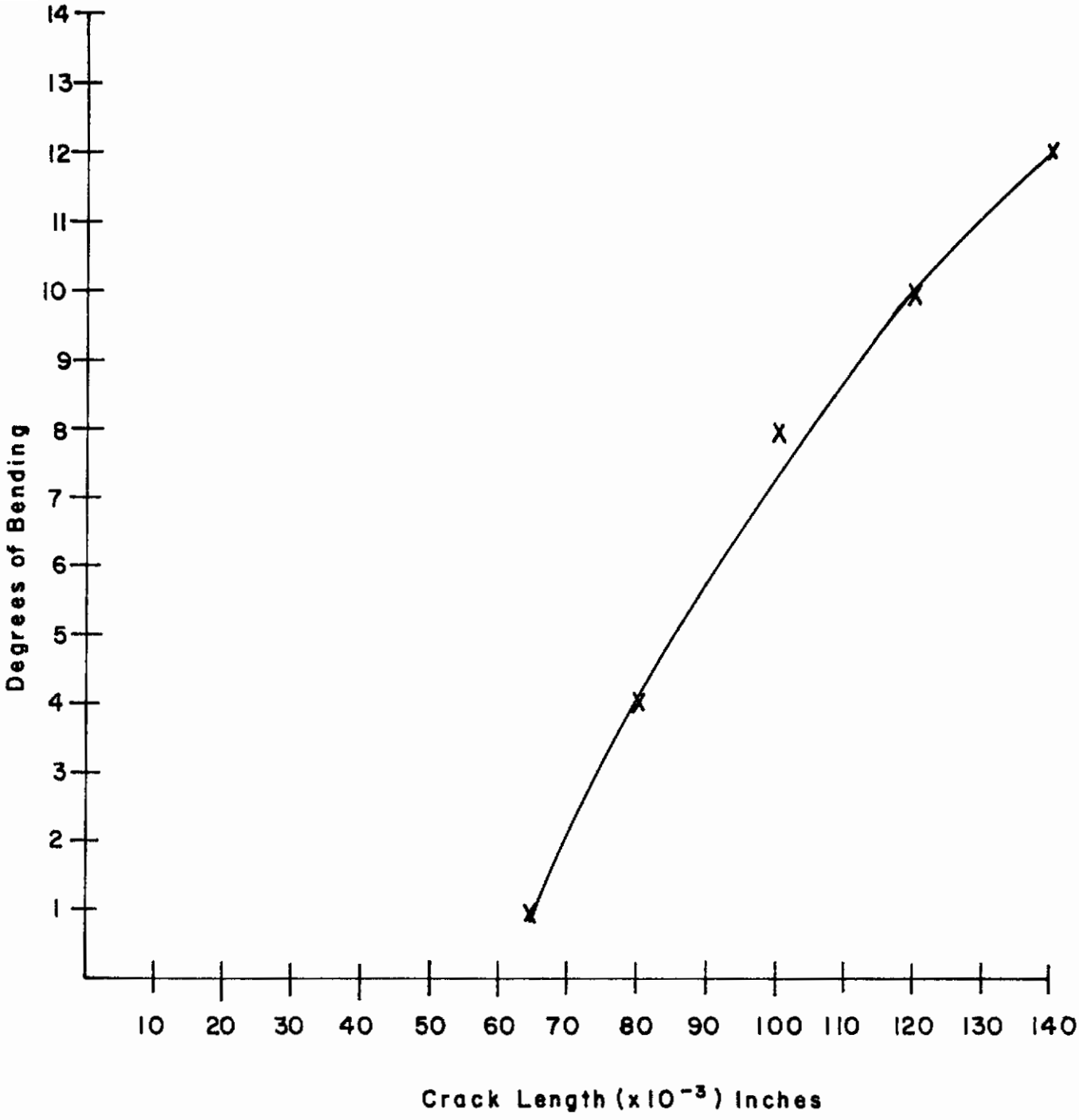

FIGURE 79 CRACK LENGTH VS. BENDING (DEGREES). (FAULT LOCATED 1/3 RD OF BLADE LENGTH FROM ROOT)

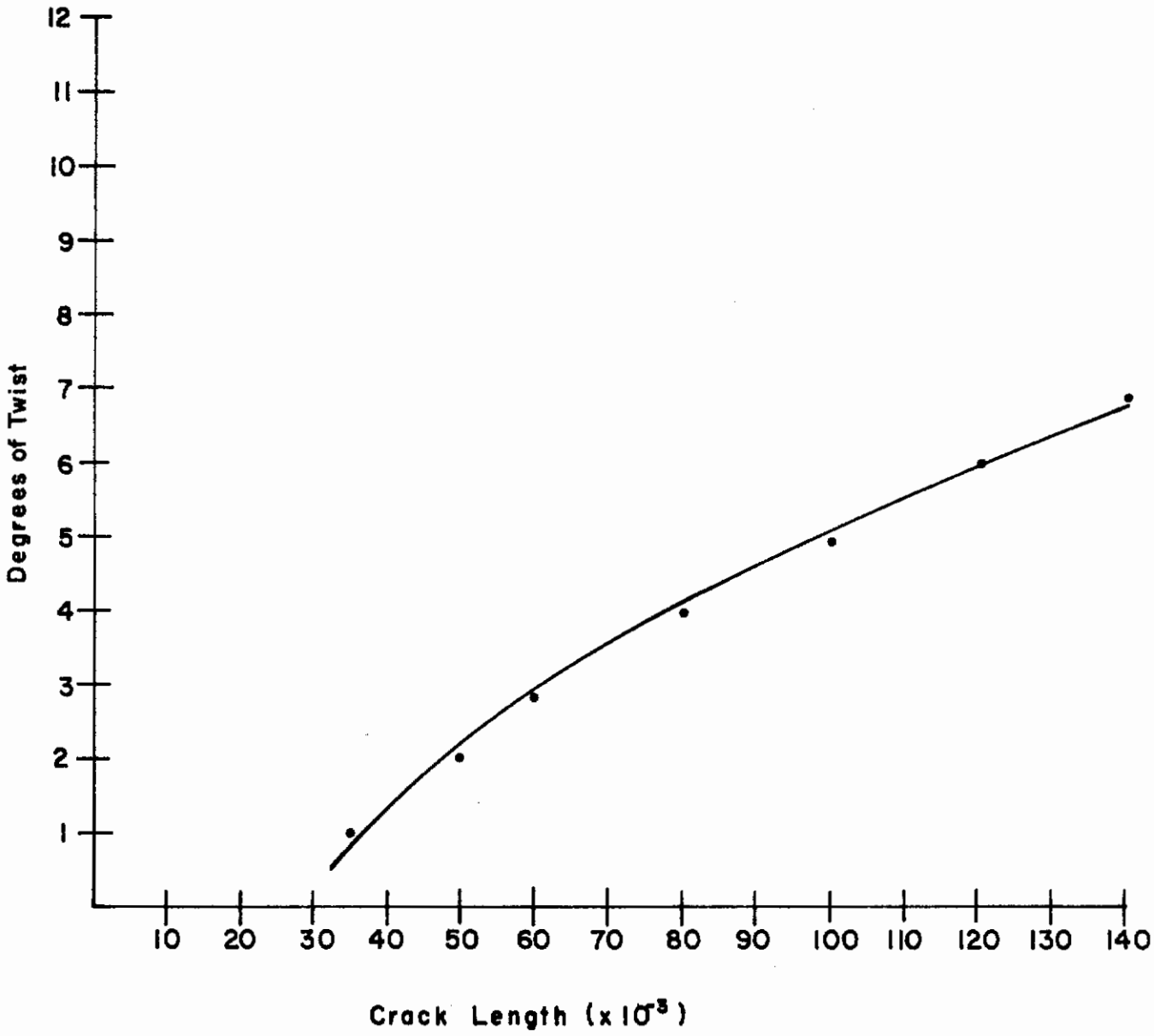

FIGURE 80 CRACK FAULT LENGTH VS. DEGREES OF TWIST
(FAULT LOCATED 1/3 RD OF BLADE LENGTH
FROM ROOT)

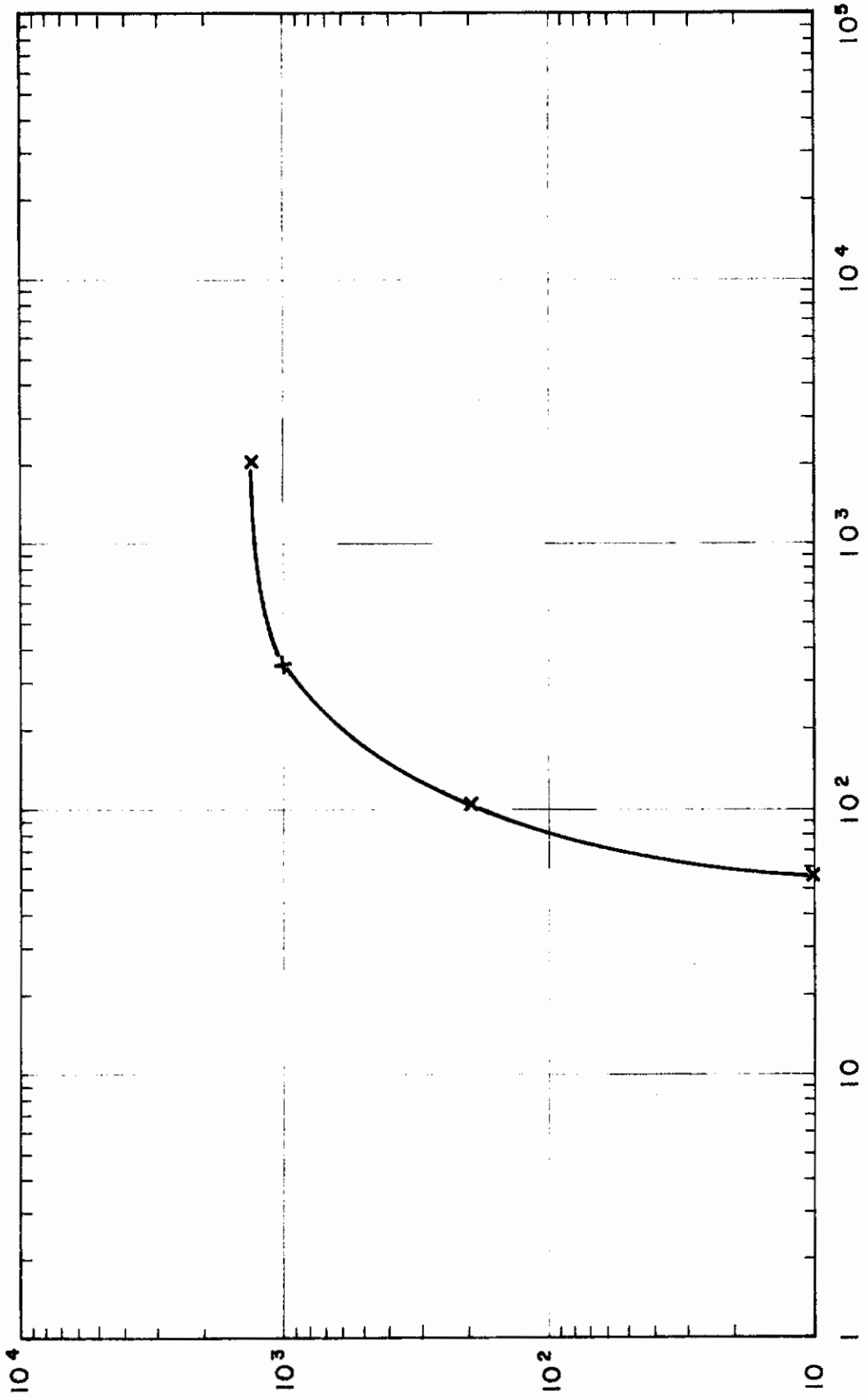

FIGURE 81 TIME VS. CRACK PROPAGATION FOR TYPE 403 STAINLESS STEEL BLADE (INITIAL LEADING EDGE DEFECT 0.125 INCHES)

53° Twist

20mv/division
10msec/division

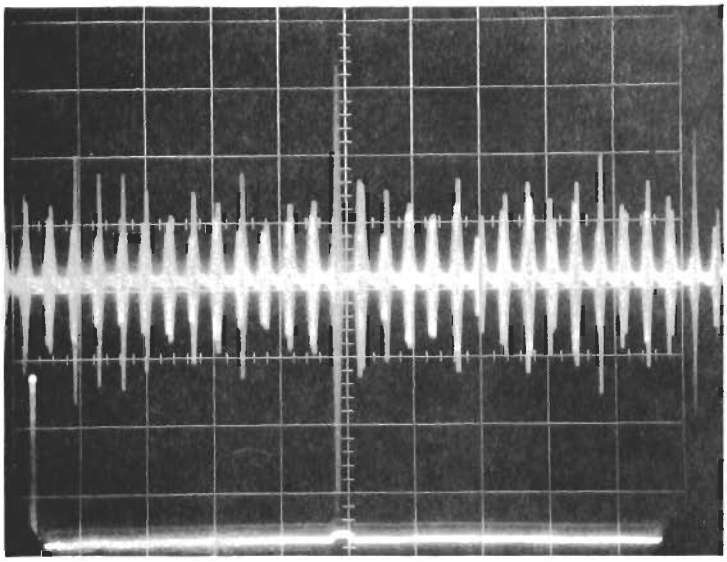

56° Twist

50mv/division
10msec/division

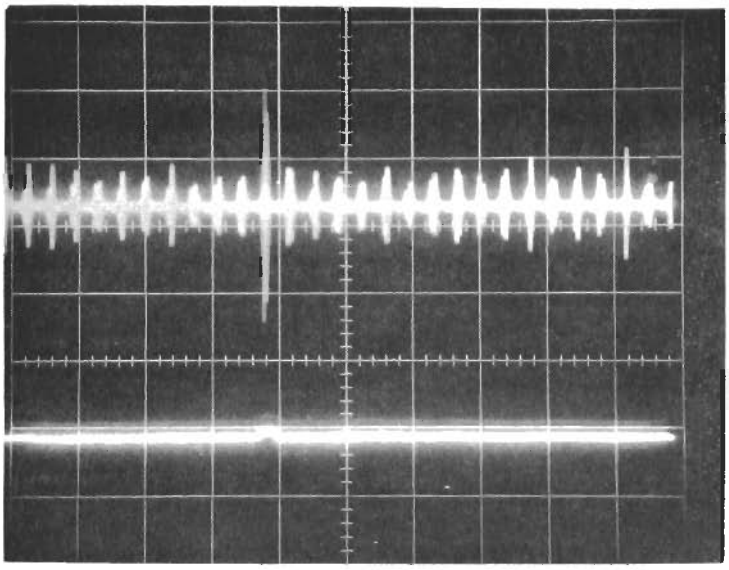

FIGURE 82 DIFFERENTIAL TIP DETECTOR OUTPUT AS A FUNCTION OF BLADE TWIST

32° Twist

20mv/division
10msec/division

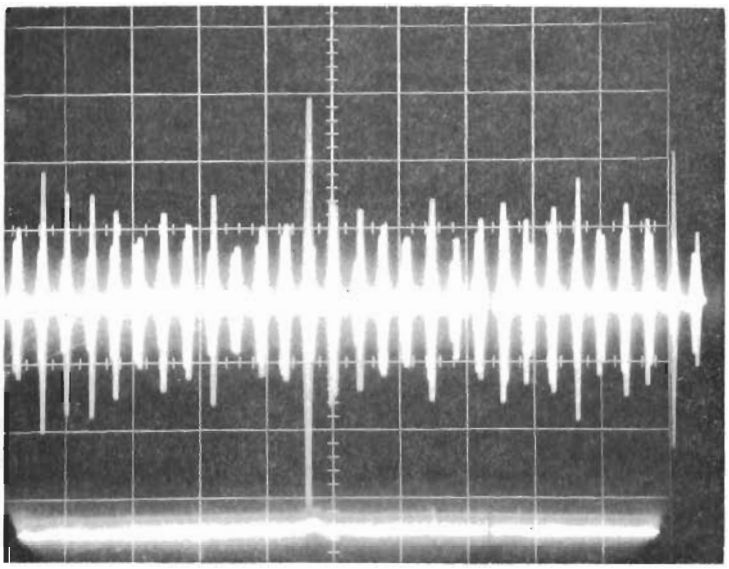

40° Twist

10mv/division
10msec/division

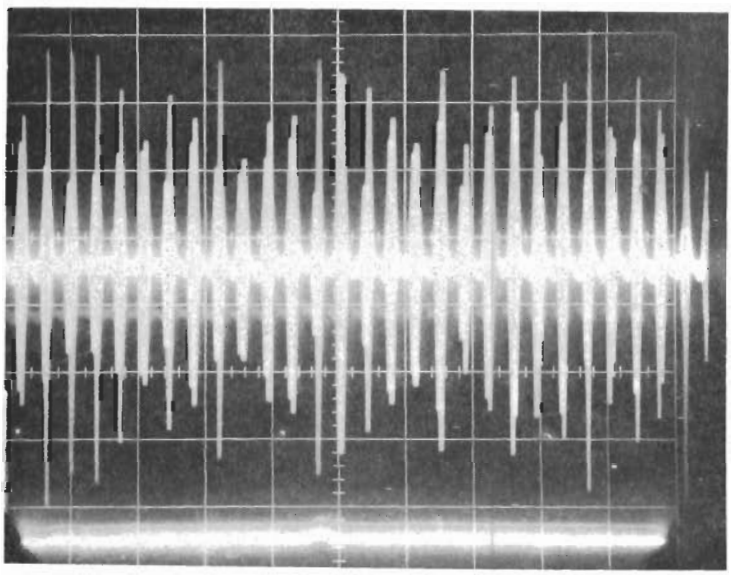

FIGURE 83 DIFFERENTIAL TIP DETECTOR OUTPUT AS A FUNCTION OF BLADE TWIST

variation in the blade angle. From Figure 79, approximately 1.0 degree of bending is the result of a .065 inch crack length.

2.3.5 Implementation of blade tip parameter detection system -- The signal processing system required to provide an indication of blade tip bending and/or twist can take several forms depending upon the number of detectors used and the blade-to-blade spacing comparison technique employed. A possible signal processing system is seen in Figure 84 . Waveforms at various points of the system are included in Figure 85 to illustrate the system operation. Here eddy-current detectors #2 and #3 are employed in a differential circuit to monitor blade tip twist. The detectors are mechanically positioned and electrically balanced to provide a minimum output for a normal blade. Blade twist results in an unbalance and, thus, an output proportional to the twist. Eddy-current detectors #1 and #2 are positioned a circumferential distance apart equal to the average blade-to-blade spacing. The output signals from detectors #1 and #2 are amplified, detected, and shaped resulting in the waveforms V_D and V_E of Figure 85. These waveforms drive flip-flops which supply gating pulses to an AND gate resulting in pulse trains, V_H, connected to a counter. Here, the counter output, V_I, is a function of the blade-to-blade spacing variation. Since the gating pulse duration is a function of compressor speed, the resulting count would be speed dependent. If, however, the waveform V_D (whose average value is proportional to compressor speed only) is used to control a voltage controlled oscillator, VCO, the count can be made independent of compressor speed. This system could easily be made to provide digital outputs proportional to spacing variations or a simple go/no-go indication depending upon the diode matrix in the binary scaler.

The system block diagram employs off-the-shelf components which are used in many systems today. Many of the blocks are, in fact, available in integrated circuit form occupying the volume of a single transistor. This system is provided only

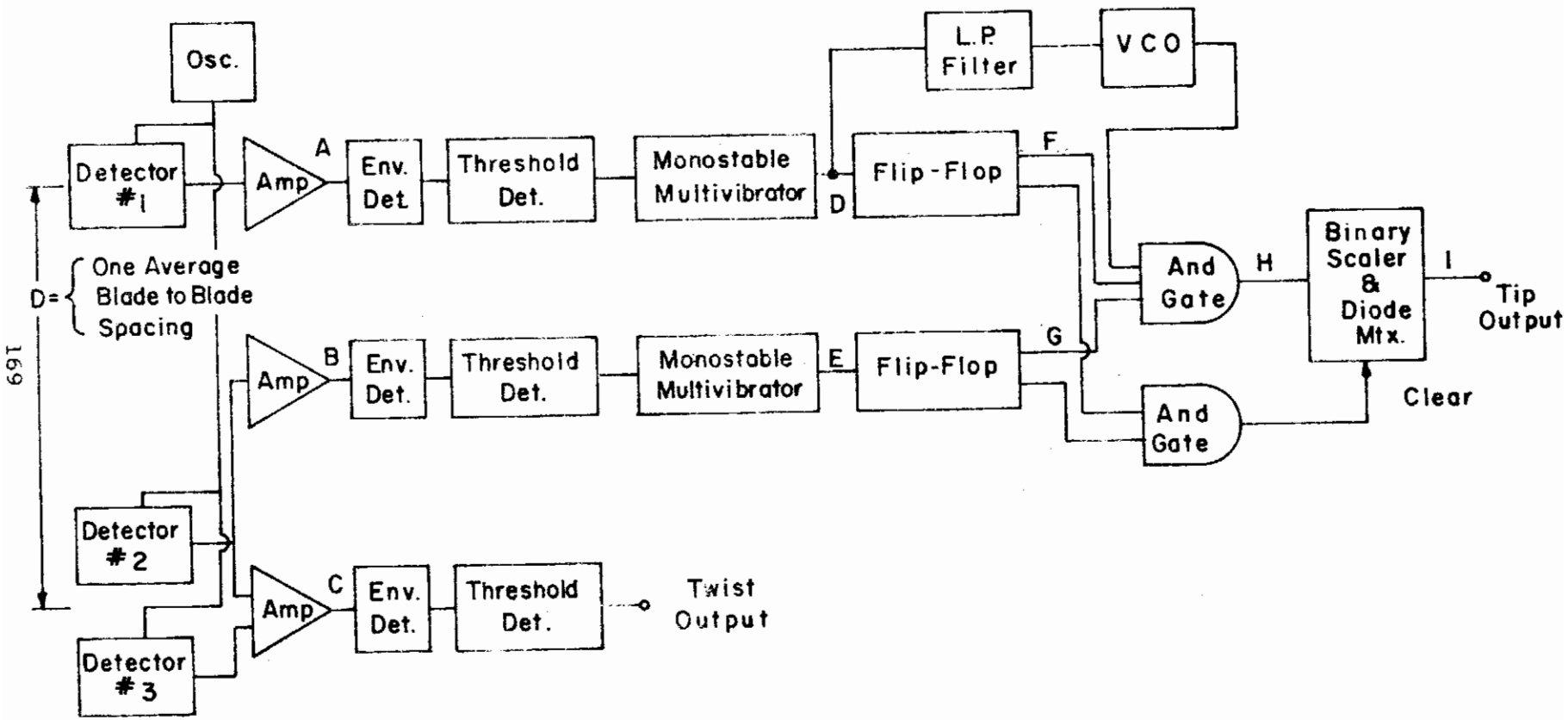

FIGURE 84 PROPOSEDTIP PARAMETER PROCESSING ELECTRONICS

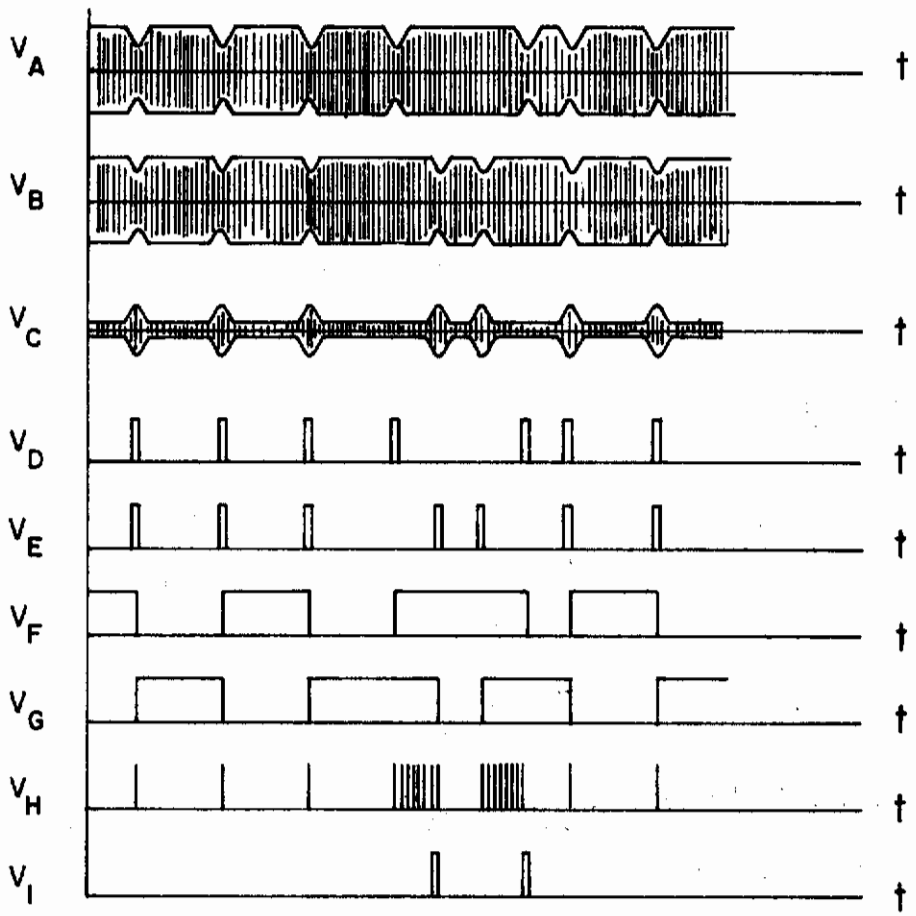

FIGURE 85 TIP PARAMETER MEASUREMENT WAVEFORMS

as an example of the amount of processing equipment required and does not represent an optimum design to perform the signal processing.

2.3.6 Conclusions -- The use of an eddy current detection scheme for monitoring blade edge defects was seen to be severely limited by the axial blade spacing or angle variations of a normal J-47 compressor section. Dynamic tests run using a differential circuit containing two parallel resonant eddy current detectors indicated that 1/8 inch diameter defects were virtually undetectable. If a signature of the detector output for a given compressor were available, the detection of 1/8 inch diameter defects should be possible with the present detectors. Subsequent static tests run on the J-47 compressor using a single detector are also presented. The results of these tests confirmed the marginal nature of the eddy-current edge defect detector.

An application of eddy current measurement techniques to monitor blade tip twist and position was seen to posses several advantages over the blade edge measurement system. Artificially introduced leading edge damage of the order of 3/32 inch x 3/32 inch was easily discernable over the normal system output or the effects of reworking the blades. Detection of blade edge defects via monitoring tip twist and tip-to-tip spacing with the compressor blades operating under an aerodynamic load were investigated. Here, a minimum blade tip twist of seven degrees as well as one degree of blade bending from its root is detectable. Although these signals are precursors of blade edge defects, they are a function of compressor speed as well as defect size and position along the blade edge and as such cannot provide a unique output as a function of defect size. Subject to a more complete analysis of damage results on actual in-use compressors, sensing twist or bending appears to be a good indicator of significant damage caused by ingestion of foreign objects.

2.4 Electrometer Techniques

2.4.1 Introduction -- The measurement of the capacitive variation between a rotating compressor rotor blade and a single stationary electrode or many small electrode plates could prove to be a useful detection technique, particularly for edge defects. During the program, two types of electrometer probes were experimentally evaluated on a small, high speed fan which was used to simulate a compressor. The first sensor evaluated was a single probe electrometer which could easily detect 0.005 inch position changes in rotating blades. The second sensor was a two probe electrometer which monitored adjacent areas on the leading edge of rotating blades. This sensor could easily resolve 0.06 inch edge defects. The main disadvantage of this sensing system is that the electrometer probe tips have to be positioned within a few thousandths of the blade edge for proper operation. Because of the normally large blade-to-blade position variation in a typical compressor (0.100 inch), the electrometer sensor was not evaluated on the J-47 compressor section.

2.4.2 Measurement techniques -- Because of the extremely small capacitance variations expected, an indirect approach to the problem of capacitance measurement was investigated. The electrometer sensor system selected is shown schematically in Figure 86.

The measured parameter in this system is the displacement current as the probe charges or discharges due to the variation in capacitance. The charge on a capacitor is given by the expression $Q = CV$; and since current is the time rate of change of charge, the displacement current is $I = \frac{V\,dC}{dt}$. Since only the changing component of capacitance affects displacement current, all stray and distributed capacitance can be neglected, provided they are constant.

For the preliminary feasibility measurements, a single probe electrometer was constructed. A small, highspeed fan was used to

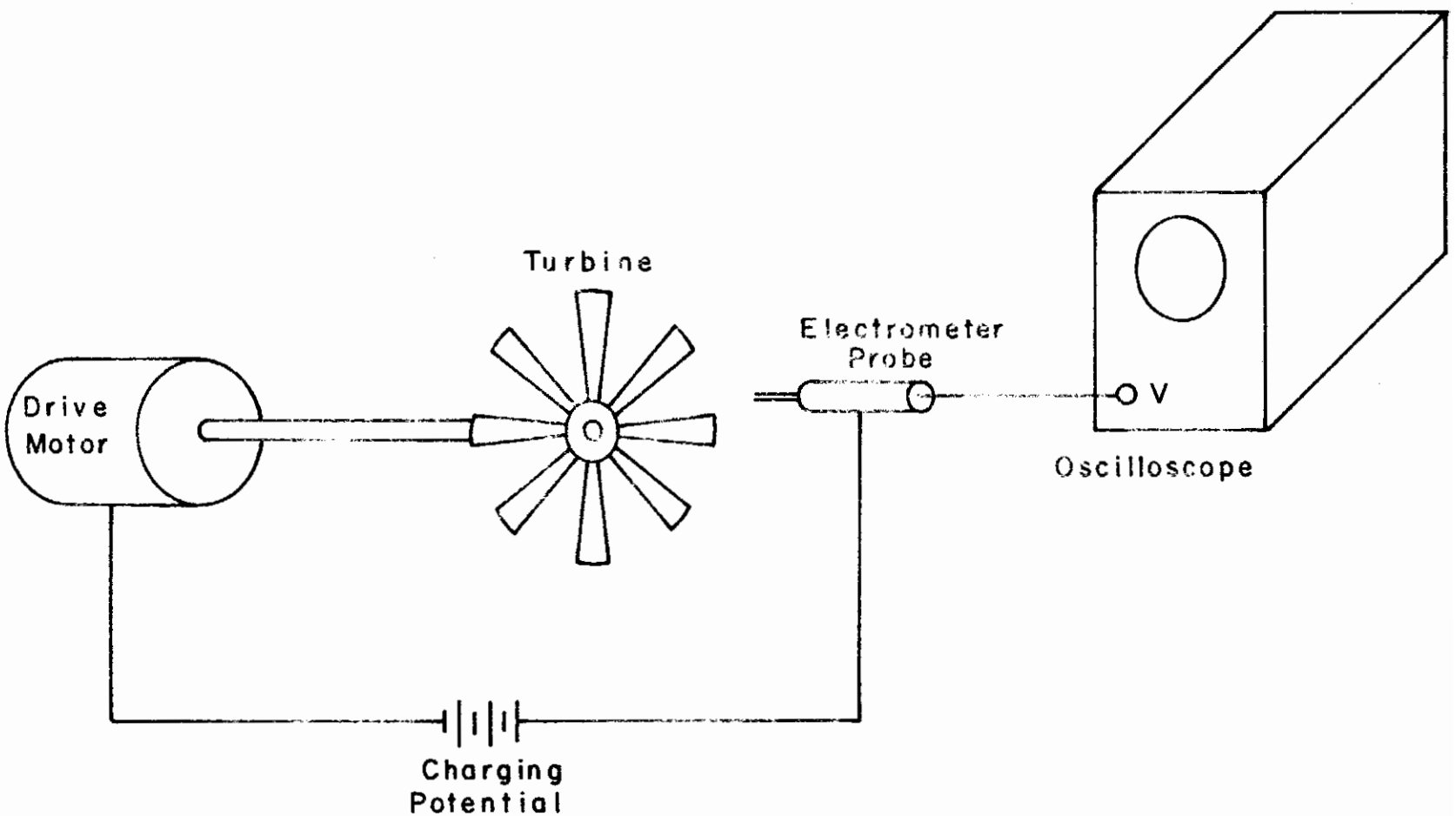

FIGURE 86 ELECTROMETER SENSOR SYSTEM

simulate the rotating compressor. The experimental set-up is shown in Figure 87. The probe was mounted on a micropositioner to permit calibration of output signal with respect to spacing. No attempt was made to distinguish defects in this experiment. The probe itself contained two transistors in a direct-coupled amplifier configuration to provide a current gain of approximately 40,000. Calibration was accomplished by adjusting the spacing between the probe and the rotating blade in discrete steps and recording the signal amplifude variations as observed on an oscilloscope. The pulse height varied from 4 mv at a 0.002 inch spacing down to 1.5 mv at a 0.012 inch spacing. From the data taken, an empirical equation was developed relating output voltage to probe spacing.

$$V = 1 + \frac{6}{S}, \quad \frac{S + 6}{S} = V, \text{ or } S = \frac{S + 6}{V} \tag{25}$$

where V = output voltage (mv)
S = probe spacing (inches).

To evaluate system sensitivity, Equation (25) may be differentiated with respect to S, resulting in

$$\frac{dV}{dS} = \frac{-6}{S^2} \tag{26}$$

As expected, the sensitivity improves as the spacing is reduced.

The output voltage was developed across a 10,000-ohm resistor so that the transfer function of the electrometer probe may be expressed as 10^5 volts per ampere. To relate this to detectable capacitance change requires establishment of a minimum detectable signal level. At this point, a definition of minimum detectable signal has not been made.

Following the preliminary tests using the simplified probe configuration, a dual input balanced electrometer sensor was designed, built, and tested. The two probe tips converge to a separation of 0.004 inches. The probe configuration is shown in Figure 88. Each probe tip is coupled directly to the input of a

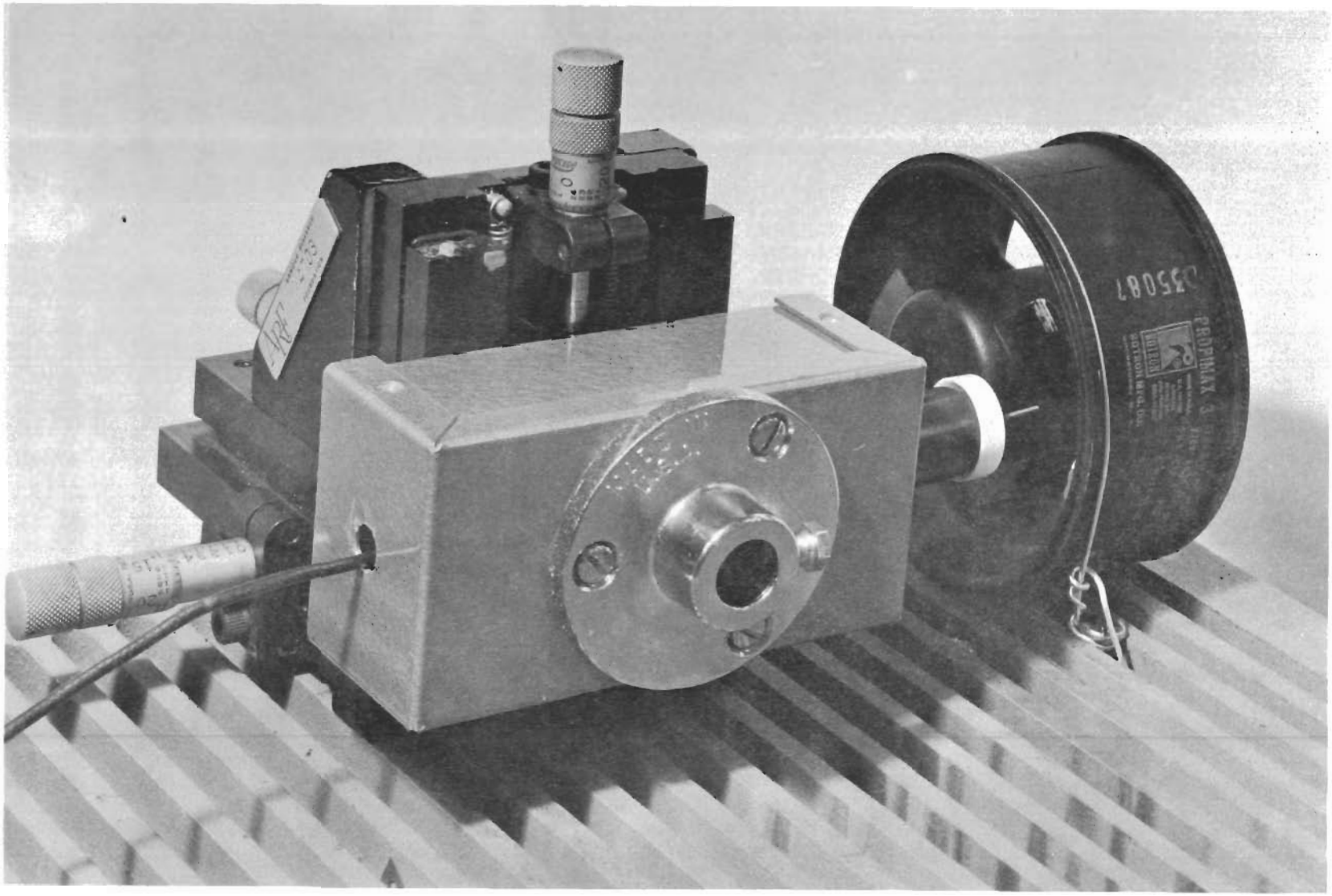

FIGURE 87 LABORATORY SET-UP FOR PRELIMINARY FEASIBILITY MEASUREMENTS OF SENSING SYSTEM

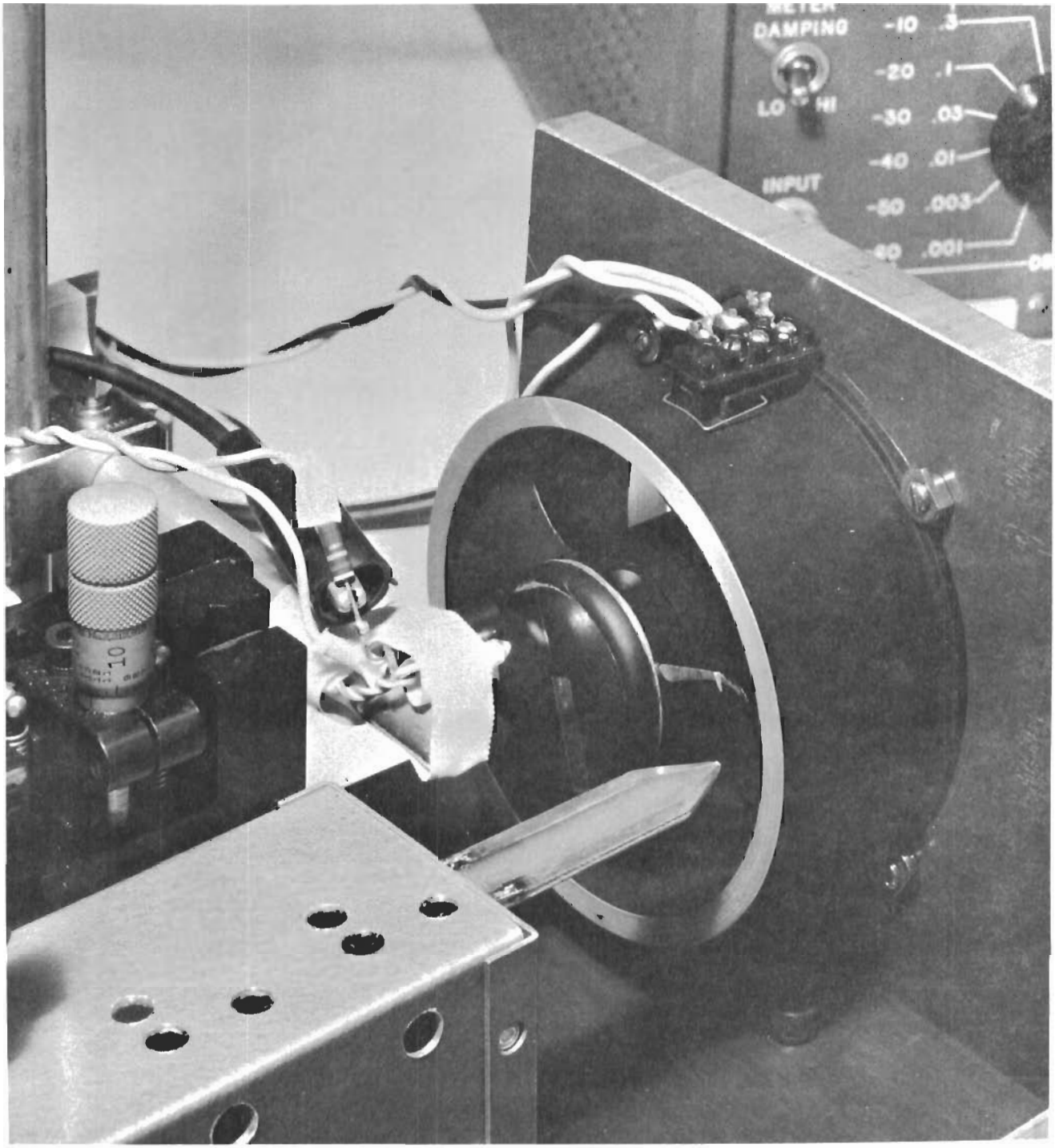

FIGURE 88 DUAL INPUT BALANCED PROBE CONFIGURATION

differential amplifier with high input impedance as shown in Figure 89. A small, high-speed fan was again used to simulate the rotating turbine engine (see Figure 88). A schematic representation of the electrometer system is shown in Figure 86, and a photograph of the experimental set-up is given in Figure 90. The sensor was mounted on a micropositioner to permit calibration of output signal with respect to spacing.

When the sensor system is completely balanced, any capacitance change which is common to both probe tips will be cancelled out. In this way, variations due to engine or sensor vibration is eliminated, as well as electrical noise from outside sources. If the sensor is brought close to the edge of a rotating compressor blade, a small defect which is closer to one probe tip than the other will produce an unbalance. The polarity of the unbalance will depend upon the location of the defect relative to the position of the probe tips. If the sensor is exactly centered over the defect, the output will again be balanced.

An experimental investigation of the two probe electrometer system was performed to determine what size defects could be detected with the system. These measurements were made on calibrated defects cut into the fan blade edges. The electrometer output pulses obtained for the two fan blades are shown in Figure 91. As can be seen, blade defects appear as variations in the amplitude of the electrometer output pulses. The amplitude of the output pulses increase as the size of the defect decreases. The pulse amplitude variation obtained for each of the two blades inspected is given below.

Blade No.	Defect Size	Pulse Amplitude
1	None	2.0 volts
1	0.063 in. x 0.13 in.	1.2 volts
2	None	1.9 volts
2	0.006 in. x 0.13 in.	$\approx$ 1.9 volts

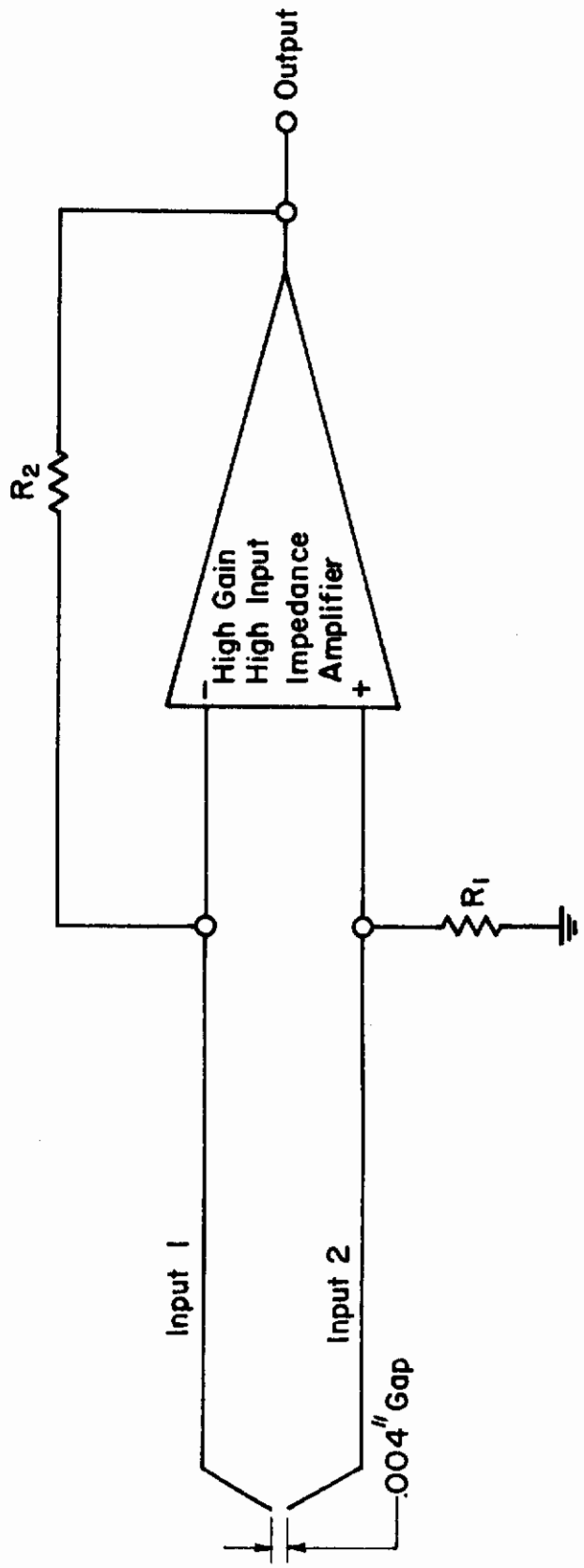

FIGURE 89 ELECTROMETER SENSOR

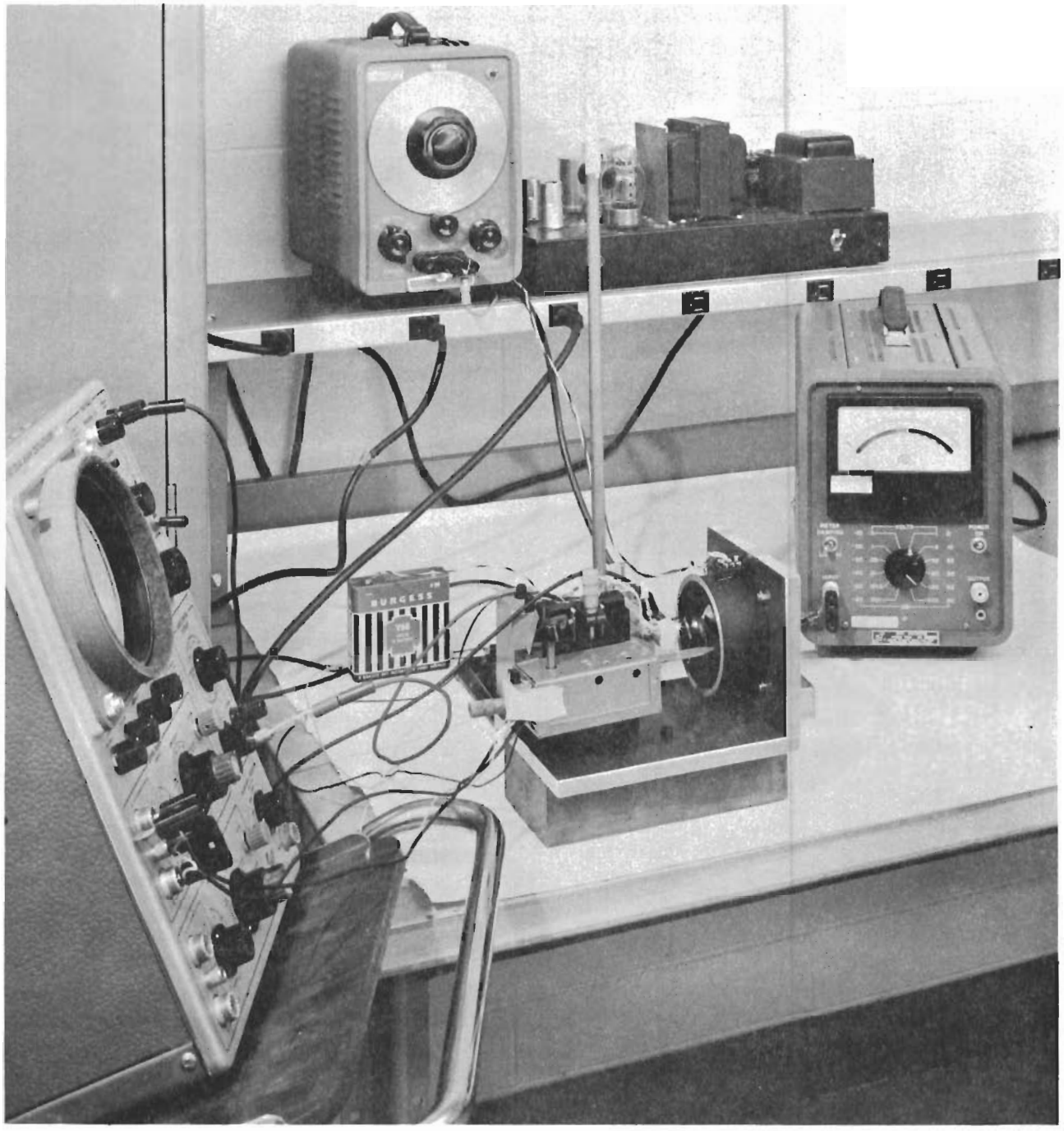

FIGURE 90 LABORATORY SET-UP OF ELECTROMETER SENSING SYSTEM

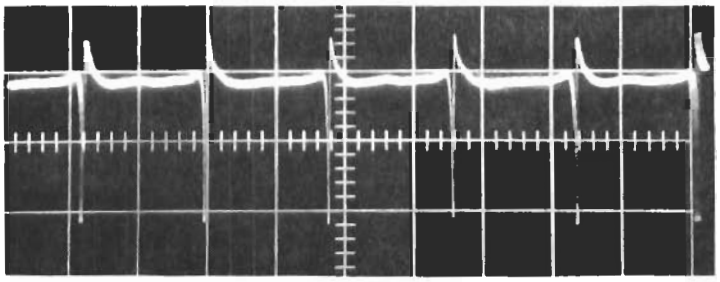

#1 #2

(a) Defect size: Blade #1 None
Blade #2 None

Horiz: 2msec/cm

Vert: 0.5 volt/cm

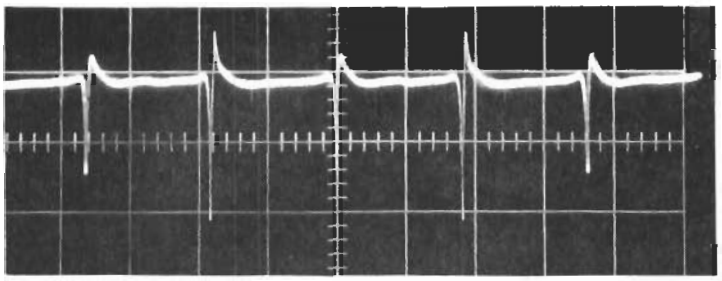

#1 #2

(b) Defect size: Blade #1 0.063 in x 0.13 in
Blade #2 None

Horiz: 2msec/cm

Vert: 0.5 volt/cm

FIGURE 91 ELECTROMETER OUTPUT PULSES

It has been demonstrated that with an adjacent area-to-adjacent area electrometer sensor, edge defects of the order of 0.060 inches can be detected. Defects of the order of 0.006 inches give only a slight pulse amplitude variation (less than 0.05 volts) which is the same order of magnitude as the variation between fan blades #1 and #2 with no defects present. The problem with implementing an electrometer as tested above is that in order to detect small defects the probe tips need to be positioned within a few thousandths of the blade edge to be inspected. This is not possible in an actual compressor. For example, the rotor blade positions for a J-47 compressor could vary by as much as 0.095 inches with respect to one another.

2.5 Optical Techniques

2.5.1 Introduction -- The number of optical approaches available to locate foreign object damage in compressor rotor blades is severely restricted by the requirement that the results be available immediately with flight line equipment. This rules out conventional photography as an approach, and visual inspection has also been ruled out by the contract work statement because of its subjectivity. The following optical concepts, however, were considered as possible approaches to the present problem:

1) Methods Depending on Reflectivity
   a. Color contrast
   b. Brightness contrast
   c. Facsimile scanning
   d. Flying spot scanning
2) Ranging
3) Thermal Emission
   a. Differential heating induced by imperfections.
   b. Differential thermal emission due to imperfections.

2.5.2 Optical considerations -- In many applications, color and color contrast provide a sensitive parameter for use in checkout. Compressor blades are, however, lacking in pronounced color attributes. Brightness contrast seems to be one of the most promising optical approaches. With appropriate implementation, it may be possible to resolve both surface flaws and edge imperfections such as nicks, dents, and pits. The implementation requires investigation of the illumination and optical imaging techniques to provide a maximum signal-to-noise ratio. This is particularly true due to the complex curvature of the blade edge. If, for example, focused light rays are used for illumination, the specular reflection from the blade edge may

provide a maximum light output for a good blade and a minimum output for a defect. On the other hand, if diffuse illumination is used, a strong specular reflection does not occur, and thus, the output from a defect may be greater than that for a good blade. The reliability may be degraded due to stains, grease spots, and re-work. The physical implementation of these concepts are discussed below.

The flexibility of optical fibers makes possible their arrangement into a wide variety of arrays. An array of special interest in this program is that of linear-to-circular configuration because of its adaptability to scanning applications. At one end, a large number of adjacent fibers are constrained to lie in a straight line by appropriate mounting, and at the other end, the fibers are formed around a circular drum to produce a circular array.

Figure 92 illustrates schematically how the above array of optical fibers may be used to scan compressor blades. The linear array of fibers is mounted at some convenient distance in front of the turbine engine compressor assembly. A camera lens, L, is adjusted to form an image of blade B in a plane containing the linear fiber array. The latter may now be thought of as an image dissector, with the image elements corresponding to the cross section of the individual fibers. Typical fibers have a diameter of 0.004 inch, but larger and smaller diameters are within the state-of-the-art. These discrete bits of information, consisting of different levels of light flux, are transmitted through their respective fibers and appear in ordered fashion at the end of the circular array.

Scanning can then be accomplished by rotating a crank-shaped fiber about the axis (extended) of the circular array, as shown in Figure 92. An appropriate detector, such as a PM tube, is mounted to receive the light flux emerging from the axial end of the crank-shaped fiber. A wide range of scan rates is possible

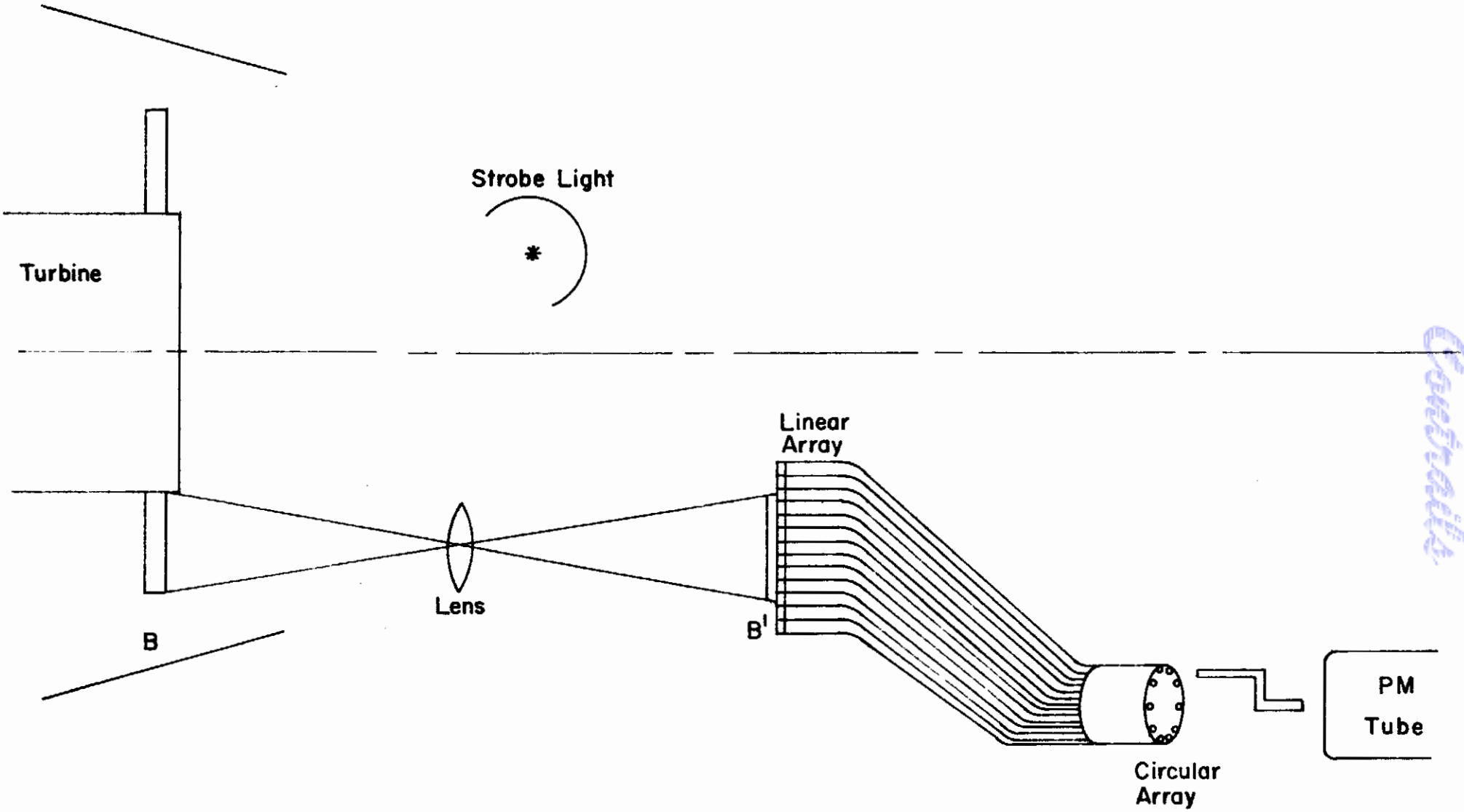

FIGURE 92 FIBER OPTICS SCANNING TECHNIQUE

with this arrangement. Because inspection is to be conducted with the turbine engine in motion, the illumination must be intermittant (stroboscopic) in order to "stop" the motion. By adjusting the strobe frequency relative to the angular frequency of the turbine it should be possible to execute an angular scan of the blades. Since three frequencies (turbine, linear scan, and stroboscopic) are involved, a careful analysis of the frequency effects will have to be conducted.

Another system that could be considered involves flying spot scanner techniques. In this approach, the flying spot would provide both the illumination and the scan. By appropriate programming, the cathode ray tube could also be made to provide the strobe frequency to "stop" the motion of the compressor blades or accomplish an angular scan of each blade in turn.

A theoretical analysis of the optical design parameters necessary for an experimental evaluation of the above optical inspection techniques involves analyzing the reflectivity of used blades. Based upon a visual inspection of typical compressor rotor blades obtained from Tinker Air Force Base, Oklahoma City, Oklahoma, reflectivity inspection techniques do not appear promising. The heavy dirt built up on the blades masks the small defects. The correction of reflectivity for large defects may also be a function of blade history. One might expect a greater reflectivity from the defect area due to its cleaning action. However, this same area may collect more dirt and thus have a decreased reflectivity after a period of operation. Thus, due to the above uncertainties the reflectivity technique was not pursued further.

Ranging as an optical inspection technique was also briefly investigated. Ranging involves the use of range finding or optical depth gauge methods. In one such method a bright narrow beam of light, e.g., a laser beam, is projected onto the compressor blade from an angle of 30 to 45 degrees to one side

and the position of the spot of light on the blade, as observed from an angle on the other side, indicates the "range," i.e., the distance of a particular point of the surface from an arbitrary base. The movements of the illuminated spot indicate the profiles of the blades. Using a lens system and an image multiplier tube to convert this optical information into electrical signals, a comparison between the successive blades can be made.

The ranging technique, however, has three disadvantages. One, the variations in blade edge to detector distance cannot be separated from that due to defects. Two, the blade edge as well as defect profile affects the angle of reflection to make the blade appear at a different position which may either mask the actual defect or make it appear larger. Three, accumulated dirt or dye spots could also cause major uncertainties.

A third optical technique that was investigated involves monitoring thermal emission from the blades. Thermal emission is a function of both the temperature and surface properties of a radiator. It is conceivable that an imperfect compressor blade will be warmer than a perfect blade because of greater aerodynamic heating. If this could be sensed while the turbine engine is revolving at a high speed, it might be possible to correlate blade temperatures with imperfections.

The ability to implement detection schemes based upon the air turbulance heating is dependent upon the absolute temperature of the blade and the temperature difference between the blade defect and the compressor background radiation. The absolute temperature of the blade determines the spectrum of the radiated energy as well as the radiated power. The use of detectors such as cooled gold-doped germanium allows monitoring radiation in the 1.0 to 9.0 micron region. Since the peak radiant emittance wavelength of a black body at 300°K is approximately 10 microns, temperatures slightly above this should be detectable. The time constant of these detectors is in the 0.1 to 1.0 μsec range placing them in the area of possible detectors. The second factor

affecting the detection of defects by this scheme involves the blade temperature rise above the background as a function of defect size. Since both good and bad blades create air turbulance, only the increased turbulance due to a defect is a precursor of the defect.

Another masking mechanism of the defect is the heat conductivity of the blades causing the heat generated by a defect to be conducted to the turbine shaft. Although detailed information is not available on heating of blades due to local turbulance, it presently does not appear that this heating mechanism would readily indicate defects of the size required in the work statement. A defect might also change the emissivity, but there is no evidence of this. Further, emissivity changes could occur due to oxidation or accumulated dirt which could mask a defect-induced "hot spot."

2.5.3 Conclusions -- The use of optical techniques in the detection of compressor rotor blade defects was not pursued beyond the theoretical phase. The variation of blade reflectivity under the operating conditions of the compressor made this parameter a relatively unreliable precursor of foreign object damage. The use of optical ranging is severely restricted by the blade spacing and tilt variations in a normal compressor. The third optical technique investigated, that of thermal emission induced by damage or by aerodynamic heating, was also rejected due to the variation in surface emissivity and small temperature differentials involved.

3.0 RELATED AREAS

3.1 Demonstration Breadboard System -- In order to demonstrate the applicability of the various sensing techniques proven feasible during the theoretical and experimental phase of the program, a turbine engine compressor section was employed. The specific type of unit used was from a J-47 class engine. This compressor assembly selection was based on:

1) Recommendations made by personnel of the Tinker Air Force Base -- Aerospace Engineer Performance Analysis and Support Section -- who have been actively engaged in compressor blade checkout during the engine overhaul phase.

2) Versatility of the system because of the method of construction employed. The rotor assemblies for the various compressor stages are readily removable as well as the blades from the rotor assembly.

3) Size of the assembly, necessary driving power, and auxiliary equipment required for operation and maintenance, such as lubrication system and special tools.

The compressor section was modified so that only two stages of stator blades were contained in the shell or housing. This arrangement is depicted schematically in Figure 93 . The purpose for removing the remaining stator stages was to decrease the power requirements for motoring the system. Since the rotor blades are of foremost interest in so far as foreign object damage detection is concerned, and since with the arrangement shown, five stages of blades are intact, the removal of the remaining blades was thought appropriate.

The compressor system was mounted on a baseplate by suspending the rotor assembly with two ball bearings and clamping the stator assembly to the bearing mounting brackets. With this arrangement, alignment between stator and rotor was readily maintained. The rotor system was coupled to a variable speed electric motor utilizing a flexible coupling. Rotational speeds,

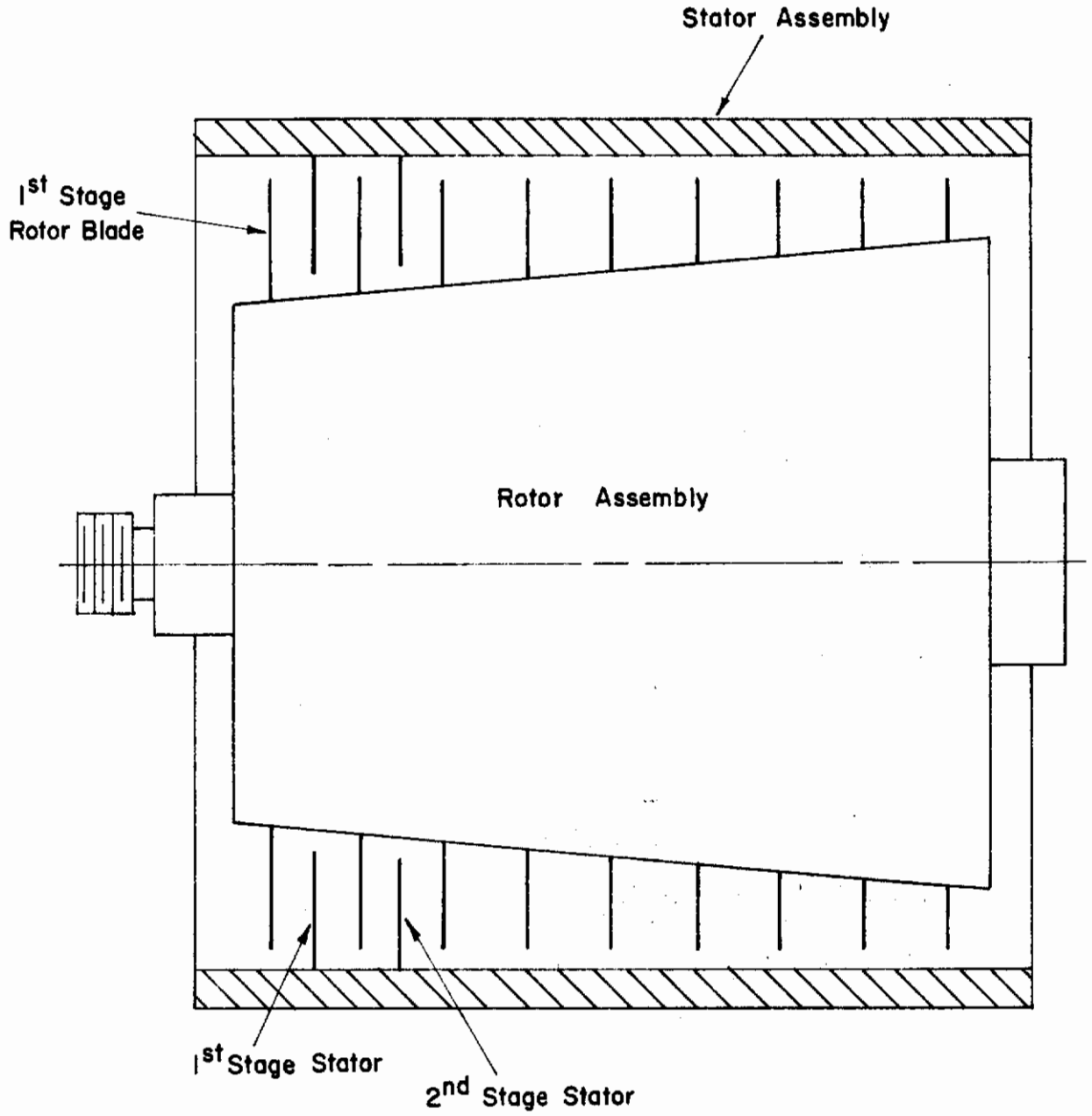

FIGURE 93 ARRANGEMENT OF DEMONSTRATION BREADBOARD SYSTEM SHOWING BLADE STAGES

variable from 780 rpm to 7200 rpm, are attainable with this system. The arrangement is schematically depicted in Figure 94.

Following initial installation, mechanical measurements were made to ensure proper operational tolerances on the system. It was determined that axial movement of the rotor was less than 0.0015-inch and radial runout was no greater than 0.0010-inch at operating speeds of 780 rpm and 1800 rpm. However, it was also noted that blade spacing and position variations not anticipated were present in the system. The tolerable fluctuations, based on Air Force specifications, are described in Section 3.2 of this report. The fluctuations observed on the compressor system were not beyond these limits. Thus, the system was termed representative of a typical jet engine compressor.

A pneumatic turbine type starter motor used with the J-47 class engine was also obtained. This motor can replace the electric drive system described previously. The pneumatic system was thought very desirable for simulating actual operating conditions because of the elimination of magnetic fields generated by the electric drive motor. In an actual turbine engine, these fields are not normally present and their presence may result in erroneous data for some of the sensing techniques. However, for all tests conducted the pneumatic system was not employed because the sensing techniques which were investigated were not affected by the electric motor magnetic fields.

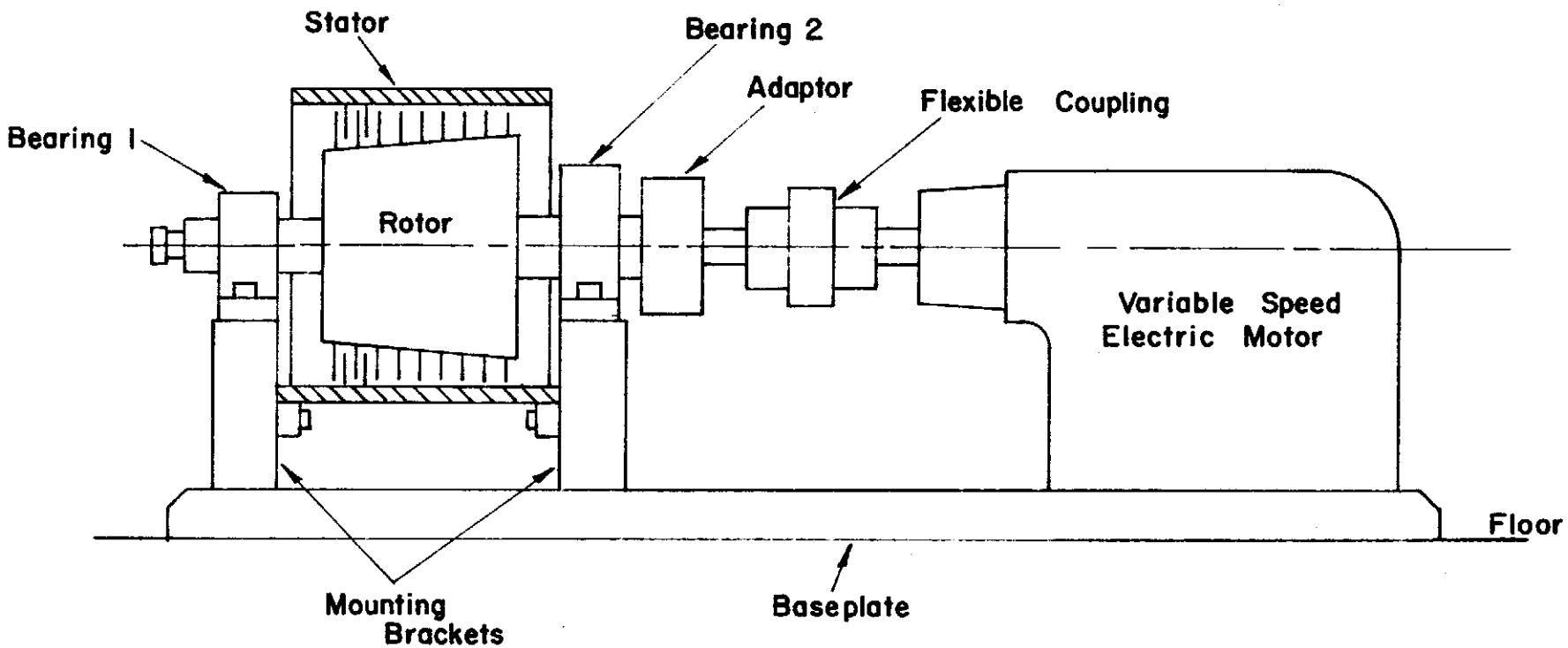

FIGURE 94 DEMONSTRATION BREADBOARD SYSTEM

3.2 J-47 Turbine Engine Compressor Section Variations

3.2.1 Compressor limits[1] -- Compressor section limits given in Table XII are used to determine the proper relationship between mating parts in any particular J-47 compressor assembly. Those limits are not for dimensional inspection at the time of tear-down and reassembly, but are used as a guide in cases of parts replacement or as a supplement to visual inspection for verifying serviceability of used parts. In most cases, dimensional inspection is necessary only if difficulty is encountered during reassembly. Clearance limits are given in inches and torque values in pound inches, unless otherwise indicated.

3.2.1.1 Clearance limits -- The limits prescribed in the tables contain the minimum clearances allowable between two parts, or, in dimensional measurements, the minimum and maximum dimensional limits of any one part. Replacement of parts is governed by the tolerance given in the "min" and "max" columns. The limits, together with visual inspection, are the indispensable guide in determining the future use, repair, or rejection of a particular part, and must be followed throughout the inspection procedure.

3.2.1.2 Definitions of symbols and terms -- The letter "A" indicates axial clearances, which are measured in a direction parallel to the rotor shaft. The letter "R" indicates radial clearances, which are measured in a direction perpendicular to the rotor shaft and are the dimensional differences between radii. The letter "D" indicates diameters which are measured in a direction perpendicular to the rotor shaft.

---

[1] This material is presented for reference by the IITRI technical staff and was taken from Technical Manual-Field Maintenance and Replacement-Turbojet Engines, Model J-47, T.O. 2J-J47-26, May 1, 1965, Section IV.

Table XII

COMPRESSOR SECTION LIMITS

Ref No.	Fig. 95 Index No.	Description	Direction Measured	Serviceable Limits In Inches Min	Max
1	1	Compressor front frame rabbet to inlet guide vane flange rabbet	D		
		Front frame rabbet OD		18.795	18.800
		Inlet guide vane rabbet ID		18.800	18.803
2	2	Compressor rotor first stage wheel shelf to inlet guide vane seal ring	D		
		First stage wheel shelf OD		17.930	17.939
		Inlet guide vane seal ring ID (Any one diameter)		17.946	17.992
		(Average of 4 diameters)		17.956	17.980
3	3	Compressor rotor first stage wheel rim to inlet guide vane seal ring	A	0.039	0.134
4	4	Compressor front frame to inlet guide vane mounting sector	D		
		Front frame ID		31.515	31.547
		Inlet guide vane mounting sector OD		31.360	31.440
5	5	Compressor stator casing rabbet to compressor front frame rabbet	D		
		Compressor stator casing rabbet ID		31.875	31.883
		Front frame rabbet OD		31.868	31.875
6	6	Compressor rotor blade tips to compressor stator casing	R		
		Stage 1		0.053	0.083
		Stage 2		0.035	0.080
		Stage 3		0.026	0.069
		Stage 4		0.027	0.068
		Stage 5		0.027	0.068
		Stage 6		0.020	0.061
		Stage 7		0.017	0.061
		Stage 8		0.018	0.052
		Stage 9		0.018	0.052
		Stage 10		0.012	0.052
		Stage 11		0.010	0.047
		Stage 12		0.010	0.041
7	7	Compressor stator blade tips to compressor rotor spacers	R		
		Stage 1		0.030	0.135
		Stage 2		0.032	0.131
		Stage 3		0.030	0.129
		Stage 4		0.035	0.145
		Stage 5		0.034	0.133
		Stage 6		0.038	0.133
		Stage 7		0.037	0.126
		Stage 8		0.032	0.103
		Stage 9		0.033	0.110
		Stage 10 & 11 (Shaft type)		0.025	0.084
		Stage 10 & 11 (Curvic coupling)		0.035	0.084
		Stage 12 (To rear frame outer air seal		0.003	0.057
		Exit stage (To compressor rear frame)		0.004	0.045

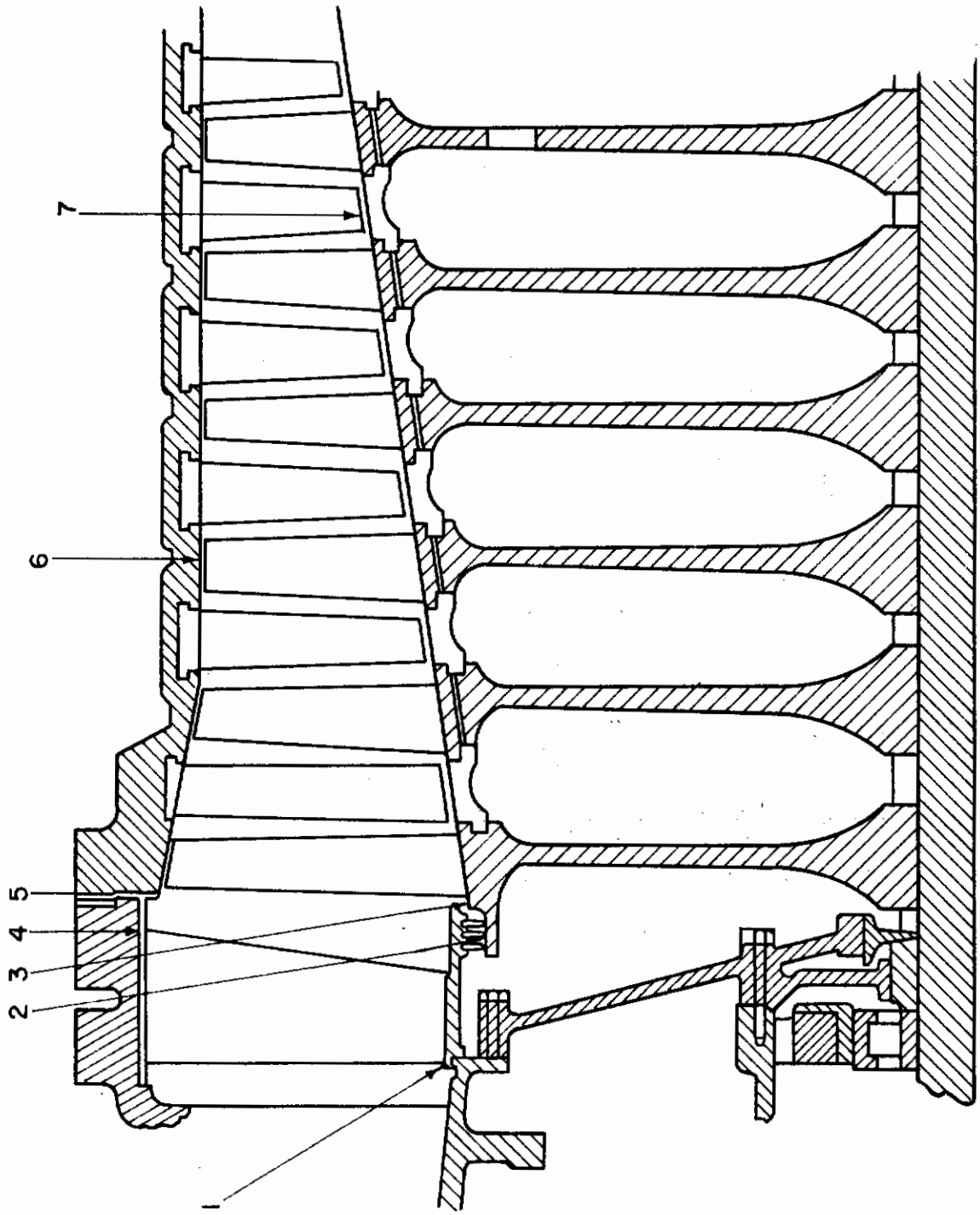

FIGURE 95 COMPRESSOR SECTION LIMITS

The column of "Serviceable Limits" indicates minimum and maximum dimensional limits or clearances permitted for parts that have been in service. If these limits are not exceeded and if no other damage is present, the part may be returned to service. The abbreviations "OD" and "ID" are used to mean "Outside Diameter" and "Inside Diameter," respectively.

3.2.2 Compressor rotor blade inspection and repair procedure[2]

3.2.2.1 General -- The maximum number of rotor blades to be reworked for leading and trailing edge damage is as follows:

1) Not more than 5 blades per stage in each 90 degree quadrant of stages 1 through 7 are to be reworked.

2) Not more than 6 blades per stage in each 90 degree quadrant of stages 8 through 12 are to be reworked.

3) Not more than 50 blades in each 90 degree quadrant of the rotor may be reworked.

Any number of repairs can be made on the leading and trailing edges of individual blades provided that the material removed does not exceed the maximum allowable for one edge and the number of blades reworked does not exceed the quantities listed above. Whenever it is necessary to remove the maximum allowable amount of material from one or more rotor blades, the engine is subjected to a vibration run on a test stand.

Any number of rotor blades may be reworked for contour surface damage and/or blade corner damage. Damage in Area B, Figure 96, such as dents, pits, mars, or scratches can be reworked if the damage does not exceed 0.010 inch deep. Any number of damages in Area A, Figure 96, are reworkable if the maximum depth of the rework does not exceed 0.031 inch.

Blade thickness in any area may not be reduced by more than 0.031 inch; i.e., damage on the blade surface may not be reworked if it is opposite previously reworked damage on the

[2]Ibid

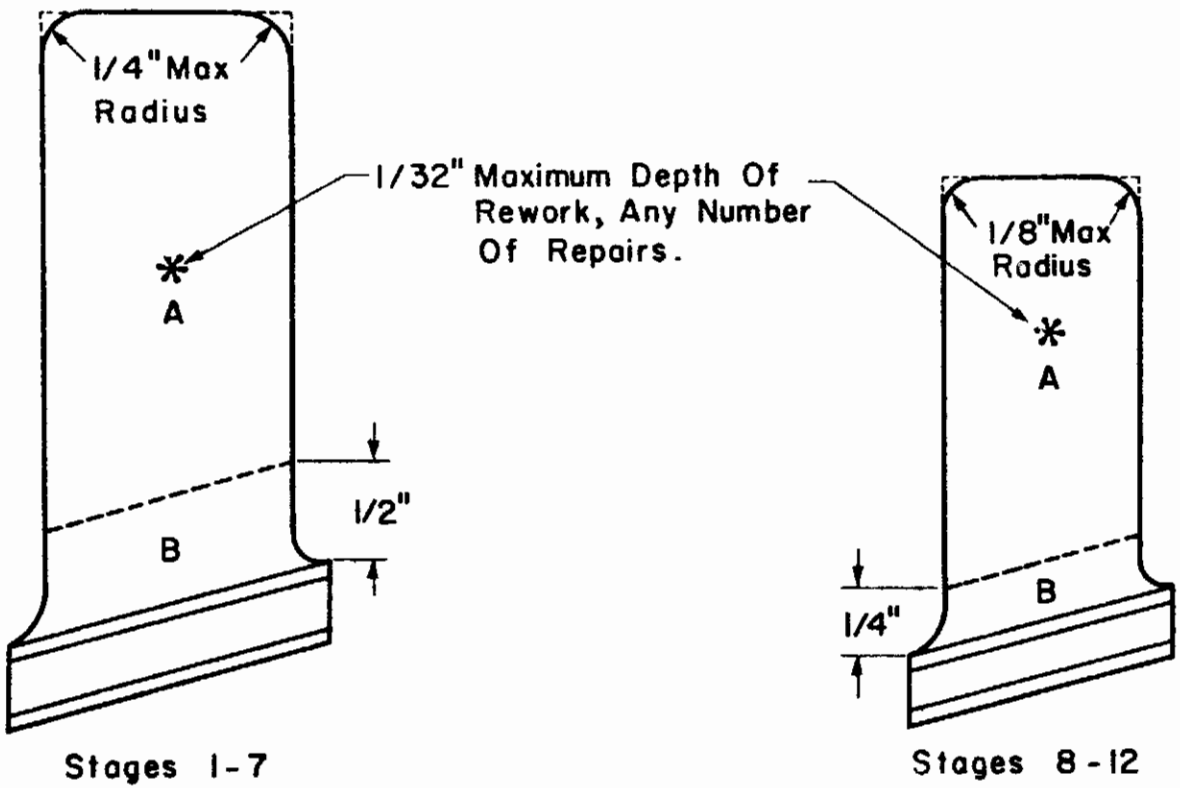

FIGURE 96 ACCEPTABLE ROTOR BLADE TIP AND CONTOUR REPAIR

reverse side of blade. Damage to blade tip corners may be repaired by forming a blend radius if the damage can be removed without exceeding the limits stated in Figure 96. Corner damage may be repaired on blades that have been reworked to the maximum limits on the leading and/or trailing edges. All limits specified are in relation to the original blade dimensions and apply to total material removed in accumulated rework. The minimum blade width (chord length) after rework is shown in Table XIII.

Blades with leading and trailing edge damage can be repaired if the damage is within the limits of the repair areas specified in Figure 97. Any blade on which the trailing edge cross section is less than 0.015 inch in thickness (knife edge) can be reworked to incorporate a radius on the trailing edge that will provide a minimum thickness of 0.015 inch. Any amount of damage (nicks, dents, pitting, etc.) in the leading and trailing edge of the blades can be repaired provided the total rework does not exceed the rework allowable for one edge. The damage should be repaired by removing the material in a long blend. The blend should begin at least 0.5 inch below the defect, or in the root area at the blade base, whichever is closer, and continue through the damaged metal. The blend should extend beyond the damage point for at least 0.5 inch, or to the blade tip, whichever is closer (see Figure 97).

3.2.2.2 Pitting inspection and repair -- Inspection of rotor blades for pitting is as follows:

1) Pitting on the leading and trailing edges to 0.015 inch diameter is acceptable. If the pitting exceeds these limits, repair procedures are to be employed.

2) Pitting on all other surfaces to 0.062 inch diameter and 0.015 inch deep is acceptable unless there are concentrated areas of pitting. Pitting is termed concentrated when the majority of the pits within a 0.5 inch circle have greater than 0.031 inch major surface dimension and are grouped closer than 0.125 inch to each other. If pitting exceeds these limits, repair procedures are to be followed.

Table XIII

ROTOR BLADE MINIMUM CHORD LENGTH
(BLADE WIDTH) AFTER REPAIR

STAGE	ROTOR
1	1.123 (tip)
	1.292 (root)
2	1.155
3	1.155
4	1.155
5	1.155
6	1.155
7	1.155
8	0.855
9	0.855
10	0.855
11	0.855
12	0.855
Exit	

The first-state rotor blades are tapered; therefore, the blade chord length is given for both the tip and root area.

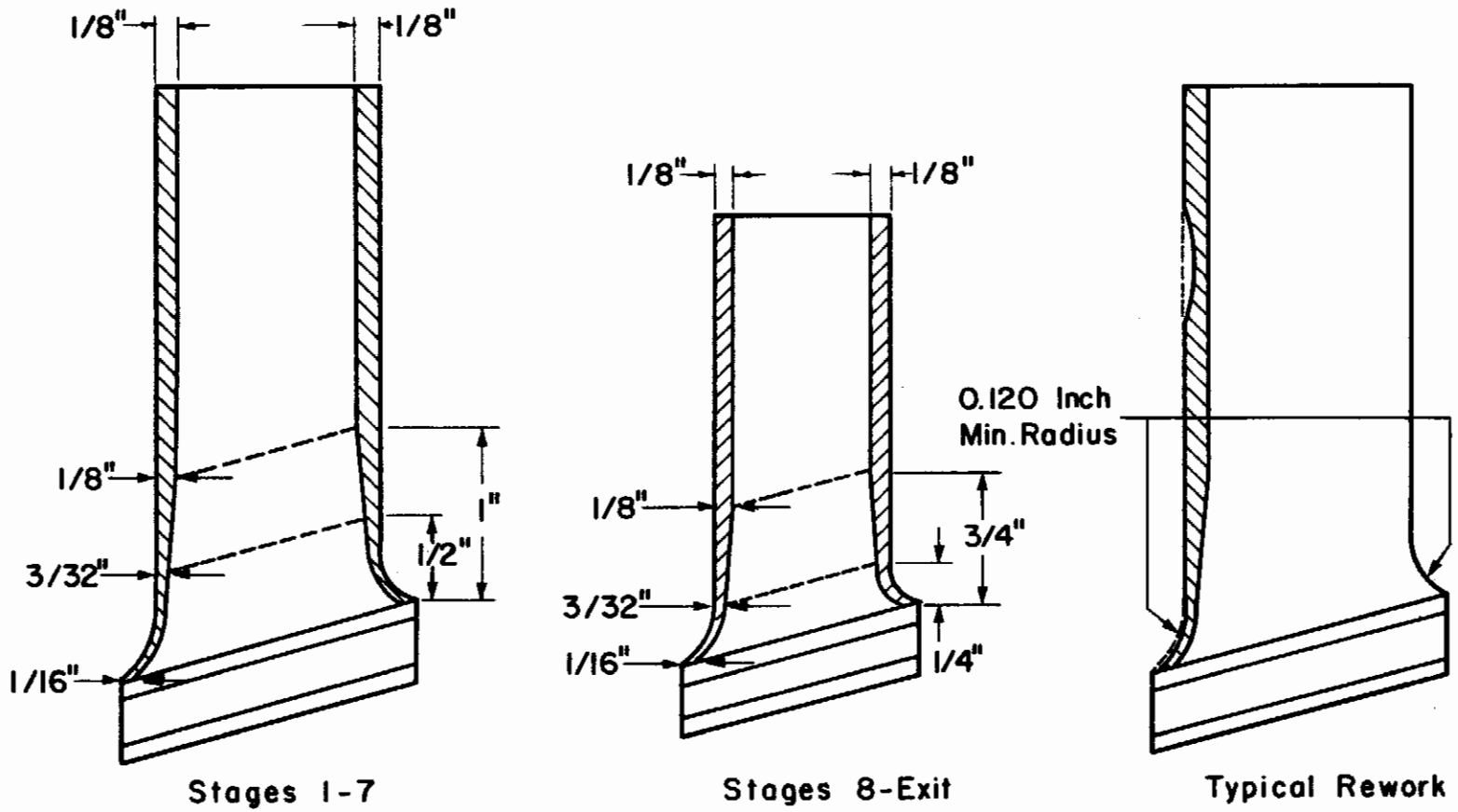

FIGURE 97 ROTOR BLADE LEADING AND TRAILING EDGE REWORK LIMITS AND AREAS.

3.2.2.3 Warpage inspection and repair -- Rotor blades must be inspected for leading and trailing edge warpage. Leading edge warpage must be repaired if all warpage can be removed within the allowable leading edge rework limits (see Figure 97). Trailing edge warpage is acceptable provided limits in Table XIV are not exceeded (see Figure 98).

3.2.2.4 Corrosion inspection and repair -- Rotor blades are to be inspected for corrosion. Corrosion which has resulted in surface build-up that can be detected by touch from the compressor blades must be removed.

Table XIV

BLADE TRAILING EDGE WARPAGE LIMITS

Stages	Area A	Area B	Area C
1 and 2	9/64-in.	5/64-in.	5/64-in.
3 through 5	7/64-in.	1/16-in.	1/16-in.
6 through 9	5/64-in.	3/64-in.	3/64-in.
10 through Exit	3/64-in.	1/32-in.	1/32-in.

3.2.2.5 Circumferential looseness inspection and repair -- Forged rotor blades must be inspected for circumferential looseness. Circumferential looseness (tip shake) is defined as the looseness between the blade and wheel or blade and ring. The blade should be grasped at the root with the thumb and forefinger and attempts to move it should be made. If movement is detected, this should be measured with a dial indicator attached to an adjacent blade. Rotor blades with circumferential looseness should not exceed the acceptable limits in Table XV. If looseness exceeds the acceptable limit but is less than the replacement limit, the blade can be peened.

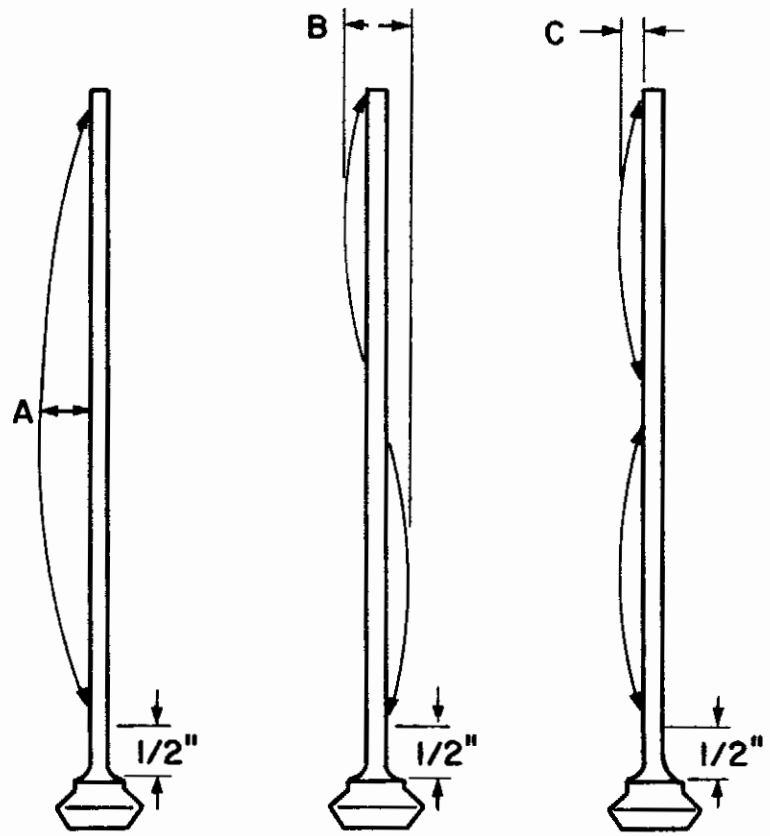

FIGURE 98 BLADE WARPAGE AREAS

Table XV

TIP SHAKE LIMITS FOR FORGED BLADES

	COMPRESSOR ROTOR BLADES	
	Acceptable Limit	Replacement Limit
Stage		
1	0.029	0.087
2	0.024	0.072
3	0.021	0.063
4	0.020	0.060
5	0.018	0.054
6	0.016	0.048
7	0.015	0.045
8	0.013	0.039
9	0.012	0.036
10	0.011	0.033
11	0.011	0.033
12	0.011	0.033

3.2.3 Compressor blade spacing measurements -- In the evaluation of a particular checkout technique, one would ideally vary only the parameter to be sensed and maintain the other system variables constant. This technique was employed in the laboratory during Phase II of the program to determine the most promising techniques to measure defects in compressor blades. Based on the information obtained during this phase, the most promising checkout techniques were then employed on the actual J-47 compressor section during Phase III. During that phase, many of the parameters which were controlled in Phase II could no longer be controlled but only monitored. The checkout system output had to be correlated to these variations. In order to evaluate the system sensitivity, calibrated defects varying from 0.0078 inch diameter to 0.125 inch diameter were cut into the blade edges as seen in Figure 64. Since variation of blade-to-detector spacing was seen to affect the sensitivity of the checkout techniques evaluated in Phase II, measurements of blade edge spacing and blade edge tilt relative to a plane perpendicular to the turbine axis were made. These measurements were taken at positions A, B, and C of Figure 64. The results of these measurements are tabulated in Tables XVI and XVII. Due to the difficulty of performing theoretical analyses of the checkout techniques, these parameters in conjunction with the detector system outputs may allow optimization of the detector parameters.

3.2.4 Definition of terms[3] -- The definition of terms associated with deviations in a turbine engine compressor assembly are given in Table XVIII.

[3] Ibid

Table XVI

COMPRESSOR BLADE SPACING MEASUREMENTS

Blade No.	Dimension A (Mils)	Slope S_{AB} (Mils/in)	Dimension B (Mils)	Slope S_{BC} (Mils/in)	Dimension C (Mils)
1	29	40.6	100	51	215
2	18	32.5	75	55	199
3	14	31.4	69	55.5	194
4	22	36	85	56	211
5	14	32	70	62.3	210
6	8	35.5	70	58.8	202
7	21	32	77	59	210
8	12	37	77	56	203
9	17	33	75	59.2	208
10	48	28	97	53.3	217
11	36	33	94	54.8	217
12	23	33	81	59	214
13	17	33	75	59	208
14	2	33.8	61	61.8	200
* 15	33	37.7	99	53.8	228
16	18	34.8	79	58	209
* 17	21	34.8	82	58	214
18	9	36.6	73	63.5	215
19	23	36.6	87	55	211
20	23	30.2	76	59.8	210
* 21	20	35	81	59	212
22	36	28	85	55	209
* 23	36	30.8	90	61.4	220
* 24	4	39.5	73	59.2	196
* 25	10	26.3	56	62.3	206
26	19	36.3	83	56.5	210
27	22	21.7	60	60	195

* Blades containing calibrated defects.

Table XVI (Continued)

Blade No.	Dimension A (Mils)	Slope S_{AB} (Mils/in)	Dimension B (Mils)	Slope S_{BC} (Mils/in)	Dimension C (Mils)
28	9	30.2	63	61	200
29	15	29.6	67	57	195
30	5	36.6	69	58.8	201
31	24	25.8	69	53.3	189
32	11	32.6	68	56	194
33	7	41	79	58.3	210
34	12	31.4	67	55.6	192
35	25	36.6	89	55	213
36	14	31.6	69	57.8	199
37	12	30.3	65	60.5	201
38	37	30.9	91	57	218
39	11	30.3	64	63.2	206
40	33	26.3	79	55.6	204
41	31	29.7	83	62.3	223

Table XVII

RANGE OF COMPRESSOR BLADE SPACING MEASUREMENTS

Parameter	Maximum (Mils)	Minimum (Mils)	Range (Mils)
A	48	2	46
B	100	60	40
S_{AB}	41	21.7	19.3
S_{BC}	63.5	51	12.5
C	228	189	39

Table XVIII

DEFINITIONS OF DEVIATIONS

Handbook Term	Definition	Associated Terms
Blister	A raised portion of a surface caused by separation of the outer layers of the parent material or a coating applied to it.	Bubble Flaking Oxide formation Peeling Scale Slag inclusion (weld)
Brittle	A change in the resiliency of the parent material, usually due to aging, extreme heat, extreme cold, chemical action, or cold working (metal).	Cold worked Hard (like an old "O" ring) Stiff
Buckle	A large-scale deformation of the original contour of a part, usually due to pressure or impact of a foreign object, unusual structural stresses, excessive localized heating, high pressure differentials, or any combination of these.	Ballooning Bend Blister (incorrect-see Blister) Bulge Crease Curl Dent (not to be confused with small-area defect in heavy material-see Dent) Depression Distortion (usually refers to heavy material) Elongated (usually refers to "out-of-round") Fold Indentation Kink (usually results in crack-see Crack) Protrusion (hollow) Rupture (result of excessive buckling) Uneven Warpage Wrinkle
Burr	A rough edge or a sharp protrusion on the edge or surface of the parent material.	
Chip	A breaking away of the edge of the parent material, usually caused by heavy impact of a foreign object.	Break Nick (similar to Chip but no parent material is removed-see Nick) Notched Spalling (usually a flat surface breaking away-see Pit)
Corrosion	A mass of small pits which cumulatively create a large cavity (usually shallow) in the surface of the parent material.	See Pit
Crack	A parting of the parent material with or without deformation of the surrounding area.	Break Crater (usually found in castings) Fatigue damage Fissure Fracture Inclusion (usually found in castings) Lap (usually found in forgings) Rupture Separation Shear (not usually considered a crack-see Missing Piece) Slit Tear
Dent	A completely smooth surface depression caused by pressure or impact of a smooth ball-like foreign object. The parent material is displaced but usually none is separated.	Peen
Deviation	An abnormal condition which causes a part to be other than the condition of a new part which agrees with the manufacturer's blueprint.	Damage Defect Flaw Imperfection Irregularity

Table XVIII

DEFINITIONS OF DEVIATIONS (cont)

Handbook Term	Definition	Associated Terms
Gouge	A general term used to describe a wide rough scratch or group of scratches, usually with one or more sharply impressed corners, and frequently accompanied by deformation or removal of parent material.	
Groove	A general term used to describe a long narrow continuous cavity or impression caused by pressure of a moving adjoining surface in contact with the parent material.	If impression is shallow and smooth-see Wear If impression is sharp-see Scratch
Loose	A part which has abnormal movement in relation to another.	Backed out Excessive movement Excessive play Insecure Leaks Loose fit Not tight Not torqued Shakes Sloppy Rattles Unbottomed Unpinned
Misaligned	A mismatching or malformation of any parts or mating parts which will either prevent perfect assembly, or result in faulty operation and/or ultimate part failure.	Eccentric Not axial Not concentric Out-of-round Unmatched Unsquare
Missing Piece	Removal or loss of a portion of parent material due to a combination of defects of damages	Break (two or more pieces) Burn (burned away) Burn-out Corrosion (eaten away) Erosion (worn away) Guttered Hole Rusted (rusted away) Sheared Smashed Torn (torn away)
Nick	A surface impression with sharp corners or bottom, usually caused by pressure or impact of a sharp-edged foreign body. The parent material is displaced but usually none is separated.	Chip (see Chip) Dent (see Dent) Notch (see Chip)
Pickup	The result of movement and/or the transfer of one material into or upon the surface of another. This is caused by: a. Contact between moving parts. b. Deposits of molten material on a cooler material.	Burr (usually tool-rub leaving high parent material) Gall (usually due to "a") High spot (if result of "a" or "b") Imbedment Inclusion (usually pickup of a dissimilar foreign material) Pile-up (usually due to "a") Protrusion (deposit on parent material) Metalization
Pinched	A condition caused by pressure on the parent material which usually results in distortion of one or more surfaces of the parent material.	Bound Compressed Flattened Seized (see Seizure) Smashed (without separation into pieces) Squashed Squeezed Tight

Table XVIII

DEFINITIONS OF DEVIATIONS (cont)

Handbook Term	Definition	Associated Terms
Pit	A minute depression or cavity, with no sharp high-stress corners, in the surface of the material. Pits are usually caused by chemical reaction (rusting, chemical corrosion, etc.)	Corrosion Crater (usually in weld or casting) Dent (incorrect-see Dent) Electrolytic cavity Erosion (usually results in hole-see Burn) Fretting (see Wear) Inclusion (as in sand castings) Oxidation Perforation (usually in weld) Pock-marked Spalled Roughness
Rub	A general term used to describe a surface cavity or impression caused by two contacting surfaces moving against one another.	If impression is shallow and and smooth-see Wear If impression is sharp-see Scratch
Scratch	A long, narrow, sharp-cornered impression caused by the movement of a sharp object across the surface of the parent material.	Abrasion Chafe Furrow Groove Rub Scarf Score
Unbalanced	A condition created in a rotating body by an unequal distribution of weight about its axis of rotation. Usually results in vibration.	

3.3 Signal Processing -- Signal processing can normally enhance the detectability of a number of checkout techniques. For example, the eddy-current methods of detecting edge defects could be considerably improved by the use of signal processing. In this case a memory system would be required. It would remember the effects of blade tilt and actual displacement for each individual blade. Such a system could be devised, built, and used successfully in conjunction with the eddy-current sensor. However, an examination of the total amount of information storage required indicates considerable cost may be involved. For example, a typical compressor section can have approximately 40 blades where each blade is roughly 6 inches long and 0.050 inches of resolution are required. At least 120 segments, therefore, must be noted for each blade. In addition, a dynamic range of over 1000 to 1 might be required. In this event, something in the order of a five megabit storage would be required. Although further sophistication might reduce this considerably. To test a motoring engine, the bandwidth of the memory system would have to be in the order of a megacycle, thus requiring the immediate accessibility offered by either a drum or disk storage. While this storage capacity is currently available in drum and disk systems, it is by no means simple and economical.

In the case of the millimeter wave detection system, some type of memory system might be required to enhance its detectability. However, since most of the signal processing is already built into the detection system, only a crude memory system might be required. In the case of the millimeter-wave, remnant-magnitization, and blade-twist and blade-bending systems, only simple analog processing appears to be required to accomplish many of the requirements. These systems would require some type of synchronization which samples the detected output at the appropriate interval, and by means of level set circuits and peak clipping circuits, for threshold indicators, the presence of foreign object damage or the effects of foreign object damage

could be resolved. For the techniques which compare the time of arrival of the blade tips, simple automatic-frequency-control circuits could lock on to the idling rotational frequency of the jet engine. The output from the sensors could be suitably shaped to square waves and the individual times of arrival compared with average time-of-arrival as developed by the automatic frequency control circuits.

4.0 CONCLUSIONS

Initially, even partial realization of the performance goals in terms of the dimensions of damage seemed difficult when a number of the promising techniques were first evaluated on the actual J-47 compressor section. Eventually, the millimeter-wave system when used as an adjacent area-to-adjacent area computer, did appear to be sufficiently immune to the normal blade tolerance variations and still possess sufficient sensitivity to resolve physical damage effects approaching those of the design goals. Since this system was one which was originally selected on a preliminary basis and on which considerable effort was expended, it was rewarding to see some of the expectations demonstrated. The use of adjacent area-to-adjacent area comparison techniques in an interferometer form permitted operation of the millimeter wave system essentially independent of the normal blade positioning tolerances. Increasing the frequency of operation, and hence the resolution, from 15 GHz to 88 GHz demonstrated that the resolution could be improved from approximately a 0.125 inch radius defect to a 0.030 inch radius defect on the leading edge of first stage compressor rotor blades. The results were considered to be very satisfactory considering the rudimentary design of the system. Further design improvements, such as increasing the frequency, increasing the source power, and employing a more sensitive receiver, should permit detections of defects 0.015 inches deep on the leading edge of the first state compressor rotor blades. In addition, there is some hope, although with less resolution, that an improved system could have the ability to resolve defects on the air foil contour area of the first stage blades and edge defects on the second stage. The millimeter wave systems best performance can probably be realized for flight line usage. In this case, a small streamlined package containing the millimeter wave radiating system could be inserted and positioned in the cowling so as to scan the various rotor

blades. The distance between the system and the blades should be as close as possible, although separation distances as far as one foot could be considered with some loss in resolution.

By considering the final objective of detecting any manifestation of foreign object damage permitted consideration of several other promising techniques. The first technique which fulfilled this criteria was the development of a sensor system to note changes in the remnant magnetization of the compressor blades caused by foreign objects striking the blades. If a foreign object is ingested into the compressor assembly and hits any premagnetized blades, the remnant magnetization will be reduced, and this reduction is a function of the size and velocity of the object. Simulated foreign object damage tests conducted at IITRI demonstrated that when ingested objects have sufficient energy to cause a 0.015 inch defect they were clearly resolvable. Before these tests could be seriously considered, a field test was conducted to demonstrate that the remnant magnetization of compressor rotor blades in an aircraft turbine engine remain unchanged under normal operating conditions. This was demonstrated by noting that the magnetization of compressor rotor blades of a J-85 jet engine in a test cell at Wright-Patterson Air Force Base remained unchanged.

Another technique which senses the manifestations of foreign object damage monitors blade-tip parameters. While not being able to sense directly the dimensional damage, this technique has several advantages. First the detector location requires only a small hole in the compressor shroud. This would allow the use of a permanently installed sensor for both in-flight and flight-line tests. Second, all stages of compressor rotor blades can be monitored, if desired. Third, the manufacturing tolerances on the rotor blade tip-to-case distances are much tighter than corresponding tolerances on the blade edges. Thus, the detector output on a normal blade is well defined and is less likely to mask the system output due to blade variations. Fourth, because of this tolerance requirement, the effect on the reliability of detection of reworked blades is also minimized. This

technique can employ either eddy-current, millimeter wave, or magnetic sensors. The simplest sensor system appears to be an eddy-current sensor approach. These sensors can monitor the blade-tip parameters for tip damage, such as tip curl. The time of arrival or twist of the blade tip can be monitored as a precursor of damage to the lower region of a blade and subsequent crack development as well as bends and twists induced by foreign objects hitting the upper portions of the blade. A third class of effects detectable using tip measuring techniques results from the aerodynamic loading of the blades. In this case, the tip twist and bending for a given dynamic load was shown to be a function of a crack length and its distance from the blade root. Artificially introduced leading edge damage of the order of 3/32 inches was easily discernible over the normal system output using tip parameter sensors.

In the case of both the remnant-magnetization and the tip-parameter detection techniques, the detector output is a function of compressor speed, defect size, and defect position. This indication may also be a function of the type of foreign object damage experienced. As such, these detection techniques cannot develop a unique output as a function of defect size. They do appear, however, to be sensitive to indirect evidences of foreign object damage or fatigue. For example, the remnant magnetization detector appears to be quite sensitive to any type of foreign object damage which would cause a minimum size mechanical defect. In addition, the tip-twist and time-of-arrival detectors appear to be quite sensitive to cracks near the root of the blade either due to fatigue or foreign object damage. Tip parameter sensors have sufficient sensitivity to detect a crack development before it has progressed much more than 0.2 inch near the root. Its use would permit timely reduction of power on a particular jet engine, assuming in-flight monitoring. Ingested object hits occurring near the top half of the blade appear less likely to cause cracks but are more likely to bend or twist the blades so that time-of-arrival

and twist change can provide a reliable indication of significant damage.

The signal processing electronics associated with either a remnant magnetization or tip parameter sensor appear to be relatively simple. While the initial breadboard designs of the signal processor, should be no greater than that of a radio receiver or bread-basket. Thus, these systems can be used not only for flight line tests but for in-flight monitoring as well.

5.0 OVERALL RECOMMENDATIONS

It would seem advisable to consider two types of checkout systems. One checkout system could be employed for in-flight applications. This system would sense if foreign object damage had taken place and provide some indication as to the seriousness of this foreign object damage. Once the foreign object damage or fatigue cracks are indicated by the in-flight monitors, the seriousness of the problem would be determined by measuring the geometrical dimension of the damage areas by flight-line equipment.

To meet the first requirements, a combination checkout system employing remnant magnetization and tip parameter sensors could be incorporated into one unit. Three sets of sensors could be installed in holes in the shroud above the first three stages of compressor rotor blades. Before actual flight tests on a large number of aircraft could be performed, it would seem appropriate to establish a more complete statistical relationship between foreign object damage and the remnant magnetization or tip-parameter effects. This could be accomplished by driving the presently available J-47 compressor section by an air motor and inducing controlled foreign object damage. In addition, the permanent nature of remnant magnetization where foreign object damage has not taken place should be further investigated for non-normal flight conditions. This would require magnetizing blades on a test aircraft and subjecting this aircraft to both common and unusual air maneuvers. A variety of airframes, both present and comtemplated, and the associated jet engines must be examined. A method for mechanically mounting the sensors in shroud holes over the first three compressor rotor stages would then be devised. A detection system including sensors, signal processor, and read-out equipment would then be built to permit evaluation of the entire checkout system on one engine of a test bed aircraft.

In addition to the in-flight monitoring equipment (which largely detects whether foreign object damage has taken place), the significance of the damage would be detected by a flight-line

system by resolving mechanical details of the foreign object damage. The system best capable of doing this is the millimeter wave interferometer. It would be used primarily for flight-line checkout. Before a field evaluation unit can be built, an additional breadboard incorporating improvements and using the highest usable frequency system should be built and tested. Based on this and the airframe survey, a field design capable of testing many jet engines should then be built to detect edge defects on the first stage rotor blades and with lesser resolution for defects on the air foil contour area of the first stage and edge defects on the second stage blades. It would then be field evaluated on a test bed aircraft.

Following this, the best designs should be revised as required and consideration given for incorporation of the checkout system into several hundred aircraft for a complete field evaluation.

REFERENCES

1. Sydney D. Berman, Jet Engineering Problems Experienced in the United States Air Force, Office of Inspector General, USAF, Norton Air Force Base, December 1953.

2. Factors that Affect Operational Reliability of Turbojet Engines, NASA Technical Report TR-R-54, Lewis Center Staff, 1960.

3. William R. Travers, Factors Against the Use of Turbojet Inlet Screens, Preprint No. 295, SAE, 1954.

4. H. Klien, Small Scale Tests on Jet Engine Pebble Aspiration, Report No. SM-14885, Santa Monica Division, Douglas Aircraft Co., August 1953.

5. Foreign Object Damage, Northrop Service News, Vol. IV, No. 7, August 1954.

6. L.A. Rodert and F.B. Garrett, Ingestion of Foreign Objects into Turbine Engines by Vortices, NACA TN 3330, 1955.

7. J.E. DeResner, Retractable Air Inlet Screens for Aircraft Gas Turbines, SAE Paper No. 296, 1954.

8. E.K. Armstrong, Research on Vibration Operational Techniques, ASME Paper No. 66-WAGT-14, February 1967.

9. A.F. Kay, Millimeter Wave Antennas, Proceedings of IEEE, Vol. 54, No. 4, pp. 641-647, April, 1966.

Security Classification

DOCUMENT CONTROL DATA - R&D

(Security classification of title, body of abstract and indexing annotation must be entered when the overall report is classified)

1. ORIGINATING ACTIVITY (Corporate author)	2a. REPORT SECURITY CLASSIFICATION
IIT Research Institute 10 West 35th Street Chicago, Illinois 60616	Unclassified
	2b. GROUP

3. REPORT TITLE

Turbine Engine Compressor Blade Checkout

4. DESCRIPTIVE NOTES (Type of report and inclusive dates)

Final Report, of study of checkout techniques, April 1966-April 1967

5. AUTHOR(S) (Last name, first name, initial)

J. E. Bridges
H. R. Hegner, et al.

6. REPORT DATE	7a. TOTAL NO. OF PAGES	7b. NO. OF REFS
1 June 1967	222	9

8a. CONTRACT OR GRANT NO.	9a. ORIGINATOR'S REPORT NUMBER(S)
AF 33(615)-3640 b. PROJECT NO. 8119 c. Task No. 811925 d.	IITRI No. E6067
	9b. OTHER REPORT NO(S) (Any other numbers that may be assigned this report) AFAPL-TR-67-59

10. AVAILABILITY/LIMITATION NOTICES This document is subject to special export controls and each transmittal to foreign governments or foreign nationals may be made only with prior approval of Support Technology Division (APF), Air Force Aero Propulsion Laboratory, WPAFB, Ohio 45433.

11. SUPPLEMENTARY NOTES	12. SPONSORING MILITARY ACTIVITY
N/A	Air Force Aero Propulsion Laboratory Wright-Patterson Air Force Base, Ohio 45433

13. ABSTRACT

The ingestion of foreign objects into jet engines causes damage in the compressor assembly which is a major safety-of-flight and maintenance problem. While the engine is installed, the checkout of jet engine compressor rotor blades is a difficult and time consuming operation. Foreign object damage is normally not found until it severely affects engine performance. Therefore, new checkout techniques need to be developed to detect foreign object damage during flight line checkout while the engine is operating.

This program was initiated with an objective to demonstrate the feasibility of one or more techniques for a portable flight line checkout system that will determine foreign object damage to the compressor rotor blades of the installed jet engine. The compressor blades are to be inspected without requiring personnel to gain access to the engine front end and while the engine is motoring, idling, and running at 100 percent power or any setting in between.

(Continued on Attached)

DD FORM 1 JAN 64 1473

Security Classification

Security Classification

14 KEY WORDS	LINK A		LINK B		LINK C	
	ROLE	WT	ROLE	WT	ROLE	WT
Ingestion of Foreign Objects into Turbine Engines Foreign Object Damage to Gas Turbine Engines (FOD) Turbine Engine Compressor Blade Checkout Automatic Checkout Equipment (ACE) Aerospace Ground Equipment (AGE)						

INSTRUCTIONS

1. ORIGINATING ACTIVITY: Enter the name and address of the contractor, subcontractor, grantee, Department of Defense activity or other organization *(corporate author)* issuing the report.

2a. REPORT SECURITY CLASSIFICATION: Enter the overall security classification of the report. Indicate whether "Restricted Data" is included. Marking is to be in accordance with appropriate security regulations.

2b. GROUP: Automatic downgrading is specified in DoD Directive 5200.10 and Armed Forces Industrial Manual. Enter the group number. Also, when applicable, show that optional markings have been used for Group 3 and Group 4 as authorized.

3. REPORT TITLE: Enter the complete report title in all capital letters. Titles in all cases should be unclassified. If a meaningful title cannot be selected without classification, show title classification in all capitals in parenthesis immediately following the title.

4. DESCRIPTIVE NOTES: If appropriate, enter the type of report, e.g., interim, progress, summary, annual, or final. Give the inclusive dates when a specific reporting period is covered.

5. AUTHOR(S): Enter the name(s) of author(s) as shown on or in the report. Enter last name, first name, middle initial. If military, show rank and branch of service. The name of the principal author is an absolute minimum requirement.

6. REPORT DATE: Enter the date of the report as day, month, year; or month, year. If more than one date appears on the report, use date of publication.

7a. TOTAL NUMBER OF PAGES: The total page count should follow normal pagination procedures, i.e., enter the number of pages containing information.

7b. NUMBER OF REFERENCES: Enter the total number of references cited in the report.

8a. CONTRACT OR GRANT NUMBER: If appropriate, enter the applicable number of the contract or grant under which the report was written.

8b, 8c, & 8d. PROJECT NUMBER: Enter the appropriate military department identification, such as project number, subproject number, system numbers, task number, etc.

9a. ORIGINATOR'S REPORT NUMBER(S): Enter the official report number by which the document will be identified and controlled by the originating activity. This number must be unique to this report.

9b. OTHER REPORT NUMBER(S): If the report has been assigned any other report numbers *(either by the originator or by the sponsor)*, also enter this number(s).

10. AVAILABILITY/LIMITATION NOTICES: Enter any limitations on further dissemination of the report, other than those imposed by security classification, using standard statements such as:

(1) "Qualified requesters may obtain copies of this report from DDC."

(2) "Foreign announcement and dissemination of this report by DDC is not authorized."

(3) "U. S. Government agencies may obtain copies of this report directly from DDC. Other qualified DDC users shall request through _____."

(4) "U. S. military agencies may obtain copies of this report directly from DDC. Other qualified users shall request through _____."

(5) "All distribution of this report is controlled. Qualified DDC users shall request through _____."

If the report has been furnished to the Office of Technical Services, Department of Commerce, for sale to the public, indicate this fact and enter the price, if known.

11. SUPPLEMENTARY NOTES: Use for additional explanatory notes.

12. SPONSORING MILITARY ACTIVITY: Enter the name of the departmental project office or laboratory sponsoring *(paying for)* the research and development. Include address.

13. ABSTRACT: Enter an abstract giving a brief and factual summary of the document indicative of the report, even though it may also appear elsewhere in the body of the technical report. If additional space is required, a continuation sheet shall be attached.

It is highly desirable that the abstract of classified reports be unclassified. Each paragraph of the abstract shall end with an indication of the military security classification of the information in the paragraph, represented as *(TS), (S), (C), or (U)*.

There is no limitation on the length of the abstract. However, the suggested length is from 150 to 225 words.

14. KEY WORDS: Key words are technically meaningful terms or short phrases that characterize a report and may be used as index entries for cataloging the report. Key words must be selected so that no security classification is required. Identifiers, such as equipment model designation, trade name, military project code name, geographic location, may be used as key words but will be followed by an indication of technical context. The assignment of links, rules, and weights is optional.

13. ABSTRACT (Continued)

The program was initiated by examining a wide variety of physical phenomena. The most promising techniques were then considered on an analytical basis, followed by preliminary laboratory evaluations on simple simulated compressor assemblies. After these investigations, the most promising techniques were evaluated on an actual compressor section from a J-47 class engine. Results pointed to the need for primary emphasis to be placed on electromagnetic techniques including millimeter wave, magnetic field, and eddy-current techniques. Electrometer and optical techniques did not prove to have promising applications on a practical basis. The feasibility of the promising techniques were verified by demonstrating them with experimental breadboards on the J-47 compressor assembly.

(This abstract is subject to special export controls and each transmittal to foreign governments or foreign nationals may be made only with prior approval of Support Technology Division (APF), Air Force Aero Propulsion Laboratory, WPAFB, Ohio 45433.)